Proceedings for the 36th Annual Conference of the
Society for Astronomical Sciences

SAS-2017

The Symposium on Telescope Science and AAVSO Spring 2017 Meeting

Editors:
Robert K. Buchheim
Jerry L. Foote
Dale Mais

June, 2017
Ontario, CA

Disclaimer

The acceptance of a paper for the SAS Proceedings does not imply nor should it be inferred as an endorsement by the Society for Astronomical Sciences of any product, service, method, or results mentioned in the paper. The opinions expressed are those of the authors and may not reflect those of the Society for Astronomical Sciences, its members, or symposium Sponsors

Published by the Society for Astronomical Sciences, Inc.
Rancho Cucamonga, CA

First printing: June 2017

Photo Credits:

Front Cover:
NGC 2024 (Flame Nebula) and B33 (Horsehead Nebula)
Alson Wong, Center for Solar System Studies

Back Cover:
Center for Solar System Studies (CS3) site, Landers, CA
Robert D. Stephens, Center for Solar System Studies

TABLE OF CONTENTS

PAPERS WITHOUT PRESENTATION

POSTER PAPERS

PREFACE

Welcome to the joint meeting that combines the 36th annual Symposium of the Society for Astronomical Sciences, and the Spring Meeting of the American Association of Variable Star Observers! This year's agenda reflects the broad diversity of interests among SAS and AAVSO participants, with papers covering photometry, spectroscopy, interferometry and astrometry; instruments ranging from eyeballs to CCDs and spectrographs to radios; and projects ranging from education to citizen-science to a variety of astronomical research targets.

It takes many people to have a successful conference, starting with the Program Committee. This year the regular committee members are:

Robert Gill	Robert D. Stephens
Cindy Foote	Jerry Foote
Robert Buchheim	Dale Mais
Wayne Green	John Menke

We thank the staff and management of the Ontario Airport Hotel for their efforts to accommodate the Society and our activities.

SAS Membership dues and Registration fees do not fully cover the costs of the Society and the annual Symposium. We owe a great debt of gratitude to our corporate sponsors: Sky and Telescope, Woodland Hills Camera and Telescopes, PlaneWave Instruments, Software Bisque, DC-3 Dreams, QHYCCD, and Sierra Remote Observatories. Thank you!

Finally, there would be no Symposium without the speakers and poster presenters, the attentive audience, and the community of researchers and educators who apply their telescopes and instruments to research activities. We thank all of you for making the SAS Symposium one of the premiere events for professional-amateur collaboration in astronomy.

Robert K. Buchheim
Jerry L. Foote
Dale Mais

2017 June

Symposium Sponsors

The Society for Astronomical Sciences thanks the following companies for their participation and financial support. Without them, this conference would not by possible.

Sky & Telescope Magazine
The Essential Magazine of Astronomy
http://www.skyandtelescope.com/

DC3 Dreams Software
Developers of ACP Observatory Control Software
http://www.dc3.com/

PlaneWave Instruments
Makers of the CDK line of telescopes and Ascension mounts
http://www.planewaveinstruments.com/

Woodland Hills Camera & Telescopes
Providing the best prices in astronomical products for more than 50 years
http://www.telescopes.net/

Sierra Remote Observatories
Remote Imaging from the Sierra Nevada Mountains
http://www.sierra-remote.com/

QHYCCD
Innovative imaging and observatory products
http://www.qhyccd.com/

Software Bisque
Enriching your astronomy experience since 1983
http://www.bisque.com/sc/

SBIG Imaging Systems
Award winning imaging systems for astronomical and laboratory use.
http://www.sbig.com/

Symposium Schedule

Time	Subject	Presenter/Author
Thursday June 15: Workshops		
0800 - 0900	Registration	
0830 - 1200		
	lunch break	
1330 - 1630		
1900	"Evening with the Pros"	
Friday June 16: Technical Papers		
8:00	Registration	
8:15	Welcome	Bob Buchheim, Stella Kafka
8:45	Monitoring the Moon for Meteoroid Impacts	Brian Cudnik
9:05	Taxonomy discrimination of the Tina asteroid family	Mattia Galiazzo
9:25	Student Observations of Cor Caroli (STF 1692)	Reed Estrada
9:45	Exoplanet Observing: From Art to Science	Dennis Conti
10:05	Coffee Break	
10:20	Eclipsing Binary NSV 03438	Carter Becker
10:40	Bright eclipsing binary zeta Phe	Tex Moon
11:00	WD 1145	Mario Motta
11:20	Spectrophotometry of Symbiotic Stars	David Boyd
11:40	Sodium doublet: A Speedometer and Thermometer	John Kenney
noon – 14:00	Lunch Break	
12:30	lunch Discussion group #1 (spectroscopy topics)	the "Spectro-gang"
14:00	Systematic Differences between Photometric Observers	John Martin
14:20	How Faint Can You Go?	Arne Henden
14:40	A Low-Cost Radio Telescope	John Hoot
15:00	All-Sky Imaging to Improve Telescope Scheduling	Gary Cole
15:20	Sponsor Infomercials	
16:00-17:30	Cash Bar in Sponsor Room	
	Dinner break	
19:00-21:00	AAVSONet: An Asset & Opportunity	Richard Berry
Saturday June 17: Technical Papers		
8:00	AAVSO Membership Meeting (1 ½ hr)	Stella Kafka
9:30	Coffee Break	
9:45	A Community-Centered Astronomy Research Prgm	Pat Boyce
10:05	Development of Student Astronomy Programs	Sean Gillette
10:25	A Decade of Published Student-Research Papers	Rachel Freed
10:45	Use of AAVSO data in Undergrad Capstone Project	Kristine Larsen
11:05	Student Research within Communities of Practice	Russell Genet
11:25	SPIRIT Telescope Initiative: Six Years On	Paul Luckas
11:45	Group Photo	
noon – 14:00	Lunch Break	
12:30	Discussion group #2 (Photometry topics) – Main Hall	

	Discussion group #3 (Astronomy in Education + Student Research) – Breakout Room	
14:00	Techniques of Photometry & Astrometry: PanSTARRS and GAIA	Wayne Green
14:40	Searching the Unknown: Detection of Fast Variability	Richard Stanton
15:00	Wide-Band SpectroPolarimetry Experiment: WR140	John Menke
15:20	Good Night and Good Luck	Bob Buchheim & Stella Kafka
17:30	Banquet (dinner service at 18:00)	
19:00	Banquet Speaker	Dava Sobel

OV BOOTIS: FORTY NIGHTS OF WORLD-WIDE PHOTOMETRY

Patterson, Joseph
jop@astro.columbia.edu

de Miguel, Enrique
edmiguel63@gmail.com

Barret, Douglas
douglasbarret70@gmail.com

Brincat, Stephen
stephenbrincat@gmail.com

Boardman Jr, James
jboardmanjr@gmail.com

Buczynski, Denis
buczynski8166@btinternet.com

Campbell, Tut
jmontecamp@yahoo.com

Cejudo, David
davcejudo@gmail.com

Cook, Lew
lew.cook@gmail.com

Cook, Michael J.
michael.cook@newcastleobservatory.ca

Collins, Donald
dcollins@warren-wilson.edu

Cooney, Walt
waltc111@att.net

Dubois, Franky
astrosun@skynet.be

Dvorak, Shawn
sdvorak@rollinghillsobs.org

Halpern, Jules P.
jules@astro.columbia.edu

Kroes, Anthony J.
akroes@netnet.net

Lemay, Damien
damien.lemay@globetrotter.net

Licchelli, Domenico
domenico.licchelli@le .infn.it

Mankel, Dylan
mankeldy@msu.edu

Marshall, Matt
marsh443@gmail.com

Novak, Rudolf
rudolf.novak@gmail.com

Oksanen, Arto
arto.oksanen@jklsirius.fi

Roberts, George
georgeroberts0804@att.net

Seargeant, Jim
jimsarge@gmail.com

Sears, Huei
searshue@msu.edu

Silcox, Austin
silcoxau@msu.edu

Slauson, Douglas
dmslauson@netscape.net

Stone, Geoff
geofstone@earthlink.net

Thorstensen, J.R
John.R.Thorstensen@Dartmouth.edu

Ulowetz, Joe
joe700a@gmail.com

Vanmunster, Tonny
tonny.vanmunster@gmail.com

Wallgren, John
jwallgren@leomail.tamuc.edu

Wood, Matt
matt.wood@tamuc.edu

ABSTRACT

Among the ~1000 known cataclysmic variables, only one appears to belong to the "Galactic halo" - the Population II stars. We report round-the-world photometry of this star (OV Boo) during March-April 2017, when it staged its first certified dwarf-nova outburst. The star is remarkable for its short binary period (66 minutes), high proper motion, metal-poor composition, substellar secondary, sharp white-dwarf eclipses, and nonradial pulsations. Something for everybody..... and it even had the good manners to erupt in northern springtime, when it transits near local midnight. Move over, SS Cyg and WZ Sge; there's a new celebrity in town!

1. INTRODUCTION

As of 2017, several thousand cataclysmic variables (CVs) are known, including ~1200 of known orbital period. Essentially all the orbital periods are short (<1 day), and most are very short (<3 hours). By definition, every CV has a Roche-lobe-filling "secondary star" transferring matter to a white dwarf, and accretion onto the white dwarf powers the luminosity. The "Roche-lobe-filling" condition implies a relation between orbital period and the density of the secondary:

$$P\sqrt{\rho} = \text{constant}$$

A few CVs (~40) have ultrashort periods - in the range 5-40 minutes - and those secondaries must therefore be of very high density. Spectroscopy of these stars shows a nearly pure helium spectrum, and the secondaries are very likely helium white dwarfs. That explains their very high density. This was lucidly explained long ago by Faulkner, Flannery, & Warner (1972).

But the other 97% of CVs show a minimum period of ~80 minutes. In fact there's a big pile-up of CVs right around 77-82 minutes ("period spike").

This is basically because the secondaries are hydrogen-rich main-sequence stars, and the smallest possible star (~0.085 solar masses) has the highest possible density - and hence the shortest orbital period, since $P\sqrt{\rho} = \text{constant}$. So we were quite shocked to find a CV with strong hydrogen emission lines and an orbital period of 66.6 minutes, far below the minimum period. This was SDSS J150722.30+523039.8 (Szkody et al. 2005). Mercifully, the Russians gave it a traditional variable-star name: OV Bootis.

You might think that since 0.085 M_{Sun} stars are the densest main-sequence stars, you could explain this oddity by merely hypothesizing a secondary of still lower mass - a brown dwarf. But not so. Lacking the central concentration of more massive "stars" (spherical self-gravitating objects), brown dwarfs are of lower density. By way of illustration, consider Jupiter - not quite a brown dwarf, but sufficient to illustrate the point. Jupiter has a mean density around 1 g/cc, like the Sun. But main-sequence stars obey roughly $R \sim M^1$, and hence $\rho \sim M/R^3 \sim M^{-2}$. Get the idea? Low-mass stars have densities far greater than the Sun (~ 100X greater, for the $R \sim M^1$ assumption). So the secondary in OV Boo is basically a low-mass star... and the spectrum is dominated by hydrogen, so the weirdly short orbital period cannot be explained by supposing it's a helium star.

So we zeroed in on this star and gave it a full photometric and spectroscopic study (Patterson, Thorstensen, and Knigge 2008). We learned the precise orbital period (66.61201 minutes). We learned the masses and radii of white dwarf and secondary, and the orbital inclination. The total eclipse of the white dwarf, along with the very high orbital inclination (85 degrees), permits very accurate measurement of these quantities. Most significantly, we measured the parallax and proper motion, which showed it to have - by a wide margin - the highest proper motion of any CV. This suggested that it might be a member of the Galactic Halo. We followed through with a study of its ultraviolet spectrum, which showed it to be significantly deficient in heavy elements: ([Fe/H] < -1.2; Uthas et al. 2011). This seemed to confirm its credentials as a Population II star – the only one known among all CVs.

Theoretical Pop II stars are slightly smaller, by ~10%, than Pop I stars of the same mass. This is because much of the opacity in the outer layers of Pop I stars comes from "metals" (elements beyond helium), and opacity tends to bloat a star. Pop II stars lack metals. Density scales as M/R^3, so at a fixed mass, that 10% translates to ~ 30% greater density. A 30% increase in ρ means a 15% increase in $\sqrt{p}$. Since $P\sqrt{\rho} = \text{constant}$, this means a 15% decrease in P. Thus the minimum orbital period for a Pop II CV should be ~15% shorter, or about 67 minutes.

Well, that's pretty good... and consistent with everything else known about this star (high proper motion, low abundance of metals). A remaining question is whether the unusual abundances might have an effect on outbursts. In March 2017, we had an opportunity to find out. This paper reports our time-series photometry over the first 40 days of OV Boo's first recorded outburst.

2. OBSERVATIONAL TECHNIQUES

Most of the data reported here comes from the Center for Backyard Astrophysics, a global network of telescopes cooperating in campaigns of time-series photometry of variable stars (CBA: de Miguel et al. 2016). The network now includes ~20 telescopes, spread sufficiently over the Earth to give very long time series relatively untroubled by local weather and daily aliasing. Our typical telescope is a 35 cm reflector, equipped with a CCD camera and recording images every 30-60 s for many hours per night. Most of the data is unfiltered (white-light, or perhaps more correctly "pink", with an effective wavelength near 6000 Å) differential photometry, although we always obtain some coverage in V light to express results on a standard scale if needed. Data from several telescopes are then spliced together to form a one-night light curve, with minimal gaps. We take advantage of overlaps in data to determine additive constants which put all our measurements on one instrumental scale (usually that of the most prolific or best-calibrated observer). These constants are usually in the range 0.01-0.05 mag, probably due to variations in transparency and camera sensitivity. Most telescopes use the same comparison star, although we also use data with other comparisons (requiring larger and more uncertain additive constants) if there is sufficient overlap. In this case we frequently used the AAVSO "115" star (GSC 3868-1067, V=11.482) and "143" star (GSC.3868-1068, V=14.290).

Research programs on faint stars with small telescopes often use white light, to enable high time resolution with good signal-to-noise. In the case of cataclysmic variables, it usually makes good astrophysical sense too, since the underlying sources of light are broad-band emitters (accretion disk, white dwarf). It is common practice to report magnitudes as "C" (or often "CV", though we will avoid this term for obvious reasons): the result of differential photometry in clear light, added to the comparison star's known V magnitude. This is also our practice.

However, because the white-light passbands are typically ~4000 Å wide, the effective wavelengths of the variable and comparison stars can easily be 500 Å apart. Therefore, C/CV magnitudes are not V magnitudes. We nevertheless prefer the C/CV scale and use it here, because it is our natural measurement scale, and because it accurately expresses the true changes in light.

Since an instrumental scale is not fully reproducible, a standard V magnitude is more desirable for archival purposes. For "good" comparison stars (B-V<1.0), our C magnitudes transform to V magnitudes via

$\Delta V = \Delta C + 0.37\ \Delta(B-V)$,

which implies $\Delta V = -0.20$ in this case, where the variable is assumed (and observed) to have B-V near 0.0. The latter assumption is pretty good for the great majority of cataclysmic variables accreting at a high rate – including OV Boo in outburst.

Atmospheric extinction is significant for us, because the program stars are usually much bluer than comparison stars (although we avoid very red stars, which are the bane of all stellar photometry). We know from experience that this differential extinction amounts to -0.06 mag/airmass for most CVs. Nevertheless, in the spirit of keeping human hands off the data as much as possible, we usually make no correction for extinction.

The summary observing log for the first 40 days of outburst is given in Table 1. (A "night" denotes a time-series of good quality lasting at least 3 hours.)

TABLE 1 - OBSERVER'S NIGHTS/HOURS (first 40 nights)

de Miguel	20/132	Boardman	5/27
Cejudo	24/122	Wood	4/32
Licchelli	29/108	Wallgren	4/32
Dvorak	16/104	Collins	8/31
Vanmunster	18/82	Seargeant	4/31
Stone	18/81	Dubois	9/23
Lemay	12/80	Slauson	4/19
Cook, L.M.	18/73	Buczynski	4/16
Kroes	13/72	Thorstensen	4/14
Cook, M.J.	11/68	Mich. State	4/11
Ulowetz	11/66	Cooney	2/12
Barret	8/57	Novak	2/8
Campbell	7/49	Halpern	2/7
Roberts	7/49	Brincat	1/3

Table 1: Summary observing log

3. THE OUTBURST

On 15 March 2017, the star was reported to be at magnitude 11.4 in the photographic sky patrol of Masaru Mukai (no relation to Koji Mukai, the famous X-ray astronomer). This was the first-ever recorded eruption. Within a few hours, telescopes around the world turned to the star, mostly with time-series photometry.

We observed the star during each of the first 40 nights of outburst, averaging ~11 hours per night. The full light curve is shown in Figure 1. We use here and hereafter a truncated Heliocentric Julian Date time stamp (true HJD - 2,457,000). The star declined by 0.10 mag/day for the first 30 days – the so-called "plateau" phase of a dwarf-nova superoutburst. Then it suddenly fell another magnitude and resumed the slow decline.

The orbital light curve changes smoothly throughout the eruption. This is shown in Figure 2, where we have singled out 4 nights spaced by 10 days, and labelled them with their 3-digit Julian days. Eclipses are seen on every night, but deepen as the star grows fainter. The complex light curve of the first two weeks gradually mutates into a more traditional "superhump" light curve (suggested by the drifting phase of the out-of-eclipse wave between JD 851 and 861).

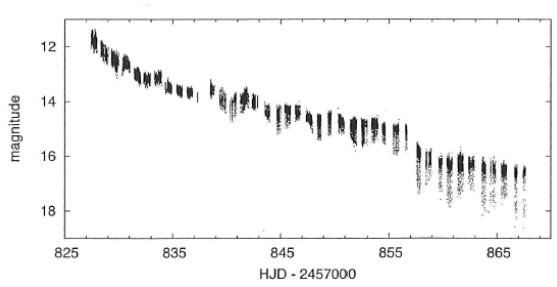

Figure 1. The full light curve over the first 40 days.

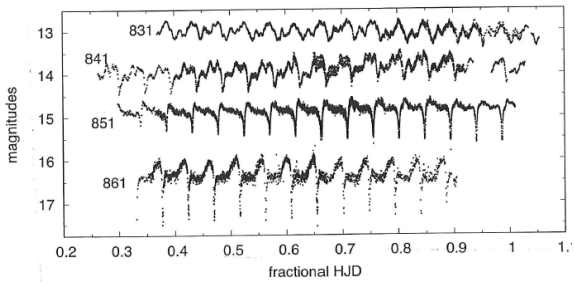

Figure 2. The changing orbital light curve. Light curves are labeled with their 3-digit Julian dates.

Actually, the light curve changes every night, not merely on the 10-day timescale which Figure 2 might suggest. This is illustrated in Figure 3, where each day looks quite distinct, and where the drifting wave can be clearly seen.

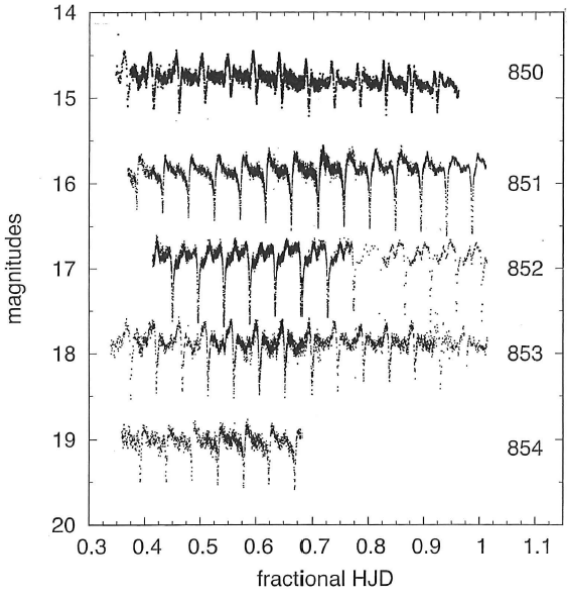

Figure 3. Nightly light curves in one 5-day segment, which illustrates the drifting out-of-eclipse wave. In this figure the magnitudes are correct for JD 850; the others are displaced downwards by 1, 2, 3, and 4 mag, to promote visibility.

To search for periodic behavior in these light curves, we first removed the sharp eclipses. We defined the eclipse portion as spanning from orbital phase 0.9 to 1.1, because that is the eclipse duration commonly found in other deep-eclipsing CVs. Then we took power spectra of segments of the overall light curve. These are shown in Figure 4. In the first 10 days of eruption, the dominant signal occurs at 21.6409 (12) cycles/day - about 0.1% displaced from the known orbital frequency. This signal is commonly found in the dwarf novae of extremely short orbital period, and is called the "outburst orbital hump" (because it occurs very close to ω_{orb}, and is a signature of superoutburst) or "early superhump" (because it is restricted to the early part of superoutburst). It fades after ~10 days, and is replaced by a dominant signal around 21.33(3) cycles/day. In Figure 4 we have parsed the latter signal into "plateau" and "post-plateau", and report their frequencies respectively as 21.3562(20) and 21.3182(20) cycles/day. This wave, dominating the raw light curves, is the famous common superhump – a universal and indeed defining signature of the "WZ Sge" class of dwarf novae. The frequency resolution is not sufficient to establish whether these are different phenomena, or just one process wandering slightly in frequency, or phase, or even amplitude. Fourier analysis is a powerful tool, but is confounded if its assumptions (constant frequency, phase, and amplitude) are not satisfied.

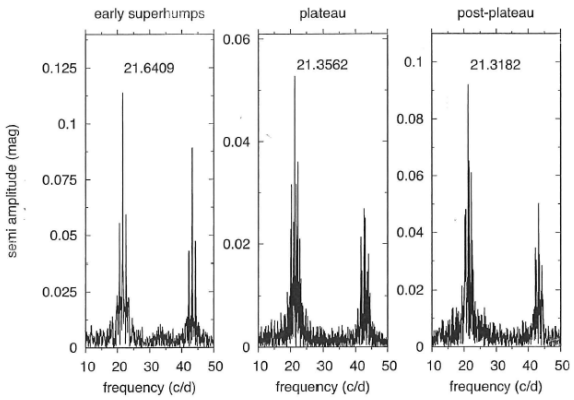

Figure 4. The amplitude spectra, parsed into three segments in time. Each peak is labeled with its frequency in cycles/day, and the fine structure in the first segment reflects the alias pattern in all of them. Therefore the signal is quite complex after the first 10 days, and the division into plateau and post-plateau may be artificial.

Eclipses are present in all light curves, but are relatively shallow, broad, and distorted (asymmetric) in the early portion of the outburst. After JD 838, they become more consistent and appear to show a regular pattern, seen in Figure 5. Here we have established a fiducial epoch of mid-eclipse (HJD 827.70155) as the expected precise time of the first mid-eclipse, based on the 2008 ephemeris. We measure the center of the sharp component seen near the bottom of every eclipse, and record the average of (usually) three consecutive eclipses. The wiggles in Figure 5 suggest a wave of ~75 orbital cycles, or 3.5 days. This appears to be the beat period between orbit and superhump, which is 3.48 days for the compromise frequency we adopt (21.33 c/d).

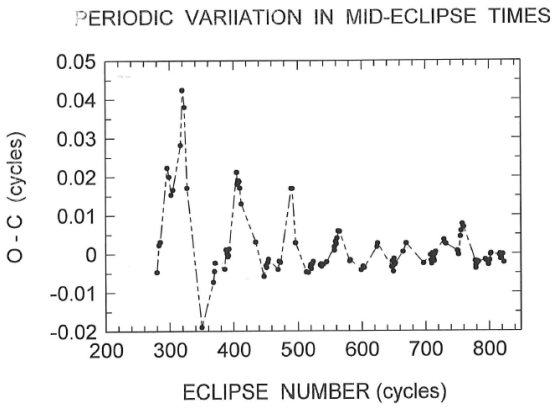

Figure 5. O-C departures from the expected time of mid-eclipse (defined as the middle of the sharp eclipse), based on the ephemeris HJD 827.70155 + 0.046258341 E. There is a wiggle with a timescale ~75 cycles= 3.5 days.

Actually, the fingerprints of "3.5 days" are all over the light curves. The upper frame of Figure 6 shows the mean brightness of the star during the plateau phase. A 3.5 day wiggle is apparent. The lower frame shows the eclipse depth in magnitudes (mid-eclipse minus mean light for the full orbit). An obvious 3.5 day modulation is present, with an apparent phase change during the transition to post-plateau.

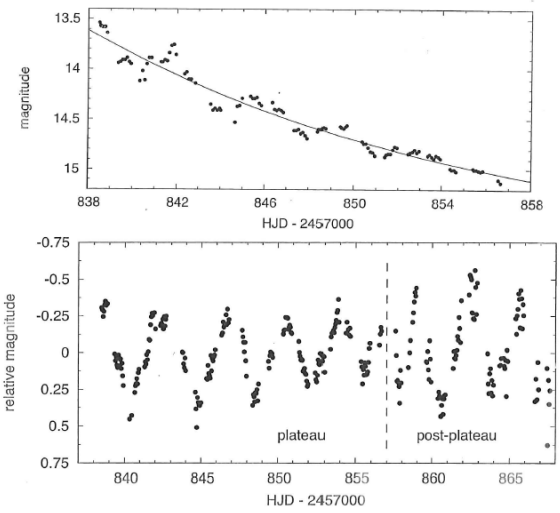

Figure 6. Upper frame, the average out-of-eclipse magnitud e per orbit, relative to the overall exponential decline. Lower frame, the eclipse depth for each orbit (post-plateau measures are noisy because of the faintness and brevity of mid-eclipse).

4. EXULTATION ... AND INTERPRETATION

We were very surprised to see how accurately we could time the eclipses. The timings appear to have a dispersion of just 4-5 s, relative to the overall trend (the "damped sinusoid" in Figure 5). Our telescopes are small, the star is faint, the eclipse is brief, the integration times are long (usually 30-40 s), and the sharp eclipse must be measured amid a broad eclipse which is variable and asymmetric. Formidable problems! But we had some advantages: the short P_{orb} implies many eclipses; the sharpness of the eclipse makes it easier to measure the mid-point; and we had very frequent overlaps in coverage, yielding the advantage of "crowd-sourcing".

As of this writing, the eruption is only 40 days old, and the star is still ~2 magnitudes above quiescence. There could be surprises just around the proverbial corner. But the periods found in our analysis are well-determined and free from aliasing, because of the large geographic spread in longitude, and because the length of coverage (40 days) is sufficient to establish the longer period (3.5 days). The outburst orbital hump ("early superhump") occurs at a period 0.1% shorter than P_{orb}; the plateau superhump occurs at a period 1.22% longer than P_{orb}; and the post- plateau superhump occurs at a period 1.40% longer than P_{orb}. From the mass ratio

$M_2/M_1 = 0.069(2)$

measured by Patterson, Thorstensen, and Knigge (2005), and the calibration of Patterson et al. 2005 [their Equation (8)], one would expect a superhump period excess of 1.38(10)%.

So, that all looks pretty good.

What exactly are superhumps?

They are large-amplitude photometric waves, with a period 1-5% longer than P_{orb}, and seen in the large eruptions ("superoutbursts") of many dwarf novae. They were discovered as early as 1972, but their origin remained puzzling until theorists made a breakthrough discovery (Whitehurst & King 1991, Lubow 1991). These studies showed that an eccentricity instability develops at the 3:1 resonance in an accretion disk. Quiescent disks are generally too small to reach that resonance. But when accretion starts, some material must spiral outward to balance the angular momentum lost by the inward-spiraling gas. It reaches the 3:1 resonance, and the disk becomes elliptical. The elliptical orbits are then perturbed by the orbiting secondary, and the orbits precess forward – for the same reason that planets in the solar system precess forward in their elliptical orbits (perturbed mainly by Jupiter). The secondary star then aligns with the disk's line of apsides on a period slightly longer than P_{orb}. This is the 67.5

minute superhump period, and the precession period itself is the beat period between the 66.6 m orbit and the superhump. And, happily, that equals 3.5 days.

That's the theory, anyway. The deep eclipses in OV Boo allow us to test the general correctness of these ideas. If the accretion disk is a precessing ellipse, then the center-of-light moves slowly around the white dwarf, and the eclipse times will show the signature of that slow precession. Figure 5 shows just this effect... and we may eventually be able to learn the degree of ellipticity, and how fast it decays.

OV Boo in superoutburst is a pretty good match for WZ Sagittae, the poster-child for all short-P_{orb} dwarf novae. The resemblance is sufficiently thorough that we can, with some confidence, answer our original questions: does the Population II composition affect the creation or properties of outbursts? No, and probably no.

But our observations and analysis are far from over. Bootes has a long observing season, and ours will be filled with extensive photometry and spectroscopy.

Of course, 666 is widely regarded as an ominous and evil number. We take no position on that subject... but for us, 66.6 (minutes) proved to be a very lucky number indeed. So are AST16-15456 and HST-GO-13630, the NSF and NASA grants that keep us going in this enterprise.

5. REFERENCES

de Miguel, E. et al. 2016, MNRAS, 457, 1447.

Faulkner, J., Flannery, B.P., & Warner, B. 1972, ApJ, 175, L79. Lubow, S.H. 1991, ApJ, 381, 268.

Patterson, J., Thorstensen, J.R., & Knigge, C. 2008, PASP, 120, 510. Patterson, J. et al. 2005, PASP, 117, 1204.

Szkody, P. et al. 2005, AJ, 129, 2386. Uthas, H. et al. 2011, MNRAS, 414, L85.

Whitehurst, R. & King, A.R. 1991, MNRAS, 249, 25.

An Ongoing Program for Monitoring the Moon for Meteoroid Impacts

Brian Cudnik, Department of Chemistry and Physics, Prairie View A&M University
P.O. Box 519, M.S. 2230, Prairie View, Texas 77446
bmcudnik@pvamu.edu

Seth Saganti, Fazal Ali, Salman Ali, Trevannie Beharie, Brittany Anugwom
Dept. of Chemistry and Physics
Prairie View A&M University

Abstract

Lunar meteor impacts are surprisingly frequent phenomena, with well over one hundred observable events occurring each year. Of these a little over half arise from members of annual meteor showers (e.g. Perseids, Leonids, etc.), with the rest being sporadic in origin. Five years ago, I introduced to the SAS Symposium the idea of observing lunar meteoroid impact phenomena and applying these observations to a space mission (LADEE-Lunar Atmosphere and Dust Environment Explorer) that launched the following year. Five years later I revisit and reintroduce the activities of the Association of Lunar and Planetary Observers-Lunar Meteoritic Impact Search (ALPO-LMIS) section and share some of the latest observations that have been received. For over 17 years now, ALPO has hosted the LMIS section, for which I have served as coordinator since its inception. In this paper, I will revisit the main ideas of the earlier paper, share some recent observations of lunar meteors, and provide new initiatives and projects interested persons can participate in.

1. Introduction

For nearly two decades, astronomers have kept a close watch on the moon for the point flashes of meteoroid impacts. Hundreds of such events have been documented over this time, leading to the conclusion that these events happen surprisingly often. This actually is not unusual when one considers the frequency of fireballs and bolides that happen in the Earth's atmosphere on a regular basis. The main differences between lunar and terrestrial meteors (Figure 1) is that the moon does not have an atmosphere to slow or stop meteoroids from striking the surface, and the mass of the moon is much less than that of Earth. These factors both play a role in the frequency of impacts that actually happen on the moon versus Earth.

Lunar meteors have historically been considered a form of Lunar Transient Phenomena, (LTP) a type of change that occurs on an otherwise changeless body. Since the invention of the telescope (and even before), hundreds of observations of such phenomena have been documented. These phenomena took on a variety of forms, from point flashes to steady glows, hazes, etc.; many of these have been reported by reputable, experienced observers. However, none of these phenomena had been unambiguously confirmed prior to 1999 (Cudnik, 2012).

With the videorecordings of the Leonid meteor impacts in 1999 we had, for the first time, a scientifically documented set of observations of this one type of LTP and were able to make many more such observations over the subsequent years. Although the vast majority of LTP remain unexplained for the most part, meteoroid impacts have now been scientifically validated as a recurring and observable phenomenon that can tell us much about the near-Earth space population of debris as well as manifestations of hypervelocity impacts.

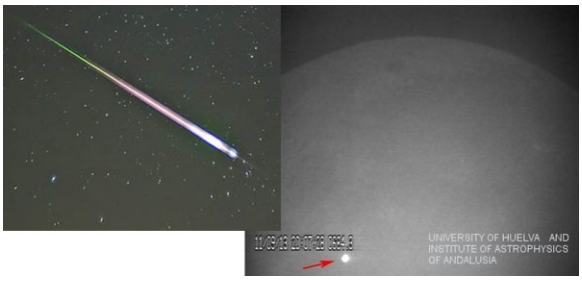

Figure 1: Atmospheric versus lunar meteor (left image credit: Navicore; right image credit: J. Madiedo / MIDAS

2. Lunar Meteor Phenomena

With the above-mentioned, scientifically confirmed observations of lunar meteor phenomena

recorded, at least one form of LTP has been validated and really exists. In addition, this set of six observed and confirmed lunar Leonid impacts gives some credibility to the historic LTP observations that resemble meteoroid impacts, namely point flashes of light; however one cannot know with absolute certainty whether each such observation, was truly a meteoroid impact as opposed to some other phenomena. This is true, even for modern observations, unless the event was observed by two widely separated and independent observers using similar equipment.

2.1 The Physical Nature of Lunar Meteors

Scientists are well aware that interplanetary space is littered with debris, such as dust, stones, rocks, boulders, and larger objects. The casual observer, with a limited knowledge of astronomy, sees evidence of this when witnessing a "shooting star". The frequent occurrence of meteors in Earth's sky reinforces the idea that interplanetary space is not completely empty but contains debris. In addition to the present-day evidence, we see historic evidence of even greater episodes of bombardment in the cratered, battered surfaces of airless planets, moons, and asteroids throughout the solar system.

One may group meteoroids into two broad classes based on their patterns of motion: annual shower meteors (from a well-defined radiant in the sky) and sporadic meteors (from seemingly random directions in the sky). In the first class, we know of dozens of meteor showers, great and small, that happen throughout a calendar year here on Earth. Most of these also affect the Moon, which increases the probability of observing one or more lunar meteors (providing the moon is favorably placed in its orbit). In the second class, these objects come from indeterminate sources and can occur at any time of the day, any day of the year. Some members of this class of meteoroid can be quite large, such as the asteroidal object that exploded above Chelyabinsk, Russia on February 15, 2013.

2.2 Where Meteors Generally Come From

We can also classify meteoroids by their source object types. Most of the annual showers come from trails of dust and debris left by the repeated passes of short period comets through the inner solar system. The Earth (and moon) intersects these trails and the result is the meteoritic phenomena we observe. Most objects within these streams are too small to generate impact flashes on the moon bright enough to be observed from Earth, but enough larger objects exist to produce flashes bright enough to be observed with ground-based equipment.

Sporadic meteoroids may either be pieces of comet debris or leftovers of collisions between asteroids, or asteroids themselves. These are often the source of some of the most spectacular impact events witnessed on either the Earth or the moon. Unlike the annual shower events, which carry a high probability of a given impact on the moon being associated with a member of the shower, it is impossible to tell the source of the impactor by a simple zero-dimensional point flash. Lunar Reconnaissance Orbiter (LRO) imagery may offer clues with the ejecta pattern of such an impact but the ability to associate a given crater with a given impact event is challenging at best.

3. Efforts to Monitor Lunar Meteors

A number of individuals, groups, and organizations have been involved in monitoring the moon (and coordinating such efforts) over the years with considerable success. Almost 500 events have been catalogued between these groups and that number continues to grow.

3.1 The ALPO-LMIS

Among other activities, the Lunar Meteoritic Impact Search (LMIS) section of the Association of Lunar and Planetary Observers (ALPO) endeavors to develop a catalog of confirmed lunar meteor impact flash observations. ALPO-LMIS was founded in early 2000 by the lead author of this paper and strives to coordinate an international effort to keep watch on the moon and document impact events. This is done using a variety of means of communication, from the ALPO-LMIS web page to e-mail reminders of events expected to occur. Over the years, the section has received more than 80 observations and reports on lunar meteor impact flash candidates.

Observer participation and activity does vary from year to year, depending on the observability of the moon during major annual showers. Each quarter an observing plan is released to the ALPO-LMIS web page and sent to the lunar-impacts@yahoogroups.com e-mail group. This plan consists of a list of intervals when the moon is favorably placed in the sky for ground-based lunar meteor observation; it also references which meteor stream(s) is(are) active during these intervals, which consist of two 5- to 7-day periods each month. The locations of the radiants of these showers help to determine which section of the Moon's disk to focus one's attention when video-taping for impact flashes.

3.2 NASA-MSFC

The Meteoroid Environment Office (MEO, https://www.nasa.gov/offices/meo/home/index.html) of NASA's Marshal Space Flight Center (NASA-MSFC-MEO) coordinates efforts to monitor the moon for meteoroid impacts using two telescopes equipped with astronomical video cameras at the Automated and Lunar and Meteor Observatory (ALaMO) at Marshall Space Flight Center in Huntsville, Alabama. The second telescope is present to rule out cosmic ray hits and other noise events. As of May 2016, when the last updated was posted, this effort had cataloged 399 candidate and confirmed lunar impact flashes over a nearly 11 year period. In addition to work with their own equipment and observatory, NASA-MSFC-MEO seeks observations from the amateur community and it has used these to make confirming observations on many occasions over the years.

With the consideration of establishing a base on the Moon (which, as far as I am aware, is not yet on the proverbial drawing board for the near future), the subject of lunar meteors is an important consideration. Individual astronauts are in little danger of being struck by a meteor but large, sprawling habitats are. The difference is simply their footprint size: astronauts cover a tiny cross-sectional area on the moon's surface while settlements would cover a much larger area, making for a much larger target for incoming meteoroids. Astronauts are not completely out of danger, however, since any moon walker unfortunate enough to be close to the blast of a meteoroid impact could be injured or killed by the shock wave and/or ejecta.

Work between ALPO, NASA and others have benefitted the study of lunar meteors tremendously. Each group offers a valuable public outreach resource and each is showing the huge value of pro-am collaborations. We hope to continue this teamwork well into the future.

3.3 Other Groups of Note

There are a number of groups active in the world, mainly in Europe and the U.S. There had seen some involvement with observers in China and Japan, but the groups from whom the ALPO-LMIS have received recent lunar meteor reports are in Europe: the British Astronomical Association, the work of Jose Madiedo and his team of professionals, the "Swiss-Italian" team of dedicated observers, and the Luna Unione Astrofili Italiani are among the groups that have been and continue to be active in the hunt for lunar meteors. The appendix at the end of the paper has web addresses for these and other relevant groups involved in lunar meteor observations. Note that this had also appeared in a previous paper but we are making it available again, with changes and updates as needed, to serve as a resource for anyone who is interested in observing lunar meteoritic phenomena.

4. Recent and Notable Observations

Next we will highlight some of the notable and recent images of lunar impact phenomena that we have received in recent years. Two events of note feature impacts recorded on March 17, 2013 and September 11, 2013. The former is the largest and brightest such event yet recorded and confirmed; if it had occurred well away from the glaring dayside, this impact may have been visible with the unaided eye.

4.1 March 17, 2013

The researchers at NASA's Marshall Space Flight Center recorded the bright flash from the impact of a meteoroid the size of a small boulder. This object impacted within Mare Imbrium with a flash almost 10 times as bright as anything recorded before. The velocity of the meteoroid the instant before impact was estimated to be 56,000 mph (90,000 km/h).

The interesting aspect of this is the unambiguous detection of an impact crater at the site of this impact by Lunar Reconnaissance Orbiter (LRO), making it one of the youngest craters ever observed on the Moon (at a little over 4 years old as of this writing, the LROC image is presented in Figure 2). The actual crater was found a short distance west of the reported coordinates, a reflection of the uncertainty in position determination from ground based impact flash measurements.

The crater generated by this impact is 65 feet (20 meters) in diameter and features a small central peak, making the crater look like a perfect miniature version of the larger craters with central peaks and ray systems. (Cassis and Jones, 2015)

It is interesting to note that this event was one of 9 lunar impact events that were attributed to a source of meteoroids known as the Virginid Complex, an unusual and little-known group of meteor showers that peak from mid-March to mid-April. There are several unusual characteristics about this complex to include their irregularities, their many radiant centers (up to 16 have been reported, but not all are active in the same year), the slow meteor motions and the proportion of larger objects within the stream. More information about this complex can be obtained from http://meteorshowersonline.com/showers/virginid_co

mplex.html. This may be something to watch in the coming years.

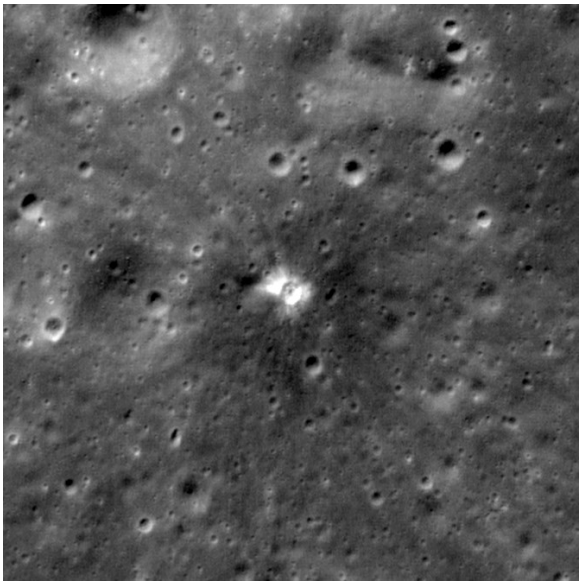

Figure 2: a brand new impact crater (center with bright spots), Credits: NASA/Goddard Space Flight Center/Arizona State University

4.2 September 11, 2013

The event that was observed and recorded on this day was the brightest confirmed impact flash recorded to date, lasting a full 8 seconds and almost matching Polaris in brightness at its peak. Jose Madiedo, of the University of Huelva in Huelva, Spain, recorded this event with two telescopes that make up the Moon Impacts Detection and Analysis System, or MIDAS observatory. This observatory is located in southern Spain.

The impact of the estimated 880 lb, 2 to 4.5 foot diameter space boulder was estimated at 37,900 mph and generated enough energy to create a crater roughly 131 feet (40 meters) in diameter. This occurred in an ancient basin known as Mare Nubium (Gannon, 2014)

4.3 December, 2013

Marco Iten, Raffaello Lena, Andrea Manna and Stefano Sposetti (the "Swiss-Italian" group) were observing the crescent moon with video and two of them, Iten and Sposetti (of Gnosca Observatory Switzerland), observed an impact through two telescopes simultaneously. This impact occurred in Mare Nubium near 11° west, 14° south and lasted approximately 80 milliseconds.

The team recorded a second, fainter impact on December 8, 2013 near lunar coordinates: 18° West, 50° South (Longomontanus crater border). This event was much fainter, lasting only an estimated 40 milliseconds. Both events may have originated from the Geminid meteor stream which was becoming active during the time of the observations.

The setups to record these flashes include 125mm and 150mm refractors each equipped with a Watec WAT902H2 Ultimate low light astronomical video camera (Sposetti, 2013)

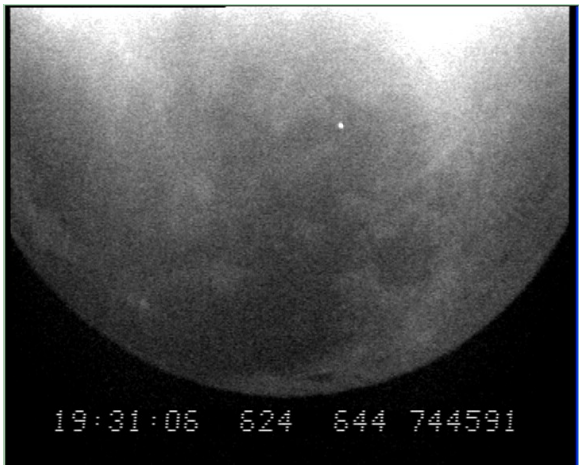

Figure 3: Video frame by Marco Iten showing the December 7, 2013 impact; image credit: Iten

4.4 November, 2015

The Swiss-Italian team observed four impacts, three on November 7 and one on November 8, each possibly a member of the Taurid complex. All four of these events had been confirmed by Jose Madiedo as being real impact events (Sposetti and Madiedo, 2013). Details of these and additional events are found in Table 1 (Cudnik, 2014).

Among the various types of instruments and cameras used by the Swiss-Italian team, the telescopes included 125 mm and 280 mm refractors, an 11-inch reflector; camera used was a Watec WAT902H2 Ultimate. The frame grab that generated the 2013 image for Figure 3 was from Iten's instrument, the 125 mm refractor.

In addition to the events described in detail, there is a number of impact events listed in Table 1 that were reported by various groups. Not included are the impact candidates observed by the NASA-MSFC team which, during the three year period from March 2013 to May 2016, catalogued 104 impact events, plus an additional 3 (also included in Table 1) reports from independent observers.

Table 1: Impacts reported recently to ALPO-LMIS between 2013 and 2017 (information for many drawn from Cudnik, 2014); note that all dates and times are in UT.

UT Date/Time and Observer(s)	Lunar Coord.	Shower source / additional comments
11 Sep. 2013 Jose Madiedo		Sporadic? Maximum brightness comparable to Polaris
7 Dec. 2013 19:31:06.6 Stefano Sposetti, Marco Iten	14°S, 11°W	Sporadic. In Mare Nubium, confirmed in two telescopes, 80 ms duration
8 Dec. 2013 19:15:58.6 Sposetti & Iten	50°S, 18°W	Sporadic. Longomontanus crater border, confirmed in two telescopes, 40 ms duration
4 Jan. 2014 23:49:57 George Varros	1.0°N, 11.6°W	Quadtrantid? Flash seen on single video field, the brightness distribu-tion matches a star more than a cosmic ray impact
5 Jan. 2014 00:12:26 George Varros	15.3°S, 25.5°E	Sporadic? Inside Crater Cyrillus F, faint single-frame event with stellar brightness profile
5 Jan. 2014 00:31:35 George Varros	15.5°S, 20.6°E	Sporadic? Faint single-frame event with stellar brightness profile
7 Jan. 2014 18:19:31.0 Sposetti & Iten	19.5°N, 15.5°W	Sporadic. In Mare Imbrium, confirmed in two telescopes, 20 ms duration
6 Mar. 2014 18:56:10.3 Sposetti & Iten	20.0°W 8.4°S	Sporadic, duration 40 ms
26 Feb. 2015 21:35:22, Iten	7.9° W 26.1° S	Sporadic, along terminator, peak mag. +8.0, possible dust plume seen
7 Nov. 2015 3:31:26 Sposetti & Madiedo	50.9° E 24.0° N	Taurid, north edge of Mare Crisium about 104 km west of Eimmart crater
7 Nov. 2015 4:14:07 Sposetti & Madiedo	48.8° E 0.70° S	Taurid, Mare Fecunditatis about 54 km north east of Messier crater
7 Nov. 2015 5:06:45 Sposetti & Madiedo	62.4° E 4.90° S	Mare Fecunditatis about 130 km north of Langrenus crater
8 Nov. 2015 5:14:09 Sposetti & Madiedo	28.4° E 7.3° S	Taurid, about 83 km south of Torricelli crater
15 Nov. 2015 18:13:57 Sposetti & Madiedo		Possible Leonid
12 Mar. 2016 18:33:03 Bruno Cantarella & Luigi Zanetta	39.9°W 8.0°S	This likely sporadic event lasted 0.08 sec, took place in the southern zone of Oceanus Procellarum, to the southwest of the crater Wichmann B

1 Jan. 2017, 17:47:15 Sposetti & Iten		Quadrantid, lasted 40 ms
3 Jan. 2017, 19:18:41 Sposetti & Iten		Quadrantid, lasted 80 ms.

4.5 March 12, 2016

Antonio Mercatali reported that two members of the Luna Unione Astrofili Italiani, Bruno Cantarella and Luigi Zanetta recorded an impact flash at18:33:03 UT. The event lasted 1/12 second and occurred in the southern zone of Oceanus Procellarum, to the southwest of the crater Wichmann B (Mercatali, 2016). The event shows fading over two frames, and the profile of the signal resembles other impacts that have been confirmed. Since this event was observed in only one telescope it remains unconfirmed, but it is considered a likely impact candidate. More information can be found at their website:
http://luna.uai.it/index.php/Lunar_Impacts_Research

5. What's Next

As I considered all that did (and did not) happen over the five years since my first presentation at SAS, I realize that it is time for an upgrade to the systems and procedures of observing lunar meteors. I plan to, over the next several years, with the help of the students listed in the paper, to upgrade our existing system and make provisions for a new system. I will do this at several levels: upgrading my own recording system and observing technique, updating the ALPO-LMIS website to improve communications, involving students at my university in an ongoing program of monitoring the moon (and eventually Jupiter) for meteoritic activity, and more.

5.1 System Upgrade

The old astronomical video system that I have been using consisted of a low-light black-and-white video camera, a KIWI-OSD time inserter with GPS, an 11-inch TV-VCR combo, and VHS cassettes. In order to work with the data, I needed to convert the analog tape to digital. I did a survey of the members of IOTA to find out what they felt was an optimal system to upgrade to. This was possible because of the fact that similar (that is, identical) equipment is used for lunar occultations as well as lunar meteor patrols. I will take the results of their input and determine the system I will purchase for home and university use.

As of this writing I have not yet decided on the final details of the system but it will be all digital with the video stream sent directly to the computer, external hard drive, or a DVD recording device. The purpose is to record the video and have it digitized "on the fly" so as to be ready for analysis without the extra step of analog-to-digital conversion. Once a setup is decided upon I will post the information on the ALPO-LMIS webpage when I update it completely during the second half of 2017.

5.2 Improving Communication

One of the first steps in improved communication is an improved website. I will be exploring ways over the coming year to improve the organization and overall usefulness of the ALPO-LMIS website and the mirror site housed within the PVAMU Physics / "Cosmic Corner" website. This will include an ongoing catalog of reported events which is regularly updated, a more detailed tutorial on getting started with lunar meteor observing and research, an updated list of resources, and a more vibrant discussion venue through yahoo-groups.

In addition I will be contacting other groups that are active around the world and maintain an open line of communication for sharing data, experiences, etc. There are at lease a half-dozen groups (most already introduced) that continue to monitor the moon on a regular basis and are recording some quality observations. As each group shares its experiences in the process this improves the experience for all participating groups. Another benefit is to coordinate among all the groups a global watch of the moon for nearly continuous coverage during annual shower events, special celestial events like a meteor outburst, looking for impacts to correlate with new craters (eventually) to be found by Lunar Reconnaissance Orbiter, and others.

5.3 The Prairie View Observatory

A project that has been in the works now for many years and has had its fits and starts is the Prairie View Observatory. We, the Physics program at PVAMU have re-acquired the Prairie View Solar Observatory (Figure 4) and are starting the process of upgrading and refurbishing the existing structure and equipment. This observatory had been used for most

of the last 19 years of its existence exclusively for solar work and will continue to be dedicated to this purpose once it is back online later this year. But this is phase 1 of the process

Phase 2 is to add two piers and two domes to the existing structure to provide facilities for both daytime and nighttime astronomy. The domes will host a 14-inch Cassegrain and a 16-inch Meade Cassegrain for use in planetary and deep sky imaging. This multipurpose facility will be instrumental in monitoring the moon for meteoroid impacts and eventually for Jupiter patrols to watch for meteors entering its atmosphere as has been observed from Earth on several occasions. The 16-inch telescope will be dedicated to the Jupiter watch while the 14-inch, with the aid of additional free-standing scopes, will be used for lunar meteor and asteroid occultation work. As of this writing, the final details of this program are being worked out but if all goes according to plan, the observatory will see first light as early as the Fall of 2018.

Figure 4: the existing Prairie View Solar Observatory, image credit: Dr. Premkumar Saganti

6. In Conclusion

As has been described already the lunar meteor phenomenon is common and readily observable with well-equipped ground-based telescopes and low-light video cameras. A number of groups and organizations have been working at recording these events since the first video-recorded and independently confirmed meteor point flashes were recorded November 1999. Since then, hundreds of confirmed and unconfirmed (but very likely genuine) lunar impact events have been documented. These meteors come from many sources and offer a glimpse into the luminous manifestation of hypervelocity collisions between a small projectile and a target.

It has been a half-decade of ups and downs since my first SAS meeting, but I am once again hopeful that the dreams and goals that I had for the lunar meteor program and for the astronomical observatory at PVAMU are now about to be realized. It will probably take more time than I am initially planning (large projects usually do) but the end result is a high quality observing facility and program that not only benefits the students and faculty and staff at PVAMU, but also interested participants and collaborators of the program both nationally and internationally.

7. References

Cudnik, B.M. (2012). "Lunar Meteoroid Impact Monitoring and the 2013 LADEE Mission" *SASS* **31**, 29-35.

Casis, N. and Jones, N. N. "NASA's LRO Spacecraft Finds March 17, 2013 Impact Crater and More", (2015). https://www.nasa.gov/content/goddard/nasas-lro-spacecraft-finds-march-17-2013-impact-crater-and-more

Gannon, M., (2014). "Record-Breaking Meteorite Crash on Moon Sparks Brightest Lunar Explosion Ever" http://www.space.com/24789-moon-meteorite-impact-brightest-lunar-explosion.html

Sposetti, S., (2013). Personal communication.

Sposetti, S. and Madiedo, J.M., (2013). Personal communication.

Cudnik, B.M. and Rahman M., (2014). "Ground-based Efforts to Support a Space-Based Experiment: the Latest LADEE Results" " *SASS* **33**, 177-182.

Mercatali, A., (2016). Personal communication

8. Appendix: Resources to Get Started

For the benefit of those who would like to participate in this effort I have listed websites that contain useful information about ongoing campaigns to monitor the moon for meteoroid impacts along with websites that provide results, share guidelines and present checklists to increase the chance of success of interested observers.

In addition, I have made available the web addresses of the various groups mentioned above to enable one to contact representatives from one or more of these groups and find help to get started. As of the writing of this paper in the spring of 2017, all of these websites were current and active.

The interested reader is also encouraged to contact me for assistance via the ALPO Lunar Meteoritic Impact Search Section (or e-mail me at the e-mail address given in this paper). For general questions, contact Robert Suggs at the NASA – MSFC Meteoroid Environment Office at Rob.Suggs@nasa.gov; to report observations to NASA-MSFC, the contact person is Danielle Moser, danielle.e.moser@nasa.gov. We encourage the sharing of observations with NASA as well as the ALPO-LMIS section to enable accurate tabulation of the data.

- ALPO Lunar Meteoritic Impact Search Section homepage: http://www.alpo-astronomy.org/lunarupload/lunimpacts.htm
- George Varros' lunar impacts resources: http://www.lunarimpacts.com/lunarimpacts.htm includes equipment lists, and a link to LunarScan 1.5, the free impact candidate detection program
- How-to "tutorial" (a guide for starting and sustaining observations): http://www.lunarimpacts.com/lunarimpacts_howto.htm
- Equipment Checklist (a.k.a. Minimum System Requirements): http://www.nasa.gov/centers/marshall/pdf/166643main_MinimumSystemRequirements4.pdf
- NASA-Lunar Impact Monitoring News, Frequently Asked Questions: http://www.nasa.gov/centers/marshall/pdf/166651main_FAQ2.pdf
- Book: *Lunar Meteoroid Impacts and How to Observe Them*, by B. M. Cudnik, ISBN 978-1-4419-0324-2, can be obtained through Amazon.com or direct from the publisher http://www.springer.com/us/book/9781441903235
- Lunar Section Research of Unione Astrofili Italiani (UAI) Lunar Impacts Research http://luna.uai.it/index.php/Lunar_Impacts_Research
- British Astronomical Association LTP section (includes lunar impact flash observations) https://www.britastro.org/lunar/tlp.htm
- Geologic Lunar Research Group, Italy http://digilander.libero.it/gibbidomine/
- Videos of lunar meteors, equipment information, and more by the GLR group http://digidownload.libero.it/glrgroup/st22web.htm

Taxonomy discrimination of the Tina asteroid family via photometric color indices

Mattia A. Galiazzo
University of Vienna, Department of Astrophysics
Turkenschanzstraße 17, A-1180 Vienna, Austria
mattia.galiazzo@univie.ac.at - mattia.galiazzo@gmail.com

Werner W. Zeilinger
University of Vienna, Department of Astrophysics
Turkenschanzstraße 17, A-1180 Vienna, Austria
werner.zeilinger@univie.ac.at

Giovanni Carraro
Dipartimento di Fisica e Astronomia, Universitá di Padova
Vicolo Osservatorio 3, I-35122, Padova, Italy
giovanni.carraro@unipd.it

Dagmara Oszkiewicz
Astronomical Observatory Institute, Faculty of Physics, Adam Mickiewicz University
Sloneczna 36, 60-286, Poznan, Poland
dagmara.oszkiewicz@gmail.com

Abstract

This work aims to expand our understanding of the physical characteristics of the Tina asteroid family in the main belt. This small group is unusual, as the only asteroid group currently known to be completely contained in the stable island of one of the principal secular resonances of the main belt, the n6. This family is almost near the center of the main asteroid belt, having its members with a semi-major axis between 2.765 au and 2.807 au. Its largest body is (1222) Tina, 21 km in diameter and an X-type asteroid. We aim to find their taxonomic types by performing correlations with their color indices.

1. Introduction

Asteroid families are groups of bodies identified in the space of proper elements or of frequencies that share a common origin in the collision break-up of their progenitors. Their dynamical evolution is shaped by the interaction with the local web of mean-motion and secular resonances, and by non-gravitational effects, such as the 'Yarkovsky' and 'Yarkovsky–O'Keefe–Radzievskii–Paddack' (YORP) effects (Carruba & Morbidelli, 2011). Usually they share similar taxonomic types, thus similar physical characteristics. Because non-gravitational forces need data like the thermal conductivity, rotational period etc., photometric and spectroscopic data are fundamental for the dynamical studies of these families which aims to find their evolution and their ages. This work is focused on the Tina family. Nowadays, only the major body of the family has its taxonomic type known, that is (1222) Tina, identified as an X-type[1], while it is classified as a metal-rich M-Type by the WISE-survey (Mainzer et al., 2011).

Thus this work aims to expand our understanding of the physical characteristics of the Tina asteroid family in the main belt. This small group is unusual, as the only asteroid group currently known to be completely contained in the stable island of one of the principal secular resonances of the main belt, the n_6. This family is almost near the center of the main asteroid belt, having its members with a semi-major axis between 2.765 au and 2.807 au. In addition it contains very faint objects by the photometric point of view, usually brighter more than

[1] In the Tholen classification the X-group consists of the following types: the E-types: asteroids with high albedo (> 0.30), composed of enstatite, forsterite and feldspar, and, the M-types: asteroids with an intermediate albedo, typical of metals such as iron and nickel, in fact, they are thought to be the progenitors of nickel–iron meteorites.

19 in Vmag, thus large telescopes (at least with a diameter more than 1 m) are needed to observe them.

We present here the first preliminary results of our observing campaign on this family with the FIGL telescope in Austria. In particular results on asteroid (99244) 2001 KV_{54} where we find its taxonomic type by performing correlations with its color indices. We have observed also a second Tina member, asteroid (112983) 2002 RV_{27} in April 17 and 18, 2015, but among the 2 nights, only one was not cloudy and this one was partially photometric and, asteroid 2002 RV_{27} was far beyond the limit in magnitudes to be observed. Asteroid 99244 has these osculating elements. In Figures 1 and 2, you can see its location (in the a-e space and in the a-i space together with asteroid 112983) in the Tina Family. More results will be given in the next future works where we will use data also from observations from via the proposal we won with the 1.3m CTIO telescope, in Chile.

2. Methods

Observations were performed at the LFOA, using the 1.5-m telescope equipped with a SBIG ST-10XME 2184 × 1472 CCD camera. The field of view is about 5.6 × 3.8 arcmin 2 with a scale 0.307 arcsec/pixel (binning 2x2). Processing of the CCD frames is done with standard routines in the IRAF[2] package. Sky flat-field frames are obtained in each filter (Bessel BVR). We collected frames of the asteroids, as described in Table 1. The photometric calibration is performed with Landolt photometric standard stars observed in the same nights as the asteroid targets. The photometric analysis, including corrections for air mass and extinction, is carried out using IRAF and Daophot II software (Stetson 1987). The standard colors and magnitudes are adopted, as derived merging together standard stars from the photometric night, after checking that they are stable. Aperture photometry is applied. We use stable field stars as reference to shift asteroid magnitudes (when there is more than one observation of asteroid per frame). Once we find the color indices we compare them with the typical color indices of the different spectral types and we find the taxonomic type more related to the asteroid. The correlations between colors and taxonomy can be found in Pravec et al. 2012 and Dandy et al. 2003 (from now on, respectively P2012 and D2003). We also estimate the asteroid diameters, which can be obtained via the relationship, $D=D_0\times10^{-0.2H/pV}$, where $D_0=1329$ km, H is the asteroid absolute magnitude and pV is the geometric albedo, assuming for the 2 asteroids, an albedo of 0.3086, the mean value of the geometric albedo for Tina family members (Carruba 2010b).

Asteroid	UT start	Filters	a	R_h [au]	D [au]
99244	22:59:10	BVR	15.2°	2.55	1.71
112983	22:12:30	BVR	10.2°	2.58	1.65

Table 1. The observing circumstances for the asteroids in this work. UT start is the time when the asteroid was started to be observed during the night of April 18, 2015. a,, Rh and D are the average respectively of the phase angle, the heliocentric distance and the geocentric distance during the observations.

3. Results

The air mass of the asteroids during the observations ranged between 1.23 and 1.62, with an average value of 1.65. The average seeing was quite high 3.68", but nevertheless we could have obtained the color indices for at least asteroid 2001 KV_{54}. The final apparent magnitudes in V-filter together with the color indices are reported together with their uncertainties in Table 2. Asteroid 2002 RV_{27} was too faint to be observed and in fact it is much smaller with a diameter D=4.56 km (H=15.4, the absolute magnitude) versus D=1.99 km of asteroid 2001 KV_{54}. Assuming they have similar albedos, because member of the same families, the size has the most important affection to the brightness.

After comparing with Table 1 of P2012 and Table 4 of D2003, we find that the results say that asteroid 2001 KV_{54} is an A-type or a V-type. If we compute the best normalized variance and we make an average of the 2 (V-R) values coming from D2003 and P2012 (because P2012 has only V-R values) we find that most likely this asteroid is an A-type. Considering also that we should consider better the values of P2012, because D2003 consider only Near-Earth Asteroids, NEAs (instead P2012, only main belt asteroids like Tinas and NEAs can have been affected by space-weathering and close encounters which can change the value of the color indices), again A-type has the minimum normalized variance (see Table 3). The equation for the normalized variance is $NV=(x-\langle x\rangle/\langle x\rangle)^2$, where x is the measured color index and $\langle x\rangle$ is the expected value (the color index given by D2003 and/or P2012).

[2] IRAF is distributed by the National Optical Astronomical Observatory, which is operated by the Association of Universities for Research in Astronomy, Inc., under cooperative agreement with the National Science Foundation.

Asteroid	99244	
V	18.2	
V_{exp}	18.24	
V-R	0.618±0.110	
$V-R_{P2012}$	0.567 (A)	0.516 (V)
$V-R_{D2003}$	0.560 (A)	0.413 (V)
B-V	0.884 ±0.147	
$B-V_{D2003}$	1.018 (A)	0.810 (V)
Spectral Type	**A**, V	

Table 2. Photometric results. V and Vexp are respectively the average apparent magnitude in visual found via our observations and the one forecasted by JPL-horizon for the observation night. Then we have the color indices for our observations and the expected one for the relative taxonomical type in parenthesis. Last column show the expected taxonomical type for the asteroid and in bold the most likely correct one.

Type	Reference	NV(B-V)	NV(V-R)
A	D2003	0.02	0.01
	P2012		0.01
	Average	0.02	**0.01**
V	D2003	0.01	0.25
	P2012		0.04
	Average	**0.01**	0.14

Table 3. Normalized variance results. First columns show the spectral type, second column the reference, apart that each third row per spectral type show the average of the values for the normalized variance. Third and fourth column show the normalized variance in respect to each spectral type and reference. In bold the minimum normalized variance.

A-type asteroids are thought to come from the completely differentiated mantle of an asteroid or even from planets, e.g. Mars. A-types are rare in the main belt, but they do not have a preferential region in the main belt (Demeo & Carry, 2013), they can be found in the inner, middle and outer main belt, therefore in the Tina family, too.

V-types are basaltic asteroids and the majority of them are in the Vesta family, however there are some of them which are spread in the other region of the main belt (Demeo & Carry 2013).

Finally the apparent magnitude in V of 2001 KV_{54} is in accordance with the value expected by the JPL-HORIZONS Web-Interface for that night, see https://ssd.jpl.nasa.gov/horizons.cgi and Table 2.

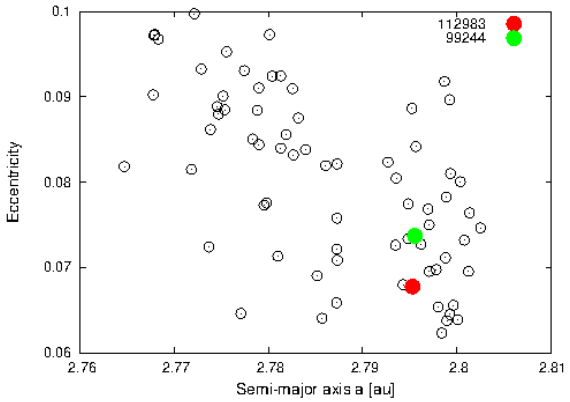

Figure 1: Tina family in the a-e phase space. The observed asteroids enlighted in red and green colors.

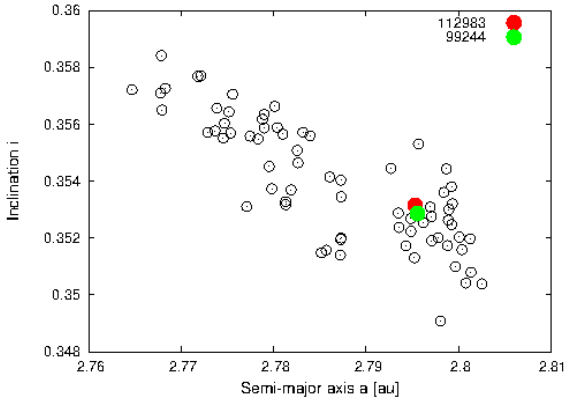

Figure 2: Tina family in the a-i phase space. The observed asteroids enlighted in red and green colors.

4. Conclusion

From our 2 night observations, one was completely cloudy and one was partially cloudy. In this last one we could observe 1 Tina asteroid: (99244) 2001 KV_{54}. We found that this asteroid is an A- or a V-type asteroid, and more likely an A-type. Because we know the parent body is an X-type, this might suggest 3 possibilities: (i) Tina family do not present physically an homogeous population, (ii)2001 KV_{54} is an intruder, or (iii) a sub-family is present in Tina family.

However the statistical sample is low , thus we plan to perform more observations in order to have more accurate and quantitative (more robust statistically) results.

5. Acknowledgements

MAG wants to acknowledge the support by the Austrian FWF project P23810-N16.

6. References

Carruba V., Morbidelli, A., "On the first ν_6 anti-aligned librating asteroid family of Tina", (2011). *Mon. Not. R. Astron. Soc.* **412**, 2040-2051.

Carruba V., "The stable archipelago in the region of the Pallas and Hansa dynamical families", (2010). *Mon. Not. R. Astron. Soc.* **408**, 580-609.

.Dandy, C. L., "Optical colors of 56 near-Earth objects: trends with size and orbit", (2003), *Icarus* **163**, 363–373

DeMeo, F. E. & Carry, B., "The taxonomic distribution of asteroids from multi-filter all-skyphotometric surveys", (2013), *Icarus* **226**, 723-741.

Mainzer, A. et al. "NEOWISE Studies of Spectrophotometrically Classified Asteroids: Preliminary Results", (2011). *The Astrophysical Journal,* **741** (2), 25.

Pravec, P. et al., "Absolute magnitudes of asteroids and arevision of asteroid albedo estimates from WISE thermal observations", (2012), *Icarus,* **221**, 365-387.

Observations of the star Cor Caroli at the Apple Valley Workshop 2016

Reed Estrada
Northrop Grumman
reed.estrada@ngc.com

Sidney Boyd
Victor Valley College
sidneymarieboyd@gmail.com

Chris Estrada
California State University, Los Angeles
pr1est0112@hotmail.com

Cody Evans
Victor Valley College
Cjevens85@gmail.com

Hannah Rhoades
Apple Valley High School
hlr@rhoadesfamily.net

Mark Rhoades
Vanguard Preparatory Parent
rhoadesma@gmail.com

Trevor Rhoades
Vanguard Preparatory School
tar@rhoadesfamily.net

Abstract

Using a 22-inch Newtonian Alt/Az telescope and Celestron Micro Guide eyepiece, students participating in a workshop observed the binary star Cor Caroli (STF 1692) and found a position angle of 231.0 degrees as well as an average separation of 18.7" This observation compared favorably with the 2015 Washington Double Star published position. This project was part of Mark Brewer's Apple Valley Double Star Workshop. The results were analyzed using bias and circle error probability calculations.

1. Introduction

A team of amateur and student observers made observations and took measurements of the double star Cor Caroli at a three-day Apple Valley Double Star workshop that was held by the High Desert Astronomical Society (HiDAS) and the Antelope Valley Astronomy Club at the Lewis Center's Luz Observatory in Apple Valley, California on July 11, 2016. Conditions on the night observations were made consisted of clear skies with some smoke in to the west. In the Washington Double Star Catalog (WDS, 2015), Cor Caroli is identified as 12560+3819STF1692AB. The right ascension and declination are listed as 125601.67+381906.2. The magnitudes of the primary and secondary stars are 2.85 and 5.52 respectively.

Typically these kind of workshop events provide excellent opportunities for first time observers to get an introduction into astronomy and the principals of scientific observations and measurement. They also provide challenges for the astronomer helping the new observers to make meaningful accurate observations.

Included in this paper is a discussion on the challenges inherent with introductory workshops, classroom exercises and group observations involving first time observers taking measurements during the short period of time afforded by the event.

With all scientific measurements the goal is to achieve both accuracy and precision. The procedures used were borrowed from Robert Argyle's book on *Observing and Measuring Visual Double Stars* and Tom Frye's published work on *Visual Double Star Measurements with an Alt-Azimuth Telescope*.

2. Equipment and Procedures

The telescope used was a 22 inch Newtonian alt/az equipped with a 12.5mm Celestron Micro Guide astrometric eyepiece. Mounted to the eyepiece was a Bell & Howell CCD video with night vision capability. This telescope was used because of its large light gathering capability that allowed the use of the Bell and Howell video camera. This set up solved several problems associated with the workshop. First the video-astro guide combination eyepiece allowed video capture of the target stars against the eyepiece scale for replay on a computer and television screen display. This allowed the team to modify the observation techniques outlined in Argyle's *Observing and Measuring Visual Double Stars*. Specifically this allowed the team to use a video playback program on a laptop computer to stop the motion of the star field and also to enhance the viewing field for a more accurate measurement.

To determine scale constant the telescope was pointed at the star Bellatrix in the constellation Orion. The telescope operator aligned the star on the linear scale of the Micro Guide Eyepiece. Once it was assured the star would drift down the middle of the linear scale a video was recorded of the drift. This procedure was repeated ten times, producing ten individual videos.

The average drift time is used in the following equation, Argyle (p 152):

$$Z = \frac{15.0411 Tavg \cos(\delta RS)}{D}$$

where Z is the scale constant in arc seconds per division, $Tavg$ is the average drift time of the reference star across the scale in seconds, 15.0411 is the sidereal motion in arc seconds per second of Earth's rotation, $\cos(\delta RS)$ is the cosine of the declination of the reference star, and D is 50, the number of divisions for the Celestron eyepiece.

The telescope was then pointed at Cor Caroli. This star was selected for measurements for several reasons. First it is easily identified visually and located with the spotting eyepiece provided on the telescope. Secondly, it is a bright pair with wide separation in the 12mm eyepiece on the 22 inch telescope. The 2.85 magnitude bright primary and its 5.52 companion showed nicely on the captured video against the lighted reticle eyepiece. There is a tradeoff between the brightness of the stars versus the lighted reticle of the eyepiece for the video camera focus and light gathering capability.

The wide separation along the scale in the eyepiece was easily measured. This is a requirement when introducing new observers to the Celestron micro guide eyepiece. Finally Cor Caroli has many past observations with relatively little change is position angle and separation over the years. This provided a good target to statistically evaluate both the precision of the team's observations and their accuracy; a measure of how well they followed procedure and protocol and how well the equipment and seeing cooperated with the nights observations.

The stars were both aligned to the linear scale (See Figure 1) where upon a series of videos was captured as they drifted across the scale. Between each video a slight adjustment was made to the telescope so that the stars drifted across a different part of the scale for each video captured.

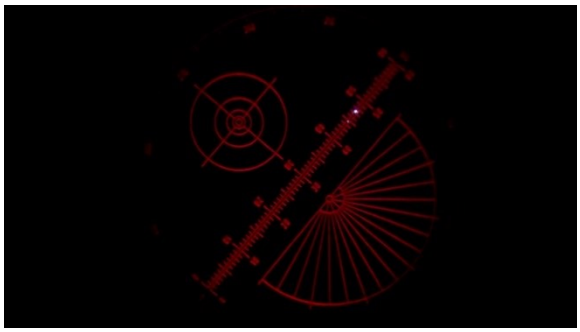

Figure 1. The stars were aligned on the linear scale where upon a video was recorded using the camera and eyepiece combination.

Finally the primary star was positioned to drift across the center of the linear scale. Once it was assured that the primary star had passed through the center a video was recorded of the star system as it drifted through the protractor rings. This process was repeated ten times creating ten individual videos.

Each video was processed using Adobe Premiere. Section of the video were evaluated and fourteen still photographs of various depictions of the position angle and the separation were saved as .jpg files

The following night the students were provided with a large television (The technique is demonstrated in Figure 2) which was connected to a computer containing the .jpg files made the previous night. Each student was tasked with making and recording observations using the picture files. The results of each individual assessment were captured in a spread sheet using algorithms from Tom Frey's

published work on *Conversion Formulas for Celestron Micro Guide Eyepiece* for analysis.

Figure 2. Students making observations on the television from data collected the previous night.

Video observations were completed the night of July 11, 2016, while observations and data analysis occurred the following morning at the Lewis Center for Educational Research in Apple Valley, California.

3. Observations and Analysis

To evaluate the observations and provide statistical data on the accuracy and precision of the data, the individual position angles and separations were loaded into an excel spread sheet for a delta bias analysis as outlined in the *Navy Test Pilot School Systems course book (p. 397)*. The WDS 2105 reported position angle and separation was assumed and plotted at the origin of a scatter chart as the X and Y*truth*. Each individual observation was then evaluated as bias from this origin point using X*bias* = X-X*truth and* Y*bias*=Y-Y*truth*. The results were plotted below. This allowed statistical analysis of each point from the last known observation as well as the average of the whole data set that will be reported as the group observation.

It was noted that the mean of the bias was X*bias* = +4, Y*bias* = -1 with an $\bar{r}$ *bias* (radial bias) of 0.24 arc seconds off the WDS 2015 observation.

The Circular Error of Probability (CEP), (Table 1) defined as the median of the radial data points plotted around the average bias, was calculated and depicted on the chart below using

CEP=*Median*(σer).

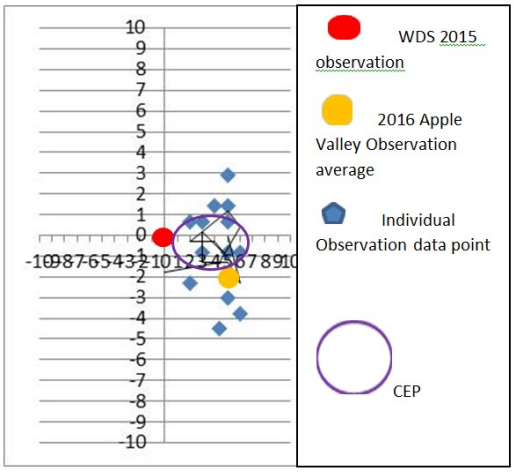

Table 1. The Circular Error of Probability

4. Conclusions

The team found by using a scale constant 7.40 arc seconds per division mark the observers average separation was 18.7 arc seconds a derived position angle of 231.0 degrees which was within 1.7% from WDS observations.

This was a bias of +4 and -1 with a radial error of 0.24 arc seconds delta from the WDS 2015 observation. This bias is the measure of the accuracy of the observations. This represents potential calibration problems with the equipment. Within this subset are errors induced by incorrect procedures as well as the quality of the seeing on the night of the observations.

The CEP is a measure of the precision of the observations and showed a shift in plotted radial error to the east and slightly north of the WDS 2015 position.

CEP errors are normally equipment problems and was also a measure of the individual team members application of the procedures taught during the workshop. (hardware and/or software).

Both accuracy and precision were both qualitatively acceptable (within 1.7% of the WDS 2015 observation) for this group of first time observers. It is a good measuring point for the appropriateness of the equipment and procedures used to overcome some of the challenges faced by first time observers measuring double stars. Continued work needs to be done to refine the equipment and the procedures to increase both accuracy and precision of these observations.

5. Acknowledgements

The observers would like to thank Mark Brewer, the High Desert Astronomical Society, and the Ante-

lope Valley Astronomy Club. The observers would also like to thank the Lewis Center for Educational Research for letting us use their facility, Walmart for their gracious donations, and Starbucks for their food donations. We also thank Russell Genet, Sean Gillette and Mark Brewer for their peer review.

6. References

Washington Double Star Catalog, 2015, Retrieved from http://www.usno.navy.mil/USNO/astrometry/optical-IR-prod/wds/WDS

Argyle, Robert. 2004. "Observing and Measuring Visual Double Stars". Springer, London.

Frey, Thomas G., and Angie M. Frey. 2010. "Conversion Formula for the Celestron Micro Guide Eyepiece Used to Determine Position Angles." Journal of Double Star Observations, Volume 6, p. 1.

Frey, Thomas G., and Angie M. Frey. "Visual Double Star Measurements with an Alt-Azimuth Telescope", Journal of Double Star Observations, Vol. 4 No. 2 Spring 2008

NTPS Navy Test Pilot School, SYS Course August 2014, Systems Course Book "Introduction to Aircraft and Systems Test and Evaluation" United States Naval Test Pilot School SYS Short Course August 2014, p 392-399.

Exoplanet Observing: From Art to Science

Dennis M. Conti, PhD
Chair, AAVSO Exoplanet Section
Annapolis, MD 21403
dennis@astrodennis.com

Jack Gleeson
AAVSO Exoplanet Database Lead
Liverpool, England
me@jackgleeson.co.uk

Abstract

This paper will review the now well-established best practices for conducting high precision exoplanet observing with small telescopes. The paper will also review the AAVSO's activities in promoting these best practices among the amateur astronomer community through training material and online courses, as well as through the establishment of an AAVSO Exoplanet Database. This latter development will be an essential element in supporting followup exoplanet observations for upcoming space telescope missions such as TESS and JWST.

1. Introduction

Exoplanet observations by amateur astronomers are now well recognized by the professional community as an important contribution to exoplanet research. For example, amateur astronomer participation in such programs as KELT (Kilodegree Extremely Little Telescope) (Pepper *et al.*, 2007) and recent Hubble pro/am collaborations (Conti, 2015 and Motta, 2017) have included:

1. followup observations of suspected exoplanets and confirmation of exoplanet candidates,
2. refinement of the ephemeris of known exoplanets,
3. participation in microlensing events, and
4. characterization of disintegrating planetesimals.

However, as active as it has been, exoplanet observing by amateurs has only recently evolved from an art to a well-established scientific process.

As new space telescopes such as TESS (Transiting Exoplanet Survey Satellite) (Ricker *et al.*, 2015) and JWST (James Webb Space Telescope) (NASA, 2017) come online in the next 2-3 years, the need for amateur astronomer participation in exoplanet research is only going to increase. In particular, followup observations of candidate exoplanets will be needed to help determine whether an observed transit is a false positive - for example, whether it is actually due to an exoplanet or to an eclipsing binary.

In order to contribute to exoplanet science, observations by amateur astronomers demand a much more rigorous approach than that required for more typical amateur astronomer endeavors, such as deep sky or planetary imaging. This paper describes the best practices that have evolved to date for conducting such research-grade exoplanet observing.

Section 2 will discuss what is meant by and the importance of high precision photometry in conducting exoplanet observations. Section 3 will discuss the best practices that have evolved for conducting research-grade exoplanet observing by amateur astronomers. Section 4 will review the training tools and aids that are available through the AAVSO to assist amateur astronomers in conducting high quality exoplanet observations, as well as how amateur astronomers can participate in the upcoming TESS program.

2. Background

Because the transit method is the dominant technique used by amateur astronomers to conduct exoplanet observations, this paper will focus on observing and modeling techniques related to this method. The transit method is useful for detecting a "hot Jupiter," namely a large planet whose orbit is close to its host star and where the planet passes directly in front of the star from the perspective of an observer on Earth. The transit method relies on measuring the flux of the suspected host star (herein also referred to as "the target star"), as well as the flux of multiple "comparison stars" that are all in the

same field-of-view. Furthermore, conducting a full transit generally involves at least 30 minutes of imaging on either side of what is typically a 4-5 hour transit. Thus, it is not unusual for a transit observing session to be 6 hours in length. It should be noted that there have been some successful attempts by amateur astronomers to utilize two other methods for performing exoplanet observations, namely Doppler spectroscopy to conduct radial velocity studies and the detection of exoplanet transits using microlensing.

Unlike deep sky imaging where the amateur astronomer is more interested in obtaining an aesthetically pleasing outcome across an entire field-of-view, the exoplanet observer employing the transit method is interested in the change in brightness (i.e., flux) of the target star and the comparison stars over several hours of time. Specifically, the exoplanet observer is interested in accurately and precisely counting photons for a given set of stars in the field-of-view. In order to understand what factors are under control of the exoplanet observer and which aren't, it is important to understand this distinction between accuracy and precision.

Accuracy is defined here as the extent to which the number of photons measured by the observer matches the number of photons emanating from the star in question. Precision, on the other hand, is used here to mean the extent to which the observer's instrumentation measures (and ultimately translates into a workable proxy) the photons arriving at the observer's site. Precision, unlike accuracy, is more a function of the type of instrumentation used by the observer, as well as the process that the observer undertakes during the measurement process.

When counting photons, another related concept is SNR – the ratio of signal to noise. "Signal" here refers to both wanted and unwanted signals. The wanted signal, of course, includes the measure of observed photons. Examples of unwanted signals include dark current, added bias, and the effects of dust donuts and vignetting on the measured photon counts. "Noise" here refers to the uncertainty in the signal. Examples of noise include shot noise (the uncertainty in the number of received photons), uncertainty in the dark current, and uncertainty due to read noise.

The following discussion relates the concepts of accuracy and precision to exoplanet observing.

2.1 Accuracy

If one were able to count the number of photons emanating from a star and then count the number of photons arriving at an observer's location, there are several factors that would affect the difference in these counts, namely the accuracy of the measurement. These factors include the following (see Figure 1):

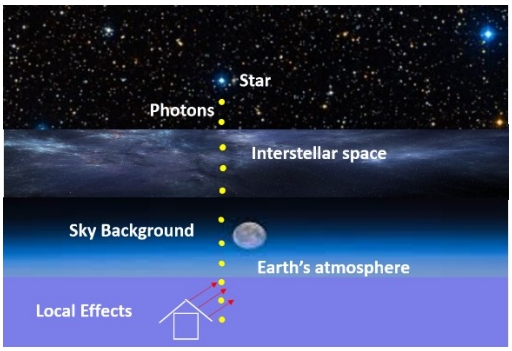

Figure 1. Factors Affecting Accuracy

1. Some photons are scattered due to the dust in the interstellar space through which the photons pass.
2. Background sky glow resulting from light pollution or moon glow may actually add to the photons arriving at a given site.
3. Some photons are scattered due to turbulence in the atmosphere, which causes rapid changes in the distribution of water vapor, smoke particles, etc.
4. Local, near-ground effects, such as heat radiating from local structures, may affect the final photon count reaching the observer's instrumentation.

Some of these factors affecting accuracy will change over the very short term (e.g., atmospheric turbulence) and some over a longer term (e.g., sky glow). Although most of these factors affecting accuracy are not under the observer's control, being aware of them will help the observer better understand variations from observation to observation, as well as the fixed limitations of the observer's site itself.

As was indicated earlier, exoplanet observing using the transit method is concerned with measuring the change in flux of the target star. The aforementioned factors that affect the accuracy of the photon counts of the target star should equally affect the accuracy of the photon counts of suitable comparison stars. "Suitable comparison stars" are meant stars that are inherently non-variable, are of similar stellar type and magnitude as the target star, and are close to the target star in the same field-of-view. Therefore, one can determine the relative change in flux of the target star by comparing its flux to that of the comparison stars.

2.2 Precision

One way to look at factors affecting precision is to ask: what are the characteristics of two different sets of instrumentation that could cause them from obtaining the same photon measurements at the same site (see Figure 2).

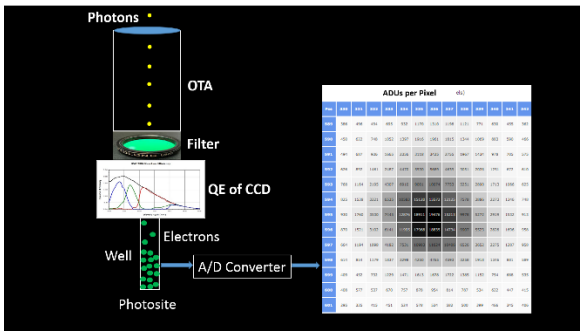

Figure 2. Factors Affecting Precision

Such factors would include:

1. Aperture size and focal length of the observer's optical tube assembly (OTA).
2. Filter used.
3. The quantum efficiency (QE), size of well, and gain of the imaging detector.
4. The size of the imaging detector's photosite. Photosite here refers to the size of the physical element on the detector that converts photons to electrons. Although often called a pixel, the term "pixel" in this paper will refer to the resulting combination of one or more (possibly binned) photosites for a given observation.
5. The extent to which inherent variations in background brightness due to dust donuts, vignetting, etc. are able to be removed through flat fielding.
6. Field rotation (i.e., star movement across the field-of-view during the entire observation session). The resulting effects of field rotation are related to the ability of flat fielding to remove inherent pixel-to-pixel variations (see Section 3.1.4).

Having addressed in Section 2.1 how the factors that affect accuracy can be compensated for through the use of comparison stars, the next section addresses the established best practices that result in the highest precision possible for a given set of instrumentation.

3. Best Practices for Achieving High Precision Exoplanet Observing

The establishment of best practices for exoplanet observing by amateur astronomers began with the publication of "Exoplanet Observing for Amateurs" by Bruce Gary (Gary, 2014). More recently, a number of pro/am collaborations have helped "refine" the set of practices that have been found to be useful for amateur astronomers, especially those wishing to conduct research-grade exoplanet observing. In addition, a freeware software package - AstroImageJ (AIJ) (Collins *et al.*, 2016) – is quickly becoming the *de facto* standard for exoplanet transit analysis and modeling by both professional and amateur astronomers. The refined best practices, as well as a step-by-step guide to AIJ, are included in "A Practical Guide to Exoplanet Observing" (Conti, 2017). The guide is also now being used as the source material for exoplanet training by the AAVSO, as well as by astronomy instructors at various educational institutions.

As will be seen, a common theme throughout this paper is "minimizing the movement of stars during the entire multi-hour observing session." This is because flat fielding can never perfectly mitigate artificial changes in flux due to a star landing on a not-fully corrected dust donut, and this artificial change in flux may then affect the precision with which we are comparing the flux of the target star relative to the comparison stars.

Prior to the observing session, it is suggested that the observer collect appropriate information about the exoplanet's host star, and if known, predictions regarding the transit itself. A spreadsheet that can be used as a guide for collecting and recording such information can be downloaded from the principal author's website (Conti, 2017).

The following sections describe the best practices that have evolved to help the exoplanet observer obtain the highest level of precision for a given instrumentation package. These best practices are organized by the respective phase of the exoplanet observing process to which they apply. The term "science image" as used herein refers to the image containing the host star of the candidate exoplanet. This is sometimes also called a "light frame" by those familiar with deep sky imaging.

3.1 Instrumentation

Certainly cost is a factor when selecting the complement of equipment to be used in exoplanet observing. And as expected, higher precision demands higher cost equipment. Thus, the choice of

equipment (and therefore precision associated with that equipment) is determined mostly by economics.

The following describes those equipment characteristics that most affect exoplanet observing precision.

3.1.1. Mount

The three most popular mount types are German equatorial mounts (GEMs), fork mounts, and alt-az (altitude-azimuth) mounts. Of the three, the alt-az mounts is the least desirable for exoplanet observing due to the continuous corrections that need to be made in three (3) axes to keep a star in relatively the same position throughout the observing session. These corrections need to be made in elevation, azimuth, and position angle. Obviously, this means that the precision associated with any of these three axis corrections will affect the observer's overall ability to minimize star movement. Position angle corrections, for example, are normally made by a rotator, and the incremental step size of the rotator, as well as the cadence of such corrections, will affect the precision with which the image chain can rotate to relatively the same pixel position throughout the observing session.

GEMs, which are popular cost-effective mounts for deep-sky imaging, have successfully been used by amateur astronomers in conducting exoplanet observations. However, GEMs will typically require a meridian flip when the target star passes across the meridian. Although some GEMs can continue tracking for some amount of time after the meridian, observations that require longer tracking will ultimately require a meridian flip. A meridian flip results in two factors affecting precision: (1) valuable data points are lost during the time it takes for the meridian flip, and (2) with no rotation of the imaging chain, the target and comparison stars will fall on the part of the imaging camera's detector that is diagonally opposite to where they were pre-flip. The implication of the latter is that the flux of stars would artificially increase or decrease due to them landing on part of a dust donut that was not fully corrected by flat fielding. Even if the image chain was rotated, getting the target and comparison stars on nearly the same pixel locations as pre-flip would be practically impossible. It should be noted that software such as AIJ can help compensate for the effects of a meridian flip, especially if it occurs near mid-transit.

Fork mounts thus are the most suitable mount for exoplanet observing because of their ability to continuously track a target star for a long duration without having to be interrupted to perform a meridian flip.

Regardless of the type of mount used, tracking precision is also a function of any periodic error in the mount's gears. Periodic Error Correction (PEC) and autoguiding will help mitigate such periodic errors. It should be noted that some of today's mounts can operate for minutes with minimal errors; this of course comes at greater expense.

Thus, as far as the mount is concerned, best practices would include:

1. polar align the mount as accurately as possible (e.g., within a few arcseconds of the pole);
2. balance the mount to help reduce RA errors;
3. in the case of a GEM mount, reduce RA backlash by always keeping the mount "East heavy" – this will help with any plate solving that might be needed after a meridian flip in order to get back on target;
4. minimize DEC backlash, which would allow for better DEC corrections during autoguiding;
5. minimize periodic error by checking for any worm or ring gear grit, as well as by using PEC to help correct any remaining errors.

3.1.2. Optical Tube Assembly (OTA)

Best practices associated with choosing and maintaining the telescope's optical tube assembly (OTA) include the following:

1. Aperture matters, so the larger the aperture, the greater ability to collect photons in a given unit of time. This is especially important for fainter target stars.
2. The OTA should be *in situ* for enough time for it to get acclimated to the temperature of its operating environment. This would help reduce any internal air turbulence due to changing temperature within the OTA.
3. In order to produce a well-formed point spread function (PSF) for the target and each comparison star, the OTA should be well-collimated.

3.1.3. Imaging Camera

A variety of cameras have been used for exoplanet transit observing. These include stand-alone CCD and CMOS cameras similar to those used for deep sky imaging, as well as DSLR's. However, for conducting research-grade exoplanet observing, the camera should be monochrome. This is so that it would be possible to use different standard photometric filters, such as the Johnson-Cousins U,V,

B, Rc, and Ic filters, or the SDSS (Sloan Digital Sky Survey) u', g', r', and i' filters. Because DSLR cameras are inherently color and therefore don't lend themselves to the use of filters, they are the least desirable imaging camera choice. It should be noted, however, that Panoptics, a citizen-science project (Edberg, 2016), is planning to use DSLR cameras for detecting exoplanet false positives.

Best practices for choosing an imaging camera to use in exoplanet observing is dependent upon factors such as:

1. The expected seeing conditions at the observer's location. This is defined as the typical FWHM of stars measured at the observer's location and expressed as arcseconds. The image scale (sometimes referred to as "pixel scale" or "plate scale"), which is expressed as arcseconds per pixel, should be matched to the location's general seeing conditions.
2. The size (i.e., format) of the camera's detector. Although a larger format allows for a greater variety of comparison stars to choose from, small format detectors have successfully been used in research-grade exoplanet observing.
3. The bias, dark current and readout noise of the camera. These factors, however, are much reduced in today's newer cameras.

In general, most modern monochrome imaging cameras that the observer has or will be acquiring for other applications such as deep sky imaging, should be satisfactory for exoplanet observing.

3.1.4. Autoguiding

Autoguiding is essential for research-grade exoplanet observing in order to minimize the drift of the target and comparison stars. The most common approaches to autoguiding and their pros and cons are:

1. Use of a separate guide scope – this is the least desirable method due to issues with flexure that may occur during the observing session.

2. Off-axis guiding – although frequently used by deep sky imagers to get pinpoint stars, this technique will still result in some amount of field rotation of the target and comparison stars in the presence of even a small amount of polar misalignment. This is true even with sub-arcsecond movement of the guide star itself. The amount of field rotation (i.e., the drift in RA and DEC) will be a function of:
    a. the distance of the guide star from the particular star in question;
    b. the amount of polar misalignment;
    c. the amount of delta movement of the guide star itself;
    d. the declination angle when the image is taken (polar misalignment will have a greater affect, especially in RA, when imaging at higher declinations).

3. On-axis guiding – this technique employs a dichroic beam splitter to separate the light path of the main image into a near infrared (NIR) path and a visible light path (di Cicco, 2012) . Here, the guide camera sees, via the infrared path, part of the same image as the imaging camera (depending on the size of the guide camera's detector). With this technique, the guide star is closer to the target and comparison stars, and therefore the effects of any polar misalignment are reduced as compared to the off-axis guiding approach. Furthermore, in the case of meridian flips with GEMs, the same guide star can be used post-flip as was being used pre-flip, thereby eliminating the need for a rotator or for a search for another guide star, if no imaging chain rotation takes place.

4. Image guiding – a relatively new autoguiding technique is to make mount corrections between exposures based on the amount of total shift of the science image itself. A variant of this is being developed (Baudot, 2017), whereby mount corrections will be made during exposures of the science images.

In addition to the above autoguiding techniques, active optics (AO) devices are also available to the amateur astronomer so that a variety of rapid gear errors can be corrected without making physical "bumps" to the mount. This technique uses a "tip-tilt" mirror or a straight-through optical window that is in the optical path to keep a guide star centered without making physical "bumps" to the mount.

Autoguiding software is optionally available for most of the popular imaging software packages. A popular freeware guiding software package is PHD2 (see http://openphdguiding.org).

3.1.5. Filters

As mentioned earlier, it is desirable that a standard photometric filter be used for exoplanet work. This is true for at least three reasons:

1. limb-darkening coefficients used during the transit modeling process are a function of the (standard) filter type, as well as stellar parameters of the target star;
2. distinguishing transits due to eclipsing binaries vs. exoplanets employs using alternating standard filters across the observing session - the transit depth of eclipsing binary will generally be different for two different filters;
3. results from two different observers can be better compared.

3.2 Flat Fielding Techniques

Because star movement over a few pixels is inevitable even with autoguiding and fairly accurate polar alignment, flat field correction is relied upon to mitigate the effects of dust donuts and vignetting. For example, Figure 3 depicts a flat field and the potential movement of a star onto a nearby dust donut. Figure 4 depicts what would happen in the case of a meridian flip, namely the star would flip across the diagonal of the detector and possible land on another dust donut. If flat field correction is not performed for either of these two cases, the flux of the star in question would artificially change.

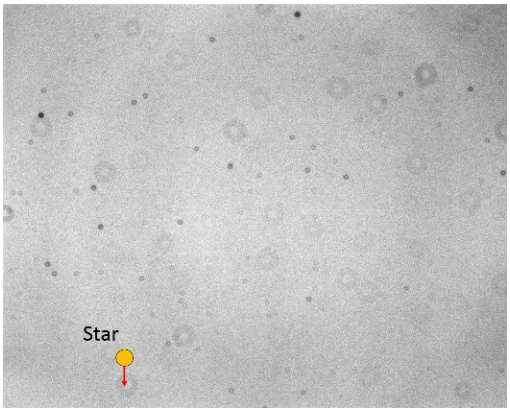

Figure 3. Star Movement in an Uncorrected Flat Field

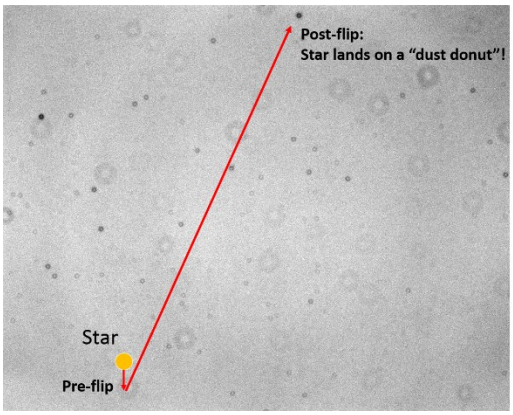

Figure 4. Star Movement after a Meridian Flip

Flat fields should ideally be created before or after each observing session, and certainly when there is any change in the imaging chain.

The following are common techniques for generating flat fields from which a master flat can then be created:

1. Twilight flats – flats are taken at dawn and dusk. Because of the speed that sky lighting conditions change, it is often cumbersome to take a good set of flats, especially if this has to be done for multiple filters. In some cases the flats may show stars if the exposure time is too long. Homemade diffusers using a white T-shirt have been a popular way to mitigate this problem.
2. Light boxes – homemade light boxes have been used by some amateur astronomers to create flats. However, using this technique to produce a uniform light field is sometimes challenging.
3. Electroluminescence panels - although at some cost, the technique has several advantages: it can create a relatively good uniform light field, its brightness can be changed to accommodate different filters, and flats may be taken at the observer's convenience.
4. Observatory flats – this technique used in permanent observatories consists of the telescope being pointed to a lit white panel on the wall of the observatory. The efficacy of this technique varies widely with the nature of the white panel, ambient lighting, etc.

It is recommended that at least 17 flats be taken for each filter type used during a given observing session. Typically flats are taken for a relatively short period of time (e.g., 3 seconds) with the center of the

resulting histogram approximately at the mid-point of the detector's ADU range. For example, for a detector with a typical maximum ADU count of 65,000, the brightness of the light source would be set such that the center of the resulting histogram is at 32,000 ADUs.

3.3 Image Capture

The full-width-at-half maximum (FWHM) of stars in the target field should be spread out over 3-5 pixels. If the imaging camera is normally setup to bin more than 1x1, accomplishing this may then mean that binning may have to be reduced.

Stars should be brought into precise focus if for no other reason than to get an accurate measure of FWHM. However, if the target star is too bright and could saturate the imaging camera, it may be necessary to defocus the OTA. If the sky background is not too high, defocusing that results in a PSF of 10-20 pixels is acceptable, as long as this defocusing doesn't result in the flux of a nearby star blending with the target star's flux.

The optimal exposure time is one that maximizes the target star's SNR, while not saturating the imaging camera's detector. For a given target star, factors that affect the optimal exposure time include:

1. the telescope's aperture size,
2. the filter used,
3. the QE of the imaging camera,
4. whether the star is rising to the local meridian, or has passed the meridian and is falling, and
5. seeing conditions.

The following best practice procedure conducted immediately prior to the actual observing session is recommended to determine the optimal exposure time:

1. At the target star's current sky position, take test images at various exposure times. First, select the exposure time with the greatest SNR for the target star where the peak ADU count is less than 75% of the saturation point of the imaging camera's detector.
2. If the star will be rising toward the local meridian, reduce the exposure time such that the detector will not reach saturation.
3. If the star will be falling from the local meridian, increase the exposure time such that the peak ADU count of the target star is equal to 75% of the saturation point of the detector.

There are some situations where the professional science team might require a certain cadence of images to be taken, which might be at the expense of the (longer) optimal exposure time. This may be the case where finer details of the pattern of the light curve are more important than the accuracy of the light curve depth itself.

Because of the natural drift in the image capture computer's clock, it should be frequently synchronized with the U.S. Naval Observatory's Internet time server. This can be done using (freeware) software such as Dimension 4 (see Dimension 4, 2017). The update period for such clock synchronizations should be set to at least every 2 hours.

Finally, the imaging system should be put in its operating environment with enough time for it to reach its desired temperature set-point, which might also require enabling of its cooling system.

3.4 Image Calibration

Image calibration eliminates the effects of the following underlying factors that affect the precision of the measurements: bias, dark current, and dust donuts and vignetting. The following are best practices for dealing with each of these factors:

1. At least seventeen (17) zero exposure, dark images (i.e., bias files) should be taken at some time before or after the observing session. These are then used to create a master bias file, ideally using median combine.
2. At least seventeen (17) dark images at the same exposure time as the science images should be taken at the end of the observing session. The reason for taking them at the end of the observing session is to make sure that they are taken at the same temperature as the science images. A master dark file is then created from them, again using median combine.
3. Since the flat files themselves have dark current and are at a different exposure time than the science images, they need to have dark current removed. Rather than creating a master dark specifically to make dark correction for the flats, another approach is to use the same master dark file created for the science images, but scale it to the exposure time of the flat files. Software such as AIJ, has such a scaling feature. Section 3.2 above describes the best practices for creating master flats.

During the image calibration phase, some software packages such as AIJ allow the user to

update the FITS headers in the science images with information such as the equivalent BJD_{TDB} (Barycentric Julian Date, Barycentric Dynamical Time) of the observation. BJD_{TDB} is the preferred timebase for reporting exoplanet transit times to the professional community. If not included in the FITS header by the image capture software, other important information such as AIRMASS can be included as well. As will be seen later, AIRMASS is one of the more commonly used detrend parameters during the transit modeling process.

3.5 Aperture and Differential Photometry

As was mentioned in Section 2, the exoplanet transit method is all about comparing the relative change in brightness between the target star and a set of suitable comparison stars. Before this comparison can be done, however, the brightness of each star needs to be adjusted for any photon counts due to the background sky that might be affecting each particular star. This is done using aperture photometry. Once this is done, the relative change in (adjusted) flux between the host star and the comparison stars can then be obtained. This process is called differential photometry. The best practices associated with aperture and differential photometry are described below.

3.5.1. Aperture Photometry

Aperture photometry involves defining both the "aperture" of a certain radius around a star, as well as an outer "annulus." The idea of the annulus is to measure the sky background around the star. Figure 5 depicts an aperture of radius 9 and an annulus starting at 16 pixels from the centroid of the star and ending at pixel location 24.

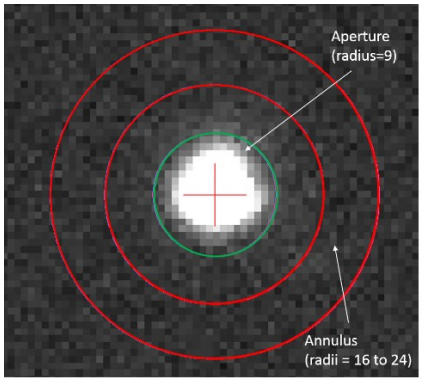

Figure 5. Aperture and Annulus

In order to compensate for background sky contribution, the ADU counts per pixel in the annulus are used to adjust the ADUs in the aperture. Some software such as AIJ also has the ability to detect and adjust for any faint stars that might happen to be in the annulus and therefore bias the background sky counts. As will be described later, the radii settings initially set for the aperture and annulus may be changed after an exoplanet model fit is done to further optimize the fit.

The following methods are recommended to select the initial size of the aperture and annulus:

Method 1: As depicted in Figure 6, some software such as AIJ can provide recommended settings for the initial radii settings.

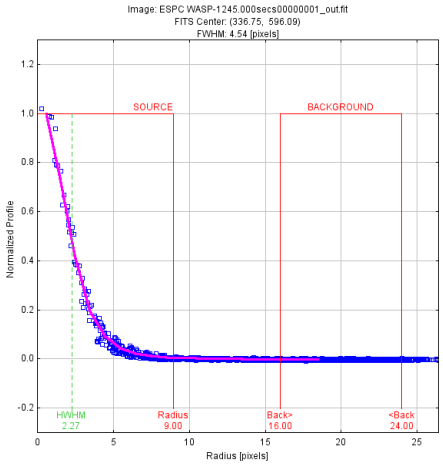

Figure 6. AIJ's Seeing Profile Screen

Here, with a FWHM of 4.54 pixels, the aperture is recommended to have a radius of 9 pixels and the annulus is recommended to start at pixel 16 and extend to pixel 24.

Method 2. The initial radii can also be determined according to the following guidelines (note that the AIJ example above is consistent with these guidelines):

1. The initial radius of the aperture (r_1) should be at least 2 times the number of FWHM pixels.
2. The initial radius of the inner annulus (r_2) should be chosen such that it and the radius of the outer annulus create an annulus region that excludes any other stars that happen to be close to the target star.
3. The initial value of the outer annulus radius should equal the SQRT($4*r_1^2+r_2^2$). This formula should produce an annulus that contains 4 times the number of pixels as are

in the aperture.

Method 3. The initial aperture/annulus settings can also be determined by using ones that maximize the SNR of the target star.

3.5.2. Differential Photometry

Differential photometry involves applying aperture photometry on the target star and multiple comparison stars and then comparing the relative differences in (adjusted) flux. The following are the best practices for selecting suitable comparison stars:

1. Ideally, at least 8 comparison stars should be chosen whose magnitudes are as close as possible to that of the target star – i.e., no greater than 0.75 in magnitude (i.e., fainter) and no less than 0.44 in magnitude (i.e., brighter) than the target star. If this is not possible, then an ensemble of comparison stars should be selected such that the average of their aperture counts are close to that of the target star.
2. The comparison stars should ideally be of similar stellar type to the target star in order to minimize the differences in atmospheric extinction. However, if the transit modeling software is able to "detrend" the effects of AIRMASS, such as is possible with AIJ, then choosing comparison stars of similar brightness to the target star is more important than choosing stars of similar stellar type.
3. The comparison stars should not be inherently variable. This can later be determined by viewing the light curve of each comparison star as described in the next section, or by using information from the AAVSO's Variable Star Plotter utility (AAVSO, 2017).

The results of the differential photometry phase will be a table of measurements that have, as a minimum, for each image: the timestamp of the image, the change in flux or magnitude of the target star (relative to the comparison stars), and its associated errors. Depending upon the differential photometry software, other valuable data could include the relative change in flux or magnitude of each comparison star (relative to all the other comparison stars), their associated errors, and changes in the X,Y pixel coordinates of the target and comparison stars.

3.6 Exoplanet Transit Modeling

Because of the growing use of AIJ by both professional and amateur astronomers, its capabilities for conducting exoplanet transit modeling will be used as the basis for discussion in this section on best practices for use during the transit modeling phase.

In addition to the measurement table resulting from the differential photometry phase, a user of AIJ would also input:

1. the timebase being used for the light curve's X-axis (e.g., BJD_{TDB}),
2. the predicted ingress and egress times,
3. the region in the time domain to be used for normalizing the model's light curve,
4. the minimum and maximum values for the X and Y axes,
5. any text legends on the light curve,
6. the predicted period of the exoplanet's orbit,
7. the host star's radius R_* (note: this value is strictly used to compute the planet's radius as discussed below),
8. appropriate limb darkening coefficients,
9. designations of what measurement values should be modeled and plotted.

AIJ also offers options for scaling, binning, and shifting resulting light curves.

Figure 7 is a sample light curve showing results from an AIJ model fit. Shown here is the relative flux changes of the target star (blue curve), the model's detrended fit through the observed data points and the RMS (root mean square) errors resulting from this fit (red curves), and the relative fluxes of three comparison stars (black, green, and purple curves). Finally, an inverse plot of predicted AIRMASS (light blue curve) vs. the total ADU counts of the comparison stars (brown dots) is indicative of any passing clouds or other atmospheric conditions.

Figure 8 is an example of the data values derived from the fit.

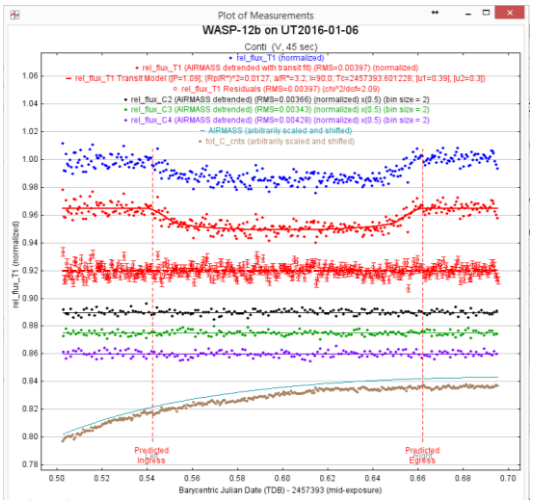

Figure 7. Example of AIJ Light Curves

Figure 8. Data values from a sample model fit

As seen in Figure 8, the following are the data values that result from AIJ's transit fit process:

1. the square of the ratio of the radius of the exoplanet (R_p) to that of its host star (R_*) – note, this is also the depth of the transit light curve;
2. the ratio of the exoplanet's semi-major orbital radius (a) to R_*;
3. the center point T_c of the transit light curve and the duration of the transit;
4. the inclination of the exoplanet's orbit relative to the observer's line-of-sight;
5. the RMS of the transit fit and the observed data;
6. the BIC (Bayesian Information Criterion) resulting from the model fit.

Given R_*, the radius of the exoplanet's host star, the first two ratios above can then be used to estimate the radius of the exoplanet, as well as the radius of its semi-major orbit.

Best practices for optimizing the transit fit after its initial run, including the following steps:

1. Initially select AIRMASS as the only detrending parameter. If a meridian flip was done, then Meridian_Flip should be maintained as a detrend parameter throughout the remaining steps below.

2. Determine the effects on RMS of various comparison stars being removed (AIJ allows the user to easily "deselect" a comparison star, in which case all of the computations associated with that star are redone). If the RMS decreases when a particular comparison star is deselected, then leave it out. It is sometimes the case that the relative flux of such stars also will show an amount of scatter greater than the target star and the other comparison stars.

3. With the above selection of comparison stars and AIRMASS remaining as the only detrend parameter (with maybe the addition of Meridian_Flip), redo the differential photometry and model fits with smaller and larger aperture and annulus radii. Determine the effects on RMS for each new radii combination. Choose the combination that results in the lowest RMS.

4. Repeat Step 2 on this new set of radii to achieve the best RMS. In addition to the resulting RMS value, record the BIC value that goes along with the best RMS.

5. Determine the effects of different detrending parameters. First, remove AIRMASS detrending and see if BIC increases by 2 or more. If it does, keep AIMASS detrending; if it does not, do not include AIRMASS. Next, add the following detrending

parameters one at a time and observe changes in the BIC value:

a. Width_T1,
b. Sky/Pixel_T1,
c. X(FITS)_T1,
d. Y(FITS)_T1,
e. tot_C_cnts,
f. time (e.g., BJD_TDB),
g. CCD-TEMP.

Of those detrend parameters that result in at least a reduction of two (2) in the BIC value, choose the 3-4 parameters that cause the greatest reduction in this value.

6. Using the resulting set of detrend parameters, repeat again Step 2 to see the effects on RMS from removing one or more comparison stars.

4. Exoplanet Observing Tools and Aids

In addition to handbooks and guides that are available (see Gary, 2014 and Conti, 2017), the AAVSO offers a 4-week online course on exoplanet observing. Appendix A contains a syllabus for the course.

The AAVSO is also developing an exoplanet database (EOD) for the amateur astronomy community to store their exoplanet observations. In particular, it is envisioned that the EOD will be the repository of qualified observations to support the TESS ground-based followup program. By contrast, the EOD will contain much more information than does the Exoplanet Transit Database (ETD). The ETD is an online archive of amateur astronomer exoplanet observations sponsored by the Czech Astronomical Society (Poddany *et al.*, 2010).

The EOD will be a relational database that will allow retrieval of information through a number of different possible queries. The following are some of the features of the EOD:

1. Since it is now well-established that a single star can host multiple exoplanets and that an exoplanet can be member of a multi-star system, the EOD will allow for a many-to-many relationship between such objects.
2. Because an exoplanet can have different names, the EOD will allow for a number of aliases associated with a given exoplanet.
3. The observer will be able to identify a star through a variety of different common names associated with that star.
4. The EOD will support the association of a primary observer, as well as several secondary observers, with a given observation. This would allow, for example, an astronomy instructor to include the names of participating students in a given science observation.
5. The EOD will be able to associate a given observation with a particular observing location and instrumentation package.
6. A web portal will allow the observer to upload a report that consists of a header with general information about an observation, as well as the observational data itself. This web portal will also allow for uploading both an image showing the stars that were used as the target and comparison stars and an image of the observer's light curve.
7. Facilities will be provided for editing and downloading observation data.

The EOD will store the following general information about an entire observation:

1. Primary observer's code
2. Host star name
3. Exoplanet name
4. Timebase used (e.g., JD_{UTC}, HJD_{UTC}, BJD_{UTC} , BJD_{TT}, BJD_{TDB})
5. Exposure time, binning, and filter used.

Optional general data elements include:

1. Software package used
2. Secondary stars, in the case of a multi-star system
3. Secondary observers
4. "Priors" used in the transit modeling
5. Transit modeling results
6. Observational notes.

Observational data that will be stored for each data point will consist of:

1. A date/time stamp
2. The differential magnitude representing the change in brightness of the target star relative to the comparison stars.
3. The error margin associated with the differential magnitude values for each of the detrend parameters.

Other observational data may also be added at a later time to support the TESS followup observation effort.

Finally, the AAVSO is developing a TESS Exoplanet Observer Qualification Program. This program will pre-qualify observers who wish to contribute to the TESS followup program. It is envisioned that qualification criteria will consist of:

1. satisfactory completion of the AAVSO Exoplanet Observing course, or evidence of exoplanet observing experience;
2. successful analysis of a set of target stars that are representative of TESS targets;
3. successful entry of an exoplanet observation into the AAVSO EOD.

5. Summary

Exoplanet observing by amateur astronomers has now matured to a set of established best practices. This movement from art to science is coming at an opportune time – namely, just when TESS will need a set of qualified exoplanets observers to conduct the many followup observations that it will require.

6. References

AAVSO: http://www.aavso.org/apps/vsp/ (2017)

Baudot, G., "*Full Frame Guiding and Focusing*," Proceedings of NEAIC 2017, April, 2017.

Collins, K., et al., "*AstroImageJ: Image Processing and Photometric Extraction for Ultra-Precise Astronomical Light Curves*," (2016), arXiv:1601.02622.

Conti, D., "*Hubble Exoplanet Pro/Am Collaboration*," Proceedings of the AAVSO 2015 Annual Meeting, November, 2015.

Conti, D.: http://astrodennis.com (2017)

di Cicco, D., "*The ONAG from Innovation Foresights*," Sky&Telescope, December, 2012.

Dimension 4: http://thinkman.com/dimension4/ (2017)

Edberg, S., "*An Automated System for Citizen Searches for Exoplanets*," Proceedings of the SAS 2016 Symposium, June, 2016.

Gary, B., Exoplanet Observing for Amateurs, Second Edition (Plus), (2014), Reductionist Publications.

Motta, M., "*Amateurs Track a Disintegrating Exoplanet*," Sky&Telescope, April, 2017.

NASA: https://jwst.nasa.gov/ (2017)

Pepper, J., et al., "*The Kilodegree Extremely Little Telescope (KELT): A Small Robotic Telescope for Large-Area Synoptic Surveys*," (2007), arXiv: 0704.0460v2.

Poddany, S., et al., "*Exoplanet Transit Database. Reduction and processing of the photometric data of exoplanet transits*," (2010) *New Astronomy.* 15: 297-301.

Ricker, G., et al., "*Transiting Exoplanet Survey Satellite*," (2015), Journal of Astronomical Telescopes, Instruments, and Systems 1 (1).

APPENDIX A:
AAVSO Exoplanet Observing Course Syllabus

This four (4) week, online course is designed to provide participants with the basics on how to conduct their own exoplanet observations. The course first briefly covers various exoplanet detection methods, but primarily focuses on the transit method. The fundamentals of high precision photometry are discussed in order to give the participants a good foundation for exoplanet observing. The various phases of an exoplanet observation are covered, as well as a detailed walk-through of an actual exoplanet observation analysis using AstroImageJ (AIJ). Finally, the future of exoplanet observing using small telescopes is discussed, as well as ways in which amateur astronomers can contribute to exoplanet research.

The course uses "A Practical Guide to Exoplanet Observing" (see http://astrodennis.com) as its primary text. Video modules are used to lead participants through each part of the course and participants are required to take a quiz after each week's assignment.

Participants must successfully pass each quiz to successfully pass the course. A private forum is available to participants in order to communicate with each other, as well as with the instructor.

The following are the topics to be covered during each week of the course:

Week 1:

1. A short introduction to the course, including its objectives and topics to be covered.
2. Some background on exoplanets and detection methods.
3. Important properties of stars and planets, and the relationships among some of these properties.
4. Some fundamentals of high precision photometry that are important to know for exoplanet observing.

Week 2:

1. An overview of the equipment and software used in exoplanet observing.
2. A description of online resources that can be used to support the various phases of exoplanet observing.
3. An overview of the various phases involved in an exoplanet observing session.

Week 3:

1. An introduction to AIJ.
2. How AIJ can be used to create master bias, master darks, and master flats and use these masters to calibrate the science images.
3. How differential photometry on the calibrated files can be performed using AIJ, as well as the meaning of the various fields in the resulting Measurements file.

Week 4:

1. A review of AIJ's Multi-plot Main screen.
2. How AIJ's Multi-plot Y-data screen can be used to plot various light curves of interest.
3. How AIJ's various "prior" parameters can be entered on AIJ's exoplanet transit modeling tool, namely its Data Set Fit Settings screen, as well as an overview of various miscellaneous AIJ screens.
4. A review of AIJ's transit modeling screen is covered, namely the Data Set Fit Settings screen, as well as how AIJ can be used to detect eclipsing binaries.
5. Finally, plans are for future exoplanet space missions are discussed, as well as how amateur astronomers can contribute to some of these future surveys.

Multiwavelength Observations of the Eclipsing Binary NSV 03438 Between January 2013 and March 2016

Carter M. Becker
Desert Pass Observatory
Green Valley, Arizona
Cbecker310@aol.com

Abstract

The eclipsing binary NSV 03438 in Canis Minor consists of two M-type stars having approximate effective temperatures of 3235○K (M4V) and 2898○K (M6V). The period for a cycle during this study was 1.535 days, essentially unchanged from that reported in 1996. A modification of the bisected chord method provides estimates of mid-eclipse Julian Dates with 95% confidence limits for 22 primary and 29 secondary eclipses. The mean depths of primary and secondary eclipses with filter B are 0.69 and 0.62 magnitude, respectively, and 0.65 and 0.61 magnitude, respectively for filter V. APASS standard stars closely associated with NSV 03438 provide a means of determining the magnitude of NSV 03438. In addition, B - V color indexes and effective temperatures of the binary can be assessed at critical stages throughout the eclipse cycle.

1. Introduction

The new catalogue of stars of suspected variability contains data on 14810 variable stars (Kholopov, P.N., editor 1982). NSV 03438 was first 0bserved by Weber (1957) as a possible Cepheid variable; however Garcia-Melendo and Gomez-Forrellad (1996) characterized it as a detached eclipsing binary star with period 1.535 days and unambiguously identified with GSC 0762.2022.

In the present study, observations of NSV 03438 were conducted over an interval of 39 months utilizing B, V, R and I photometric filters. The period for a complete cycle appears independent of the observing wavelength. Mean times for all primary and secondary eclipses with 95% confidence limits are determined utilizing a modification of the bisected chord method (Pickard, R., Director 2011). These values over the duration of the study establishes the period for the eclipsing binary.

The B-V color index is utilized to determine the effective temperatures and spectral type of the eclipsing binary and its component stars. Data obtained with R and I photometric filters could not be compared directly with APASS standard stars resulting in considerable uncertainty in color indexes involving R and I photometric filter data.

2. Observing Facility and Equipment

All observations were conducted at Desert Pass Observatory using a Paramount ME robotic mount and Celestron EdgeHD 1400 telescope equipped with an SBIG ST-8XME camera, a HyperStar C14 HD Lens and Micro Touch Autofocuser. TheSky6 Astronomy Software and CCD Soft provide for control of the mount and camera, respectively

All equipment is housed within an HD-6S Home-Dome controlled by Digital Dome Works, Model 4, Version 5.0. The dome is anchored to a concrete foundation having a central well about two feet deep. Combined with the height of the dome, the well provides height for standing of about six feet at the center. Dome control and software for all equipment within the dome are served by an HP Desktop (Dome-PC) with Vista operating system. Observing runs are accomplished robotically with wireless communication via remote desktop to the Dome-PC from an adjacent building.

3. Observations

Observations of NSV 03438 were made between January 2013 and March 2016. The majority were in January or February of a given year with a smaller number in March, April and October. During all observing runs images were captured at an interval of 180 seconds. To conform with APASS criteria, exposure times generally were 180 seconds with no delay between exposures for images with a B filter or 90 seconds with 90 second delay for images with V, R and I filters. Observations are labeled by the month, day and year the run started and ended and whether the run is E, W or E/W with respect to the meridian flip of the mount (e.g. 0217-1815 W).

The camera temperature for all observations was -5°C. and prior to all runs sky flats were acquired with 5 second exposures, 20 pooled for a master flat. During an observing period dark frames were

acquired at -5°C. and with appropriate exposure times to calibrate images and flats. Images were downloaded to the Dome-PC and later transferred to another PC for calibration and photometric analyses utilizing AIP4WIN 2.0 software, Berry, R. and Burnell, J. (2005).

4. Results and Discussion

A total of 51 eclipses (22 primary and 29 secondary) were observed at four wavelengths: B (10), V (26), R (7) and I (8). The period for a complete cycle appears independent of the observing wavelength. Plots of Delta Magnitude vs Julian Date for all eclipses were analyzed to estimate the JD for the mean minimum with 95% confidence limits. A modification of the bisected chord method (Pickard, R., Director 2011) for estimating mid-eclipse was utilized as illustrated in figure 1 for NSV 3438 0217-1815 W. Complete data for this primary eclipse are shown in figure 3 (Chart 1) and figure 4 (Chart 2).

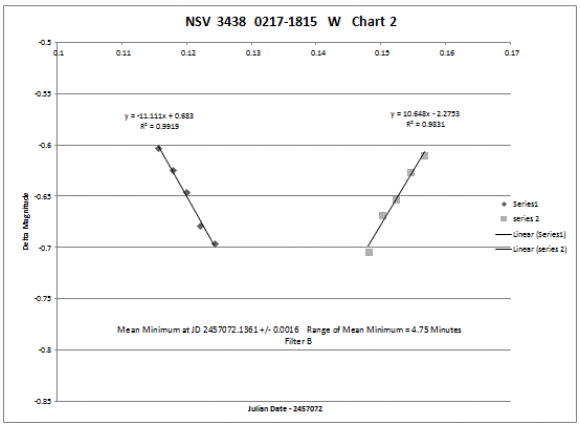

Figure 1. Determining the estimated mean minimum for mid-eclipse with confidence limits.

For all eclipses, Chart 1 generally shows a plateau before or after the eclipse and a complete minimum. Chart 2 generally shows 19 to 23 data points including the minima and extending before and after the minima to about the same level of delta magnitude before and after the eclipse. As show in figure 1, five data points are utilized at the beginning of the descending limb and end of the ascending limb of data points to determine linear estimates approaching the minimum. The point of intersection of the linear estimates is the estimated JD for the mean minimum. The magnitude at the intersection is more negative than the actual minimum, but the focus here is on establishing the mean time for the minimum.

A plot of the Julian Date of mean minimum vs the 51 eclipses analyzed is shown in figure 2. The slope of the plot line, 1.535 days gives the period for the eclipsing binary. This period is essentially the same as found by Garcia-Melendo and Gomez-Forrellad in 1996.

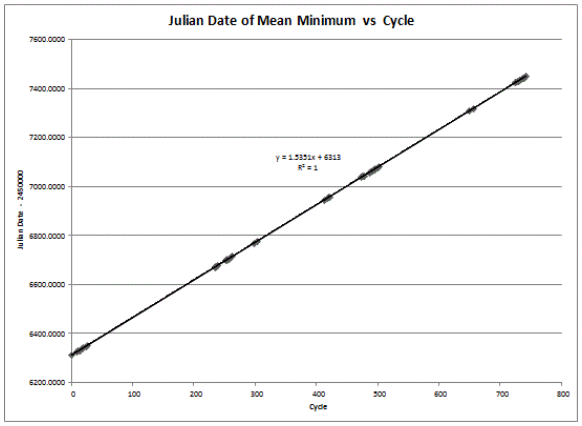

Figure 2. Julian Date of Mean Minimum vs Eclipse Cycle.

In order to determine the degree of uncertainty in the mean time for minima, 95% confidence limits were established as follows. The two linear estimates in figure 1 directed toward and away from the minimum each have a slope and intercept. There are mean values for the two slopes and intercepts as well as high and low values depending on the 95% confidence limits. Therefore, four parameters (two slopes and two intercepts), and for each of these three values (high, mean and low) could represent a range of reasonable values. Thus, there are 3^4 or 81estimates of the mean minimum. Of course there are innumerable values for each of the four parameters within the high and low limits, but these would generate additional estimates of the mean minimum within the range established by the 81 estimates as given above.

In chart 2 for each of the eclipses, the JD for mean minima are given along with 95% confidence limits. Based on the confidence limits, the possible ranges for times of the minima are given in minutes with the means at the center of the ranges.

In figures 3 through 12, Chart 1 data are shown for primary eclipses with filter B (figure 3) and filter V (figure 5). Chart 2 data are seen for primary eclipses with filter B (figures 4 and 7) and filter V (figures 6 and 8) as well as secondary eclipses with filter B (figures 9 and 10) and filter V (figures 11 and 12). As shown in the next section, magnitudes at primary and secondary eclipses along with magnitudes at plateaus are utilized to determine B-V

color indexes and effective temperatures of the component stars of the binary.

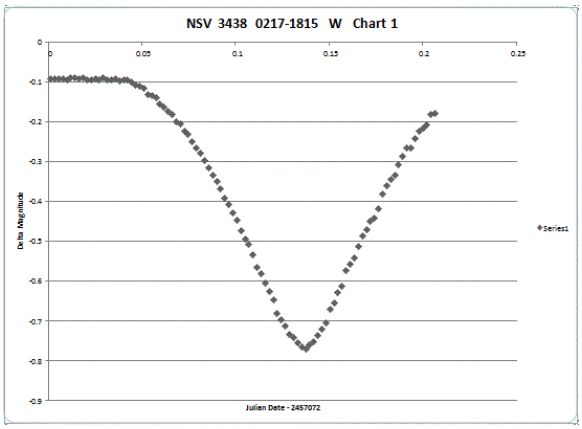

Figure 3. NSV 3438 0217-1815 W Chart 1 primary eclipse with filter B.

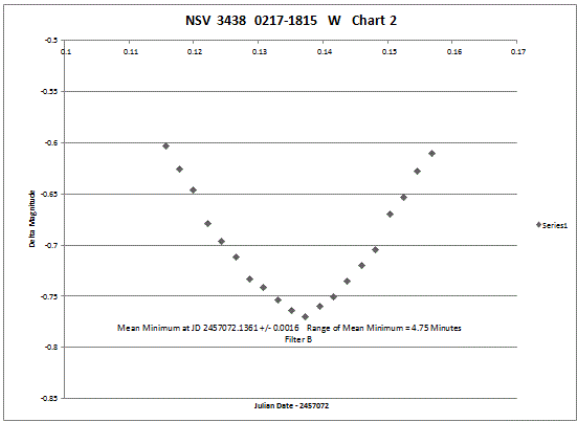

Figure 4. NSV 3438 0217-1815 W Chart 2 primary eclipse with filter B.

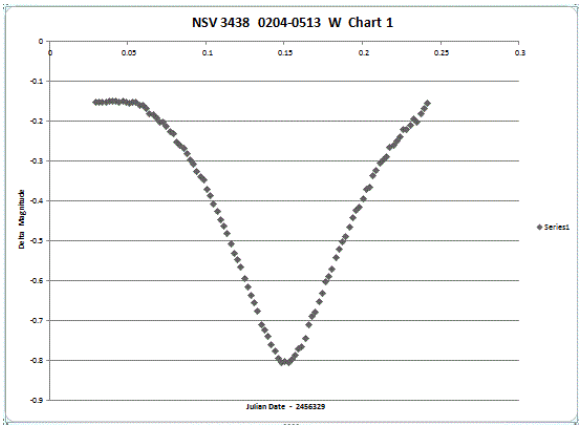

Figure 5. NSV 3438 0204-0513 W Chart 1 primary eclipse with filter V.

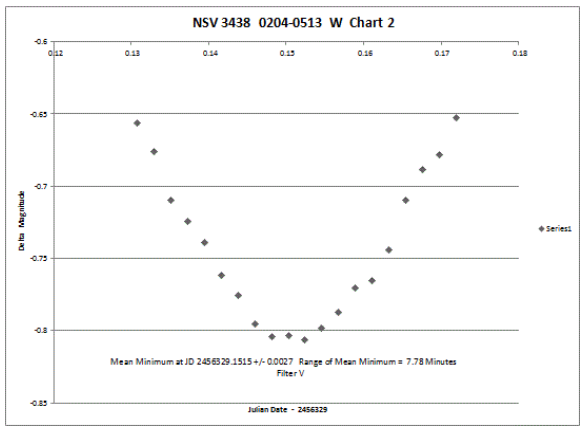

Figure 6. NSV 3438 0204-0513 W Chart 2 primary eclipse with filter V.

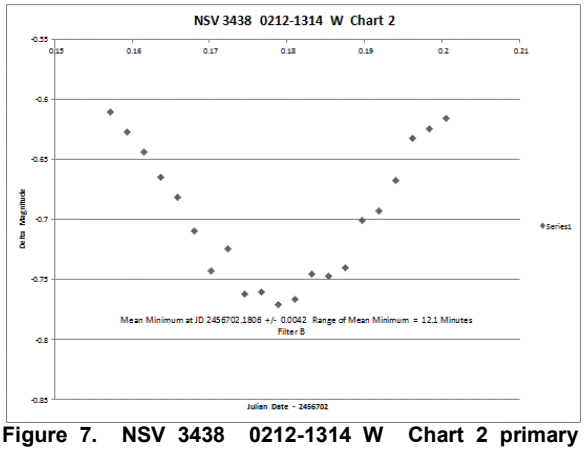

Figure 7. NSV 3438 0212-1314 W Chart 2 primary eclipse with filter B.

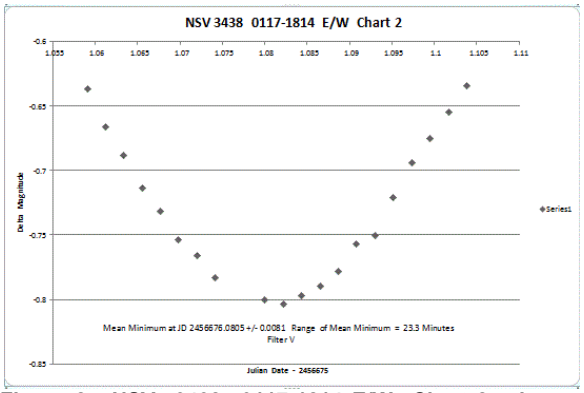

Figure 8. NSV 3438 0117-1814 E/W Chart 2 primary eclipse with filter V.

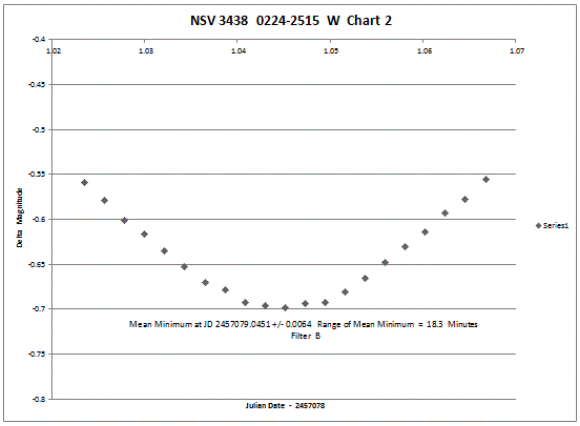

Figure 9. NSV 3438 0224-2515 W Chart 2 secondary eclipse with filter B.

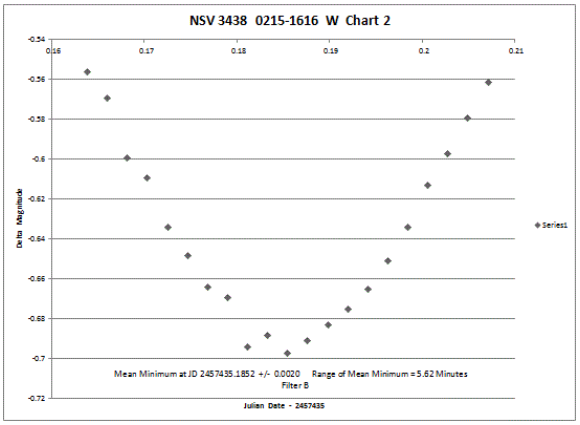

Figure 10. NSV 3438 0215-1616 W Chart 2 secondary eclipse with filter B.

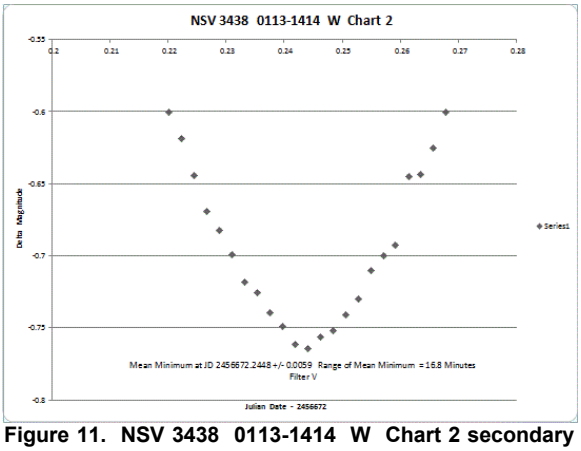

Figure 11. NSV 3438 0113-1414 W Chart 2 secondary eclipse with filter V.

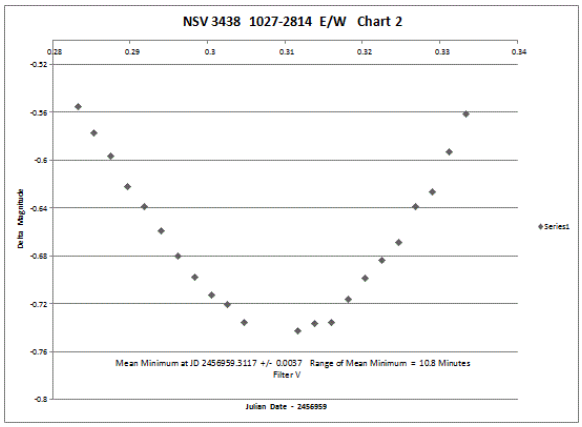

Figure 12. NSV 3438 1027-2814 E/W Chart 2 secondary eclipse with filter V.

5. Effective Star Temperatures

Data for observations shown in figures 3 through 12 were utilized to determine the total temperature of the binary system as well as effective temperatures and spectral classification of the two component stars. Listed by filter (B or V), the eight observed eclipses utilized in temperature calculations are given in Table 1.

Table 1

Observation	Date	Mount	Eclipse
B - 1	0212-1314	W	primary
B - 2	0217-1815	W	primary
B - 3	0224-2515	W	secondary
B - 4	0215-1616	W	secondary
V - 1	0204-0513	W	primary
V - 2	0117-1814	E/W	primary
V - 3	0113-1414	W	secondary
V - 4	1027-2814	E/W	secondary

For each of these observing dates, the magnitude of NSV 03438 as identified with GSC 0762.2022 was determined by comparing the star-sky photometric signal, Berry and Burnell (2005) with two closely associated APASS (AAVSO, 2011) standard stars, GSC 0762.2280 and GSC 0762.2164. The magnitude of NSV 03438, m_1, is then given by:

$$m_1 = -2.5 \log (C_1/C_2) + m_2$$

where C_1 is the star-sky photometric signal of NSV 03438, and C_2 and m_2 are the star-sky photometric

signal and the APASS magnitude, respectively, of the standard star.

Comparing the results of all calculations show a consistent ~ 0.2 higher magnitude when GSC 0762.2280 is used as the standard star than with GSC 0762.2164. The mean of the two results was used in further calculations. For filters B and V, the magnitudes of NSV 03438 in plateau as well as at primary and secondary minima are given in Table 2. The means of two similar observations are also shown including differences between plateaus and minima.

Table 2

Filter B			
Observation	B - 1	B - 2	Mean
Primary plateau	11.290	11.292	11.291
Primary minima	11.992	11.973	11.983
Plateau-minimum	-0.702	-0.681	-0.692
Observation	B - 3	B - 4	Mean
Secondary plateau	11.289	11.285	11.287
Secondary minima	11.903	11.907	11.905
Plateau-minimum	-0.614	-0.622	-0.618
Filter V			
Observation	V - 1	V - 2	Mean
Primary plateau	10.768	10.759	10.764
Primary minima	11.420	11.416	11.418
Plateau-minimum	-0.652	-0.657	-0.654
Observation	V - 3	V - 4	Mean
Secondary plateau	10.755	10.766	10.761
Secondary minima	11.374	11.364	11.369
Plateau-minimum	0.619	-0.598	-0.608

The mean values in the right-hand column of Table 2 are utilized to calculate B - V color indexes at primary and secondary plateaus and minima. Effective temperatures are then determined using the relation in figure 13, representing data from Pecaut and Mamajek (2013) for pre-main-sequence stars and supported by Pecaut et. al. (2012) for main-sequence stars.

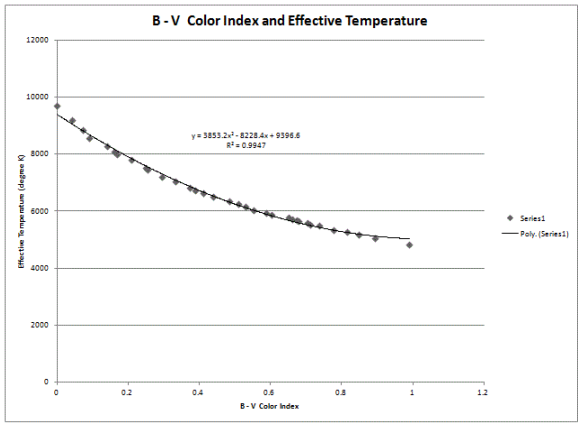

Figure 13. Relation of B - V Color Index and Effective Star Temperature.

Equation 1 stipulates the effective temperature (T) for a given B - V color index.

$$T(^{\circ}K) = 3853\,(B\text{-}V)^2 - 8228(B\text{-}V) + 9397 \qquad (1)$$

In table 3 the B - V color indexes and effective temperatures are given for primary and secondary plateau and minima observations.

Table 3

Observation	B - V	T °K
Primary plateau	0.527	6130.4
Primary minima	0.565	5977.6
Secondary plateau	0.526	6134.6
Secondary minima	0.536	6093.2

The combined temperatures of the binary stars in the primary and secondary plateaus are similar (no eclipse) and the mean value is rounded to 6133 ○K. The rounded values for the primary and secondary eclipses are 5978○K and 6093○K, respectively.

Equations 2, 3 and 4 stipulate the conditions to be met

$$S1 + S2 = 6133^{\circ}K \quad \text{(no eclipse)} \qquad (2)$$

$$aS1 + S2 = 5978^{\circ}K \quad \text{(primary eclipse)} \qquad (3)$$

$$S1 + bS2 = 6093^{\circ}K \quad \text{(secondary eclipse)} \qquad (4)$$

where S1 and S2 are the effective temperatures of the brighter and fainter stars, respectively, and a and b are empirical factors representing the decrease in

brightness from S1 (a) and S2 (b) during the primary and secondary eclipses, respectively.

Equations 2, 3 and 4 are solved numerically to find the values of the four unknowns providing the best solutions for equations 2, 3 and 4. To four decimal places, a = 0.9521 and b = 0.9862. The effective temperatures of the brighter and fainter stars are estimated to be S1= 3235°K and S2 = 2898°K, respectively.

6. Conclusions

NSV 03438 is an eclipsing binary with component stars having estimated effective temperatures of 3235°K (spectral type M4V) and 2898°K (spectral type M6V). The period appears to have remained constant at 1.535 days since its characterization as an eclipsing binary in 1996. A modification of the bisected chord method provides estimates of the mid-eclipse Julian Date with 95% confidence limits for the 22 primary and 29 secondary eclipses observed.

As shown in table 2, the mean depths of primary and secondary eclipses are 0.69 and 0.62 magnitude, respectively, when observed with filter B and 0.65 and 0.61 magnitude, respectively, when observed with filter V. The magnitudes are determined by comparing the star-sky photometric signals of NSV 03438 with two APASS standard stars and using the mean.

The B - V color index could be used with confidence to estimate effective temperatures of the component stars in the binary. Unfortunately, color indexes involving R and I filters are not optimal for temperature estimates due to considerable variation in transformation of R and I filter data to Sloan r' and i' for APASS standards, Chonis and Gaskell (2008).

For future photometric studies at the longer wavelengths, Sloan filters will be utilized to allow direct comparison with APASS data. Possible model solutions for NSV 03438 are being explored using Binary Maker 3, Bradstreet and Steelman (2004). However, this effort may be somewhat limited by the absence of radial velocity data.

7. References

APASS (AAVSO, 2010-2015) This research has made use of the APASS database, located at the AAVSO web site. Funding for APASS has been provided by the Robert Martin Ayers Sciences Fund.

Berry, R. and Burnell, J., "The Handbook of Astronomical Image Processing, 2nd Edition"(2005) Willmann-Bell, Inc.

Bradstreet, D. and Steelman, D., "Binary Maker 3" (2004) Contact Software.

Chonis, T. S. and Gaskell, C. M., "Setting *UBVRI* Photometric Zero-Points using Sloan Digital Sky Survey *ugriz* Magnitudes" (2008) University of Nebraska.

Garcia-Melendo, E. and Gomez-Forrellad, J. M., "NSV 03438, A New Detached Eclipsing Binary Star in Canis Minor" (1996) Information Bulletin on Variable Stars, Number 4410.

Kholopov, P. N., editor, "New catalogue of stars suspected of variability containing data on 14810 variable stars which have not received definitive nomenclature until 1980" (1982) USSR Academy of Science Publisher (Nauka), Moscow.

Pecaut, M. J. and Mamajek, E. E., "Intrinsic Colors, Temperatures, and Bolometric Corrections of Pre-Main-Sequence Stars" (2013) ApJ Supp. 208:9.

Pecaut, M. J. et al., "A Revised Age for Upper Scopius and the Star Formation History Among the F-Type Members of the Scorpius-Centaurus OB Association" (2012) ApJ 746:154.

Pickard, R., Director, "Eclipsing Binary Handbook" (2011) British Astronomical Association - Variable Star Section, Shobdon.

Weber, R., "Photographic research of variable stars" (1957) Astronomy 71:34.

New observations and analysis of zeta Phe

Coen van Antwerpen
Coki Observatory
8 Carman Close, Hillbank, SA 5112, Australia.
coenva15@gmail.com

Tex Moon
Centauri Observatory
14 Ada St, Scottsdale, TAS 7260, Australia.
texmoon0@gmail.com

Abstract

From new and published photometry of the eclipsing binary ζ Phe (HR 338) a period of 1.66977220(3) days was determined and a new epoch of HJD 2432500.021511 selected. Using the 60+ years of photometry, published radial velocities and new values for the period and epoch, the physical characteristics of the ζ Phe system were modeled using a software package called PHOEBE. Of note, the masses of the B6V and B9V components were determined to be 3.75 and 2.35 $M_{\odot}$, somewhat less than previous determinations. The period of apsidal motion of ζ Phe's eccentric orbit was calculated to be 53.7±0.3 years indicating that one full cycle has been completed since photoelectric measurements of this star were first undertaken in 1950.

Key words: binaries: eclipsing

1. Introduction

ζ Phe (HR 338; HD 6882; HIP 5348) is classified as an eclipsing binary of the Algol type; the components being B-type main sequence stars. The depth of the primary minimum is about half a magnitude and the period is about 1⅔ days. This system is of particular interest as:

- it is the brightest eclipsing binary where primary and secondary eclipses are both of appreciable depth (Popper 1970; Dachs 1971);
- it belongs to a small subset for which astrometric observations have also been made (Zasche and Wolf 2007);
- its orbit is eccentric (Clausen *et al*. 1976a, b);
- there is measurable apsidal motion (Giménez *et al*. 1986a, b) over a relatively short time frame (Zasche and Wolf 2007);
- it has two visual companions that may be physically associated with it (Andersen 1983).

Further measurement and a new analysis was thus seen as useful, particularly in light of the new modeling software available (PHOEBE) and the importance of determining masses at the luminous end of the main sequence.

2. New and Published Data

New photoelectric measurements of ζ Phe were made by one of the authors (Moon) from 8 October 2009 to 31 January 2012 using equipment and techniques as described in Otero and Moon (2006). For the 192 new measurements in V-band and 179 in B-band, η Phe (HR 191; HD 4150; HIP 3405) was used as the comparison star with κ Eri (HR 721; HD 15371; HIP 11407) used as the check star. The measured magnitudes were corrected for atmospheric extinction and transformed to standard V and B-V values. These new measurements are presented in Table 1 while Table 2 lists the other (previously published) photometry used.

See TABLE 1 at end of paper

The photometry assembled for modeling and analysis of ζ Phe included Hipparcos 'H_p' and Tycho 'V_T' measurements which were transformed to V-band using the relationships given by Bessell (2000). This resulted in corrections of 0.022 and 0.016 being applied to H_p and V_T respectively. The GCPD (Mermilliod *et al*. 1997) lists a mean V magnitude for η Phe of 4.358. This was selected for standardizing all measured differences between ζ Phe and η Phe. Noting that the different data sets are likely to have different internal and transformation errors, we suggest adopting a value for the photoelectric

measurement error of 0.01 magnitude (Budding and Demircan 1973).

The data of Hogg (1951) were adjusted by subtracting 40 minutes in HJD to align them with the other data sets. This was similar to the adjustment applied to some other 1950s photoelectric measurements (see discussion by Moon and van Antwerpen (2009; 2010)). Hogg made his 'blue-sensitive' photoelectric measurements before the establishment of the UBV system. An adjustment of -0.085 was needed to bring them into alignment with other V band measurements. The combined, homogenized photoelectric data set for ζ Phe thus comprised 2967 magnitude measurements spanning more than 60 years.

Photometric Dataset	Number of Measurements
Hogg (1951)	77
Dachs (1971)	200
Clausen (1976a)	1744
Mallama (1981)	12
Gimenez (1986)	200
Hipparcos (1990)	143
Tycho (1990)	211
Shobbrook (1996)	188
Moon (2012)	192

Table 2. Sources of photometric data used in the analysis

Radial velocities for ζ Phe have been measured by Hagemann (1959), Popper (1970), and Andersen (1983). When reviewing these 3 sources of radial velocity we noticed that Hagemann's measurements around secondary minimum were inconsistent with those of both Popper and Andersen. Consequently, Hagemann's data for secondary minimum were discarded leaving a total of 123 measurements of radial velocity around primary eclipse and 48 around secondary eclipse for our subsequent analysis.

3. Analysis

Our approach to analyzing ζ Phe followed that we used for μ^1 Sco (van Antwerpen and Moon 2010). Central to this analysis was the software PHOEBE (Prša 2003; Prša and Zwitter 2005; Prša et al. 2008; Prša 2009).

2.1 Estimating effective temperatures from photometric indices

Being at a distance of about 83 pc, interstellar reddening for the ζ Phe system is expected to be small. Using UBV and uvby color indices for ζ Phe listed in the GCPD, we followed the approach taken in our analysis of μ^1 Sco (van Antwerpen and Moon 2010) to estimate the combination of spectral types that would best reproduce the reddening-free color indices of ζ Phe.

Assuming a standard reddening law applies to ζ Phe, an E(b-y) = 0.018 was calculated, consistent with its independently calculated E(B-V) value. Values of $(B-V)_0 = -0.115$ and $(b-y)_0 = -0.057$ were then adopted for the reddening-free B-V and b-y color indices of ζ Phe. Using Table 4 of van Antwerpen and Moon (2010), a spreadsheet was constructed to calculate the combined B-V and b-y color indices obtained from combinations of various spectral types. The best match was obtained for spectral types of B6V+B9V, in agreement with Zasche and Wolf 2007.

From the B-V, T_{eff} relationship of Flower (1996), effective temperatures for the components of ζ Phe were calculated to be 13200 K and 10600 K (typical error being ±400 K).

With a measured parallax of 10.92±0.39 mas (van Leeuwen 2007) and a V=3.9 for the combined light of the components, M_V was calculated to be -0.9 (again consistent with the spectral types).

3.2 Choice of epoch and determination of period

Colacevich (1935) first determined an accurate period for ζ Phe of 1.66958 d. Later observations have confirmed and refined this value. For a better determination of the period based on 60+ years of photoelectric measurements we started with the period and an epoch given by Shobbrook (2004) and made small adjustments until all the data sets aligned visually.

Using PHOEBE we then iterated to determine a period and recent epoch that best fits all the 60+ years of photometry. Figure 1 shows there is good agreement of all measurements with the light curve when these new values are adopted.

3.3 The system's orbital characteristics

PHOEBE (Prša 2003; Prša and Zwitter 2005; Prša *et al*. 2008; Prša 2009) is based on the Wilson and Devinney (1971) model and includes theoretical

developments by Kallrath and Milone (1999). The limb-darkening model adopted is based on a logarithmic law and van Hamme's tables (van Hamme 1993). In PHOEBE the type of eclipsing binary to be modeled is selected from a range of options.

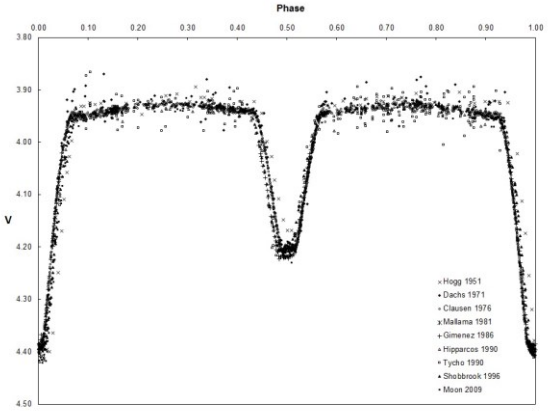

Figure 1. All photometric data for ζ Phe plotted using the newly determined epoch and period.

After selecting the detached binary option, PHOEBE was run to determine the orbital parameters that best fit the combined, harmonized photometry and published radial velocities. In the iterative approach taken we:

1. Normalized the luminosities of the data sets;
2. Fitted the Epoch and Period;
3. Fitted the semi-major axis, mass ratio and center of mass velocity;
4. Fitted the eccentricity, inclination and argument of periastron as a group;
5. Fitted the inclination, eccentricity, argument of periastron and time derivative of the argument of periastron;
6. Adjusted the semi-major axis, mass ratio and center of mass velocity;
7. Fitted the potential profiles for the stars;
8. Fitted the gravity brightening and albedo profiles for each star; and
9. Fitted the synchronicity parameter for each star.

For each step the selected parameters were allowed to vary while all other parameters were held constant. The initial values adopted were based on system characteristics determined by Zasche and Wolf (2007). An 'initializing' run was undertaken using the photoelectric measurements of Shobbrook and Moon. This provided the starting parameters for subsequent modeling using all available data.

Figures 2 and 3 show the fit of the system solution we modeled compared to the photometry around primary and secondary minimum respectively.

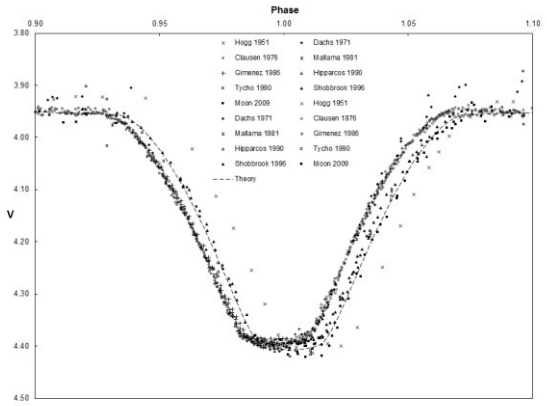

Figure 2. System solution for primary minimum from PHOEBE modeling compared to photoelectric measurements.

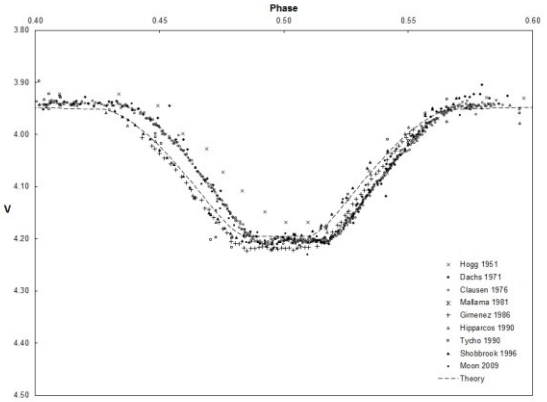

Figure 3. System solution for secondary minimum from PHOEBE modeling compared to photoelectric measurements.

Using the system parameters determined (see Table 3) PHOEBE was then used to calculate magnitudes for the time interval HJD 2432499 to HJD 2455958 in increments of 0.25 d.

Primary star's spectral type	B6V
Primary star's mass	3.75 $M_{\odot}$
Primary star's radius	2.84 $R_{\odot}$
Primary star's temperature	13200 K
Secondary star's spectral type	B9V
Secondary star's mass	2.35 $M_{\odot}$
Secondary star's radius	1.78 $R_{\odot}$
Secondary star's temperature	10600 K
Mass Ratio	0.625
Centre of Mass velocity	15 kms^{-1}
Semi-major axis	10.82 $R_{\odot}$
Inclination	86.52°
Eccentricity	0.01067
Argument of Perihelion	170.4°
Time derivative of Argument of Perihelion	0.018365 °/day
Epoch (HJD)	2432500.021511(208)
Period	1.66977220(3) day

Table 3. System parameters for ζ Phe determined using PHOEBE with new and published data.

Figure 4 compares the system solution obtained to all observed data demonstrating that the derived parameters, including the aspidal motion, fit the combined, homogenized data set.

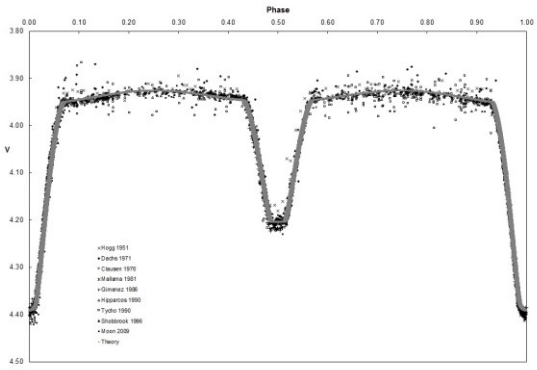

Figure 4. V magnitudes calculated from PHOEBE for the time interval HJD 2432499 to HJD 2455958 compared to photoelectric measurements.

4. Conclusions

From modeling and analysis using published and new data it is concluded that:

1. The variations of ζ Phe are stable over the 60+ years for which photoelectric measurements exist. Using a combined, homogenized data set, a period of 1.66977220(3) days was determined.

2. An epoch of HJD 2432500.021511 would be suitable for further monitoring and analysis of this system.

3. ζ Phe is a fully detached binary with an eccentric orbit that has an apsidal period of 53.7±0.3 years.

4. Derived masses for the components are 3.75 and 2.35 $M_{\odot}$, somewhat less than previously determinations.

In order to check and refine the period of the apsidal motion it is recommended that further photoelectric measurements be collected approximately every five years. With the semi-major axis of the orbit subtending 1.21 mas at its estimated distance, ζ Phe may be also a suitable target for SUSI (Davis 2006; Davis et al. 2007).

ζ Phe photometry used in this analysis has been entered into the AAVSO database (WebObs).

5. References

Andersen, J. (1983), *Astron. Astrophys*. **118**, 255.

Bessell, M. S. (2000), *Publ. Astron. Soc. Pacific* **112**, 961.

Budding, E. and Demircan, O. (1973), *Introduction to Astronomical Photometry*, Cambridge University Press, Cambridge, 2nd edition.

Clausen, J. V., Gyldenkerne, K., and Grønbech, B. (1976a), *Astron. Astrophys. Suppl*. **23**, 261.

Clausen, J. V., Gyldenkerne, K., and Grønbech, B. (1976b), Astron. Astrophys. **46**, 205.

Colacevich, A. (1935), *Publ. Astron. Soc. Pacific* **47**, 84.

Dachs, J. (1971), *Astron. Astrophys*. **12**, 286.

Davis, J. (2006), *Pub. Astron. Soc. Australia* **23**, 94.

Davis, J., Ireland, M. J., Chow, J., Jacob, A. P., Lucas, R. E., North, J. R., O'Byrne, J. W., Owens, S. M., Robertson, J. G., Seneta, E. B., Tango, W. J., and Tuthill, P. G. (2007), P*ub. Astron. Soc. Australia* **24**, 138.

European Space Agency (1997), *The Hipparcos Main Catalogue, Hipparcos Epoch Photometry*, URL: http://webviz.ustrasbg.fr/viz-bin/VizieR-S?HIP%2082514

Flower, P. J. (1996), *Astrophys. J*. **469**, 355.

Giménez, A., Clausen, J. V., and Jensen, K. S. (1986a), *Astron. Astrophys*. **165**, 306.

Giménez, A., Clausen, J. V., and Jensen, K. S. (1986b), *Astron. Astrophys*. **159**, 157.

Hagemann, G. (1959), *Mon. Not. R. Astron. Soc*. **119**, 143.

Hogg, A. R. (1951), *Mon. Not. R. Astron. Soc*. **111**, 315.

Kallrath, J. and Milone, E. F. (1999), *Eclipsing Binary Stars – Modeling and Analysis*, Springer Verlag, New York.

Mallama, A. D. (1981), *Publ. Astron. Soc. Pacific* **93**, 774.

Mermilliod, J. C., Hauck, B., and Mermilliod, M. (1997), *Astron. Astrophys. Suppl.* **124**, 349, URL:

http://obswww.unige.ch/gcpd/gcpd.html

Moon, T. and van Antwerpen, C. (2009), *J. Amer. Assoc. Var. Star Obs*. **37(1)**, 3.

Nikolov, A. and Maslev, K. (1987), *Astrophys. Space Sci*. **135**, 283.

Ochsenbein, F., Bauer, P., and Marcout, J. (2000), *Astron. Astrophys. Suppl. Ser*. **143**, 230, URL: http://webviz.ustrasbg.fr/viz-bin/VizieR

Otero, S. and Moon, T. (2006), *J. Amer. Assoc. Var. Star Obs*. **34**, 156.

Pojmanski, G. (2002), *Acta Astronomica* **52**, 397.

Popper, D. M. (1970), *Astrophys. J.* **162**, 925.

Prša, A. (2003), in U. Munari (ed.), *ASP Conf. Ser*. **298**, p.457, San Francisco: ASP.

Prša, A. (2009), URL: http://phoebe.fiz.uni-lj.si/

Prša, A., Guinan, E. F., Devinney, E. J., DeGeorge, M., Bradstreet, D. H., Giammarco, J. M., Alcock, C. R., and Engle, S. G. (2008), *Astrophys. J*. **687**, 542.

Prša, A. and Zwitter, T. (2005), *Astrophys. J*. **628**, 426.

Samus, N. N., Durlevich, O. V., Kazarovets, E. V., Kholopov, P. N., Kireeva, N. N., and Tsvetkova, T. M. (2004), *General Catalogue of Variable Stars*, Vol. IV, Strasbourg Astronomical Data Centre, 4th edition, http://vizier.u-strasbg.fr/

Shobbrook, R. R. (2004), *J. Astron. Data* **10**, 1.

van Antwerpen, C. and Moon, T. (2010), *Mon. Not. R. Astron. Soc.* **401**, 2059.

van Hamme, W. (1993), *Astron. J*. **106**, 2096.

van Leeuwen, F. (2007), *Astron. Astrophys*. **474**, 653, URL: http://vizier.cfa.harvard.edu/vizbin/VizieR?-source=I/311

Wilson, R. E. (1914), *Lick Obs*. **8**, 80.

Wilson, R. E. and Devinney, E. J. (1971), *Astrophys. J*. **166**, 605.

Zasche, P. and Wolf, M. (2007), *Astron. Nachr* **328**, 928.

Table 1. New V and B-V photoelectric measurements of ζ Phe.

HJD	V	B-V	HJD	V	B-V	HJD	V	B-V
2455112.951	4.124	-0.067	2455521.980	4.207	-0.098	2455577.986	4.309	-0.082
2455112.997	4.003	-0.087	2455521.983	4.205	-0.087	2455577.992	4.261	-0.059
2455122.927	4.207	-0.085	2455521.989	4.209	-0.095	2455577.997	4.225	-0.065
2455122.940	4.212	-0.099	2455521.992	4.204	-0.094	2455582.955	4.416	-0.071
2455122.957	4.196	-0.084	2455521.998	4.218	-0.097	2455582.961	4.411	-0.040
2455122.984	4.097	-0.104	2455522.001	4.218	-0.091	2455582.966	4.421	-0.072
2455122.998	4.050	-0.103	2455522.005	4.204	-0.079	2455582.971	4.405	-0.040
2455123.957	3.949	-0.100	2455522.011	4.209	-0.092	2455582.977	4.418	-0.062
2455123.989	3.945	-0.084	2455522.014	4.219	-0.097	2455582.982	4.400	-0.073
2455125.931	3.916	-0.059	2455522.022	4.208	-0.082	2455582.988	4.364	-0.088
2455125.981	3.925	-0.080	2455522.025	4.200	-0.079	2455592.951	4.38	-0.010
2455130.931	3.936		2455522.031	4.207	-0.090	2455592.957	4.392	0.00
2455131.924	3.946		2455522.040	4.186	-0.094	2455592.962	4.397	-0.01
2455140.931	3.937		2455522.046	4.176	-0.098	2455592.968	4.388	-0.01
2455140.964	3.930		2455522.051	4.162	-0.099	2455592.974	4.404	0.00
2455143.937	3.969	-0.110	2455522.057	4.135	-0.095	2455592.98	4.416	0.01
2455143.988	3.957	-0.072	2455522.063	4.111	-0.097	2455592.985	4.399	-0.01
2455144.935	3.926	-0.078	2455522.068	4.097	-0.089	2455592.991	4.397	0.01
2455144.994	3.918	-0.062	2455532.951	4.006	-0.066	2455592.996	4.397	-0.01
2455146.942	3.933	-0.068	2455532.958	4.002	-0.095	2455593.008	4.311	0.04
2455146.974	3.936	-0.061	2455532.970	3.960	-0.107	2455593.017	4.259	0.04
2455166.957	3.944	-0.095	2455532.985	3.933	-0.107	2455600.947	3.93	-0.091
2455171.957	3.939	-0.070	2455532.998	3.941	-0.096	2455605.946	3.934	-0.101
2455172.010	3.949	-0.068	2455533.012	3.954	-0.137	2455608.952	3.963	-0.108
2455172.030	3.957	-0.059	2455551.959	3.94	-0.077	2455611.938	3.93	-0.084
2455172.048	3.970	-0.068	2455551.997	4.044	-0.064	2455916.965	4.212	-0.096
2455172.076	3.972	-0.085	2455552.008	4.089	-0.082	2455916.971	4.179	-0.091

2455173.971	3.982	-0.101	2455552.016	4.128	-0.088	2455916.98	4.116	-0.088
2455178.969	3.992	-0.079	2455552.024	4.148	-0.088	2455916.985	4.092	-0.084
2455185.002	3.932	-0.077	2455552.034	4.192	-0.097	2455916.991	4.068	-0.095
2455185.969	3.921	-0.075	2455552.043	4.188	-0.091	2455917	4.033	-0.103
2455190.970	3.926	-0.086	2455552.049	4.214	-0.078	2455917.009	3.994	-0.097
2455194.967	3.929	-0.080	2455552.055	4.199	-0.090	2455917.015	3.973	-0.087
2455199.969	3.938	-0.085	2455552.062	4.190	-0.091	2455917.021	3.967	-0.097
2455200.965	3.941	-0.097	2455552.068	4.200	-0.103	2455917.027	3.958	-0.083
2455201.966	3.955	-0.104	2455552.077	4.229	-0.119	2455917.032	3.946	-0.073
2455202.964	3.945	-0.085	2455552.083	4.196	-0.081	2455917.038	3.951	-0.088
2455203.977	4.181	-0.087	2455552.092	4.199	-0.084	2455917.044	3.955	-0.099
2455203.995	4.083	-0.080	2455552.101	4.181	-0.099	2455917.05	3.961	-0.093
2455204.008	4.029	-0.103	2455552.108	4.153	-0.098	2455917.055	3.937	-0.087
2455204.020	3.989	-0.113	2455552.114	4.131	-0.094	2455917.069	3.95	-0.076
2455204.029	3.974	-0.108	2455552.961	4.167	-0.078	2455925.087	3.944	-0.067
2455204.041	3.937	-0.067	2455552.972	4.117	-0.088	2455925.093	3.948	-0.083
2455204.046	3.959	-0.093	2455552.986	4.046	-0.095	2455925.099	3.958	-0.093
2455209.966	3.941	-0.077	2455552.999	4.003	-0.102	2455925.11	3.965	-0.109
2455214.987	3.944	-0.097	2455553.015	3.967	-0.090	2455925.116	3.944	-0.089
2455215.965	3.935		2455553.962	3.934	-0.090	2455925.122	3.938	-0.065
2455215.980	3.918		2455557.957	4.266	-0.120	2455925.133	3.941	-0.069
2455215.995	3.931		2455557.965	4.196	-0.092	2455925.14	3.939	-0.074
2455490.966	3.971	-0.114	2455557.974	4.152	-0.089	2455925.147	3.962	-0.082
2455493.959	3.943		2455557.981	4.112	-0.106	2455925.153	3.963	-0.08
2455494.931	3.939		2455557.988	4.066	-0.114	2455950.972	3.921	-0.09
2455494.951	3.927		2455557.995	4.040	-0.100	2455950.979	3.923	-0.086
2455504.932	3.941	-0.097	2455558.002	4.008	-0.112	2455950.988	3.93	-0.04
2455504.957	3.941	-0.095	2455558.008	3.992	-0.090	2455950.999	3.947	-0.106
2455504.977	3.930		2455558.015	3.981	-0.074	2455951.009	3.957	-0.112
2455504.995	3.929		2455558.029	3.947	-0.082	2455951.014	3.953	-0.093
2455517.945	3.970		2455558.056	3.960	-0.098	2455951.02	3.923	-0.079
2455521.950	4.095	-0.089	2455566.964	3.941	-0.083	2455957.954	3.936	-0.076
2455521.957	4.109	-0.082	2455577.957	4.399	-0.080	2455957.96	3.944	-0.097
2455521.963	4.142	-0.097	2455577.964	4.395	-0.061	2455957.966	3.937	-0.076
2455521.968	4.160	-0.089	2455577.969	4.384	-0.086	2455957.972	3.938	-0.076
2455521.972	4.174	-0.092	2455577.975	4.380	-0.095	2455957.978	3.943	-0.079
2455521.978	4.196	-0.102	2455577.980	4.324	-0.088	2455957.983	3.948	-0.075

WD1145+017

Mario Motta, MD, AAVSO
19 Skipper Way
Gloucester, MA 01930
mmotta@massmed.org

Abstract

WD1145 is a 17th magnitude white dwarf star 570 light years away in Virgo, that was discovered to have a disintegrating planetoid in close orbit by Andrew Vanderburg a graduate student at Harvard CFA, while data mining the Kepler 2 mission. He contacted me to obtain transit data to elucidate the nature of its rather bizarre transit light curves. I obtained multiple observations of WD1145 over the course of a year, and found a series of complex transit light curves that could only be interpreted as a ring complex or torus in close orbit around WD1145. Combined with data from other amateur astronomers, professional observations, and satellite data it became clear that WD1145 has a small planetoid in close orbit at the Roche limit and is breaking apart forming a ring of debris material that is then raining down on the white dwarf. The surface of the star is "polluted" by heavy metals by spectroscopic data. Given that in the intense gravitational field of a white dwarf any heavy metals could not for long last on the surface, this confirms that we are tracking in real time the destruction of a small planet by its host star.

If someone had told me 20 years ago, I would someday be documenting the destruction of a small planet around a white dwarf star, I would've considered that a flight of fantasy. Yet, nowadays, I and a number of amateur astronomers are accomplishing that and much more. WD1145+017, is a 17th magnitude white dwarf star in the constellation Virgo near the Leo border, 570 light years away. This white dwarf is in the process of destroying and devouring one or more of its planet "children"

When the Kepler satellite lost the second of its four of its reaction wheels back in May of 2013, it could no longer continue to point steadily at its assigned field with the high precision needed for its original mission. Therefore NASA undertook a modified plan that could still use the satellite to perform science within its limitations of a slow drift. In November of 2013, the new Kepler 2 mission was announced with several fields chosen along the ecliptic plane, field 1 being the Virgo-Leo area. Due to the inherent small drift caused by the malfunction of its reaction wheels it would not have the same high precision of the original Kepler mission, but could continue to collect valuable scientific data of transiting planets around distant stars. On March 21, 2015, Andrew Vanderburg, a Harvard astrophysics-graduate student, was reviewing data from the K2 mission and found that WD 1145 had a most unusual photometric signal. He arranged for observational follow-up to be made at 1.2 meter telescope at the Whipple Observatory in Arizona, and on April 11, 2015 found WD1145's transits similar in nature to what had previously been reported from disintegrating planets around main sequence stars by Dr. Saul Rappaport of MIT. Andrew quickly realized that the bizarre photometric signal from WD1145 was similar to the data that Saul Rappaport previously reported. This however would be the first time a disintegrating planet would be documented around a white dwarf star.

White dwarf (WD) stars are the extremely compact dense cores of stars at the end of their evolutionary life. White dwarfs are what are left after extensive mass loss of old evolved stars, after they have shed their outer layers that result in spectacular planetary nebulae displays. The helix nebula is a fine example of that, showing the mass loss of an expanding shell, and the remnant core of the star, a newly formed white dwarf in the center. The mass loss during this process can be from one third up to 75% of the mass of the star. Any planetary system in orbit, however, would still retain its original orbital momentum. With the mass loss, the planets that had been in stable orbit would migrate out. Planetary systems, such as our solar system, remain stable over billions of years because they have settled into stable orbits after an initial chaotic formation time with multiple interactions. With the out migration of the planetary system, the remaining planets are now thrown into new chaotic planetary orbits that lead to multiple planetary interactions. Some interactions will fling planets out of the system; others may force a small planet inward as must've occurred in the case of WD1145.

Although we have seen evidence for debris remnants on the surface of WD's before, with

WD1145 we are witnessing a star destroying a planet and having fragments of that disintegrating planet "rain down" onto the white dwarf surface in real time, a never before seen event.

White dwarf stars have an extremely intense surface gravity due to their compact nature, and therefore any "metals" should sink to the center over a relatively short period of time. Yet many white dwarfs on spectral analysis have been shown to have their surface "polluted" with heavy metals, such as iron, magnesium, aluminum, and silicon. Vanderburg's co-authors Warren Brown and Patrick Dufour demonstrated that this was also the case with WD1145 using data from the MMT telescope on Mount Hopkins. It had been theorized that white dwarfs with heavy metals on their surfaces must have been rained down on by leftover planetary disc material such as planets to account for this spectral anomaly. With WD1145, Andrew Vanderburg had found the "smoking gun" of a planet disintegrating and raining down on the white dwarf star that confirms this assumption.

What appears to be occurring at WD1145 is that a small planet no larger than the planetoid Ceres has spiraled in and is currently in orbit at a distance of only 500,000 miles above the surface of the white dwarf, roughly twice the distance of the Earth moon separation. At this remarkably close distance the planet faces intense heat from the star, and has reached the Roche limit where intense tides within the planet are ripping it apart. It is so close, that the planet is whipping around the star completing an orbit in only 4.5 hours. At this speed and separation, given that a white dwarf core is not much larger than the size of the Earth; a transit should last on the order of a minute or so. What is seen however are multiple transits that vary in photometric depth and duration, and that evolve from week to week. This implies an expanding cloud of debris, similar to a coma around a comet. Throughout the 4.5 hour “year” there are fluctuations in the photometric signal of WD1145, indicating the likelihood of a debris ring of material in orbit around the star.

Andrew realized early on that he would need to enlist a number of professional and amateur observers to collect enough data to properly study this unusual and scientifically interesting star. He therefore collaborated with other investigators such as Bryce Croll at Boston University, and a few advanced amateurs such as Bruce Gary, Tom Kaye, and myself to obtain enough data to properly analyze this object. Andrew contacted me in the summer of 2015, came over to my home and 32 inch telescope and observatory in Gloucester Massachusetts, where we discussed this fascinating system. We tested my telescope's capabilities on some other transiting systems at the time. WD1145 is a 17th magnitude star, and given the rapid transit time predicted, he required one minute cadences of data collection to capture the granularity of details of the orbiting debris field. Although the Kepler satellite boasts a 1 meter telescope, it images on 30 minute cadences, smearing out the fine detail needed to truly understand this fascinating object.

Virgo is not observable until winter and spring from New England, but of course as luck would have it New England had a very cloudy winter of 2016, therefore I was not able to start collecting data until March of 2016. Fortunately Andrew had other advanced amateurs in parts of the world with better weather who were also collaborating and were able to collect data in January and February such as Bruce Gary. My data from March 30 of 2016 (Figure 1) is illustrative and interesting shows an initial sharp depression caused by the transit of the planet itself, but a much deeper photometric depression than would be expected for such a small body.

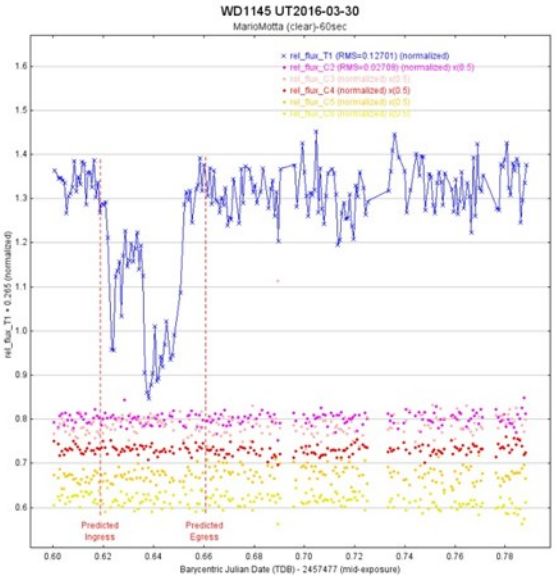

Figure 1: UT 2016-03-30 photometry (clear filter, 60 sec exposures).

This implies that a "cloud" of material surrounds the small planet itself leading to a substantially larger obscuration of the parent star. It is followed by an even deeper flux depression in a very wide transit interpreted as a large trailing cloud of debris expanding in size. Note that the rest of the orbit indicates wide fluctuation in light flux intensity indicating the likelihood of a debris field that has

formed a complete ring around WD1145. The control stars shown on the graph are very steady in comparison, showing that this fluctuation has nothing to do with error or atmospheric effects. Compare these wild fluctuations of WD1145 to a typical transit profile and you immediately see what drew Andrew's initial attention to this object. Instead of the typical transit event flux drop of a few milli-magnitudes, with WD1145 you have up to a 70% drop in light output during its transits! Interestingly, the transits were only about 1% deep in the Kepler light curve. This is partially because they were smeared out by the 30 minute exposures, and partially because the transits were just not as deep in summer 2014 when Kepler was observing WD 1145.

Viewing a sequence of additional transits over the course of two months, one can see the dramatic changes in transit depth and shape, indicating the dynamic nature and continual evolution of the debris field as it is disrupted from the planet body, and eventually falls onto the surface of the star. (Figures 2-6) We are witnessing in real time the destruction of this planet. Given the small size of this planet, this situation is not likely to last much longer.

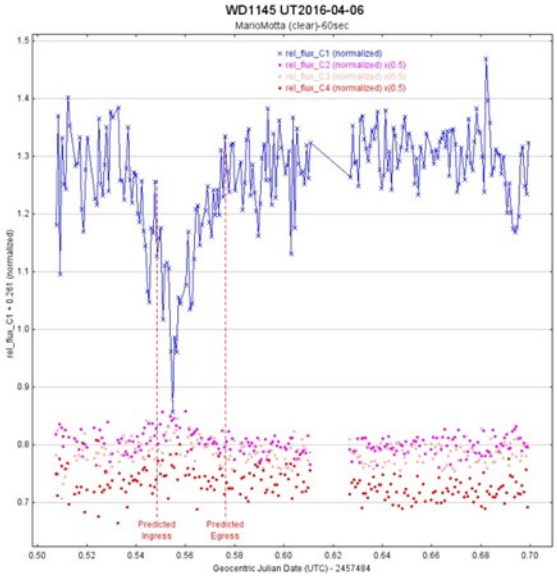

Figure 2: Photometry UT 2016-04-04

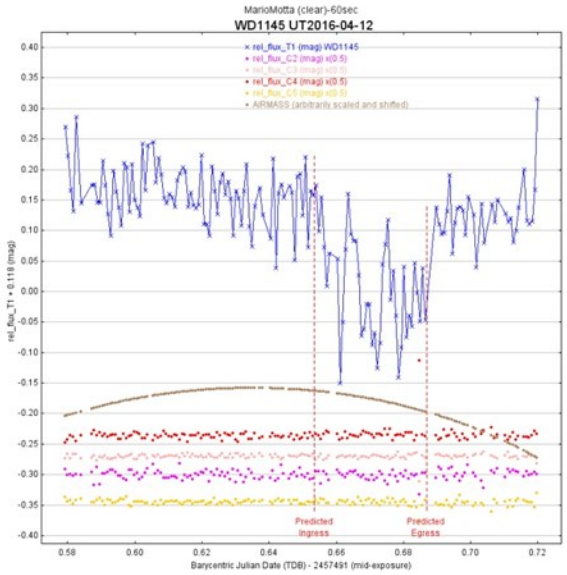

Figure 3: Photometry UT 2016-04-12

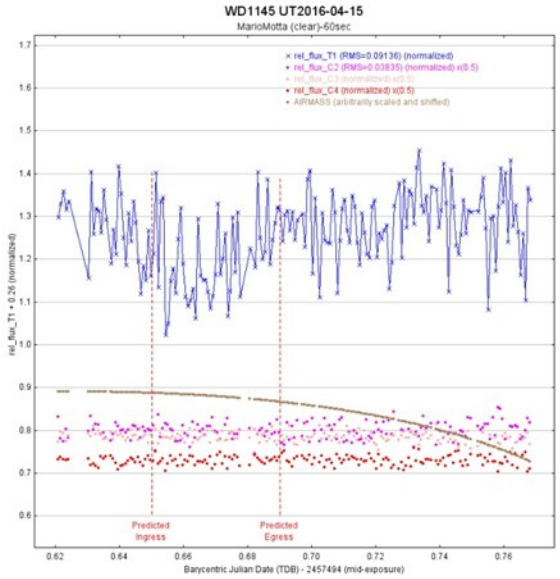

Figure 4: Photometry UT 20016-04-15

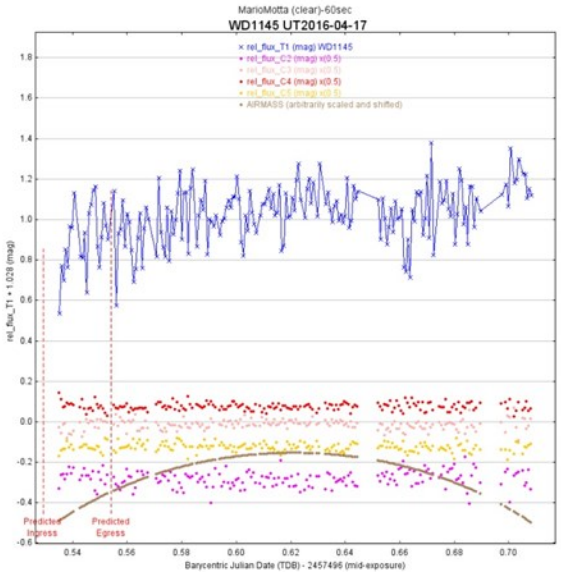

Figure 5: Photometry UT 2016-04-17

During my last spring season observation on May 31 2016 (Figure 7) before lost behind the sun for the summer and fall, there seemed be very little activity.

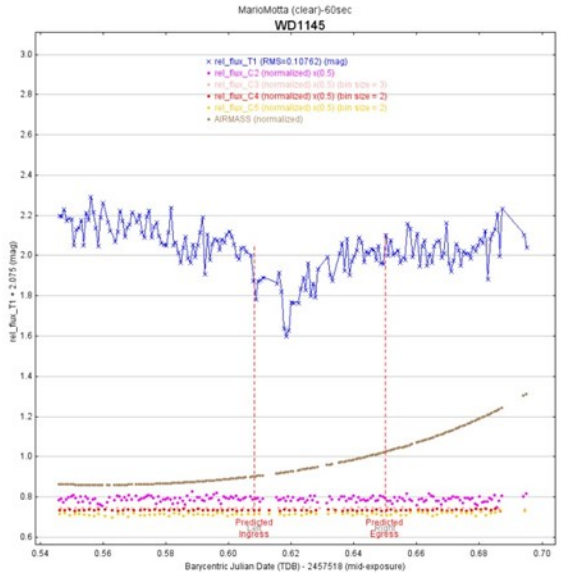

Figure 6: Photometry UT 2016-05-10

Much to my surprise, in late November of 2016, Bruce Gary was first to find renewed activity of WD1145! I was not able to get good data until December 26 when weather cleared in New England, and sure enough either there is new disruption of this planetoid, or it is possible another small body is now being destroyed (Figure 8) On February 17 of 2016, (Figure 9) I was able to collect data simultaneously with the Hubble telescope, with Hubble collecting UV light, and myself using clear filter, to help determine particle size. A paper will be soon be published on this set of observations by the Harvard CFA.

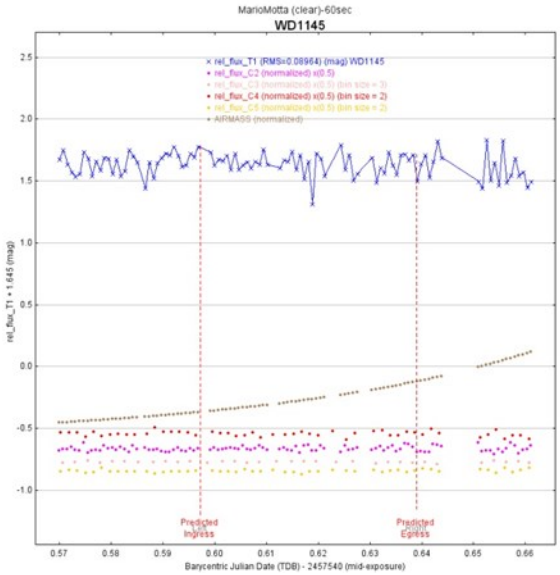

Figure 7: Photometry UT 2016-06-01

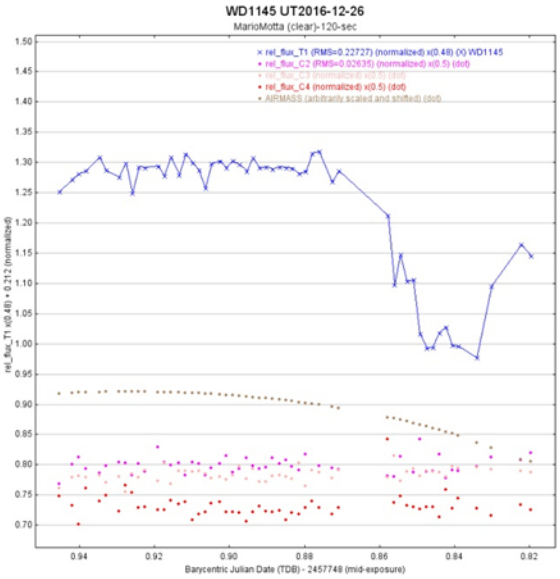

Figure 8: Photometry UT 2016-12-26

More observations will be collected over time to demonstrate the continuing evolution of the WD1145 system. To collect the vast volume of data that is needed to properly analyze this system, however, scientists like Vanderburg, Croll, and Rappaport are dependent on an extensive professional-amateur

collaboration. Pro-am collaborations have proven essential as more discoveries are made and data is requested, and continues to expand exponentially as more exoplanets are found. Beyond WD 1145, as of this writing well over 3500 exoplanets have been verified, with many of them needing follow-up observations, and many more in the pipeline to be verified and catalogued. This is where the value of a worldwide network of amateurs can contribute greatly to science, using equipment they already possess. There are several collaborative projects under way, all of which would welcome further amateur contributors. A particularly useful way to start would be to contact the American Association of variable Star observers (AAVSO), and join the exoplanet section, headed by Dennis Conti, or join the KELT collaboration. An amateur with imaging and variable Star skills, already has the skill set to contribute incredibly useful data to science.

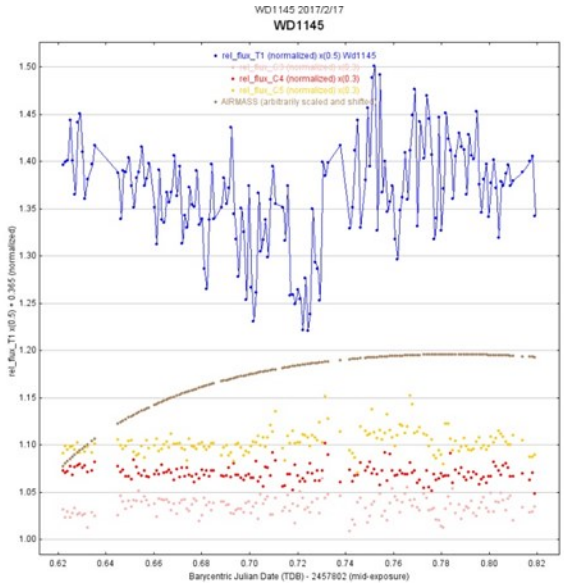

Figure 9: Photometry 2017-02-1

Spectrophotometry of Symbiotic Stars

David Boyd
5 Silver Lane, West Challow, Wantage, OX12 9TX, United Kingdom
davidboyd@orion.me.uk

Abstract

Symbiotic stars are fascinating objects – complex binary systems comprising a cool red giant star and a small hot object, often a white dwarf, both embedded in a nebula formed by a wind from the giant star. UV radiation from the hot star ionises the nebula producing a range of emission lines. These objects have composite spectra with contributions from both stars plus the nebula and these spectra can change on many timescales. Being moderately bright, they lend themselves well to amateur spectroscopy. This paper describes the symbiotic star phenomenon, shows how spectrophotometry can be used to extract astrophysically useful information about the nature of these systems, and gives results for three symbiotic stars based on the author's observations.

What are symbiotic stars?

In 1932 Merrill and Humason at Mt Wilson Observatory reported that three stars, AX Per, RW Hya and CI Cyg, had unusual "combination spectra" containing strong hydrogen Balmer and ionised helium emission lines. These lines were similar to those seen in planetary nebulae and indicative of a hot ionising source, and were superimposed on a continuum showing the TiO molecular absorption bands usually associated with cool M-type stars. Research showed that both AX Per and CI Cyg had experienced two outbursts within the previous 30 years. Over the next decade, about two dozen variables showing similar combination spectra were identified. The variable Z And was adopted as the prototype for this new class of objects whose variability was found to be unpredictable on timescales from minutes to years. Merrill coined the term "symbiotic" stars in view of what appeared to be an unusual and apparently close relationship between a cool red star and a hot companion.

After debate over many years, it is now generally accepted that symbiotic stars are wide, long-period binary systems comprising a cool red giant star, usually but not always M-type, and a small hot companion, usually but not always a white dwarf, with both stars immersed in a nebula created by a wind from the giant star. Their spectra show molecular absorption features arising in the photosphere of the cool star and strong nebular emission lines of H I, He II and forbidden lines of [O III], [Ne III], [Ne V] and [Fe VII] as UV radiation from the hot white dwarf ionises the nebula. The spectra of many symbiotic systems also show two broad emission features at 6825 Å and 7088 Å, features which are only seen in symbiotic stars with high-excitation nebulae. These are due to Raman scattering of the O VI 1032 and 1038 Å resonance lines by neutral hydrogen close to the cool giant star (Schmid 1989).

Most catalogued symbiotic stars contain normal giant stars and have orbital periods in the range 1 to 10 years. These constitute ~80% of symbiotics and are classified as S-type (stellar). The giant stars in some of these may exhibit semi-regular variability due to stellar pulsation. The other ~20% contains Mira variables surrounded by dust shells and may show evidence of dust in their spectra. They are referred to as symbiotic Miras and are classified as D-type (dusty). They typically have orbital periods ten times longer than S-type systems and show regular photometric variation due to Mira-type pulsation. The symbiotic phase is believed to be a relatively short stage (~10^6 years) in the life of these binary systems.

A comprehensive catalogue of recognised and suspected symbiotic stars was published by Belczynski et al. (2000). More recently a catalogue with almost twice as many confirmed and candidate symbiotic stars has been presented by Akras et al. (2016).

What do we know about symbiotic stars?

A relatively small proportion of the giant's hydrogen-rich wind is attracted gravitationally onto the surface of the white dwarf and if the temperature and pressure at the bottom of this layer is high enough the hydrogen may undergo quasi-steady nuclear fusion burning. This heats the white dwarf to a temperature in excess of 10^5 K with a luminosity of ~10^3 $L_\odot$. X-ray and UV radiation from the hot white dwarf ionises a segment of the nebula generating strong emission lines. Because of pressure of the wind from the giant star, this preferentially happens in the direction away from the giant star (see Figure 1). If the material aggregating onto the white dwarf

surface is not ignited the white dwarf remains cooler, there is less ionisation of the nebula, and any emission lines are much weaker. In these circumstances the cool star tends to dominate the spectrum.

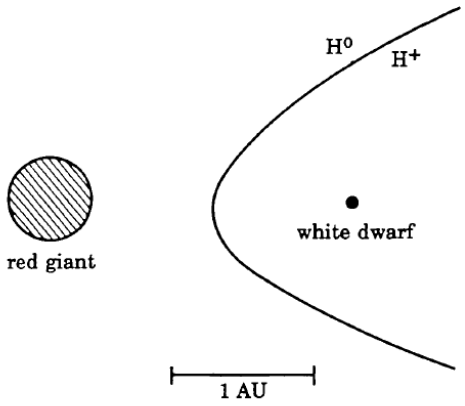

Figure 1. This shows a possible extent of the neutral and ionised nebula relative to the cool and hot stars in a symbiotic system. The neutral part of the nebula is marked H0, the ionised part H+. Diagram adapted from Kenyon (1990).

If there is a build-up of hydrogen-rich material on the surface of the white dwarf not consumed by steady burning this can lead to a thermonuclear runaway eruption called a symbiotic nova. This is similar in principle to a classical nova explosion but in a symbiotic nova the process may happen more slowly with the rise taking many months and the eventual decline back to quiescence taking decades. Some symbiotic stars have been seen to have more than one nova explosion and these are referred to as recurrent symbiotic novae. The behaviour of symbiotic novae appears to be correlated with the white dwarf mass. The more massive the white dwarf, the faster, brighter and more frequent the symbiotic nova explosions. Overall, less than ten percent of symbiotic stars have been seen to experience nova explosions.

Symbiotic stars may be potential progenitors of type 1a supernovae if a built up of material over time leads to the white dwarf mass reaching the Chandrasekhar Limit ($1.4M_{\odot}$). In the long run, many symbiotic stars will evolve to double white dwarf binaries whose components may merge to create type 1a supernovae.

Many symbiotic stars experience outbursts, referred to as classical symbiotic outbursts, in which the star brightens by a few magnitudes in a matter of weeks and then slowly fades over many months. They recur on a frequency of approximately a decade. These events are less powerful than symbiotic novae and the reason they happen is still not understood, although possible mechanisms including increased nuclear shell burning and thermal instability in an accretion disc have been proposed.

Accretion discs form around the white dwarf in many symbiotic stars. Thermal instability in the disc can lead to an outburst similar to what happens in a cataclysmic variable but in symbiotic stars with large binary orbits the accretion disc may grow much larger than in a short period cataclysmic variable causing the outburst to last much longer. Symbiotic stars with an accretion disc may also exhibit flickering due to the stochastic nature of the accretion process. In some symbiotic stars the tenuous outer atmosphere of the giant star fills its Roche lobe and loses material through the L1 Lagrange point leading directly to the formation of an accretion disc around the white dwarf. The light output of a symbiotic star may also be modulated at the orbital period by heating of the surface of the giant star facing the white dwarf.

A small number of symbiotic stars have been observed to produce collimated jets in which material is expelled at high velocity in opposite directions at approximately right angles to the plane of the disc. The formation of jets in symbiotic stars is not fully understood but appears to be related to the presence of both an accretion disc and a strong white dwarf magnetic field. These jets are transient, appearing during or soon after an outburst and then fading over many months.

In practice symbiotic stars show a wide range of behaviour and, as Scott Kenyon says in his book *The Symbiotic Stars*, “The outbursts of symbiotic stars have generally attracted much attention, and each eruption is a new adventure in complexity.” (Kenyon 1986).

Symbiotic stars involve many of the physical processes currently at the forefront of astrophysical research including accretion discs, high velocity jets, mass transfer, colliding winds, soft and hard X-ray emission, and the evolution of binary systems. They are the subject of ongoing research and therefore need to be kept under surveillance. This is where amateurs have a valuable role as they can potentially achieve more persistent coverage of these objects using their own equipment than professional astronomers who have to share access to large telescopes on a competitive basis.

It is clear from the above that symbiotic stars enjoy a rich diversity of behaviour. Later in this paper I will describe my observations and analysis of three symbiotic stars but first I should explain how I collect this data.

Observing symbiotic stars

Spectrophotometry of symbiotic stars involves using a combination of photometry and spectroscopy to measure their brightness in standard magnitudes and their spectral energy distribution in absolute flux units. This provides information about their behaviour which is of direct use to professional astronomers trying to develop a better understanding of these fascinating objects.

My spectra are recorded with an equatorially-mounted 0.28m SCT equipped with a LISA spectrograph from Shelyak Instruments fitted with a SXVR-H694 imaging camera and SXV-EX guider, both from Starlight Xpress. Camera control and mount guiding are performed with the software Astroart. A second equatorially-mounted 0.35m SCT scope equipped with Astrodon BVRI filters with known spectral profiles and a SXVR-H9 camera is used to take a short series of B and V images of the symbiotic star field concurrently with recording the spectra. Differential aperture photometry performed on these images with respect to an ensemble of nearby stars with known B and V magnitudes produces instrumental magnitudes of the symbiotic star which are then transformed to B and V magnitudes on the Johnson-Cousins standard photometric system (Boyd 2012). These magnitudes are routinely uploaded to the AAVSO and BAA variable star databases (AAVSO, BAA).

Spectra are bias- and dark-subtracted, flat-fielded, sky-subtracted and wavelength-calibrated using Argon-Neon lamp spectra taken before and after each series of symbiotic star spectra. They are then corrected for instrumental and atmospheric losses by recording spectra of a reference star with known spectral profile, typically from the MILES Spectral Library (MILES), as close as possible in altitude and close in azimuth to the symbiotic star.

In preparation for generating absolute flux spectra of symbiotic stars, absolute flux spectra of a number of spectrophotometric standard stars from the CALSPEC Calibration Database (CALSPEC) were convolved with the profile of my V filter to find the absolute flux transmitted by this filter and hence its spectroscopic zero point which enables conversion of a V magnitude to an absolute flux. A measured relative flux spectrum of the symbiotic star convolved with the spectral profile of the V filter gives the relative flux transmitted by the V filter. Knowing the V magnitude of the symbiotic star, its relative flux spectrum can be scaled to produce an absolute flux spectrum in ergs/cm^2/s/Å. This is the spectrum that would be measured by a perfect detector above the atmosphere.

An estimate of the accuracy of these absolute flux calculations can be made by comparing them with published absolute flux spectra. Since comparing spectra taken at exactly the same time is generally not possible this can only be an approximate check but indicates that flux measurements made in this way have an accuracy of approximately 10%.

Depending on the direction and distance of the symbiotic star, interstellar extinction and reddening may significantly affect its spectrum. A correction for this can be applied based on the colour excess parameter E(B-V) and is calculated here using the parameterisation of extinction given by Cardelli et al. (1989). Values of E(B-V) for extinction in the visible region of the spectrum for many symbiotic stars are published in Parimucha & Vanko (2006). This finally gets us as close as possible to the spectrum actually emitted by the symbiotic star.

One of the challenges in observing these systems is the long timescale involved in some of these changes so regular monitoring and archiving of spectra is necessary. My symbiotic star spectra are routinely uploaded to the ARAS database (ARAS). Sudden and unpredictable changes do occur in some systems. These are usually detected first in optical photometry but could easily be missed if they are not observed regularly.

Analysis of three symbiotic stars

Below I present results of analysing spectra of three symbiotic stars. They are all bright enough to yield astrophysically useful information with amateur equipment. A rich resource of amateur observations is available in the ARAS database for anyone wishing to undertake their own analysis of any of these stars and many others.

One source of information about symbiotic stars comes from measuring the flux of their emission lines. According to the method originally described in Iijima (1981) and quoted more accessibly in Sokoloski et al. (2006), the temperature of the hot ionising source in a radiation-bounded nebula can be calculated by measuring the flux of the He I (4471), He II (4686) and Hβ lines. The He I (4471) line flux is usually assumed to be zero as it is very much weaker than He II and Hβ. Several other methods have been proposed for calculating the hot source temperature. These do not always give consistent results so there is some uncertainty about the absolute accuracy obtained by any particular method. However results obtained using the same method should be internally consistent and give a good indication of the relative variation of the hot source temperature over time.

AX Persei

AX Per is an S-type eclipsing symbiotic star consisting of an M4.5 III red giant star and a hot component, probably a white dwarf, that may occasionally be surrounded by an accretion disc. Leibowitz & Formiggini (2013) give the orbital period as 681.48 ± 0.43 days based on their analysis of 125 years of data with early measurements coming from Harvard photographic plates. However they note that the time between individual minima may vary by tens of days from this value so the minima are clearly not attributable to a purely geometrical eclipse. They suggest this apparent irregularity is due to oscillations in the red giant star and its wind which in turn affect the accretion process onto the hot component and eventually the light output of the system.

Figure 2 shows the visual light curve from the AAVSO database (AAVSO) for the last 50 years showing a distinct orbital modulation. There are several occasions during this period when the system brightened by up to 3 magnitudes above quiescence. The last such period of brightening began in 2009 with higher than normal peaks in 2009, 2012, 2014 and 2016. According to Skopal et al. (2011), the accretion disc forms during periods of enhanced activity but disappears during quiescence. The current orbital amplitude of 2 magnitudes is larger than its quiescent range so it appears that the current period of enhanced activity is continuing. Figure 3 presents (a) the AAVSO V magnitude light curve of the star from July 2014 to the present showing two minima and (b) these minima phased on the ephemeris in Skopal et al. (2011) demonstrating the variability in timing and depth of eclipses noted by Leibowitz & Formiggini (2013). According to Skopal et al. (2011) phase 0 corresponds to inferior conjunction of the giant star and therefore eclipse of the region around the hot component.

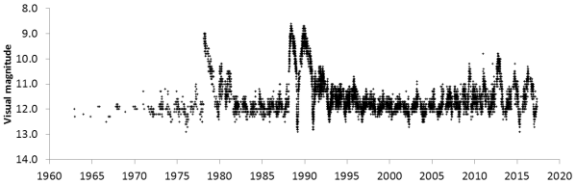

Figure 2. AAVSO visual light curve of AX Per from 1965 to the present.

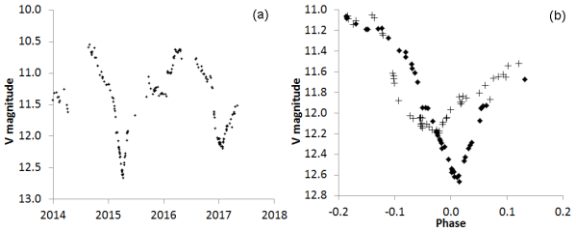

Figure 3. (a) AAVSO V magnitude light curve of AX Per from July 2014 to the present showing two minima, and (b) these two minima phased on the ephemeris in Skopal et al. (2011).

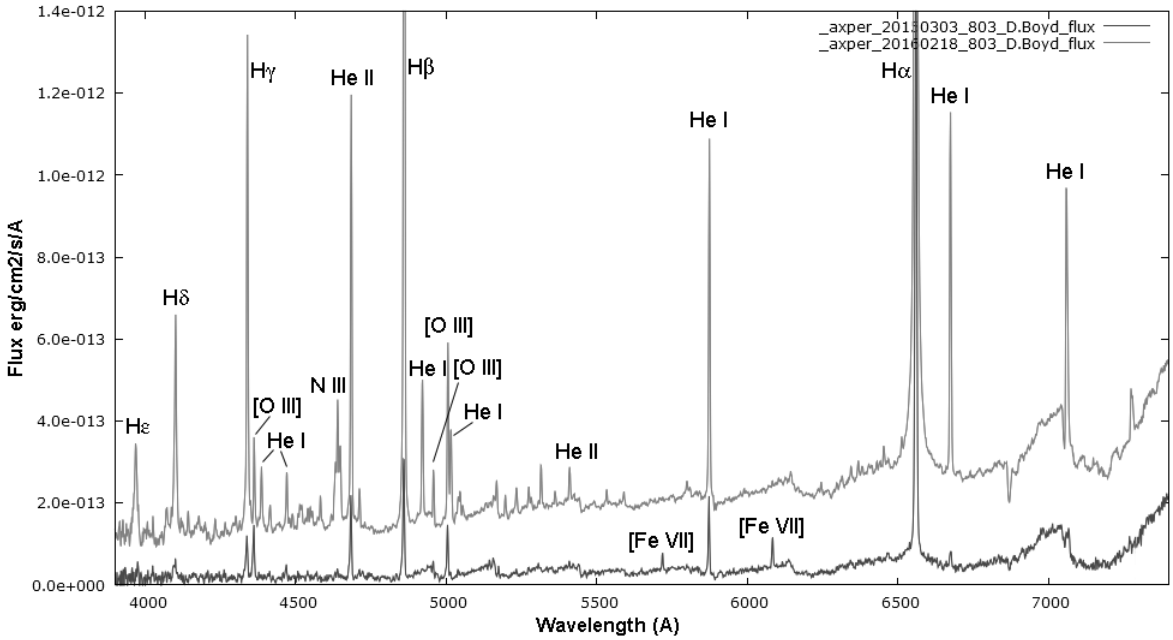

Figure 4. Two absolute flux spectra of AX Per, the lower one recorded on 3 March 2015 during eclipse at orbital phase 0 and the upper one on 18 February 2016 at orbital phase 0.5. Prominent emission lines are identified.

Between January 2014 and March 2017 I recorded 42 absolute flux spectra of AX Per. In all cases flux was calibrated using concurrently measured V magnitudes as described earlier. Figure 4 compares two absolute flux spectra, the lower one recorded in March 2015 during eclipse at orbital phase 0 and the upper one in February 2016 at orbital phase 0.5. In the latter case the continuum level has increased and there are prominent emission lines of H I, He I, He II, N III and [O III]. This is consistent with phase 0.5 being superior conjunction of the giant star at which time the ionised region of the nebula will be facing us. In eclipse at phase 0 many of these lines fade or disappear, the strength of the [O III] lines relative to the H I lines grows, and [Fe VII] lines at 5721 Å and 6087 Å appear. In neither spectrum was there any sign of the broad emission features at 6825 Å and 7088 Å due to Raman scattering of O VI resonance lines.

Line fluxes were corrected for interstellar extinction and reddening with E(B-V) = 0.24 from Parimucha & Vanko (2006). Figure 5 shows that the Hα line flux varies by a factor five over the orbit reaching maximum around orbital phase 0.5. This is consistent with the prominence of emission lines in the spectrum at this phase.

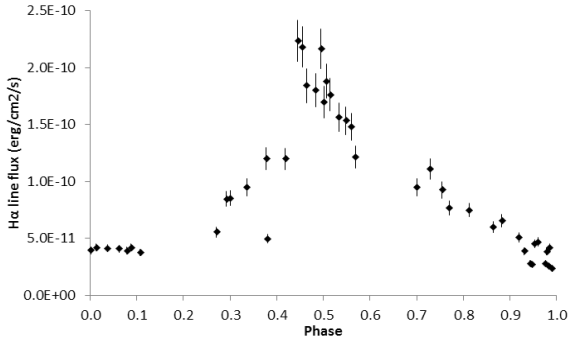

Figure 5. Variation of Hα line flux in AX Per with orbital phase using the ephemeris of Skopal et al. (2011).

Using Iijima's method based on the He II/Hβ line flux ratio (assuming the nebula is radiation-bound) to calculate the variation of hot source temperature with orbital phase gave the results in Figure 6. The hot source temperature varied between ~190,000 K at orbital phase 0 and ~130,000 K at phase 0.5. If the Iijima formula is valid in this case, this indicates the temperature of the hot source is higher when it is on the far side of the giant star in eclipse than half an orbit later when it is closer to us. This is unexpected.

According to Mürset & Nussbaumer (1994) a proxy for the radiation temperature of the hot source is 1000 χ_{max} where χ_{max} is the maximum observed ionisation energy. In the spectrum of AX Per the ion with the highest ionisation energy (125ev) is [Fe VII] indicating a temperature of the hot source of at least 125,000 K, consistent with the minimum temperature above. Figure 7 shows how the [Fe VII] line flux varies with orbital phase. This variation is similar to Figure 6 and also indicates that the largest flux corresponding to the hottest temperature occurs close to phase 0.

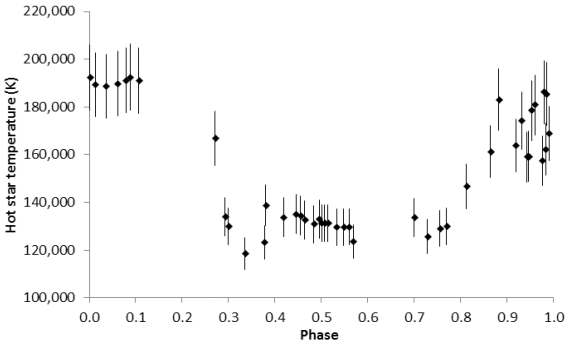

Figure 6. Variation of hot star temperature in AX Per calculated by the method in Iijima (1981) with orbital phase using the ephemeris of Skopal et al. (2011).

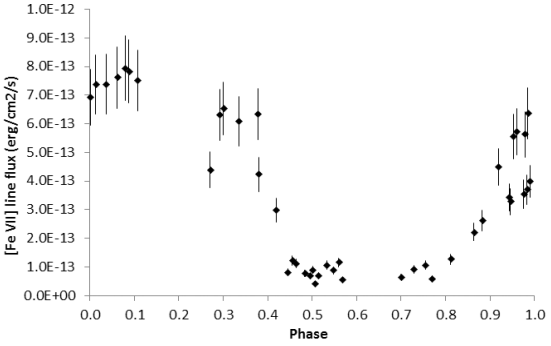

Figure 7. Variation of [Fe VII] line flux in AX Per with orbital phase using the ephemeris of Skopal et al. (2011).

V694 Monocerotis

V694 Mon (= MWC 560) is another S-type symbiotic star consisting of an M4-type red giant star and a hot component comprising a white dwarf and bright accretion disc. The luminosity of the disc indicates it is being well fed by accretion from the wind of the giant star and is the main source of the strong emission lines. A high velocity jet is being emitted towards us along our line of sight.

First noted in 1943 as an emission line object with deep blue-shifted absorption features, it caused excitement in the professional community when it suddenly brightened by several magnitudes in 1990. At this point the amateur community also began monitoring the star. Figure 8 shows the AAVSO

visual light curve from 1990 to the present. Another even brighter outburst occurred in 2016.

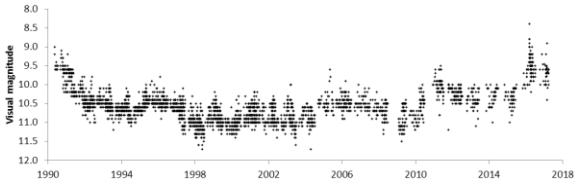

Figure 8. AAVSO visual light curve of V694 Mon from 1990 to the present showing a bright outburst occurring in 2016.

Period analysis of magnitude measurements of V694 Mon going back to 1928 by Leibowitz & Formiggini (2015) found a period of 1943 days. Other analyses found similar periods with a spread of about 5%. Munari et al. (2016) argued this is too long for the orbital period of a system in which the giant star appears to be filling its Roche lobe and sustaining a high mass transfer rate to the accretion disc. Uncertainty about the binary period has been attributed to the system having a low orbital inclination and this is consistent with the failure so far to find a spectroscopic orbital period.

I recorded V magnitudes and absolute flux spectra of V694 Mon on 21 dates in 2015, 2016 and 2017. My observing season for V694 Mon is short because, at a declination of -8°, it never rises higher than 30° above my southern horizon. Extra care is necessary when correcting for atmospheric extinction to ensure that the reference star used is at the same altitude as V694 Mon. The light curve of V 694 Mon shows persistent flickering, normally evidence of the accretion process.

Figure 9 compares spectra taken in February 2015 before the recent outburst and at the peak of the outburst in February 2016 when the spectral flux had increased by a factor of 3.7. The continuum and emission lines are primarily from the hot accretion disc with faint evidence of TiO bands from the red giant beyond Hα. The narrow emission lines of H I and Fe II, plus fainter lines of other singly ionised metals, have wide, blue-shifted troughs caused by absorption within the jet coming towards us. The flux levels at the bottom of the absorption troughs of the Balmer lines are very similar before and during the outburst, indicating that these absorptions may well be saturated. As the outflow velocities within the jet change, so the profile and blue-shift of the absorption troughs also change, sometimes over just a few days.

Figure 10 shows how the absorption troughs of the Hβ and Fe II lines changed between 14 and 20 March 2017. Radial velocities in the jet can be estimated from the wavelengths of the blue and red edges of the Hα and Hβ absorption troughs relative to the rest wavelengths of these lines. These are listed in Table 1 and have estimated uncertainties of ±75 km/s. Jet velocities were substantially higher during the outburst in 2016. No corrections have been applied for the Earth's heliocentric motion, typically -10 to -25 km/s during the V694 Mon observing season, or the systemic velocity of +37 km/s.

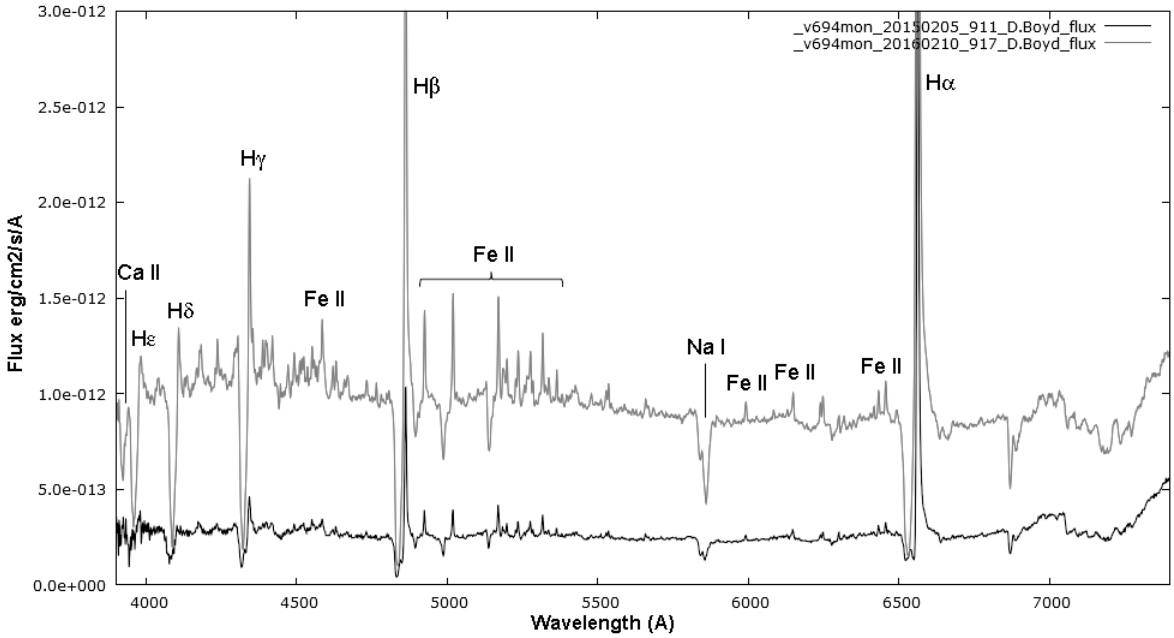

Figure 9. Absolute flux spectra of V694 Mon on 5 February 2015 before the recent outburst (lower) and at the peak of the outburst on 10 February 2016 (upper) with the prominent emission lines identified.

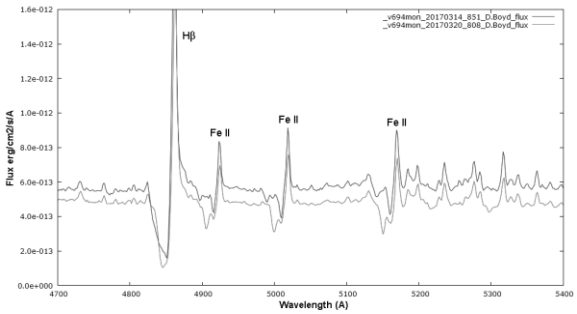

Figure 10. Changes in the absorption troughs of Hβ and Fe II lines between 14 March 2017 (upper) and 20 March 2017 (lower).

	Hα absorption trough (km/s)		Hβ absorption trough (km/s)	
Date	Blue edge	Red edge	Blue edge	Red edge
05-Feb-15	-2536	-391	-2884	-373
08-Feb-15	-2711	-444	-3270	-445
09-Feb-15	-2743	-454	-3289	-451
21-Feb-15	-1678	-348	-2302	-280
26-Feb-15	-1480	-377	-2172	-312
04-Mar-15	-1537	-468	-1989	-434
08-Apr-15	-1617	-383	-2152	-319
20-Jan-16	-2927	-335	-3365	-254
03-Feb-16	-2888	-420	-2980	-369
10-Feb-16	-3003	-617	-3301	-469
14-Feb-16	-3064	-637	-3328	-496
18-Feb-16	-3039	-776	-3349	-461
23-Feb-16	-3058	-713	-3376	-432
28-Feb-16	-3099	-590	-3375	-376
07-Mar-16	-3021	-512	-3437	-271
17-Mar-16	-3059	-467	-3322	-322
25-Mar-16	-2924	-621	-3140	-363
05-Feb-17	-1697	-462	-2204	-371
13-Feb-17	-2021	-498	-2141	-309
18-Feb-17	-2006	-484	-2289	-401
02-Mar-17	-1504	-475	-2111	-278
14-Mar-17	-2003	-481	-2174	-396
20-Mar-17	-1536	-384	-2154	-322
06-Apr-17	-1606	-454	-2192	-248

Table 1. Radial velocities of the blue and red edges of the absorption troughs of Hα and Hβ relative to the rest wavelengths of these lines.

Line fluxes were corrected for interstellar extinction and reddening using E(B-V) = 0.15 from Schmid et al. (2001). Figure 11 shows (a) the Hα line flux in 2015, 2016 and 2017 with a sharp peak lasting only 3 weeks during the 2016 outburst, and (b) the relationship between Hα line flux and V magnitude over the same period. The outburst appeared to follow the general trajectory of this relationship. The B-V colour index did not change during the outburst suggesting the rise in luminosity was due to an increase in the size of the accretion disc and not its temperature.

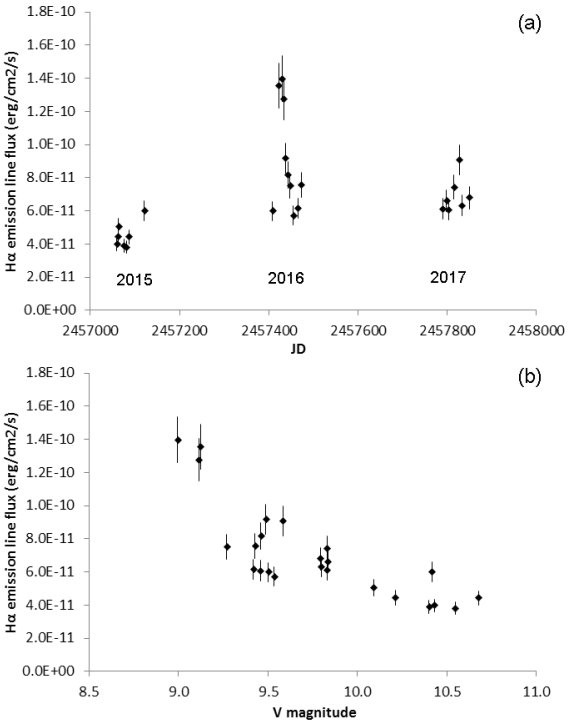

Figure 11. (a) Hα line flux in V694 Mon in 2015, 2016 and 2017, and (b) relationship between Hα line flux and V magnitude over the same period.

Astrophysically, V694 Mon is a particularly interesting object because of its complex jet structure which we observe almost end-on. The contribution of amateurs in collecting data on the object is therefore especially important.

V1329 Cygni

V1329 Cyg (= HBV 475) is now recognised to be a symbiotic nova comprising an M4-type giant star, a white dwarf and a surrounding nebula. Prior to 1964 it was an apparently normal 15th magnitude eclipsing variable with minima at least 2 magnitudes deep (Schild & Schmid 1997). Our line of sight is therefore approximately in the orbital plane. In 1964 it experienced a thermonuclear nova explosion on the surface of the white dwarf, presumably from material slowly accumulated from the giant wind over many years. The star brightened by 2.5 magnitudes and radiation from the hot white dwarf began ionising the wind from the giant star producing numerous

emission lines superimposed on the giant star spectrum. Evidence of the event was discovered in 1969 by Kohoutek when he detected a new 12th magnitude star where there had previously been a faint variable (Kohoutek 1969). Subsequent research revealed its previous history with observations dating back to 1894. Over the last 50 years V694 Mon has been slowly fading as expected for a slow symbiotic nova.

Figure 12 shows the AAVSO visual light curve from 1970 to the present. The minima in the light curve appear to be consistent in period with the previous eclipses and are therefore assumed to be orbital in origin. Arkhipova et al. (2015) give the orbital period as 955.3 days and the ephemeris of the orbital minimum as

JDmin = 2442005.4 + 955.3 * E

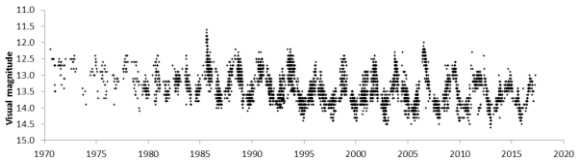

Figure 12. AAVSO visual light curve of V1329 Cyg from 1970 to the present showing a steady fading.

Figure 13 shows the AAVSO V magnitude data phased on this ephemeris. At phase 0 the white dwarf is on the far side of the giant star. The high points are from a noticeably brighter maximum during 2006. The shape of the orbital light curve suggests that the current source of light is now larger than the bare white dwarf originally being eclipsed and is only partially eclipsed by the giant star. Maximum brightness occurs at phase 0.5 when the white dwarf and the ionised nebula are between us and the giant star.

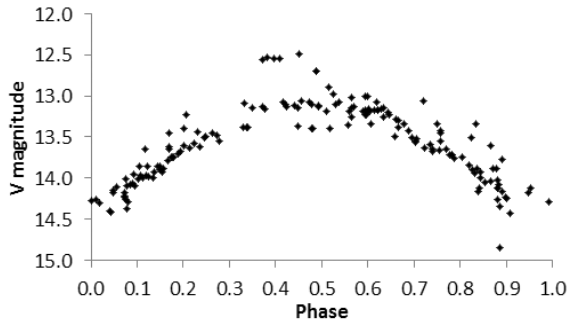

Figure 13. AAVSO V magnitude data phased on the ephemeris in Arkhipova et al. (2015).

I recorded 6 absolute flux spectra of V1329 Cyg between August 2015 and December 2016 with concurrent V magnitudes. Figure 14 shows a spectrum of V1329 Cyg taken on 14 August 2016 at V magnitude 13.38 and orbital phase 0.34 in which the principal emission lines have been identified. Note the presence of the Raman scattered O VI lines at 6825 Å and 7088 Å, a trademark of symbiotic stars with high excitation nebulae.

Figure 15 shows how the absolute flux of emission lines in these 6 spectra in 2015 and 2016 varies with orbital phase, together with similar data between 2000 and 2014 from Arkhipova et al. (2015). Good consistency between these two sets of data shows that the star continues to behave as it did in previous years and is evidence of the accuracy of my flux calibration. As the published data had not been corrected for extinction or reddening, my data in this plot have not been corrected. The orbital profile of these line fluxes shows that emission is a minimum at phase 0 when the white dwarf is behind the giant star and a maximum at phase 0.5 when the white dwarf and ionised nebula are in front of the giant star.

Using Iijima's formula for calculating the hot component temperature using the ratio of fluxes of the He II and Hβ lines gives the variation of temperature with orbital phase shown in Figure 16. This has been corrected for extinction and reddening with E(B-V)=0.33 from Parimucha & Vanko (2006). As was the case with AX Per, the hottest temperature is around orbital phase 0 when the white dwarf is behind the giant star.

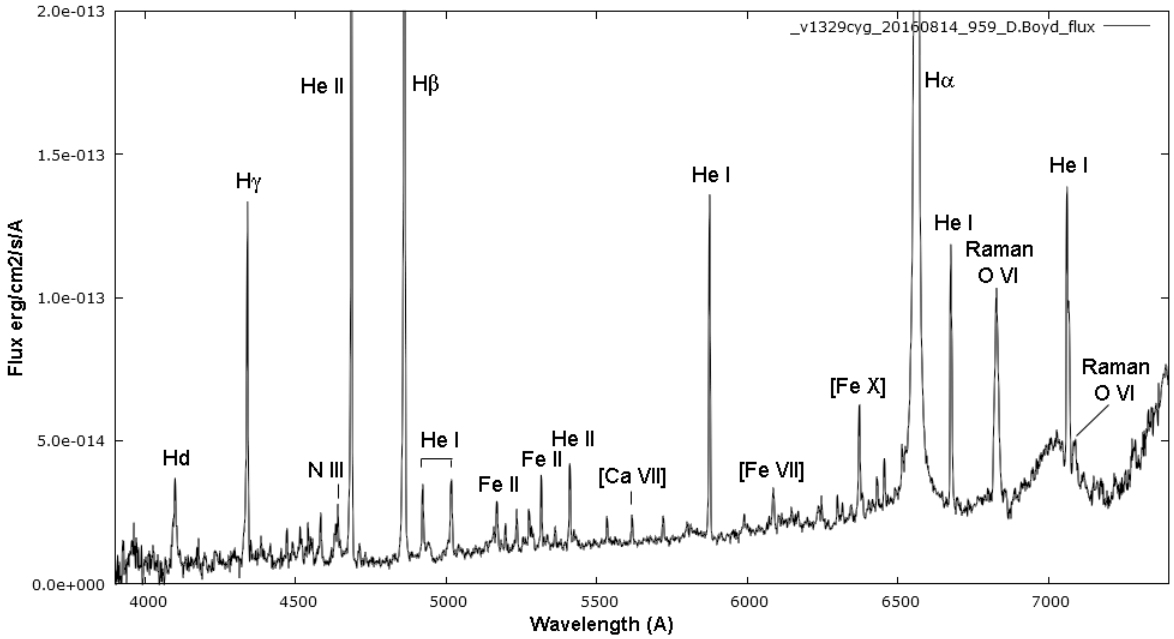

Figure 14. Absolute flux spectrum of V1329 Cyg recorded on 14 August 2016 when the V magnitude was 13.38 with prominent emission lines identified.

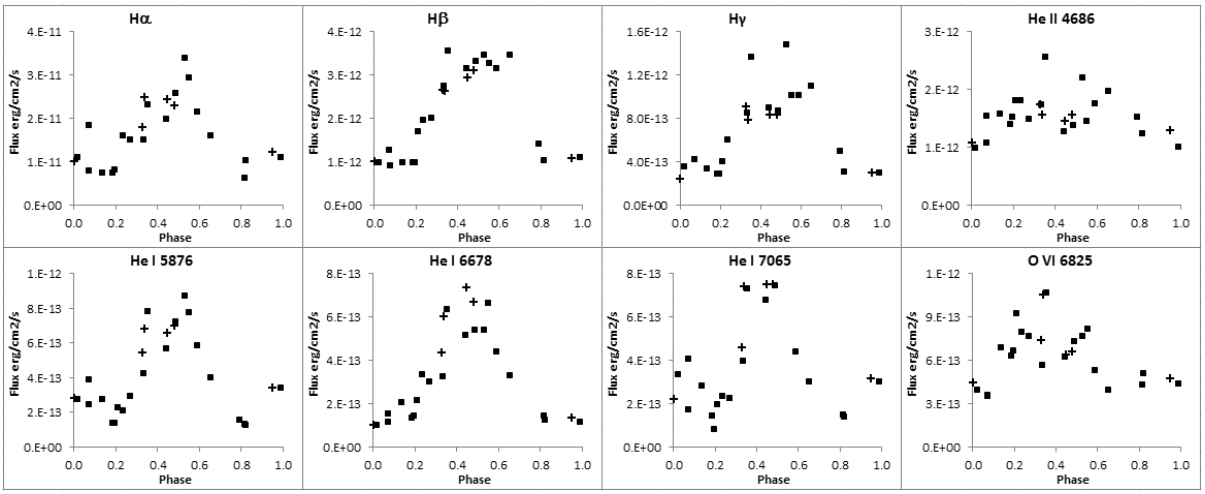

Figure 15. Variation of absolute flux of emission lines with orbital phase in spectra of V1329 Cyg recorded by the author during 2015 and 2016 (crosses), together with similar data from Arkhipova et al. (2015) between 2000 and 2014 (squares).

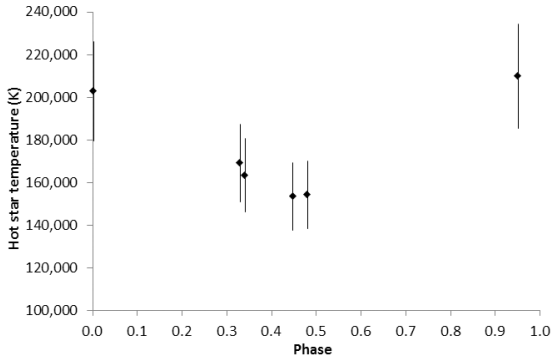

Figure 16. Variation of hot star temperature in V1329 Cyg calculated by the method in Iijima (1981) with orbital phase using the ephemeris in Arkhipova et al. (2015).

Conclusion

These examples show that careful observation of symbiotic stars using photometric and spectroscopic equipment available to the amateur can produce useful results which complement and extend those obtained by professional astronomers who, while having access to larger instruments, are not able to maintain as persistent cover as the amateur community.

There are currently over 40 symbiotic stars bright enough for useful amateur observation. More are still being discovered for which almost no data exist and those provide an excellent opportunity for amateurs to help establish a base of knowledge.

Acknowledgements

I am grateful to Francois Teyssier for his advice and encouragement and for curating the ARAS database which provides a rich resource of symbiotic star spectra for the amateur and professional communities. I acknowledge with thanks the variable star observations from the AAVSO International Database contributed by observers worldwide and used in this research, and also the work of the AAVSO in providing comparison star charts.

References

AAVSO, https://www.aavso.org/aavso-international-database (2017)

Akras, S. et al., Oral presentation at the Conference on Accretion Processes in Symbiotic Stars and Related Objects, La Serena, Chile (2016)

ARAS database, http://www.astrosurf.com/aras/Aras_DataBase/DataBase.htm (2017)

Arkhipova, V. P. et al., Astronomy Letters, 41, 128 (2015)

BAA, http://www.britastro.org/vssdb/ (2017)

Belczynski, K. et al., Astronomy & Astrophysics Supplement Series, 146, 407 (2000)

Boyd, D. R. S., Journal of the AAVSO, 40, 990 (2012)

CALSPEC, http://www.stsci.edu/hst/observatory/crds/calspec.html (2017)

Cardelli, J. A., Clayton, G. C. & Mathis, J. S., Astrophysical Journal, 345, 245 (1989)

Iijima, T. in Carling, E. B., Kopal, Z., eds, Photometric and Spectroscopic Binary Systems. Kluwer, Dordrecht (1981)

Kenyon, S. J., Proceedings of the 6th Cambridge Workshop, Astronomical Society of the Pacific, 206 (1990)

Kenyon, S. J., *The Symbiotic Stars*, Cambridge University Press, ISBN 978-0-521-26807-3 (1986)

Kohoutek, L., Information Bulletin on Variable Stars, 384 (1969)

Leibowitz, E. M., Formiggini, L., Astronomical Journal, 146, 117 (2013)

Leibowitz, E. M., Formiggini, L., Astronomical Journal, 150, 52 (2015)

Merrill, P. W., Humason, M. L., Publications of the Astronomical Society of the Pacific, 44, 56 (1932)

MILES, http://www.iac.es/proyecto/miles/pages/stellar-libraries/miles-library.php (2017)

Mürset, U., Nussbaumer, H., Astronomy & Astrophysics, 282, 586 (1994)

Munari, U. et al., New Astronomy, 49, 43 (2016)

Munari, U., Zwitter, T., Astronomy & Astrophysics, 383, 188 (2002)

Parimucha, S., Vanko, M., Astronomical Society of the Pacific Conference Series, 349, 309 (2006)

Schild, H., Schmid, H. M., Astronomy & Astrophysics, 324, 606 (1997)

Schmid, H. M., Astronomy & Astrophysics, 211, L31 (1989)

Schmid, H. M. et al., Astronomy & Astrophysics, 377, 206 (2001)

Skopal, A. et al., Astronomy & Astrophysics, 536, A27 (2011)

Sokoloski, J. L. et al., Astrophysical Journal, 636, 1002 (2006)

How to Use Astronomical Spectroscopy to Turn the Famous Yellow Sodium Doublet D Bands into a Stellar Speedometer and Thermometer

Joshua Christian

Matthew King

*John W. Kenney, III**
Chemical Physics Laboratory
Concordia University
1530 Concordia West
Irvine, CA 92612
**Corresponding Author*

Abstract

The twin, closely spaced D bands of sodium, which appear in the spectra of many stars, turn out to be easy to identify and, owing to their intensity, easy to use as "speedometer bands" via spectral Doppler shifts for the analysis of differential radial velocities in binary star systems and other systems for which astronomical velocity measurements are needed. Moreover, temperature data can be extracted from an analysis of the widths of the sodium band profiles. In order to demonstrate the effectiveness of these techniques and calculations, terrestrial sources of sodium and a simulated Doppler shift were used. A visible and quantifiable difference in band profile widths was seen corresponding to temperature, encouraging further studies.

1. Introduction.

The yellow sodium doublet D1 and D2 spectral bands are a nearly ubiquitous stellar phenomenon, readily seen in the absorption and emission spectra of many stars. The consistency and commonality of this spectral band pair is so great that it can be used with relative ease to measure the characteristics of stars and, more specifically, temperature and relative velocity. This paper provides an overview of the sodium doublet, the quantum mechanical origins of these effects, and a guide to using these effects to measure stellar parameters.

2. Background

The sodium doublet consists of a pair of spectral bands, residing at 589.15788 nm (D_1) and 589.75537 nm (D_2) Moore (1). arising from the quantum mechanical coupling of the spin and orbital angular momenta of the valence sodium electron Harris and Bertolucci (2). These bands are present in both stellar and terrestrial sources as emission bands (specific photons emitted by electronic transitions from high to low energy states) and as absorption bands (gaps in the spectrum caused by electrons absorbing specific photons to jump from a low to a high-energy state). The positions of these bands in the spectrum are constant for a stationary source and observer, providing an excellent reference point. The usefulness of these lines comes from their sensitivity to Doppler effects.

Velocities via Doppler shifts. In the familiar audio Doppler shift, a given audio frequency emitted from an approaching object will sound as though it were at a higher frequency than if it is emitted from an object going away from a stationary hearer. Similarly light emitted by objects approaching the observer will appear to be at higher frequency (more blue) than light emitted by objects traveling away from the observer (more red). This effect shifts the position of the spectral lines in proportion to the velocity of the light emitting or light absorbing object relative to the observer, for example a star or galaxy. Thus, with a spectral observation, one can determine the relative speed of a star with respect to an observer or to another star with remarkable accuracy and simplicity. The velocimetry vs. wavenumber formula, based on the Doppler effect, is

$$\tilde{\nu} = \tilde{\nu}_0 \sqrt{\frac{c \pm v}{c \mp v}}, \quad (1)$$

where $\tilde{\nu}$ is the Doppler shifted frequency (in wavenumbers: cm^{-1} or m^{-1}), $\tilde{\nu}_0$ is the frequency with no Doppler shift, v is the velocity in ms^{-1} of the source relative to the observer and *c* is the speed of light. The frequency, expressed in wavenumbers, is the reciprocal of the wavelength; i.e., $\tilde{\nu} = 1/\lambda$. The upper signs in Eq. (1) apply when the source and observer are approaching each other and the lower signs apply when the source and observer are moving away from each other.

Thermal broadening of spectral bands. Though far less familiar, thermal broadening of the spectral lines is also due to the Doppler effect. Random thermal motion of atoms results in some of the atoms having a high velocity toward the observer, and some having a high velocity away from the observer. This results in a percentage of the atoms appearing red shifted or blue shifted, though the macroscopic source of the emission or absorption need not be moving. Since the thermal broadening is dependent on the particle's mass, temperature, and characteristic spectral wavelength, this effect allows for an excellent temperature estimation to be made for the target, or targets, being observed.

In this study, the effects of thermal broadening of sodium spectral bands were investigated using the sodium D absorption bands of sun and in terrestrial sodium D emission sources (sodium lamps and flames). Spectral broadening was measured using the full width at half maximum of the spectral bands, expressed in wavenumbers (cm^{-1}). The spectra were graphed with respect to wavenumbers to highlight the linear increase in energy with wavenumber, considerably simplifying data analysis. Using the width at half height and spectral offset parameters discussed below, it is possible to calculate the temperatures and velocities of unmeasured stars by comparing their spectra to those of stars with known temperatures and velocities, or by ground-based spectral measurements.

3. Theory

The yellow color in a sodium flame arises from the de-excitation of the sodium valence electron from the $3p^1$ excited configuration to the $3s^1$ ground configuration. The reverse process describes the absorption of yellow light to promote the valence sodium electron from the $3s^1$ to the $3p^1$ configuration. Quantum mechanically, two closely spaced yellow bands are present, caused by the excited $^2P_{1/2}$ and $^2P_{3/2}$ states transitioning to the ground ^2S state by photon emission. The sodium doublet absorption results from the reverse of this effect, with the ground ^2S state absorbing photons of specific wavelengths to transition to the excited $^2P_{1/2}$ and $^2P_{3/2}$ states. The $^2S\ ^2P_{3/2}$ transition is the higher energy D_2 transition and the $^2S\ ^2P_{1/2}$ transition is the lower energy D_1 transition. The energy of these $^2P_{1/2}$ and $^2P_{3/2}$ states is offset from the normal ^2P states by spin-orbit coupling factors of $\frac{Ah}{4\pi}$ for $^2P_{3/2}$ and $-\frac{Ah}{2\pi}$ for $^2P_{3/2}$, where A refers to the spin-orbit coupling constant in $J^{-1}s^{-2}$ and *h* is Planck's constant in J s. This offset is clearly seen in the Doppler-free sodium D spectral bands, whose maxima appear at 589.15788 nm (D_2: 16973.379 cm^{-1}) and 589.75537 nm (D_1: 16956.183 cm^{-1}), resulting in a spin-orbit splitting of 0.59749 nm, (17.196 cm^{-1}) Moore (atomic energy levels) (1).

The Doppler broadening of spectral lines, the key to temperature determination, is caused by the velocity distribution of atoms arising from random thermal motion. As the temperature rises, so does the average speed of the atoms, thus causing more and more to be red or blue shifted with respect to a stationary observer. This effect, along with Lorentz broadening and other effects, results in the peak becoming wider, especially toward the base. The formula for the specific thermal broadening effect is given by

$$\Delta\tilde{\nu}_{avg} = \frac{2\tilde{\nu}_0}{c}\sqrt{\frac{2kT\ln 2}{m_0}} \quad (2)$$

where $\Delta\tilde{\nu}_{avg}$ is the spectral bandwidth at half height in wavenumbers (cm^{-1} or m^{-1}), $\tilde{\nu}_0$ is the measured center position of the peak in wavenumbers, *k* is the Boltzmann constant, *T* is the temperature in Kelvin, m_0 is the particle mass (e.g., the mass of one sodium atom), and *c* is the speed of light in a vacuum.

It should be noted that Eq (2) is not an exhaustive solution for all the effects in stellar spectra, but characterizes the specific broadening due to thermal conditions. For the temperature determination, a more useful and convenient arrangement of Eq. (2) is

$$T = \frac{m_0 c^2}{8k \ln 2}\left[\frac{\Delta \tilde{\nu}_{\text{max}}}{\tilde{\nu}_{\text{max}}}\right]^2 . \qquad (3)$$

It should be noted that temperature in Eq. (3) is not the temperature of the surface of the star, $T_{surface}$, but a temperature (or a range of temperatures) of the gas cloud (in this case containing light absorbing sodium atoms) surrounding the star and well away from the star's surface. For a given star, $T_{surface}$ may be arrived at by measuring the intensity of emitted light at a number of different wavelengths (or frequencies) to generate a light curve from which the star's surface or color temperature may be calculated.

4. Apparatus

Measurements were conducted on a modular spectrophotometer in which the incident light was dispersed through a JY ISA HR-640 monochromator (640 mm optical path, 1800 groove/mm holographic grating, micrometer adjustable entrance and exit slits) and detected via a thermoelectrically cooled Hamamatsu R943-02 photomultiplier tube whose photocurrent output was measured with a Keithley 411 picoammeter and digitized by a Hewlett-Packard 3497A data acquisition unit. Monochromator scanning was implemented via a computer-controlled Arcus DMX-UMD-23 stepper motor. All spectra were acquired through a 2.15 mm OD, 1.00 mm ID, multi-strand fiber optic cable 35 m in length. A photograph of the spectroscopic apparatus is shown in Figure 1.

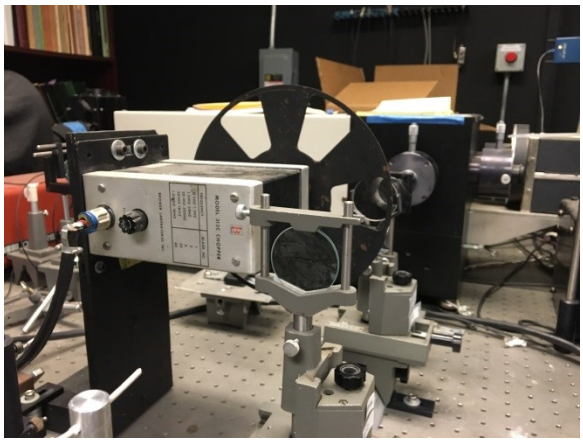

Figure 1. Monochromator and focusing lenses, fiber optic cable in foreground.

Use of the fiber optic cable allowed all spectroscopic measurements to be carried out with the light sources remote from the instrument (flame, lamp, sun, or star). The sodium lamp spectra were acquired using a Gates SLA-5C low-pressure sodium lamp, while the sodium flame spectra were acquired using a piece of borosilicate (Pyrex) glass heated red hot and white hot with a natural gas-oxygen glassblowing torch. This was possible due to the high sodium content in borosilicate (Pyrex) glass. The solar spectrum was measured by setting up a ring stand and positioning the fiber optic cable in the clamp such that sunlight could be collected and sent to the monochromator. Finally, the white hot and red hot glass spectral comparisons were accomplished by using a lens to focus the flame from a natural gas-oxygen glassblowing torch into the fiber optic cable. For the "red hot" glass spectra, the glass was rotated and played through the flame to keep it just above its melting point (Figure 2), while for the "white hot" spectra, the glass was heated to the point of dripping from the rod (Figure 3).

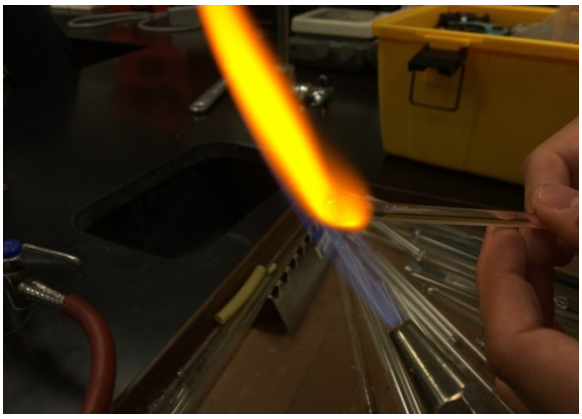

Figure 2. Red hot glass in flame

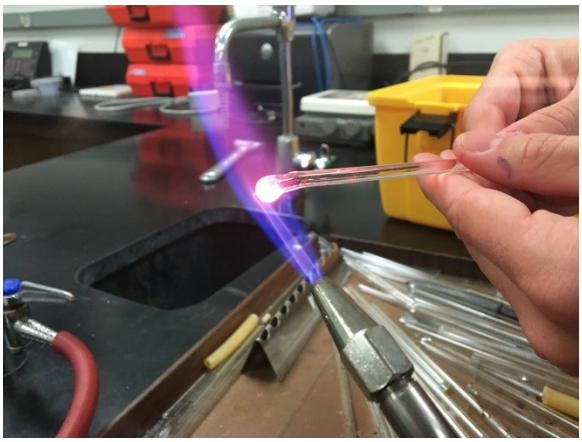

Figure 3. White Hot glass with Sodium fine filter

These photos show a clear difference between the temperatures of the glass used for each spectrum.

5. Results

The spectra of the sodium doublet of borosilicate glass heated to red hot, just above its softening point (T = 820 □C) and white hot (T □ 1400 □C) were recorded, converted to wavenumbers, and plotted on the same graph (Figure 4). Band width at half height was found to be 5.7 cm-1 and 6.4 cm-1 and 9.8 cm-1 and 10.2 cm-1 respectively (the latter being nearly 3/2 the former). In the same way, the spectra of the sodium doublet of borosilicate glass when white hot, the SLA-5C sodium lamp, and the Sun were recorded, converted into wavenumbers, and plotted on the same graph (Figure 5). The widths of the bands at half height were found to be 9.8 cm-1 and 10.2 cm-1, 5.7 cm-1 and 5.8 cm-1, and 7.1 cm-1 and 7.2 cm-1 respectively which correspond to the expected relative temperatures of the sodium sources.

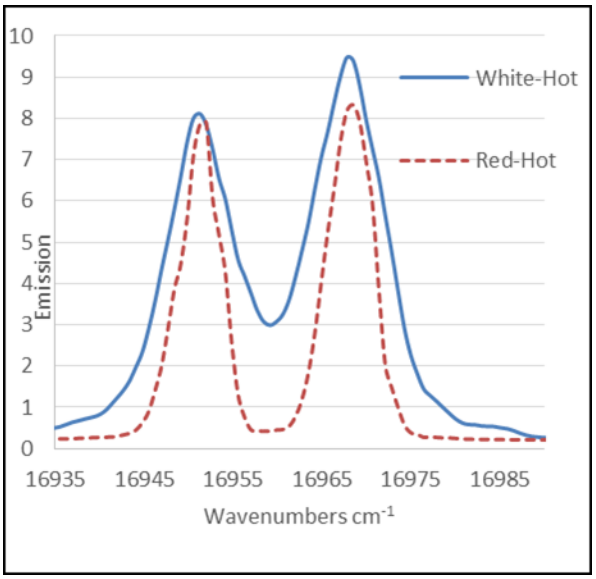

Figure 4: Thermal Broadening of Sodium Doublet in Borosilicate glass

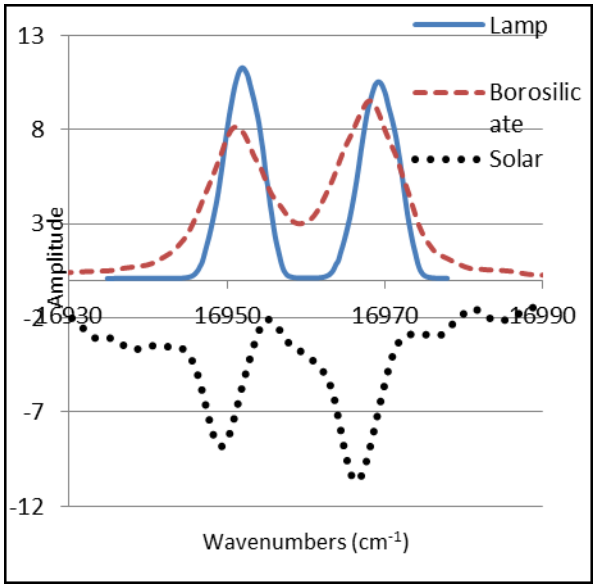

Figure 5: Sodium D line bandwidth comparison: hot glass emission (___), sodium lamp emission, (---), and solar sodium D absorption (….).

6. Discussion

The results display the potential that these simple observations have to determine the temperature of stars from basic spectral measurements. Due to the cumulative effects of the various broadening conditions, equation (2) from the theory section cannot be directly applied to a stellar spectrum. By taking the non-thermal broadening conditions into account, it is possible to compensate for their effects on the spectra. This calibration and correction is material for future study, but is beyond the scope of this paper, the focus of which is primarily a comparative determination of temperature. The graph of the white hot vs red hot glass is an excellent example of a visible thermal broadening of a spectrum even under terrestrial conditions with temperature differences only on the order of 102 K. As such, amateur astronomers equipped with a simple spectroscope can qualitatively compare temperatures of the gas clouds surrounding unknown stars and, via comparison to known stellar bodies, perform quantitative evaluations as well. In addition, spectroscopic determination of stellar velocity is well within the reach of the same spectroscope. For reference, a simulated spectrum is included below, where the velocities of the stars were calculated to be approximately -5.0 x 104 ms-1 (red shift) and 1.0 x 105 ms-1 (blue shift), Figure 6.

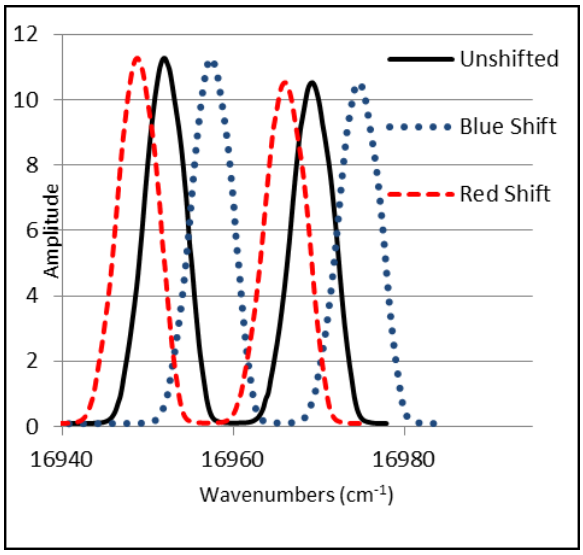

Figure 6: Simulated sodium D spectra: unshifted (___), Doppler red shifted (----), and blue shifted (….).

Not only are the techniques discussed above simple, but, as evidenced by given examples, incredibly powerful as well. In order to increase the accessibility of the given equations and provide astrometric examples of their usefulness, additional investigation is required and currently underway.

7. References

Moore, C. E. Atomic Energy Levels Volume 1. NBS Circular 467, U.S. Government Printing Office: Washington, DC 1949 p. 892.

Harris, D. C.; Bertolucci, M. D. Symmetry and Spectroscopy; Oxford University Press: New York, 1978 pp 235-245.

Modeling Systematic Differences In Photometry by Different Observers

John C Martin
University of Illinois Springfield
One University Plaza MS HSB 314, Springfield, IL 62704
Jmart5@uis.edu

Abstract

Photometric monitoring campaigns commonly increase their cadence and length of coverage by combining measurements from multiple observers (typically using different telescope/detector systems). However, systematic offsets between the calibration of different contributors can cause problems which may threaten to degrade the quality of an effort when analyzing the results. This is particularly common when the collaboration is put together post-hoc after the campaign but it can also be an unwelcome surprise for even the most carefully planned joint efforts. Here we will explore some of the issues and explore solutions which can be helpful for identifying and mitigating systematic offsets between observers during post-hoc analysis.

1. Introduction

The cadence or duration of coverage in an observing campaign can be enhanced by enlisting many different observers and telescopes at different locations. Sometimes, there is also a need to combine uncoordinated observations of an event. With both planned and post-hoc collaborations, it is unrealistic to assume all observers will have identical observing setups. In photometric campaigns, most of the differences in filters, plate-scale, detector sensitivity, f-ratio, and average atmospheric conditions are accounted for by uniform reduction using the same comparison stars and applying color transformations to a standard photometric system. However, small differences between observers can persist.

For many applications, the remaining systematic differences may be harmless. They are usually more pronounced in photometry of non-stellar sources in fields with nebulosity or other background. Their modeling and removal can improve the precision with which the timing of events is measured in a light-curve. The differences between observers may also be more significant in long duration observing campaigns or between observations combined post-hoc (as opposed to campaigns planned and coordinated with foreknowledge). A tool to model and remove them could greatly increase the utility and ease of use for data collected from many unrelated observers al la the AAVSO database.

Munari and Moretti (2012) describe how differences in filters and telescope f-ratios introduce small differences into the brightness measured in broadband filters by telescopes in the ANS collaboration. Munari et al. (2013) and others describe a light-curve merging method (LMM) to characterize and remove those differences. Here I will review and extend that work, outlining the possible causes of these small differences. I will also relate experience gained trying to model and remove them from supernova light–curves.

There may be no clear benefit to cleaning many datasets. Sampling theory limits what can be interpreted from any data and no data cleaning algorithm is going to make new results suddenly appear. Cleaning may make it easier for automated data processing algorithms to recognize and measure the significance of patterns and features. However, considering the ability of the human brain to discern patterns, if a feature is invisible to human inspection before the cleaning then one should be highly suspicious.

2. Contributing Factors

Several factors contribute to systematic differences between photometry measured by different telescope systems. Here I focus on factors that are not addressed by uniform analysis using the same comparison stars and performing color transformations to a standard photometric system.

2.1 Filter Response

Under most circumstances, the effective filter response for a telescope/observer is accounted for by transforming the magnitudes to a standard photometric system. The color transformation coefficients must be determined uniquely for each observer. Observers with same filters will not always

have the same photometric response since it also depends on the transmission/reflection of the telescope optics and spectral response of the CCD detector. The transformations may also change over time as the optics and CCD age and/or become dirty.

Munari & Moretti (2012) provide a detailed list of filter transmission factors that may not all be removed by applying color transformations. Those include: red leaks, dirty filters, and aging of filter coatings.

The color transformations coefficients are usually calculated under the assumption that the sources observed are stellar and of a similar metallicity to the standard stars used to calculate them. Photometry of targets with non-stellar spectra, including those with strong variable emission lines (i.e. supernovae) or unusual bands of absorption, can transform to a standard photometric system with residuals that vary from observer to observer. Observations of nova, supernovae, symbiotic stars, R CrB variables, Wolf-Rayet stars, and quasars are at greater risk of this effect.

2.2 Angle of Incidence on Filter

The angle of incidence of light on a filter can significantly change the wavelengths transmitted through it. Multi-layer dielectric filters and fast f-ratio optical systems are more sensitive to this effect while slow optical systems and traditional "sandwich" filters show less change (Munari & Moretti, 2012). When this effect is present it may cause the response of the filter to vary across the image so that the relative brightness of comparison stars and the target will depend on their positions in the field. This may also change in fast f-ratio optics when the filter shifts it's the orientation in its mount.

This effect is difficult to model and can manifest itself as a systematic difference between photometry measured by different optical systems or maybe even with the target positioned in different parts of the field on the same system.

2.3 Non-Linearity of CCD

Most modern CCDs have a good linear response over their full well depth. But some lower quality CCDs have a non-linear response at high illumination before the pixels reach saturation. Flux is typically under-measured for pixels which are exposed in the non-linear regime. Photometry measured can be brighter or fainter depending on how non-linearity affects the measurements of relative flux between the target and comparison stars.

3. Modeling Offsets

Munari et al. (2013) introduced a light-curve merging method (LMM) to characterize and subtract the systematic offsets between photometry measured by different observers. Their method is a three-parameter model:

$$\Delta_{i,j} = \theta_j + \phi_j \times \left[t_{i,j} - t_j^0\right] \quad (1)$$

The index j refers to the observer and i is the index of the individual measurement by observer j. $\Delta_{i,j}$ is the difference between magnitude i measured by observer j and the *true* light-curve at time $t_{i,j}$. The *true* light-curve is approximated by a template. In Munari et al. the template is the average of what was measured by the individual observers. They determined the parameters θ, ϕ, and t^0 for each observer by a minimizing the sum:

$$\chi^2 = \sum_i \sum_j \left(\frac{\Delta_{i,j}}{\varepsilon_{i.j}}\right)^2 \quad (2)$$

Where $\varepsilon_{I,j}$ is the total error for observation i from observer j.

Equation 1 can be reduced to a mathematically equivalent two-parameter form:

$$\Delta_{i,j} = \theta_j + \phi_j \times \left[t_{i,j}\right] \quad (3)$$

In that from the parameters θ and ϕ are estimated by a linear least-squares fit with Δ as the difference between the measured brightness and a template adopted for the *true* light-curve.

3.1 Light-curve Templates

Assumptions made by the template will be propagated through to the results. Therefore, the best template to use depends on the intentions of the astronomer. One should choose a template with assumptions that do not bias the result in an undesirable way.

Munari et al. (2013) effectively assumed a template for the light-curve that is an average of the light-curves measured by each individual observer. This approach assumes that each of the light-curves are of equal quality and no observer was more accurate than any other.

A weighted average may be more appropriate when some observers are more "trusted" relative to other observers. For example, the average light-curve could be computed with a weight assigned to each observer or each individual observation could be weighted as a function of its quoted error.

The average light-curve will be on a system that is an average of the systems which are incorporated

in it. The use of any average template (weighted or un-weighted) will introduce ambiguity about which "system" the processed photometry is on. This could be undesirable when determining the brightness of a peak or depth of dip in a light curve to high precision.

In another scenario, the intent may be to supplement one very well sampled light-curve with data from other observers. In that case, the well-sampled light-curve may be adopted as the template. That effectively transforms the supplemental data to the system of the well-sampled data set.

If the nature of the target is well known it may closely follow a theoretical prediction. In that case, a theoretical light-curve fit to the raw measurements may be the best template. This approach risks masking true deviations from the theoretical light-curve. But assuming the shape of the template may help improve the precision of timing measurements for events. An iterative approach is advisable. First the theoretical light-curve is fit to the observations. Then the deviations between the observations and the theoretical template are calculated and applied. Next the template is rebuilt from the transformed observations, repeating until the process converges.

No approach for building a template is universally superior. To make the best choice the biases introduced need to be weighed against the benefits and goals.

3.2 Constant Offset

Our experience shows that most of the systematic differences between observers can be accounted for with a constant offset (solving equation 3 for θ_j with $\phi_j = 0$). The linear term gains importance in datasets spanning long intervals of time or when the color of the target changes significantly. Recall that the factors discussed in Section 2 all depend on color of the target and/or changes to the CCD and filters occurring over time. In circumstances where a constant term completely accounts for the offset between observers, it can also be used to compute corrections for observerations which are not color transformed to a standard system.

Assuming the linear term is zero, θ_j is calculated as the average difference between observer j and the template.

3.3 Linear Term

The linear term (ϕ_j) becomes more significant in light-curves that are longer duration and/or when the target's color changes significantly. We confirm the finding of Munari et al. (2013) that there can be a significant linear term in the systematic offsets between observers of a supernova light-curve. But we are not able to show conclusively if it is the long duration or the changing color that are the primary contributor to that term. Based on our experience with other light-curves, we hypothesize that the latter is responsible. In limited testing, observations of variables whose color does not change significantly were sufficiently modeled by the constant term and do not require a linear term.

If that hypothesis is proven true then it would be appropriate to modify the systematic offset model and replace linear dependence on time with a linear dependence on color. For example:

$$\Delta_{i,j} = \theta_j + Q_j \times [c_{i,j}] \qquad (4)$$

Where $c_{i,j}$ is the color of observation i by observer j and Q_j is the linear dependence of the correction from observer j to the template as a function of the color of the target.

4. Future Direction

We will undertake additional tests to determine whether the linear term in the systemic offset model should depend on time or color. Regardless of that result, it is consistent with the factors that have been identified to further explore modeling systematic offsets between observers in terms of color instead of time.

5. Acknowledgements

This research is supported by the Henry R. Barber Astronomy Research Observatory and Endowment at the University of Illinois Springfield. Some of the data modeled and the origin of this project is associated with National Science Foundation Grant AST 1108890.

6. References

Munari, U. & Moretti, S. 2012, Baltic Astronomy, 21, 22.

Munari, U. et al. 2013, New Astronomy, 20, 30.

How Faint Can You Go?

Arne Henden
arne@aavso.org

Abstract:

For many scientific projects, knowledge of the faint limit of your exposure can be extremely important. In addition, it can be just plain fun to know how faint your equipment can go under varying circumstances. This paper describes the concept and gives some guidance as to how to increase the scientific value of your reports.

1. Introduction

You are trying to be one of the few amateurs who have discovered the optical afterglow of a gamma ray burst (GRB). After the initial alert giving an error box, you image the entire error box, but don't see anything new. Can you report a non-detection? What if you see a faint fluctuation in the background? Is it a real object? Do you want to report such a faint discovery, and have huge professional telescopes relying on your result? Or perhaps you are participating in a campaign to monitor a cataclysmic variable (CV) for an HST visit. The object must be in quiescence and not outbursting for the HST observation to take place. Is a non-detection worthwhile? How long does the exposure need to be to detect the quiescent object? All of these projects, and many more, rely on a concept called "limiting magnitude" or "plate limit": the faintest object that you can reliably detect on your CCD frame.

Schaefer (1998) wrote an article for Sky and Telescope about the concept, and provided a BASIC program for calculating the limiting magnitude for your system. Schaefer (1999) also ran a "contest" to see who could obtain the deepest image of a specified field, with the "winner" being Paul Boltwood, imaging fainter than 24th magnitude in 20 hours of unfiltered exposure with his homemade 16-inch telescope.

This paper will describe the concept of the limiting magnitude, as well as giving you a field where you can experiment and see how faint you can actually go. The primary emphasis is for variable-star work, and so the tools provided by the American Association of Variable Star Observers (AAVSO; https://www.aavso.org), along with the Johnson/Cousins filter passbands, will be highlighted.

2. The Faint Limit

The concept of the limiting magnitude seems pretty simple: look for the faintest object that you can see, determine its magnitude in some fashion, and report that value. The devil is in the details. How do you find this "faintest object"? Perhaps more importantly, how do you determine its magnitude? How do you know that the object is real? Finally, how do you optimize your system and exposures to go even fainter?

2.1 A Theoretical Definition

There are basically two types of limiting magnitude. First, if you are just trying to find the faintest object on a frame, most researchers define the faintest object to be one that is 5 standard deviations (5σ) above the sky background; or roughly equivalently, that has a signal-to-noise ratio (SNR or S/N) of 5. This may seem conservative to you, as it means (assuming a normal population) that the probability of the detection being real is 99.99994%. However, the assumption is that you have not properly accounted for everything, and there will be small, non-real, fluctuations in your background.

You can use a less-stringent requirement if you have additional information about the possible object. For example, if you know the position of a real object, most researchers will relax the requirement to 3σ, or SNR=3, as the probability of a small non-real fluctuation happening right at the known position is smaller.

3. Factors Affecting Limiting Magnitude

The factors affecting limiting magnitude are the same ones affecting any photometry. Howell's CCD Equation (Howell 2006) can be rewritten if you are taking long exposures such that the read noise is not important:

$$SNR = \frac{N_S}{\sqrt{N_S + N_b}} \qquad (1)$$

where
SNR = signal to noise ratio
N_s = number of photons from the star
N_b = number of photons from the background inside of the aperture

These terms can be further defined as

$$N_s = F_s t \quad (2)$$

$$N_b = n_{pix} F_b t \quad (3)$$

F_b = background flux (photons/pixel/sec)
F_s = star flux (photons/sec)
n_{pix} = the number of pixels in the aperture
t = exposure time (seconds)

Note that if we assume perfect conversion from photons to electrons, the photon flux rate is in electrons/sec, not ADU. You need to multiply the ADU counts by your system gain. Ways to increase the SNR are listed below.

There are two limiting cases for this equation. If the star flux is much larger than the sky flux, then SNR becomes:

$$N_s = SNR^2 \quad (4)$$

For an SNR of 3 and an exposure of 100 seconds, the total star flux needs to only be 9 electrons. This is 7.6 magnitudes fainter than a star that has SNR = 100.

If the sky flux is larger than the star flux, then rearranging the equation,

$$N_s = SNR \sqrt{N_b} \quad (5)$$

For a sky flux rate of 100 electrons/sec, an exposure of 100 seconds, and an aperture of 79 pixels, you reach SNR = 3 for a total star flux of 888 electrons. This is 2.6 magnitudes fainter than a star with SNR = 100.

3.1 Telescope Aperture

Obviously, the larger the aperture of the telescope, the more light collecting area and therefore the more flux (star photons) that will be recorded by a given object. This factor scales as the square of the telescope diameter. That is, a telescope that is twice as large (say, a 60cm telescope instead of a 30cm telescope) will collect four times as much flux. If we were purely Poisson-noise dominated, the signal/noise would grow as the square root of the signal, or an increase of two in the signal/noise for this case.

3.2 Exposure Time

The amount of collected flux scales linearly with exposure time. Changing the exposure time by a factor of four will increase the flux by four, or an increase of two in the signal/noise for this case, if we are Poisson-noise dominated.

3.3 Sky Background

For most faint sources, the sky background dominates the signal from the source. Reducing the sky background therefore reduces the "noise" part of the CCD Equation. This can be accomplished by observing at a darker site, or when the moon is not visible, or by using an aperture that includes fewer pixels so that less sky is included. Note from the earlier equation examples that the smaller the sky flux, the fainter you can go. This is one of the main reasons why the Swift satellite's UVOT direct-imaging instrument, with only a 30cm aperture, can routinely measure sources below 21st magnitude in a two-minute exposure.

3.4 Seeing

For stellar objects, the star profile is Gaussian in shape with an exponential fading from the central peak. The usual parameter for describing the stellar profile is full-width-at-half-maximum, or FWHM. For most amateur sites, FWHM of a stellar target is typically 2-3arcsec. For quality professional sites, it can often be subarcsec. The smaller the image, the less sky background that contributes to the measurement as you can use a smaller measuring aperture.

For extended objects such as galaxies or comets, the FWHM is no longer the proper unit of measure. You have to know the angular size of the galaxy and use a measuring aperture that is large enough to include the majority of the flux from the object. For this reason, you generally can't see galaxies as faint as you can stellar objects.

3.5 Airmass

Extinction rears its ugly head when determining limiting magnitude. As you observe farther away from zenith, you look through larger and larger amounts of air. The parameter that measures the amount of air you look through is called airmass, with its value being 1 at the zenith and increasing by the cosecant of the zenith angle. At zenith angle 60 degrees (30 degrees above the horizon), the airmass

is 2; at 70 degrees, the airmass is 3; and so on. For each wavelength, there is an extinction coefficient that measures the amount of flux loss per unit airmass. For example, the V filter (central wavelength around 550nm) has a typical extinction of about 0.25magnitudes per airmass. This means you lose 0.25magnitudes of flux for an object directly overhead, and 0.50magnitudes for an object at a zenith distance of 60 degrees. For the deepest frames, you want to observe as close to the meridian as possible.

3.6 Detector Quantum Efficiency

Sensors that have higher sensitivity will detect more flux from a star. Typical front-illuminated, microlensed CCDs might have 60% Quantum Efficiency (QE) at 550nm, meaning they detect 60% of the V-band photons that fall on the sensor. A thinned, back-illuminated sensor might have 90% QE at this same wavelength. As you go to very blue or very red wavelengths, the back-illuminated sensor advantage becomes much larger. The more photons you detect, the fainter you will be able to image.

3.7 Filter

The light that reaches the sensor has to reflect off of the primary/secondary mirrors (or pass through an objective lens); then pass through a filter that limits the passband of light you are measuring; then potentially pass through several other optical elements, like focal reducers, field flatteners, camera entrance windows, etc. before finally reaching the sensor. Each of these optical elements has imperfect transmission, and you lose light all along the telescope path. The filter is probably the primary limitation, as not only does it restrict the wavelengths of light that reach the sensor, but does not have perfect transmission even within its passband. In addition to this, the sensor itself has a wavelength-dependent QE. For the Johnson/Cousins V and R_c filters, the peak response of the sensor falls pretty much near the region transmitted by the filters, and these are likely to be the filters you will use when trying to go deep. On the other hand, the wavelength of the filter might also affect the limiting magnitude, as redder filters suffer less atmospheric extinction, and red stars might be brighter in those filters than a shorter-wavelength filter like B or V. So there is some optimization as to what filter to use. As filters from different vendors have different transmission, you may want to purchase a filter with higher throughput even if it is somewhat more expensive.

4. Calculating the Limiting Magnitude

There are three main ways to calculate the limiting magnitude in a given image: using the faintest known comparison star in your image; using a prior deep comparison image to learn what your typical limiting magnitude is for a given exposure time; and measuring the magnitudes and errors for stars in the current image.

If your target star has an AAVSO comparison-star sequence, there will be stars in your field of view with known magnitudes, usually covering the entire known range of variation. Sometimes for fainter targets, such as cataclysmic variables, the sequence may only be for the outburst stage, and there will be no stars near the quiescent magnitude. If you use the VSP chart plotter, you can identify the known comparison stars in your image. For stars fainter than the faintest comparison star, you can report that the target is fainter than the comparison star. For example, if the faintest comparison star is V=17.4, and that star is visible but the target star is not visible, you can report a "fainter-than" estimate, or <17.4, to the AAVSO. This works well for visual observers, where often the sequence goes fainter than they are able to see, and reporting a "fainter-than" is pretty close to their actual visual limit. For CCD systems, however, the faintest comparison star might be 17.4, but your image goes to 20th magnitude, and reporting <17.4 is an extremely conservative report.

Another technique is to gain an understanding of how faint you can go with a typical exposure. To use this technique, you need a deep comparison image of some field, and then you need to take a deep exposure of the same field. Comparing your image against the deeper image with well-identified stars with known magnitudes will give you an idea of how faint you can go.

Probably the best technique is to use your photometry analysis tool, if it includes a good estimate of the uncertainty in the measurement. A good estimate is one that makes use of the CCD Equation, including at least the sky noise in addition to the target Poisson noise. Measure 3-5 faint objects that are barely detectable; identify those that have SNR around 3, average the values and report that as the limiting magnitude (for a known object).

5. Caveats

When working at faint magnitudes, one of the large concerns is the even fainter background. For a star with SNR=100, a contaminating faint star that is 5 magnitudes fainter will cause a 0.01mag error in your photometry. These faint companions are very difficult to know about if you are already working

close to your plate limit. An even worse case is when the companion is somewhat brighter (say, 3 magnitudes fainter than the star being measured), but near the edge of the measuring aperture. A 0.1mag error can result, depending on whether the companion is included or excluded from the aperture. So if possible, either use a deeper image (from another source, or from a special "deep-field" image taken on a good night) to look for these faint companions.

Another issue at plate limits is that the number of galaxies is rapidly increasing, especially out of the plane of the Galaxy. Tyson (1988) notes that, at magnitude 21, the number of stars and the number of galaxies is about equal. Combined with relatively poor seeing, these faint galaxies are difficult to distinguish from stars, yet yield very different photometry as their profile is not Gaussian.

Another potential problem is centroiding. You can see the faint object on the display, and can move the cursor over it. However, some software packages then try to refine the position of the desired object, and that centroiding can fail for faint objects. You may need to turn this feature off, and point as precisely as you can.

6. More Techniques for Going Deep

Here are some very simple additional guidelines when attempting to go as faint as possible with your setup.

Use a filter that optimizes the response. Usually an R-like filter is optimal, obtaining the maximum QE from your CCD. This filter also decreases the sky background and lessens the effect of the moon.

Use the best possible guiding. If your mount cannot track unguided for very long, then use autoguiding or limit exposures to the maximum untrailed exposure time.

Use subframes. Typically the sky noise dominates the readnoise with an exposure of a few minutes, so taking subframes of, say, 5-10 minute duration, and stacking them in software later gives the same SNR as a single longer exposure, yet provides safety against observing problems, such as satellites, trailed images, cosmic rays, etc. Dithering between subframes also gives the advantage of removing hot pixels since they can be filtered out. Using a median filter, or some single-pixel rejection algorithm such as sigma clipping or min/max, will remove artifacts while retaining most of the true signal. That said, the FWHM of stars will usually degrade with stacking, compared with autoguiding a longer exposure, as the registration step needs to be done without interpolating pixels, and integer pixel moves will spread the flux slightly.

7. Example: M67

The open cluster M67 is on the observing queue for several of the AAVSOnet telescopes, both to continue calibrating it on photometric nights at good sites as well as for using it to calculate transformation coefficients for those systems with few photometric nights. This cluster is a nice target for demonstrating limiting magnitude techniques.

Shown in Figure 1 is a single 900-second V-band image (with 0.8arcsec seeing) from the CFHT 3.6m telescope in Hawaii. This particular field is northwest of the cluster center, with a field center of 08:51:05 +11:51:20 (J2000). There are a couple of dozen marked stars in this image, with their magnitudes given in Table 1. Stars A-G are part of the standard-star sequence for this cluster, with the magnitudes obtained from the photometry table provided by the AAVSO VSP chart plotter. The remaining magnitudes are from the CFHT image, obtained by using a "bridge" exposure from the Isaac Newton 2.5m telescope. The INT exposure does not saturate the AAVSO standard-star sequence, and has good signal/noise on the brightest unsaturated CFHT stars. The limiting magnitude in the CFHT image is about V=25.

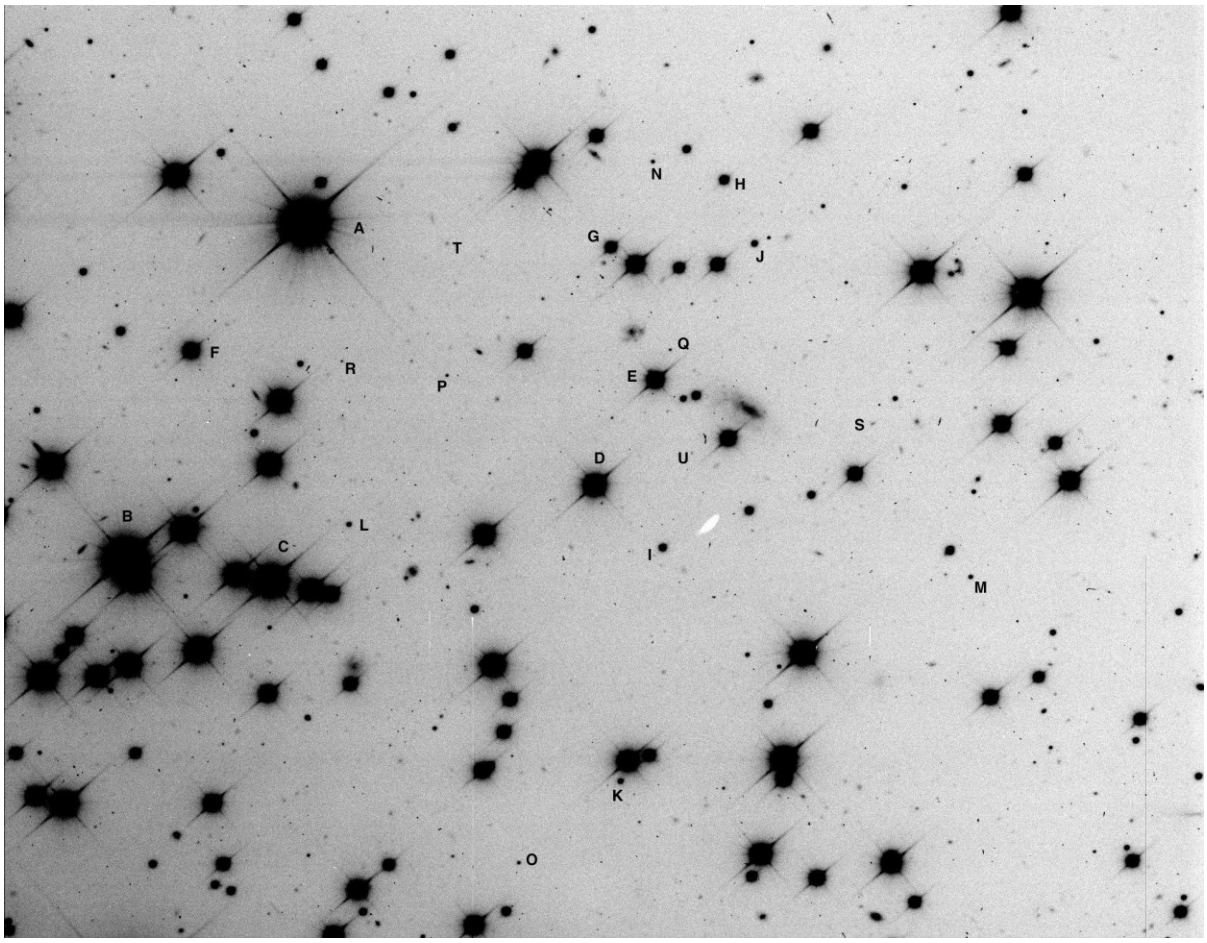

Figure 1: Deep image from CFHT. North is up, East is left, field of view about 7 arcmin square.

The depth of the CFHT image is roughly equivalent to a 36-hour exposure with a 30cm amateur telescope, but with much better seeing. This magnitude-bridging technique is common in the professional world, as most of the standard stars are too bright for large telescopes.

Shown in Figure 2 is a stack of eight 80-second images from the New Mexico Bright Star Monitor (BSM_NM) telescope. This is only part of its 3-square-degree image, covering the same field as the CFHT image. The image shows one of the drawbacks of such a wide-field system. The 5arcsec pixels create severe blending in the crowded cluster region. The system is optimized for observing bright stars rather than going faint.

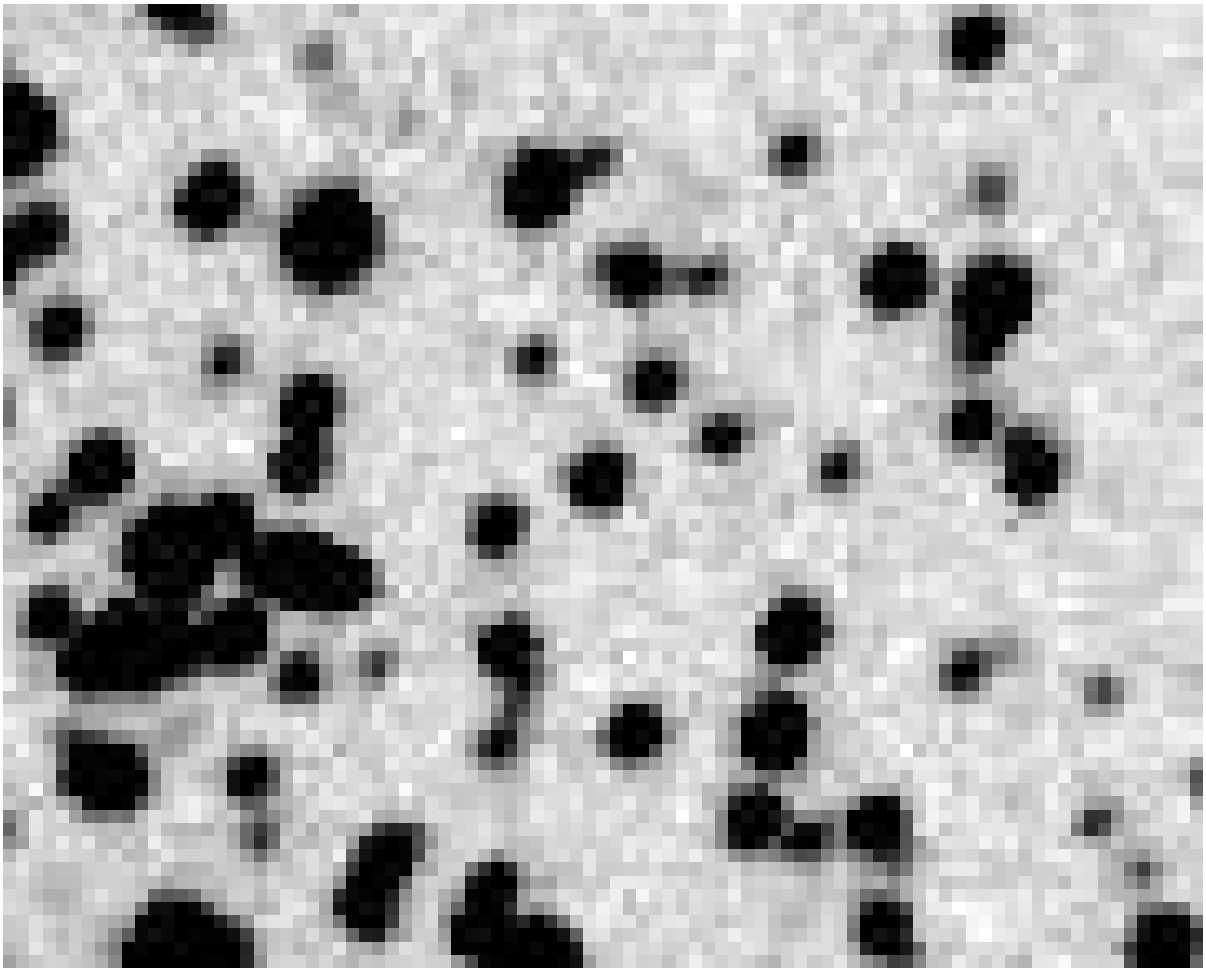

Figure 2. Deep stack from BSM_NM of the same field as the CFHT image.

ID	Mag	Err
A	10.289	0.016
B	11.132	0.014
C	12.213	0.012
D	13.310	0.019
E	14.045	0.018
F	15.006	0.027
G	15.738	0.026
H	16.78	0.03
I	17.84	0.03
J	18.57	0.03
K	19.42	0.03
L	19.98	0.04
M	20.54	0.04
N	20.97	0.04
O	21.51	0.05
P	22.00	0.05
Q	22.60	0.05
R	22.98	0.07
S	23.35	0.08
T	24.02	0.10
U	24.56	0.15

Table 1. V-band magnitudes for identified stars in Figure 1.

As mentioned above, the simplest technique is identical to the visual estimating method: find the faintest sequence star on your image, and report that the target (or limiting magnitude) is fainter than that sequence star. For the BSM image, the faintest sequence star is magnitude 15.3, and so the report would be a limiting magnitude of at least 15.3, or if this were a report for a variable star, <15.3.

For estimating the limiting magnitude by finding the faintest recognizable star on the CFHT image, the BSM image barely shows star H, so the limiting magnitude is about 16.8. Note that the eye is pretty good at detecting shapes, and so this is probably optimistic, and somewhat below SNR=3. Still, not bad for a 6cm telescope! However, the real restriction is the poor angular sampling, so finding isolated faint stars is very difficult. If you need to go faint, a BSM system is not the wisest choice!

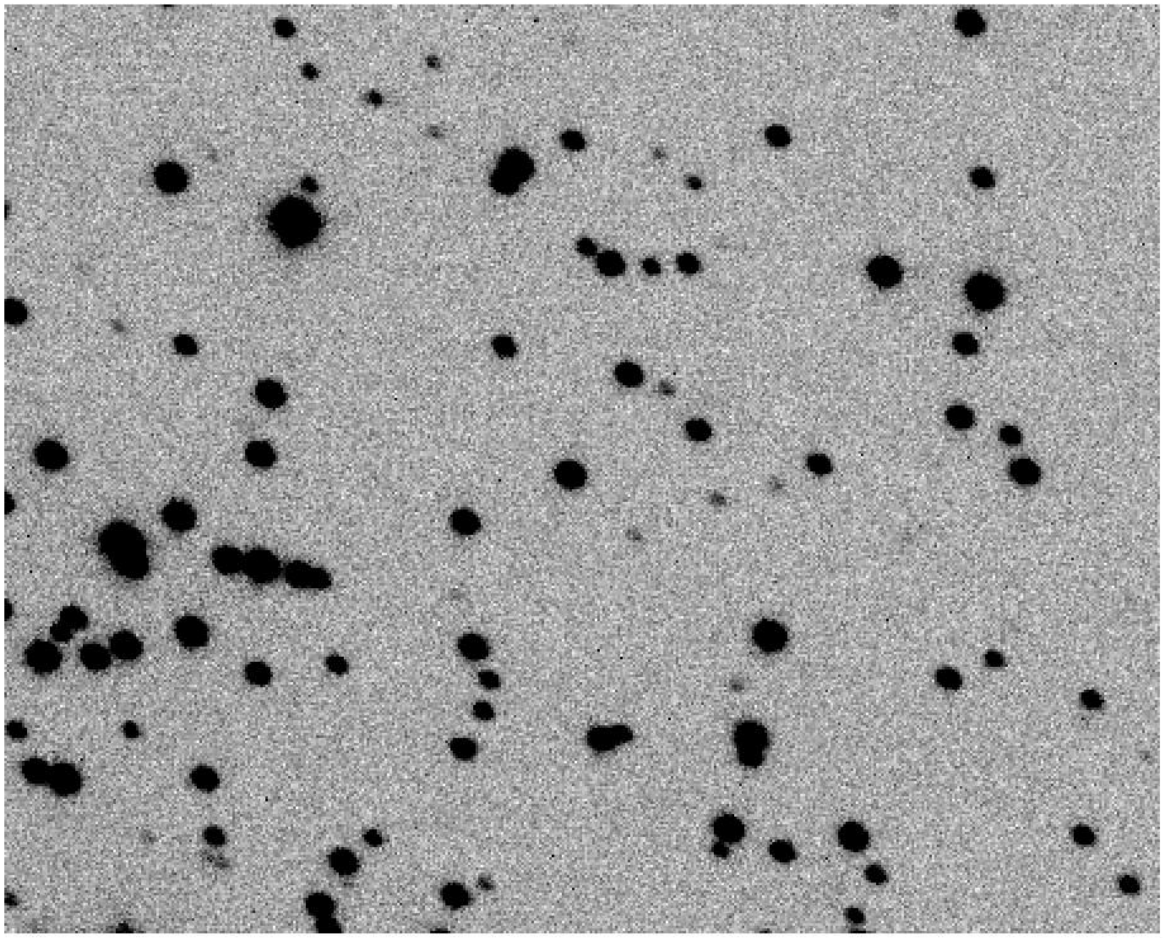

Figure 3. Single image from SRO50 of the CFHT field.

Shown in Figure 3 is a single 90-second exposure with the Sonoita Research Observatory 50cm telescope (SRO50). Note that the angular resolution is dramatically improved compared to BSM_NM, though the FWHM is still 4 pixels = 3.6arcsec. The faintest star visually is star J. Using aperture photometry with diameter = 2 FWHM, star I yields 0.10 error (SNR ~ 10), and star J has SNR=3. For this image, this yields a limiting magnitude of about 18.6 magnitude. The exposure time is 7 times less than for the BSM_NM image; the collecting area is 69 times larger, so the net flux difference is 9.9, for a magnitude difference of about 2.4, which roughly corresponds to the different limiting magnitudes.
.

8. Conclusion

Determining your limiting magnitude can be scientifically useful for many projects. There are some simple techniques using known comparison stars, or more complex ones using photometric measurements of faint stars. Observing a known field such as M67 can help in understanding the limiting magnitude for a given exposure time, and also be used as a test field for improving your techniques.

You can make your own deep field for comparison purposes. The images from SDSS (http://skyserver.sdss.org/dr13/en/home.aspx), the Isaac Newton group of telescopes (http://casu.ast.cam.ac.uk/casuadc/ingarch/query), and other websites for specific projects for several of the worldwide 3-4m telescopes are also available. You may need to find a "bridge exposure" to be able to calibrate the much fainter large-telescope imagery.

9. Acknowledgements

This paper makes use of data obtained from the Isaac Newton Group Archive which is maintained as

part of the CASU Astronomical Data Centre at the Institute of Astronomy, Cambridge. This paper is also based on archival data retrieved from the CFHT archive. Images from AAVSOnet telescopes have also been used; the work by the many volunteers operating that network are gratefully acknowledged.

10. References

Howell, S. B., "Handbook of CCD Astronomy," (2006), Cambridge University Press.

Schaefer, B. E., "Limiting Magnitudes for CCDs," (1998), Sky and Telescope 96, 117.

Schaefer, B. E., "Going to the Limit," (1999), Sky and Telescope 97, 126.

Tyson, J. A., "Deep CCD Survey: Galaxy Luminosity and Color Evolution," (1988), Astron. J. 96, 1.

Shoestring Budget Radio Astronomy

John E. Hoot
SSC Observatory, Center For Solar Systems Studies, Las Campanas Remote Observatory
1303 S. Ola Vista, San Clemente, CA 92672
jhoot@ssccorp.com

Abstract

The commercial exploitation of microwave frequencies for cellular, WiFi, Bluetooth, HDTV, and satellite digital media transmission has brought down the cost of the components required to build an effective radio telescope to the point where, for the cost of a good eyepiece, you can construct and operate a radio telescope.

This paper sets forth a family of designs for 1421 MHz telescopes. It also proposes a method by which operators of such instruments can aggregate and archive data via the Internet. With 90 or so instruments it will be possible to survey the entire radio sky for transients with a 24 hour cadence.

1. Introduction

Radio astronomy blossomed shortly after the Second World War. Advances in microwave radar, and the observations of naturally occurring signals by those who operated them stimulated the birth of a new branch of astrophysics, Lovell (1990), Kraus (1966). Radio wavelengths, provide a window to observer high energy events, the interactions of intense magnetic fields with particles. Because of radio's longer wavelengths, radio signals penetrate interstellar clouds that are opaque to optical astronomy. Finally, cool matter and molecular clouds all radiate the majority of their energy at radio frequencies.

Radio astronomy discovered pulsars, quasars, and even the echo of the birth of the universe in the cosmic background radiation.

Until very recently, observing at radio wavelength was beyond the means of most amateurs, small institutions, and other citizen scientists. Radio astronomy was associated with large steerable dish antennas, complex and expensive cryogenically cooled receivers and super computers. For example the Parks Radio Telescope in Australia cost over 5.6 million dollars to fabricate in today's dollars.

However, in the last decade, improved semiconductor materials and shrinking dimension of integrated circuit components has brought microwave radios into our homes and pockets. Commercial technology now brings us HDTV from geostationary satellites with dishes less than ¼ square meter. We take for granted the distribution of hundreds of megabits per second over microwave routers that sit in our homes, offices and businesses. We carry cell phones that use a single, frequency agile microwave radio transceiver to make phone calls, text images, communicate with WiFi, and receive faint signal from a constellation of GPS satellite in Earth orbit while sitting in metal cars. The cheap availability of this microwave technology now allows anyone with the desire and a modest budget to start to explore the universe with radio!

I am always on the lookout for commercial technologies that can be repurposed for science. I was quick to recognize the benefits when CCD chips started to go first into video and then still cameras. I was galvanized by early experiments with The CCD Cookbook Camera, Berry et al. (1994). Later, the CMOS sensor revolution brought photometry within the means of the masses, Hoot (2004, 2007). Recently, I have been following two other recent component developments that herald a dramatic cost reduction in the development of radio telescopes.

In the last 4 years the price of ARM processor based, fully featured, multi-core single board Linux computers has dropped into the $30 range. Additionally, the market has been flooded with USB digital TV receiver dongles. Clever folks have reverse engineered those TV receiver dongles and found that they contain a two chip software defined radio receiver that can operate on frequencies from 24 MHz to 1.8 GHz, Fry, E., Palosaari, A (2011) ,RTL-SDR (2017).

I, and others, East, P.W (2014), realized that by combining these two consumer products, you can build an interfermetric radio telescope for under $500. This paper outlines designs for three different radio telescopes that can be built by an individual with hand tools, moderate computer and electrical skills. It also provides a brief summary of the kinds of observations for which these instruments are useful. Finally, it elaborates how those owning such instruments can cooperate over the Internet to

provide monitoring of radio transients with a 24 hour cadence.

2. The Sources of Naturally Occurring Radio Signals

The three primary mechanisms that generate natural radio waves are: thermal Black Body radiation, thermal emission from ionized gas, and synchrotron radiation. Most are familiar with black body radiation, as it is the mechanism that drives most optical signals. Planck's curve describes how the temperature of a body determines how it radiates at different wavelengths.

Thermal emission from ionized gas is also familiar to optical astronomers. These emissions are triggered by thermally initiated transition between quantum energy states, emitting or absorbing discrete wavelength photons. The difference being, that at longer radio wavelengths, the temperature-energy relation is strongly influenced by the optical depth of medium.

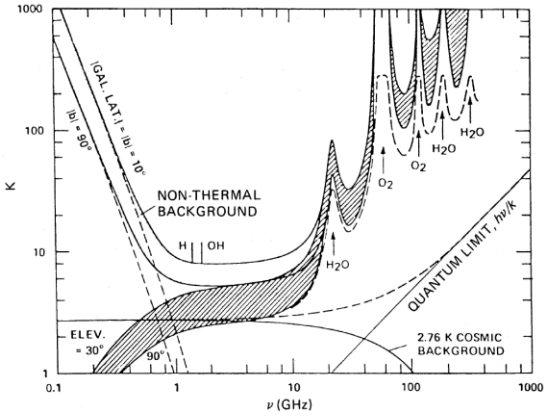

Figure 1: Terrestrial Microwave Window (From Nasa SP-419)

Synchrotron radiation is emitted when free electrons are accelerated to relativistic velocities in a magnetic field. The wavelengths emitted are a function of the strength of the magnetic field. Stronger fields give rise to shorter wavelengths, lesser magnetic fields to longer wavelengths. Synchrotron radiation accounts for nearly all non-thermally generated radio waves.

The telescopes described in this paper are designed to operate around a center frequency of 1.420405752 GHz, a wavelength of 21.106 cm. This is the frequency emitted when a neutral hydrogen atom is thermally excited and its electron spin state flips direction. It is the wavelength chosen for several reasons. Firstly, most of the ordinary matter in the universe is hydrogen, so it is a good choice. Next, it is in a window in which our atmosphere is transparent to radio waves. Finally, its wavelength is short enough that it has a good response to black body radiation, and long enough to detect synchrotron radiation. So it is kind of a "goldie locks" frequency.

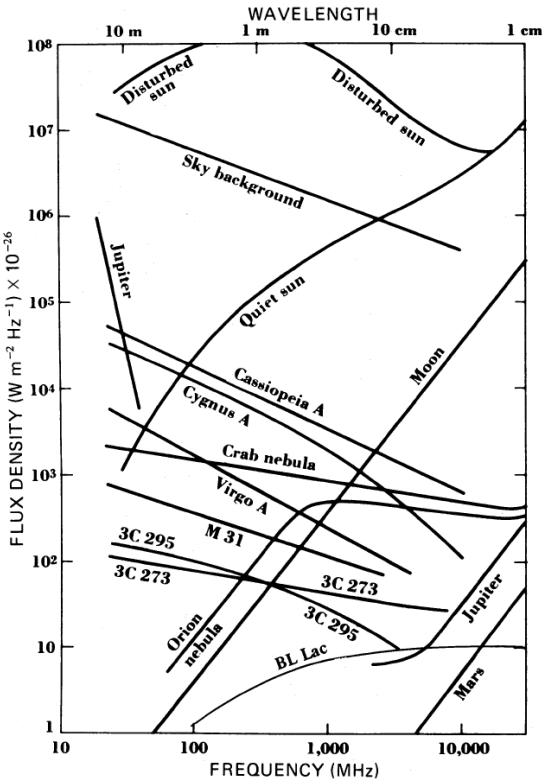

Figure 2: Spectral Power Of Typical Radio Source, Kraus (1966).

While the design herein is for 1420 MHz, it can easily be adapted to any other frequency changing the antenna and filters, and plugging different frequencies into the software.

3. Radio Telescope Basics

Simple radio telescopes consist of two basic components. A directional antenna and a receiver that measures the received flux/unit time for a given frequency bands, or multiple frequency bands. It is essentially a type of radio spectrometer or radiometer. Its key parameters are the aperture of its antenna, frequency, bandwidth, sensitivity, and signal/noise ratio. Since radio wavelengths are much longer than visible light, they require large apertures to resolve features in the sky. The formulas in Figure 3 shows an example of how the beam of a circular filled aperture is modeled.

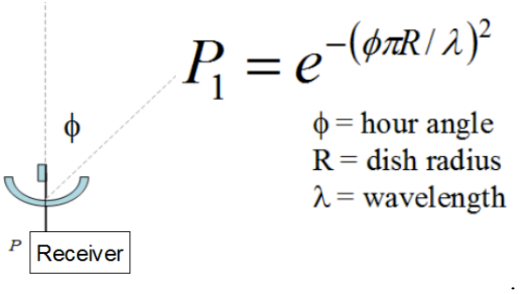

Figure 3: Response of a filled aperture antenna to an off axis signals as a function of the angle of offset from the primary axis.

We define an aperture's angular resolution as the width of the angle to the ½ power sensitivity point. From the formula in Figure 3, the formula below shows how we calculate the angular resolution of a 3m dish at 1420.405 MHz.

$$\theta = \text{angular resolution}$$

$$\theta \approx 1.22 \frac{\lambda}{D}$$

$$\theta \approx 1.22 \frac{0.211m}{3m} = 4.9^\circ$$

Figure 4 shows what the response of the antenna is out as far as about 6 degrees.

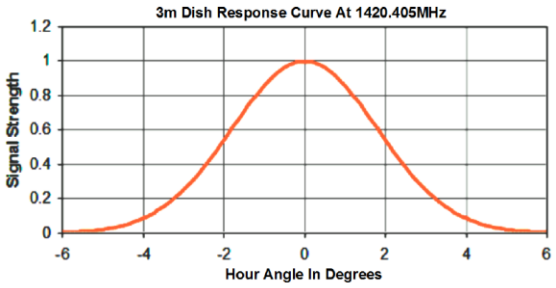

Figure 4: Antenna Beam Sensitivity For a 3M Dish At 1.42 GHz.

One way to view this result is, that for single antenna telescopes, unless you can have enormous apertures, the entrance of your spectroscope is very large. There are mathematics, such a maximum entropy deconvolution, that can generate plausible maps of point sources with a single aperture, but small single aperture telescopes are limited in what they can resolve. Nonetheless, they still can do science.

4. A Simple Software Defined Telescope

The simplest and easiest radio telescope consists of a single high gain antenna, a set of high gain amplifiers, a DVB-TV dongle and a Raspberry Pi (Rpi) single board computer. Figure 5 shows a black box level schematic of the system.

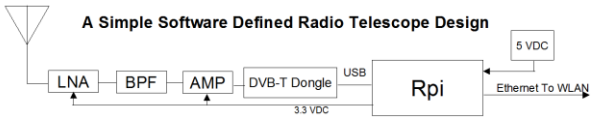

Figure 5: Block diagram of a single element software defined radio telescope.

The antenna used in the initial test configuration was an axial mode helical antenna. It consists of a helical coil of wire with each turn approximately one wavelength long. In this case, 20.7 cm with a pitch spacing of 4.65 cm using 34 turns of #10 AWG insulated wire. The antenna was fabricated using a piece of 1"x2" lumber and UV resistant cable ties to attach the helix and maintain spacing. The antenna was then elevated 1.5 wavelengths above its base using wooden struts pinned with dowel rods so that no metal fasteners were near the structure to distort its radiation pattern. Figure 6 shows the antenna mount on a German equatorial mount for initial tests.

Figure 6: Helical Antenna Test Configuration

Figure 7 shows a spreadsheet, derived from Kraus (1988) that derives the optimal dimensions for

helical antennas. Although calculated as over 20 dB, in practice, these antennas are perform a couple of dB below theory in their longer instances. They are however, relatively easy to fabricate and reasonably broad banded.

number of turns n	frequency f [GHz]	wavelength λ [cm]	reflector diameter D [cm]	winding length L [cm]	winding spacing S [cm]	wire diameter d [mm]	lobe angle ϕ [°]	gain G [dBd]	resulting coil length l [cm]
		30/f[GHz]	0.75*λ	0.98*λ	0.22*λ	0.13*λ	root(12300/n)	10 log(3.2*n)	n*S
8	1.420	21.1207	15.84	20.70	4.65	2.75	39.21	14.08	37
10	1.420	21.1207	15.84	20.70	4.65	2.75	35.07	15.05	46
20	1.420	21.1207	15.84	20.70	4.65	2.75	24.80	18.06	93
34	1.420	21.1207	15.84	20.70	4.65	2.75	19.02	20.37	158

number of turns	lobe angle	gain (dBd)
15	28.636	16.81
16	27.726	17.09
17	26.899	17.36
18	26.141	17.60
19	25.443	17.84
20	24.799	18.06
21	24.202	18.27
22	23.645	18.48
23	23.125	18.67
24	22.638	18.85
25	22.181	19.03
26	21.750	19.20
27	21.344	19.37
28	20.959	19.52
29	20.595	19.68
30	20.248	19.82
31	19.919	19.97
32	19.605	20.10
33	19.306	20.24
34	19.020	20.37
35	18.746	20.49
36	18.484	20.61
37	18.233	20.73
38	17.991	20.85
39	17.759	20.96
40	17.536	21.07
41	17.321	21.18
42	17.113	21.28
43	16.913	21.39
44	16.720	21.49
45	16.533	21.58

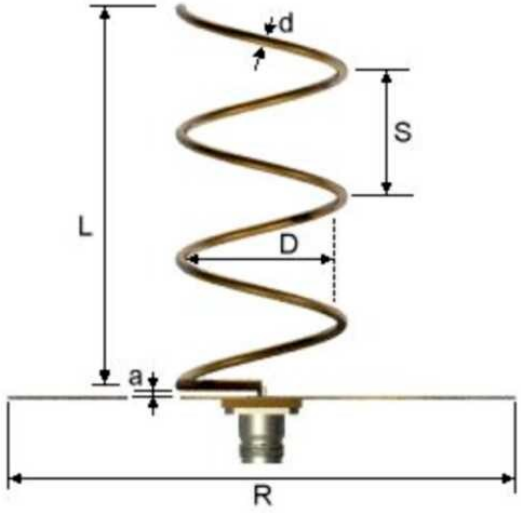

Figure 7: Here is a spreadsheet with formulas for calculating dimensions for a high gain helical antenna. Formulas are derived from Kraus (1988)

Figure 8: ¼ wave matching strip line.

A helical antenna's characteristic impedance is about 150 ohms. To again leverage commercial products, this design uses commonly 72 ohm RG6 satellite grade CATV cable. The cable is good up to 3GHz and connectors and adapters are commonly available. In order to transform the antenna impedance to match the cable and prevent signal reflections and lose, a ¼ wave matching slip line section connects the helix to the coax connector.

Strip Line Matching Calculator

$$Z_{match} = \sqrt{Z_{source} * Z_{load}}$$

Input Z	72 Ohms
Output Z	150 Ohms

1/4 wave ▶ 103.92305 Ohms

(Motorola) $$Z3 := \frac{377 \cdot D}{\sqrt{\varepsilon} \cdot b \cdot \left[1 + 1.735 \cdot \varepsilon^{-0.0724} \cdot \left(\frac{b}{D}\right)^{-0.836}\right]}$$

Frequency	f	1420.405 Mhz
Conductor Dist. To Grnd(mm)	D	5 mm
Conductor Thickness(mm)	d	0.5 mm
Dielectric Constant	eps	1

Quarter Wavelength(mm)	Len	5.2801842 mm
Conductor Width(mm)	**b**	**Impedance**
	8.8	102.9
	8.9	102.2
	9.0	101.6

Figure 9: Antenna Matching Calculations

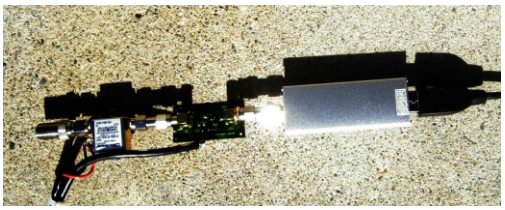

Figure 10: Amplifier chain and DVB-T SDR

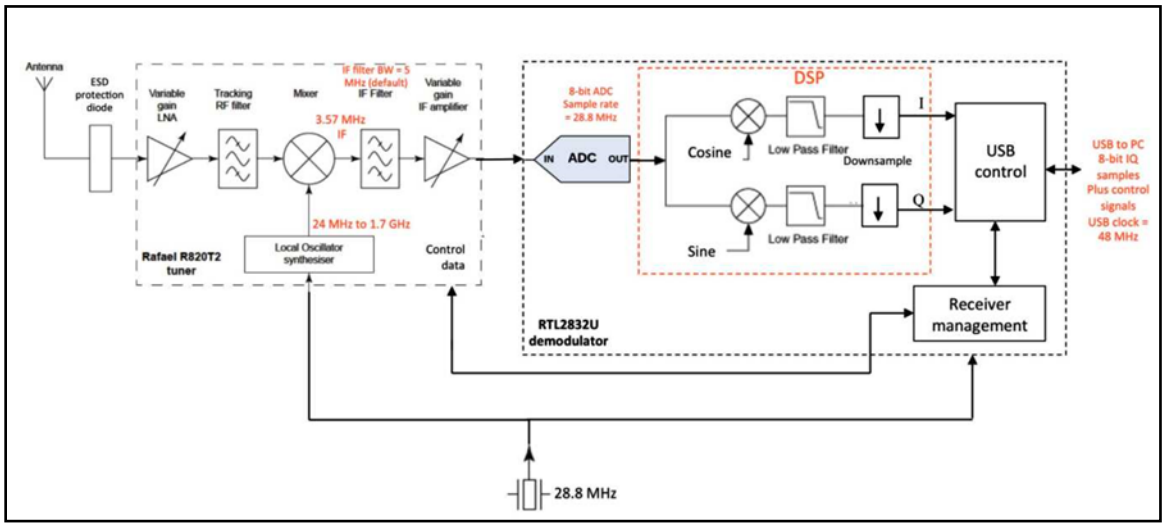

Figure 11: Block Diagram of DVB-TV Dongle

A cascade of two amplifiers boosts the signal from the antenna. The first of these is a MiniCircuits ZX60-P162LN+ device. It provides over 20db of gain and adds only 0.6 dB of noise at 1.4GHz. A less

expensive broadband amplifier follows with a 25dB gain at 1.4GHz and a noise figure of 2.5db. Analysis shows that the noise figure of the entire system is primarily determined by the noise figure of the first antenna in the chain, East (2014), so less expensive amplifiers can be used for later stages.

Figure 10 shows the amplifier cascade in the prototype. For a permanent configuration all the elements will need to be enclosed and weather proofed.

The output of the amplifier chain feeds the input of the DVB-T dongle. Figure 11 shows a block diagram of the DVB-T dongle. The DVB-T dongle's front end can boost the incoming signal from 0dB to 49.6 dB, under software control. This puts the overall max signal gain at a whopping 112.6 dB. This much gain is necessary because the DVB-T dongle has only an 8 bit dynamic range, so gain must be carefully adjusted to boost the source signal into the dynamic range, but not so much that it saturates.

The DVB-T and Rpi computer are heart of the system. The DVB-T implements a software defined radio (SDR) receiver in two chips on a circuit board about 3 cm x 7cm. An SDR uses an oscillator whose frequency is digitally controlled to feed a mixer that multiplies it with the incoming signal. Mixing two signal frequencies in this way produces the following terms:

$$f_{osc} \otimes f_{in} \Rightarrow$$
$$a_1 f_{osc} + a_2 f_{in} + a_3\left[f_{in} + f_{osc}\right] + a_4\left[f_{in} - f_{osc}\right]$$

The resulting signal is then passed through a low pass filter. Note that the first 3 terms are all at least above the oscillator's frequency. Only the final term has low frequency components if the desired reception frequency is near the oscillator's frequency. Thus the desired received frequency, translated down to the range of 0 Hz to 3.57MHz passes through to the backend which digitizes the signal in a phase conserving I-Q format. This I-Q digital data is what is passed to the Rpi computer, which uses digital signal processing (DSP) routines, to extract the desired information from the signal.

For this design, a small low power Rpi Linux computer performs the DSP work. The workhorse software is RTL-SDR (2017). Versions are available for Linux, Windows and OSX. Because the telescope is designed to run drift scan mode, the system will be operating 24 hours a day. A 5 watt system is much preferred over dedicating an expensive power hungry PC running all day long. Additionally, the Rpi is run in "headless" mode. No monitor or keyboard is attached. It runs a Virtual Network Console (VNC) server that allows phones, tablets or PCs to connect to and remotely operate it over a network link.

Table 1 shows the total cost of this simple Radio Telescope is under $200.

Simple Radio Telescope Cost

SubSys	Qty	Item	Unit Cost	Extension	Sub Sys
Antenna					
	1	8' 1x2 lumber	$ 0.89	$ 0.89	
	1	50' spool #10 wire	$ 23.00	$ 23.00	
	1	50 cable tie package	$ 4.00	$ 4.00	
	1	Al. Sheet	$ 2.00	$ 2.00	
	1	F connector	$ 0.55	$ 0.55	
					$ 30.44
Amplifiers					
	1	MiniCircuits ZX60P162LN+	$ 57.00	$ 57.00	
	1	Broadband 1-2400 MHz Preamp	$ 8.00	$ 8.00	
	2	SMA M-M Connectors	$ 4.50	$ 9.00	
	2	F Male Crimp Connectors	$ 0.37	$ 0.74	
					$ 74.74
SDR					
	1	DVB-T Dongle (ebay)	$ 8.00	$ 8.00	
	1	3m USB Extension Cable	$ 4.50	$ 4.50	
					$ 12.50
Computer					
	1	Rpi B+ Computer	$ 25.00	$ 25.00	
	1	16 GB Micro SD Card	$ 7.10	$ 7.10	
	1	USB 2.0 Amp Power Supply	$ 7.33	$ 7.33	
					$ 32.10
Software					
	1	Wheezy Linux	$ -	$ -	
	1	Open Office	$ -	$ -	
	1	RTL_SDR	$ -	$ -	
	1	Radio Sky Eyes	$ 39.95	$ 39.95	
	1	Real VNC Client	$ -	$ -	
					$ 39.95
			Total Cost		$ 189.73

Table 1: Materials cost for the simple radio telescope

5. Observing With An SDR Radio Telescopes

Typically, the telescope is operated by mounting the antenna on a tripod or other stationary mount. The antenna is pointed at the meridian. Its elevation is selected to scan a swath of sky centered on a particular Declination. As the Earth rotates, it pans the antenna through Right Ascensions (RA) corresponding to the current Local Sidereal Time (LST).

The telescope takes data by starting RTL_POWER program. The program's parameters include:

a. The frequency range to measure
b. The bandwidth of each power bin
c. The integration time for each measurement
d. The name of the desired output file

The program takes enough samples to cover the requested bandwidth and performs a Fast Fourier Transform (FFT) on that sample set, measuring received power in each power bin. It repeats that process during the integration interval, averaging the power in each bin. At the end of the integration interval, it outputs a text line to the output file, using comma separated value (CSV) format, compatible with many spread sheet and plotting programs. It

repeats that process for a specified period of time, or until it is interrupted.

The result is a matrix of data containing the power measurements. Each row of the matrix is the power spectra at a specific time for the integration interval. Each column of the matrix is the power at a specific frequency. If you sum columns you end up with the the power over the entire frequency range as a function of time(RA). If you sum the rows, you get the power spectrum as a function of frequency, which is easily converted to power as a function of wavelength.

Figure 12 shows a typical Power vs RA plot for a 13 hour session. Figure 13 is the same data plotted with a section of the radio sky from the Radio Sky Eyes program. Radio sky eyes is the radio equivalent of a planetarium program for radio astronomy. It has maps of the radio sky at different frequencies, identifies radio sources, calculates elevations, transit time, fringe periods, and will even controls and script a steerable radio telescope antenna.

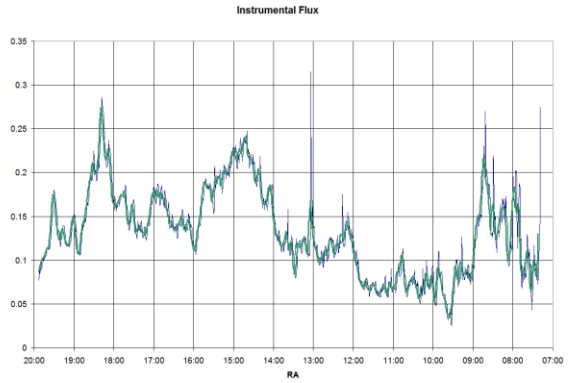

Figure 12: 13 Hour Drive Scan At Declination –5°

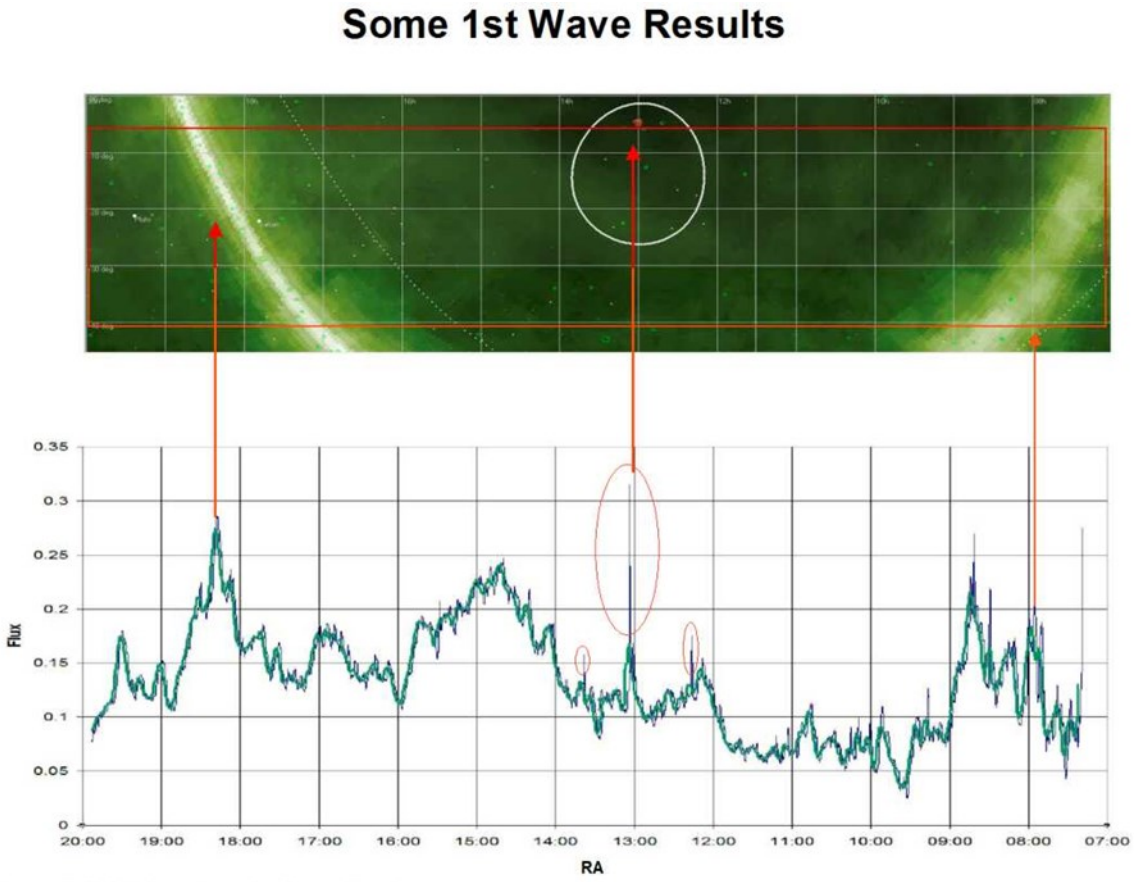

Figure 13: Drift data aligned with a radio sky map

The red arrows indicate the likely sources of increased energy in various parts of the trace. On the left and right you can see the response to neutral hydrogen in the arms of our galaxy.

In the center, the large spikes are apparently caused by activity at Jupiter. Investigation of the data shows that this was the largest of at least 3 such events captured. Each event is very short lived, taking approximately 30 seconds. Figure 14 zooms in a single, 30 second, integrated spectra centered very close to 21.1cm rest wavelength of neutral hydrogen. There are three peaks, the first centered at –14.25 km/s. The two flanking peaks have blue and red shifts of +11.52 km/s and –52.68 km/s.

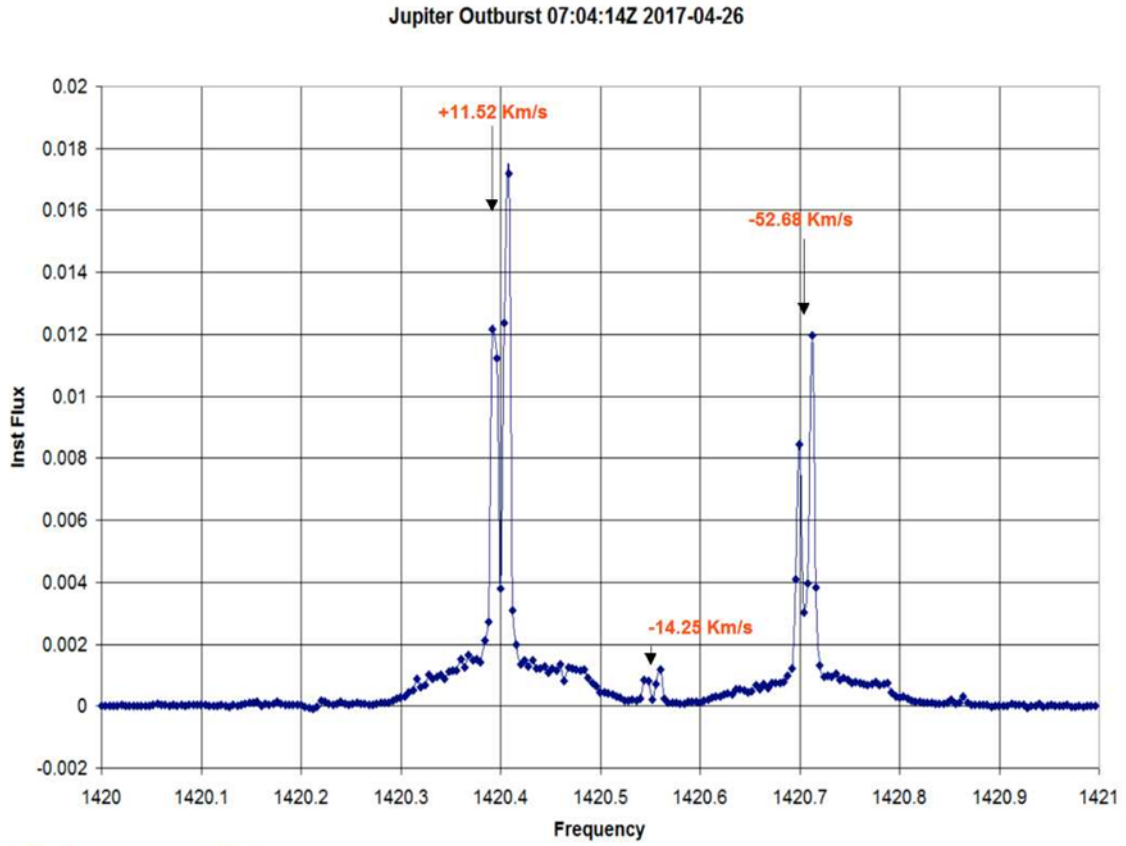

Figure 14: Jupiter Outburst Event

One hypothesis suggested by the data is that a cloud of neutral hydrogen moving away from the Sun collided with Jupiter. Atoms in the cloud were accelerated by Jupiter's strong bipolar magnetic field. The fields bent one stream back at us and the other shot away. The delta velocity changes are symmetric at +/- ~32 km/s. Another piece of supporting evidence for this being a synchrotron event caused by strong magnetic fields is that each of the 3 lines are double, a possible sign of Zeeman splitting!

Figure 15 is a scatter plot of power during the scan where the color/symbol indicates the observation's frequency and the observation's energy by the color/symbol's Y position. From this plot the points with the highest energy in each arm, were selected and their red shifts annotated on the figure. From this calculation the recessional velocity is between 92 km/s and 93 km/s. This number is below the published values, but not a bad start for wide field instrument taking a single sample.

Figure 16 is a subsequent 24 hour scan at Declination of $+12^{o}$ that has been RA calibrated, annotated and overlaid with a sky map of the swath. Reasonable guesses as to the causes of prominent features have been marked. One of the results of this analysis is that strong signal sources, well out of the predicted beam diameter, appear in the plot. The beam is not a sharply defined entity. It has a roll off, and side lobes of increased sensitivity far off axis. Clearly, while adequate sensitivity has been demonstrated, more resolution is required!

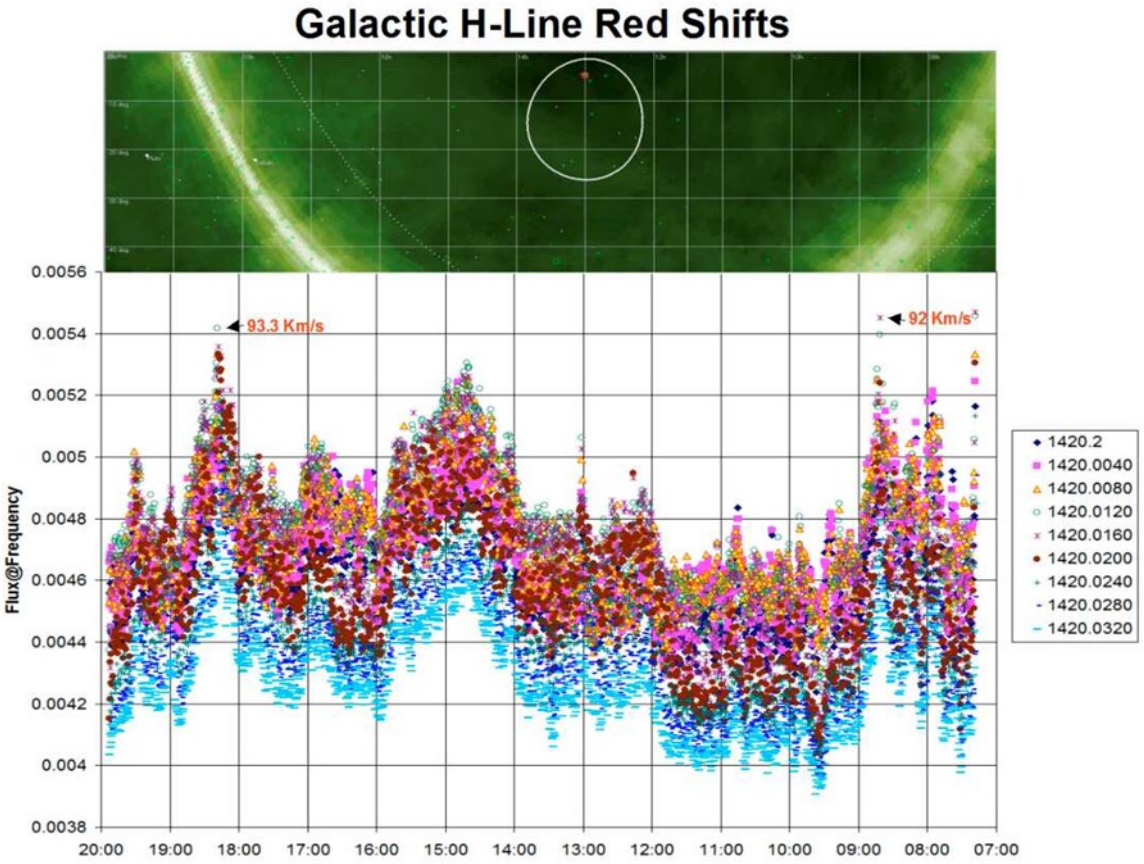

Figure 15: Galactic Arm Redshifts

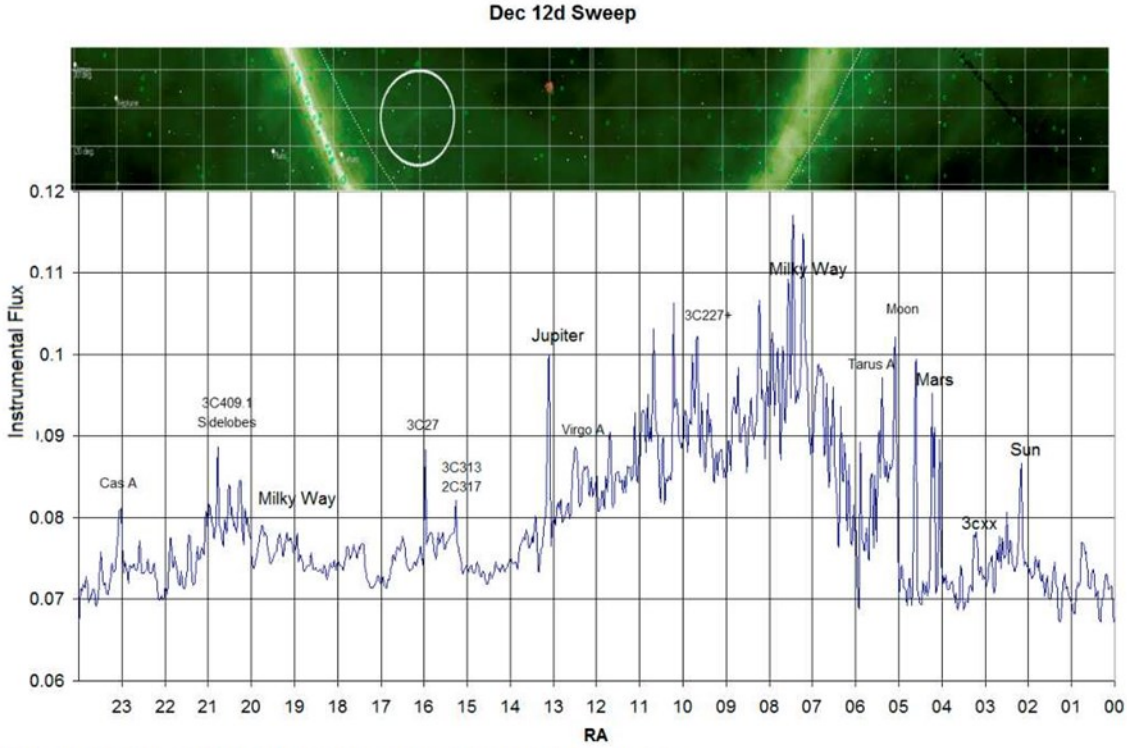

Figure 16: Annotated Drift Scan Centered At Declination +12.11 Degrees

6. Upgrading to an Interferometer

Increasing the length of an axial antenna's boom to achieve a resolution of 1 degree is physically impossible. For most, increasing the aperture of a dish or feed horn to achieve 1 degree resolution is fiscally impossible. Fortunately there is another alternative, interferometry. Figure 17 shows formulas that model the response of a pair of antennas separated by a known difference respond to a source.

$$P_2 = e^{-(\phi \pi R/\lambda)^2} \cos^2\left(\frac{\psi}{2}\right)$$

$$\psi = \frac{2\pi s}{\lambda}\sin(\phi)$$

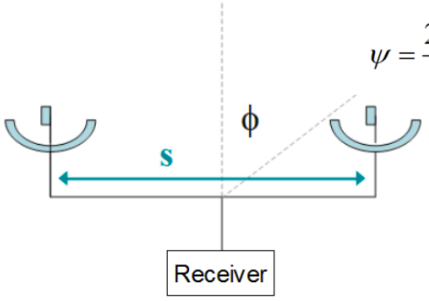

Figure 17: Mathematical model of interferometer beam formation

Basically as the aspect of the target changes, for a given frequency, the signal's phases change with respect to each other, causing the signals to alternately constructively combine, and then destructively cancel each other as they reach a phase difference of 180 degrees. The formula below shows how near on axis signal as a function of aspect change.

$$\theta \approx \frac{\lambda}{S} = \frac{0.2112m}{15.24}$$

$$\theta \approx .8^o \qquad \text{(for s = 50 feet)}$$

The total response of the system is the convolution of the interference pattern and the individual antenna's native beam response. Figure 18 shows the resulting system response.

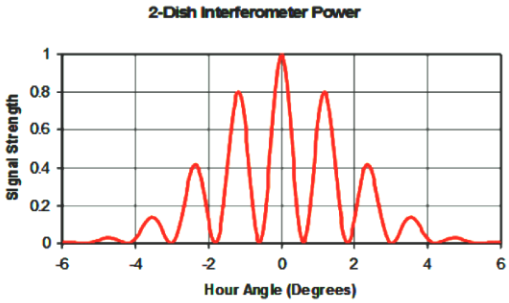

Figure 18: Response of 3m dishes spaced 50 ft apart.

7. A 3 Element Interferometer

To achieve a 1 degree resolution, three antennas are placed in a Y configuration as shown in Figure 19. This gives a beam width of 0.8 degrees east to west, and a north to south beam width that is 0.8 degrees/sin(target elevation). A north south distance of 75 feet was chosen to assure a beam width less than 0.8 degrees for targets above 45 degrees elevation. The interferometer is intended to be a meridian drift scan system where all antennas are pointed at the same elevation when observing.

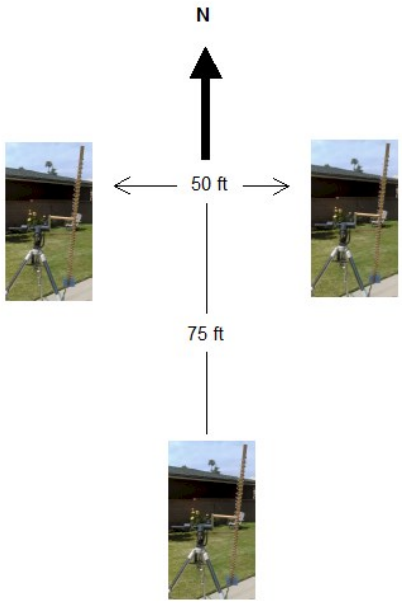

Figure 19: Meridian transit radio telescope configuration with resolution <1 degree.

In order to upgrade the simple radio telescope design above to a simple interferometer, two additional antennas need to be fabricated. Figure 20 shows a block diagram of how the simple interferometer is fabricated.

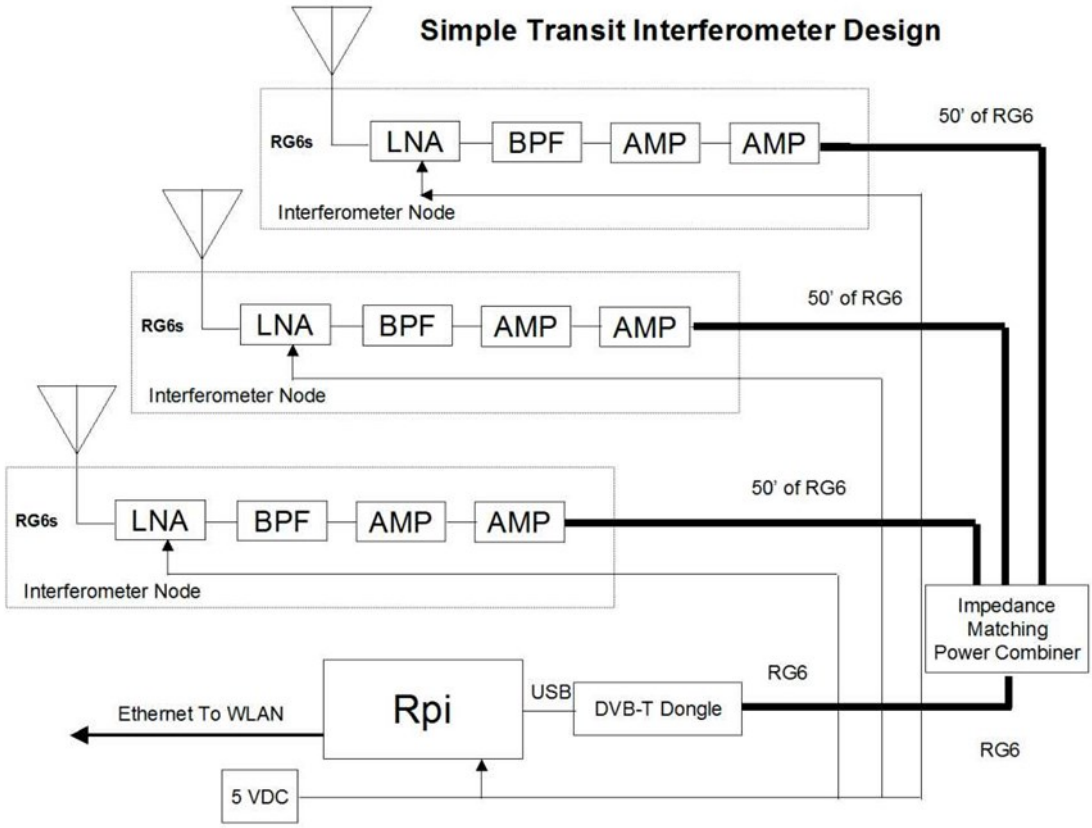

Figure 20: Block diagram of the simple transit radio interferometer

In this design in addition to fabricating 2 additional antennas, three 50 foot lengths of low loss RG6 cable are added to carry the signal from the antennas to the signal combiner. To overcome the cable losses, an additional booster amplifier is added at each antenna. The signals are combined using a standard satellite grade 3:1 signal splitter. Table 2 summarizes the total expense. It shows that for around $500, an interfermetric radio telescope can be assembled that can resolve sources to within ~1 degree.

8. Future Directions

As mentioned earlier in this paper, poor rejection of strong off-axis signals by helical antennas is a weak point in this first iteration of the design. A new feed horn design has just been completed. It anticipates adding 2 dB of additional gain to the antennas, improving side lobe rejection and adding little in additional cost. Design details are contained in Figure 21. The antennas are to be fabricated from ¼ inch plywood with aluminum foil laminated to the interior surfaces. Additionally, they will be fitted with dual feed posts, one feed to the receiver and the other feed from a switched calibrated noise source. This addition will provide the ability to calibrate the system noise and track system gain, East (2014).

Once these changes are complete and the first unit is operating and permanently installed at The Center For Solar Systems Studies, SSC Observatories (SSCO) will publish complete plans and parts lists to encourage others to duplicate the system. If participants are willing, they shall be assigned Declinations, and software will be provided to them to upload their daily scans to a database that will generate a web accessible daily image of the radio sky and automatically detect and post transients for follow up observations.

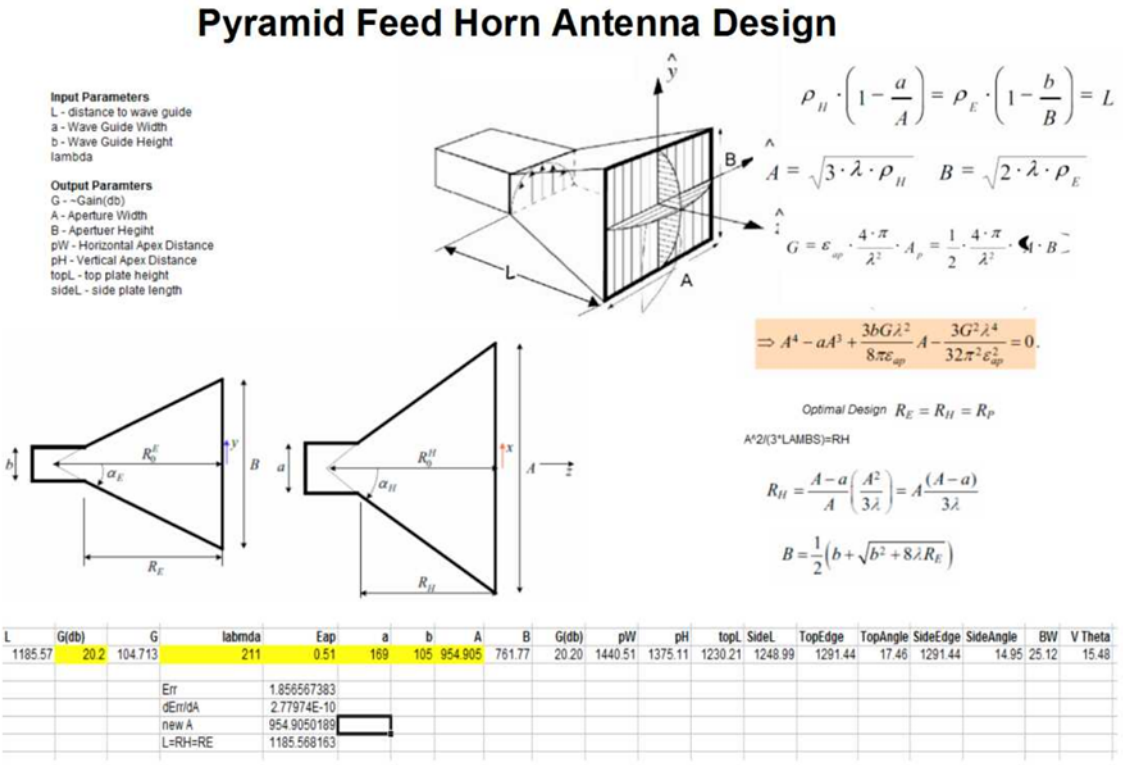

L	G(db)	G	labmda	Eap	a	b	A	B	G(db)	pW	pH	topL	SideL	TopEdge	TopAngle	SideEdge	SideAngle	BW	V Theta
1185.57	20.2	104.713	211	0.51	169	105	954.905	761.77	20.20	1440.51	1375.11	1230.21	1248.99	1291.44	17.46	1291.44	14.95	25.12	15.48

Err	1.856567383
dErr/dA	2.77974E-10
new A	954.9050189
L=RH=RE	1185.568163

Figure 21: Pyramid Feed Horn Design For Hydrogen Line Astronomy

Simple Interfermetric Radio Telescope Cost

SubSys	Qty	Item	Unit Cost	Extension	Sub Sys
Antennas					
	3	8' 1x2 lumber	$ 0.89	$ 2.67	
	2	50' spool #10 wire	$ 23.00	$ 46.00	
	3	50 cable tie package	$ 4.00	$ 12.00	
	3	Al. Sheet	$ 2.00	$ 6.00	
	3	F connector	$ 0.55	$ 1.65	
					$ 68.32
Amplifiers					
	3	MiniCircuits ZX60P162LN+	$ 57.00	$ 171.00	
	6	Broadband 1-2400 MHz Preamp	$ 8.00	$ 48.00	
	9	SMA M-M Connectors	$ 4.50	$ 40.50	
	2	F Male Crimp Connectors	$ 0.37	$ 0.74	
					$ 260.24
Feed Lines					
	3	50 ft RG6 Cable	$ 20.00	$ 60.00	
	1	150 ft spool #16 wire	$ 12.00	$ 12.00	
	1	Satellite Signal Splitter	$ 10.00	$ 10.00	
					$ 82.00
SDR					
	1	DVB-T Dongle (ebay)	$ 8.00	$ 8.00	
	1	3m USB Extension Cable	$ 4.50	$ 4.50	
					$ 12.50
Computer					
	1	Rpi B+ Computer	$ 25.00	$ 25.00	
	1	16 GB Micro SD Card	$ 7.10	$ 7.10	
	1	USB 2.0 Amp Power Supply	$ 7.33	$ 7.33	
					$ 32.10
Software					
	1	Wheezy Linux	$ -	$ -	
	1	Open Office	$ -	$ -	
	1	RTL_SDR	$ -	$ -	
	1	Radio Sky Eyes	$ 39.95	$ 39.95	
	1	Real VNC Client	$ -	$ -	
					$ 39.95
			Total Cost		$ 495.11

Table 2: Simple Interfermetric Radio Telescope Costs

Finally, Figure 22 is a block diagram for a DSP steerable phased array implementation. The interferometer uses SDRs at each antenna. Raw I-Q data will be streamed over CAT5 cable to an additional processor that will implement phase delayed correlation. This should allow the synthesized beam to track +/- 10 degrees above, below, east and west of the nominal focus point. Phase coherence will be maintained by modifying the DVB-T dongles to accept clocking from a central oscillator over the same CAT5 cable that handles the network traffic, and distributes power to the nodes.

9. Conclusion

The successful operation of this family of prototype Radio Telescopes, based on inexpensive consumer products, demonstrates that Radio Astronomy is within everyone's means. The time has come for amateurs, educators and small institutions to start observing at radio wavelengths. As with optical astronomy, large institutions have instruments of exquisite resolution and high sensitivity, but their resources are narrowly focused and scarce. The capability now exists for a legion of citizen scientists to observe much more of the sky with the chance of finding missed transients and new phenomena.

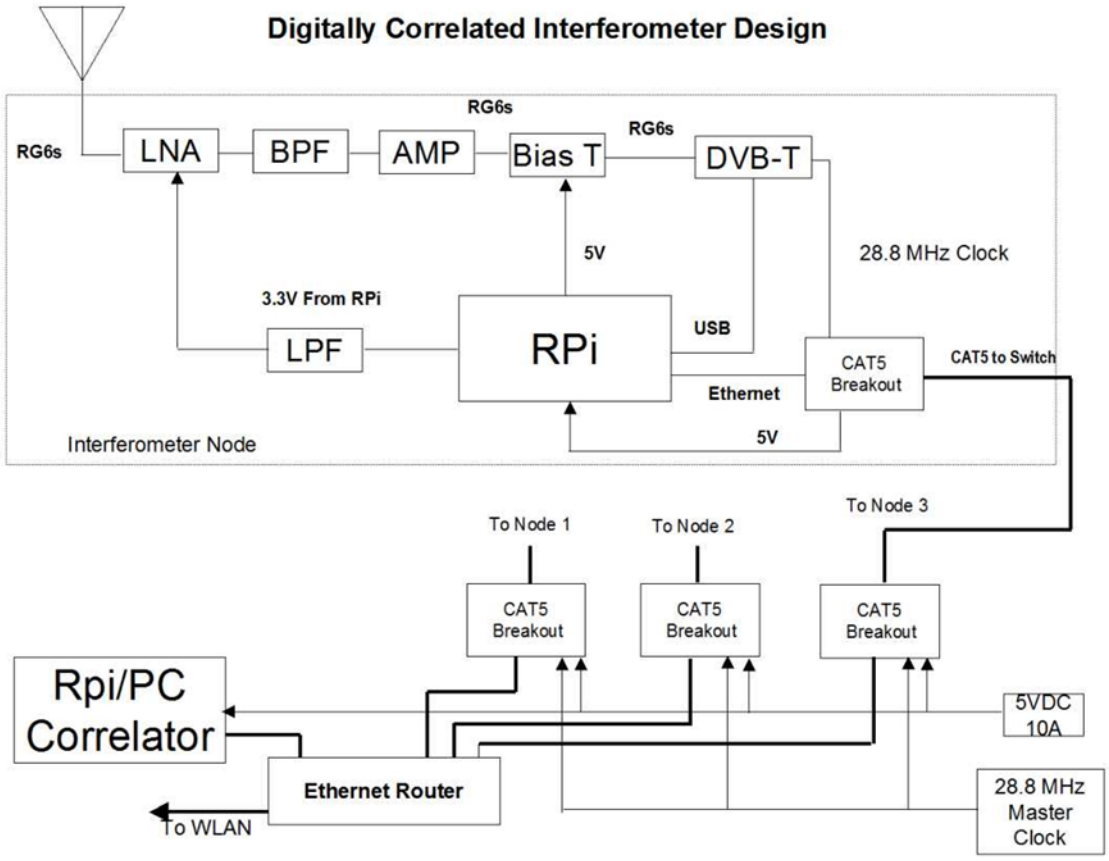

Figure 22: A DSP Steerable Phased Array Interferometer Design

10. Acknowledgements

I wish to acknowledge my gratitude to the late Dr. Eduardo Vega for his support and encouragement to pursue radio science. To my wife Layla, for her patience with my obsessive curiosity and to the Center For Solar Systems Studies for providing a site for the pilot system.

11. References

Berry, Kantoa and Munger, *The CCD Cookbook Camera*, Willmann Bell, 1994.

East, P.W., "Hydrogen Line Radio" (2014), http://y1pwe.co.uk/RAProgs/index.html

Fry, E., Palosaari, A "Private Corresponence" (2011) *Open Source Mobile Communications,* http://osmocom.org/projects/sdr/wiki/rtl-sdr

Hoot, J.E. "Uncool Science: Photometry and Astrometry with Modified Web Cameras and Uncooled Imagers" (2004), *The Society for Astronomical Sciences 23rd Annual Symposium on Telescope Science. 23-33.*

Hoot, J.E., "Photometry With DSLR Cameras". (2007), *The Society for Astronomical Sciences 26th Annual Symposium on Telescope Science,* 67-72.

Kraus, J.D., *Radio Astronomy,* McGraw-Hill, N.Y 1966.

Kraus, J.D., *Antennas,* McGraw Hill, N.Y. 1988.

Lovell, Bernard, *Astronomer By Chance,* The Arthur P. Sloan Foundation, NY 1990.

RTI-SDR, "About RTL-SDR" (2017), http://www.rtl-sdr.com/about-rtl-sdr/

Using All Sky Imaging to Improve Telescope Scheduling

Gary M. Cole
Starphysics Observatory
14280 W Windriver Ln, Reno, NV 89511
garycole@mac.com

Abstract

Automated scheduling makes it possible for a small telescope to observe a large number of targets in a single night. But when used in areas which have less-than-perfect sky conditions such automation can lead to large numbers of observations of clouds and haze.

This paper describes the development of a "sky-aware" telescope automation system that integrates the data flow from an SBIG AllSky340c camera with an enhanced dispatch scheduler to make optimum use of the available observing conditions for two highly instrumented backyard telescopes.

Using the minute by minute time series image stream and a self maintained reference database, the software maintains a file of sky brightness, transparency, stability, and forecasted visibility at several hundred grid positions. The scheduling software uses this information in real time to exclude targets obscured by clouds and select the best observing task, taking into account the requirements and limits of each instrument.

1. Background

While many observatories now have all-sky cameras, full integration with telescope scheduling is still uncommon.

The most recent published work the author is aware of comes from a conference paper by Mandeville, et al. (2015). In that work methods of calibration for all sky images are developed and shown to capable of providing cloud detection for telescope targeting.

In the current work, the author describes his own methods for rapid sky analysis, introduces forecasting techniques, and explains the integration of sky data into the scheduling process.

The system described herein is in nightly operation in the author's backyard.

2. Introduction

Automated astronomical observing systems are controlled by telescope scheduling software. These schedulers generally begin with the assumption that the entire sky is clear, transparent, and stable.

While this may be an excellent assumption for large mountaintop observatories, it does not necessarily apply very well to typical backyard observing sites.

The work outlined in this paper has been to integrate the image stream of an off the shelf all-sky camera into the decision process of existing automatic telescope scheduler.

The primary goal has been to ensure that each target selected for observation will be actually observable, findable, and have sky conditions suitable for the duration of the intended measurements.

There are two parts to the software that has been developed for this project. The first is called the Sky Processor (SP). The second is called the Sky-Aware Telescope Scheduler.

The Sky Processor uses the real-time image stream coming from the all sky camera to maintain a real time database called the Sky Report.

This software performs a time series analysis of the image sequence to construct brightness, transparency and stability values for each point in a preset grid of sky positions.

It also generates, when sky conditions permit, a forecast for the duration of the observing window.

The Sky Aware scheduler an upgrade of an existing telescope scheduler previous described in Cole (2008).

This upgrade modified the scheduling process to take the sky conditions and the instrumentation into account before committing to begin a new observation.

3. The Observatory

The author's backyard hosts a C-14 and a C-11 telescope in addition to the AllSky camera. The C-14 has a 10'x15' FOV at f9, the C-11 is 18'x29' at F6.2.

Homeowners association rules prevent permanent structures. Telegizmos 365™ covers are put in place whenever bad weather is expected.

A variety of instruments are installed to support PEP and imaging photometry, polarimetry, spectroscopy, spectropolarimetry, filtered and polarized imaging. Ten CCD cameras and two photometers collect data.

Figure 1 The author's backyard observatory

The system is controlled by a 16GB Mac mini running a current version of OSX which serves as an outer software layer.

Within it, three WindowsXP™ virtual machines (C14VM, C11VM, and AllSkyVM) operate under the control of a Parallels™ hypervisor.

The control and data files (some 600Gb) are accessed directly from the shared OSX file system.

The C14VM and the C11VM each run a version of the sky-aware scheduler as well as their full complements of astronomical software.

The Sky Processor and the camera software run within the AllSkyVM.

4. The Camera

The SBIG AllSky-340c camera used in this work uses a KAF 340 ccd. It is equipped with a high quality fisheye lens enclosed in a weatherproof housing.

The sky is imaged through an acrylic plastic dome. The camera assembly is strapped to a fencepost chosen to have a clear view of the sky seen by the telescopes.

The short 1.4mm focal length and fast f/1.4 ratio create a plate scale of approximately 18 arc minutes per pixel.

Figure 2 – The AllSky Camera

Given that stars appear to move on the meridian at 15 arc minutes per minute, all the light from a star will be captured in one or at most two pixels during a 60 second exposure.

The result is an imaging system that, in my suburban backyard, records stars to about 5.5 magnitude, which is as good or slightly better than the naked eye limit. It also very clearly shows the large scale structure of the Milky Way.

The camera generates color images using a Bayer mask. As a result, bright stars change color as they move across the sky.

Note that the AllSky camera must be within about 100 feet of the telescope(s) so they both see the clouds in the sky from the same perspective.

The camera uses a serial interface linked with a 50ft Db9 cable attached to the computer using a Keyspan™ usb converter. The download time is just under a minute at 115K baud. Hence the average age of the image when displayed is about 90 seconds from mid-exposure. The next image is taken during the download process so virtually the entire night time is recorded.

There is one serious problem with this system. Bright moonlight internally illuminates and scatters on one side of the plastic dome, overwhelming the starlight from part of the sky. A discussion of this will be found later in this paper.

Figure 3 – The Night Sky in Reno

5. The Camera Software

The SBIG AS340 software automates camera operations to provide current and time lapse displays of the sky images. Once started, it operates reliably and continuously for long periods of time.

Exposure is dynamically adjusted up a maximum preset exposure (nominally 60 seconds) used during dark night imaging. Automatic dark frames are taken as exposure changes are made.

The software creates a FITS format file of each image into a user designated directory.

The image file names are sequential numbers making it very easy to process them in order.

The FITS headers provide the exposure time and the UTC time of the image.

6. The Sky Processing Software

The Sky Processing software (SP) is an independent program written by the author which runs continuously within the same virtual machine as the SBIG camera software.

Upon start, the Sky Processor determines the highest numbered image that has been recorded. Once this image has been processed, it then waits for the next higher numbered image to appear. This repeats until a flag set by a user command terminates operation.

The output of the Sky Processor is a text file called the Sky Report for use by the telescope scheduler. A new version is created as each new image is processed.

An important design goal for this software is for it to be able to complete its work before the arrival of the next image. This ensures that the sky information provided to the telescope scheduler is no more than 2 minutes old.

The Sky Processing software is written in VBScript, augmented by the API of CCDSoft™ and by a small group of image processing functions written in Visual Basic™.

6.1 Sky Processing – Part I

Once a new image is available, the Sky Processor executes a Windows script command to launch the CCDSoft application using a command line containing the file name of the image.

CCDSoft opens with the image file loaded. Using the scripting API, the Sky Processor extracts the UTC date-time and the exposure time from the FITS header.

Next, the Sky Processor sends a Window's shell command to CCDSoft to extract and save the luminance layer. In the current implementation the color information is ignored.

A final shell command (Show Inventory) is issued which executes the Sextractor process of CCDSoft on the luminance image.

Sextractor locates stars and other extended objects within the image through a detailed examination of local variations in brightness.

The Sextractor result is called the SRC LIST. For each object it lists, in text format, the X and Y centroids, apparent magnitude, full width half maximum (FWHM), ellipticity, and other details.

6.2 Sky Processing – Part II

The Sky Processor defines a logical fixed grid on top of the image. This consists of 10x10 pixel square segments.

The total grid consists of 64 by 48 cells. Of these, approximately 2000 enclose the visible sky. Each cell represents an area of about 3° x 3°. An information record in the Sky Report will be generated for each cell for possible use by the telescope scheduler.

The actual sky area in each cell varies slightly due to the projection of the camera optics.

The system next measures the background luminosity of the sky in each grid cell. This is done by first sorting the pixels into a histogram of intensity and then accumulating the total value of the lower 90% of the pixels within each cell. The resulting value is adjusted by the exposure time, the pixel count, and bias so that luminosity is recorded on a unified scale.

Since a star image is contained within just a couple of pixels, this process is effective in ignoring the contribution of stars in the cell. Note that, even in the dark sky conditions, only half of the grid locations will contain a star.

The software maintains a moving time series of the last 30 minutes of these luminosity values. The telescope scheduler will receive both the current value and the time series variance at each grid position.

At this point the sky processor is done with the image itself. Subsequent analysis is done using SRC LIST.

6.3 Sky Processing – Part III

The list generated by Sextractor contains stars and many other items that create brightness variations. Such items include edges and interior variations in clouds, rooflines, trees and foliage along the horizon. These items also include internal reflections generated within the plastic dome of the camera, primarily from moonlight. There are also occasional hot pixels in the images which masquerade as stars.

The object list from Sextractor is fed through a filtering process containing the following steps.

The first step is to exclude all objects outside of the circle centered on the Zenith point and extending to the physical horizon. In the author's site the lowest physical horizon is at approximately 10° of elevation.

The next step is to exclude all objects whose FWHM is less than one or greater than three pixels. This has the effect of eliminating most of the artifacts generated by the roof lines, foliage, and cloud edges that tend to be larger and ellipsoidal in shape.

If the moon is in the sky, objects within a 30° circle centered on the moon are removed. This is necessary because of light scattering within the plastic dome surrounding the camera.

Finally, all the objects in the remaining list are compared with the lists generated in the two previous iterations. Any object whose position is constant in all three lists is excluded. This last filtering step removes any hot pixels that may have found their way into the image and which otherwise look just like bright stars.

Note: objects in a small circle centered on the north star are not excluded by this process because stars in this location will not show any movement over a few minutes.

6.4 Sky Processing – Part IV

If clouds are present, there will be parts of the sky in which no stars are to be found. The Sky Processor iterates over all grid cells contained within the sky radius in order to identify those areas which are totally obscured and those which are not.

There only a 50% likelihood, even in dark conditions with 500 or so stars visible, that a star will be found within an individual grid cell. Therefore, a larger region, centered on the cell, is used as a filter against the star list.

Note that we are using a fairly large area in which to locate stars. This is necessary because, when a bright moon is above the horizon, dim stars are not detected.

If no stars are found in this search, the cell is marked as a cloudy cell. If any stars are found, the cell is marked as a clear cell.

An integer is used to record the state of the cell. If the cell value is already positive, it will be incremented if the cell is now clear. If the cell is already negative, it will be decremented if the cell is now cloudy. If the cell state has changed, a new value of +1 or -1 will be set.

This simple process provides a record of how long the cell has remained in the current state. For example, a value of 13 means that the cell has been clear for the past 13 reporting cycles. The averaged values provide a useful index of overall sky stability.

6.5 Sky Processing – Part V

Even an ideal atmosphere induces a measurable level of extinction that is correlated with airmass. Although an important factor from a scientific perspective, normal airmass extinction rarely impacts the ability to find and measure sky objects.

Other factors can exercise a much larger effect upon telescope performance. These include cloud edge haze, thin cirrus cloud layers, dust trapped in local inversion layers, and smoke from wildfires.

The author identifies the additional reduction in star brightness from non-airmass sources as "excess extinction" or "obscuration." The degree of excess extinction is position dependent and time variable.

Significant excess extinction can make a particular observation impossible in an area of the sky which would not be marked as cloudy.

It was realized by the author that the unusual observing system allowed a very simple method of obtaining this particular information with much less complexity than the full extinction analysis (for monochrome cameras) described in Mandeville (2015).

It is a fact that there are only a limited number of unique clear sky images (excluding the moon, planets, comets, meteors, and airplanes) from a fixed camera at this focal length and plate scale.

Given the use of one minute exposures, and the fact that a star spends 1 minute or more on a specific pixel, there are only 1440 distinct images, one for each unique sidereal minute.

Thus, if an another image, taken at the current sidereal minute in clear sky conditions is available, the instrumental star magnitudes can be directly differenced to determine the excess extinction.

Optical distortions and CCD pixel response will be the same in both images.

Naturally the source of such comparison images must be the camera itself. Its optical system must be fixed, and the camera itself must not move over time. For an all sky imager, these are reasonable constraints.

6.5.1 Maintaining the Reference Database

In this system a collection of image data made during periods of excellent sky conditions is maintained in a folder called the "Reference Database".

Within this collection the filename of each record contains the text value of the sidereal minute of the original image.

Every image with a total star count greater than a preset threshold is considered as a candidate for membership in this collection. Using a threshold excludes moonlit, hazy and cloudy images.

When the current candidate has a has a higher star count than the existing reference for that sidereal minute, the reference will be replaced with current data.

In this way the collection evolves to have the very best sky data for each minute.

The reference files are the fully filtered star lists produced during the Part III processing.

Note that the generation of a useful reference database occurs very quickly because several hundred potential reference observations are made during each clear night.

6.5.2 Determining the Excess Extinction

As described in a previous section, the star count for a grid position is determined by defining an extended search region around that position. The same filter is applied to the star list obtained from the reference database for the sidereal minute of the current image.

A short list of the brightest objects from each of the star lists is created. These items are paired using the X and Y pixel positions. This correlation is necessary to exclude a planet or other transient item that may have been included in the current or reference star lists.

The differences in magnitudes for each of the star pairs are averaged to determine the "excess extinction" value for that grid position. Only positive results (an actual reduction in brightness from the reference) are used. Negative results are recorded as zero.

This process is repeated for every grid position that has not already been marked as cloudy.

In addition, the sky processor maintains a time series of these calculated values for each grid position. The variance of the data within the time series is made available to the telescope scheduler as an additional metric of local sky stability.

7. Forecasting

The telescope scheduler needs know that a target's sky position is likely to remain clear for the duration of the intended measurement.

Forecasting cloud movement is complicated and computationally intensive. See Lam (2015) for a solar energy example. See Mandat (2014) for a night sky example.

This application, fortunately, is not so demanding. Simple heuristics and time series analysis provide short term projections that are both useful and easy to obtain at two levels. The full sky forecast deals with the evolution of the whole sky. The grid forecast provides a local projection for each cell.

7.1 Full Sky Forecasting

This is done by monitoring the percentage of the sky which has been marked as cloudy. As with other data, this is maintained in a time series within the Sky Processor. So long as the total cloud coverage is less than a minimum threshold (nominally 10%,) no forecast is generated.

When that threshold is exceeded, a simple linear slope is computed using the two most recent images and two points from 5 and 6 cycles in the past. If this slope indicates increasing cloudiness, a "CloseIn" value, expressed in minutes, is reported as a summary parameter in the Sky Report.

The telescope scheduler has been programmed to prevent issuing any task expected to take more than the projected closure time. It effectively stops scheduling when the forecast is for less than 10 minutes.

Note that it is the short term change in cloud coverage that drives this parameter, a steady level of cloudiness does not of itself prevent telescope activity.

7.2 Grid Level Forecasting

The Sky Processor calculates a forecasted "lifetime" for every clear grid position.

The cell forecast is calculated from a time series data set maintained at each grid position. A minimum number of data points must be accumulated before a forecast is generated. The time series is cleared when the cell becomes cloudy. As a result, a minimum duration of clarity must occur before a forecast is calculated.

Starting from the grid cell location, the Sky Processor executes what could best be thought of as a spiral search around that cell. The search continues until a predefined maximum search radius is reached, or until a cloudy cell is found. The "distance" to the nearest cloudy cell is recorded in the time series.

The most recent distance and the rate of change measured from the previous time series entries are used to generate a number. If positive, it is the number of cycles remaining before the cell becomes cloudy. This is based upon an assumption of constant linear cloud motion. That assumption is often wrong.

Note that the time computed must be reduced to take into account the 2+ minute delay between the exposure and its availability in the scheduler. The reduced value is the one actually put into the sky report.

7.3 Meta Forecasting

The grid forecasts are based upon the simple assumption that clouds are moving in a uniform and relatively slow manner across the local sky dome. This is a reasonable assumption some of the time, and absolute nonsense at other times.

The conditions which enable useful forecasting are those where the cloud edge is moving at the rate of 2 grid cells or less per minute. A grid cell spans about 3°. A cloud edge angular movement of 6° will turn two cells from clear to cloudy. When the cloud layer is a mile above the observing site, 6° represents a linear movement of 550 feet and a speed of about 6 miles per hour.

In this situation, a forecast of 3-5 minutes would be meaningful. Slower motion would create longer forecasts.

Long lived, virtually static and well defined cloud banks are not uncommon in Northern Nevada. Grid forecasts made in these condition are quite reliable.

At other times clouds appear in multiple layers moving in very different directions at significantly different speeds. In such circumstances the basic forecasting assumption of linearity is invalid, and the forecasting procedure generates worthless data.

What is needed is a way to differentiate between conditions that generate good forecasts and and those that do not without complex sky analysis.

For this purpose, the author has implement a form of meta analysis in which the system evaluates the degree to which its own recent forecasts have proven to be accurate.

For example, if a forecast of 10 minutes was computed for a particular grid position, the status of that cell can be tested during each of the subsequent 10 minutes.

If the cell becomes cloudy, or if the forecast has become shorter at a rate faster than the progression of time, then the original forecast was invalid.

If on the other hand the cell remains clear and the forecast either decreases as expected or actually increases, then the original forecast was a good one.

Aggregating this over all the cells where forecasts have been created provides a percentage of success of forecasting at each point in the recent past.

When a high success rate is observed, the Sky Report tells the scheduler that it may rely on the the cell level forecasts. A cell with a history of unreliable forecasts will be marked as a poor place for observation.

8. The Moon

Image analysis is significantly impacted by the presence of the moon. On nights when the moon is nearly full, about 15% of the sky image is obliterated by a circle of overexposed moonlight and optical artifacts spreading from the center of illumination.

This problem is created by scattering within the camera's protective plastic dome. The dome material is glowing from internal refraction. The long exposure time makes this scattering visible.

To minimize the effects, the sky processor software determines the moon position using a formula and excludes objects within a significant radius of that point. This means, within a circle of about 30°, no useful data is collected.

Bright sky hides dim stars, but the instrumental magnitude of the remaining bright stars is not significantly impacted. The means that the excess extinction values are valid for the rest of the sky.

9. The Sky Report

The Sky Report is a text file approximately 300K in size. The most current version of this report can be accessed by the telescope schedulers.

The report contains Keyword and Grid records. Keyword records provide parameters needed to interpret the report and overall sky conditions. Some of the more significant are shown in Table 1 below. Note the the items marked with ** are used by the scheduler to convert Alt-Az coordinates into grid cell positions.

9.1 Keyword Parameters

CenterX, CenterY	Position of the Zenith Pixel**
PoleAng	Angle from Zenith to Polaris.**
AltScale	Pixels per degree on radial from Zenith**

CloudPct	Percentage of sky which is cloudy.
ClearAvg	Average lifetime of clear cell.
CloudAvg	Average lifetime of cloudy cell.
CloseIn	Forecasted minutes till 100% cloudy
SkyFlux	Luminosity in Zenith Region.
StarCnt	Number of stars found.
Source	Original Image File name
SRCTime	UTC of original Image
SRCLST	Local Sidereal Time of original image
MoonX, MoonY	Pixel coordinates of Moon if in image
ZDepth	Sky Processor cycle count
GoodCnt	Star count of reference image for this LST
FcstPct	Percent of cell forecasts the were correct.

Table 1 – Sky Report Keyword Data (subset)

9.2 Grid Parameters

A grid record is a fixed format line of text consisting of numeric values for the items shown in Table 2.

X	Horizontal Grid Cell Index
Y	Vertical Grid Cell Index
CC	A count representing the time that the current state (cloudy or not cloudy) has persisted.
L	The background luminosity at each grid position. A value of 26 is a dark sky, 150 is bright moonlight.
LV	The variance of luminosity over time.
H	A measurement in stellar magnitudes of the excess extinction in the region surrounding this grid cell.
HV	The calculated variance of this extinction over time at this sky position.
F	Positive value is minutes of remaining clarity. Zero indicates no information. Negative indicates instability.

Table 2 - Sky Report Grid Record

10. The Telescope Scheduler

10.1 Introduction

A Telescope Scheduler is a software process which takes observation requests and generates instructions to operate the telescope system. When this is done in real time, as herein, it is called a "dispatch" scheduler.

At the author's observatory a scheduler of this type has been in use since late 2007 and has completed over 35,000 automated observations. Its original design is described in some detail in Cole (2008). A short synopsis is presented herein to illustrate how the selection process has been adapted for sky awareness.

10.1.1 The Telescope Automation Cycle

When the night begins, or the telescope becomes idle, the scheduler is run to select a task to undertake.

When the scheduler is unable to find a task to perform, it will stop and restart after a minute elapses.

Otherwise the highest scoring of the candidate tasks is selected. An entry is made into an activity list to prevent the same task from being selected again until its normal interval has expired.

The scheduler creates and initiates an observing script. This script will execute the programs required to run the telescope mount, camera, spectrograph, etc. to collect the required measurements. Most measurements take at least 5 minutes to complete.

Upon completion of that script, the scheduler is restarted. The cycle repeats until morning.

In the author's observatory, each telescope has its own independent scheduler.

10.1.2 The Scheduling Data

An automated scheduler needs an astronomical database in order to to translate the object's identification (e.g. "M32") into RA and Dec coordinates.

The authors' system uses a combination of "TheSkyX™" and the "Simbad" astronomical data server for this purpose.

In the author's system, each observing task is written as a line of text that specifies the object name, constraints on when the observation is to be done (fixed time, periodic interval) and a list of the measurement(s) to be taken. The collection of these files containing these task descriptions is available to the scheduler.

The Sky Report provides the hyperlocal weather data needed to support sky-aware scheduling.

10.2 Standard Scheduling

The original scheduler created by this author assumes that the sky is clear, transparent, and stable.

The function of the scheduler is to evaluate the potential observing tasks and eliminate from consideration those which are not possible at the current time. Those tasks which are possible are assigned scores for final selection. These are the key steps:

a) Determine if the observation is permitted at the current time by the constraints set by the user.

b) Lookup the object name to find its RA and DEC. Use the current sidereal time to convert RA/DEC to Alt/Az coordinates. Determine if the target is accessible to the telescope at this time. It must be above the local horizon, not behind a tree, not too close to the moon, etc.
c) Calculate the observing duration for the desired measurements. Determine if the observation can be completed before the meridian flip or before the target falls below the allowable western horizon.
d) Determine if observations of supporting objects (comp stars, calibration objects) are needed and if these are observable.
e) Compute a score for the task. Scoring allows factors such as airmass, waiting time, and the user's priorities to be taken into account.
f) Initiate the observation of the highest scoring task, if there is one, or delay for a minute and run the scheduling process again.

10.3 Sky-Aware Scheduling

A modest amount of additional logic makes the process sky-aware and cloud adverse. This greatly reduces the likelihood of observation failure.

10.3.1 Sky-Aware Startup

The current Sky Report is loaded. The values of the keyword parameters are retrieved. The grid data is stored for use when needed.

The keyword parameters are checked to ensure that there is some potential for observation. This means verifying that the CloseIn time is greater than 10 minutes, that the SkyFlux is no higher than that of a full moon and that CloudPCT is less than 80%.

Unless these startup conditions are met, the scheduling process stops with no task selection and restarts a minute later when a new sky report will be available.

10.3.2 Sky Aware Task Selection

This is a simply a more elaborate version of standard scheduling. In the list below, the new steps have been *italicized* for emphasis.

a) Determine if the observation is permitted at the current time.
b) Lookup the object name to find its RA and DEC. Use the current sidereal time to convert RA/DEC to Alt/Az coordinates. Determine if the target is accessible to the telescope. It must be above the local horizon, not behind a tree, not too close to the moon, etc.
c) Convert the Alt/Az coordinates into a sky grid position and retrieve the contents of that grid record for subsequent use.
d) Determine if the sky is clear at that grid position, if not, go on to the next target.
e) Determine whether or not the telescope will be able to find the object after slewing. This can depend upon the brightness of the object and the degree of obscuration at that sky position. Dim objects are centered by "plate solving" the initial image. This process fails when the astrometric reference stars are obscured. Find another candidate when this appears likely.
f) Determine if the sky conditions at this time meet the requirements for each of the measurements specified for this task. This is detailed in the following section.
g) *Calculate the time for each individual measurement, adjusting as necessary for the degree of obscuration. Sum these estimates into a total observing time requirement.*
h) *Compare the required time with available forecast data for the cell or for the sky as a whole. Skip this candidate unless it has a reasonable chance to be completed.*
i) Determine if the observation can be completed before the meridian flip or before the target falls below the allowable western horizon.
j) Determine if observations of supporting objects (comp stars, calibration objects) are needed and if these stars are observable *and in a clear sky location*.
k) If all these conditions have been met, compute a score for this target.

When a task is skipped over for any reason, it will be re-evaluated on each subsequent pass of the scheduler. Thus when clouds dissipate, those targets that were previously suppressed will become viable candidates.

10.3.3 Measurement Specific Rules

Each task contains a list of the measurements to be made. Each kind of measurement (broadband imaging, polarimetry, low resolution spectroscopy, etc.) is associated with a set of sky conditions needed to obtain useful results.

These are collectively referred to as "measurement rules." They can specify conditions for the all uses of an instrument, or can be specific to a combination of instrument options and object properties.

The scheduler is programmed to compare the sky conditions with the measurement rules for each measurement specified in the task description. Unless the conditions are acceptable, the task will be deferred to a later time.

Example of measurement rules:

- ***Photo Electric Photometry****(PEP) observations require skies that are relatively dark, haze free, and stable in both transparency and luminosity.*
- ***RGB Imaging*** *of diffuse, low surface brightness objects requires very dark, haze free skies, but stability is not particularly important.*
- ***Stellar Polarimetry, Spectroscopy, and Spectro-polarimetry*** *(which are staples of this observatory) tolerate bright unstable skies but take much longer to execute in hazy conditions.*

Whenever a target is rejected, a note is added to the schedule log indicating the specific reason. This is to facilitate the tuning of the measurement rules over time.

The additional steps have virtually no effect upon the time needed for scheduling. The whole process normally completes within 15 seconds or less.

The following diagram (Figure 4) shows the entire process from the AllSky image to the initiation of telescope action.

11. Data Flow Diagram

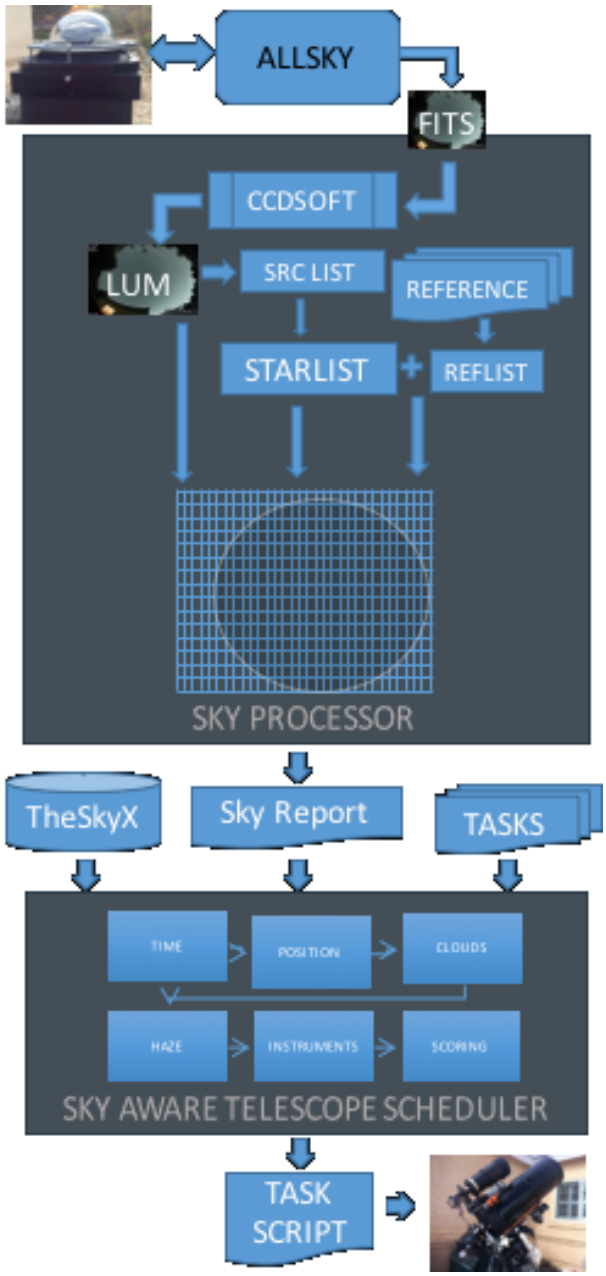

Figure 4 – Sky Aware Telescope Operation

12. Conclusions

This author believes that this work fills a gap in observatory operations technology between protection services (rain sensors, lightning detectors, and automatic dome controls) and the blind target selection methods of existing queue based scheduling systems.

In the Reno area, about 200 nights per year are suitable for observing, but less than a third are true photometric nights.

Sky imperfections cause many failed observations over the course of each year. Avoiding such problems is the principle motivation for this project.

This system has already improved the operation of the author's observatory. Tasks that would have been selected based upon priority, but would have failed due to clouds, are now simply delayed. Lower priority tasks located in clear sky regions are scheduled.

13. Future Work

- Use sky color and local brightness to improve the precision of cloud detection.
- Track bright stars over long intervals on clear nights to determine true extinction.
- Calibrate and report sky background luminosity in true magnitudes.
- Adjust the star search region size to sky conditions for more precise cloud detection.
- Refine the measurement rules to make the best use of the instrumentation available.
- Make the current sky state available to the observing scripts as well as the scheduler. Add programming to adjust the measurement processes to changing conditions.

14. Acknowledgements

This research has made use of the SIMBAD database, operated at CDS, Strasbourg, France.

The author acknowledges the inclusion of software code provided by Keith Burnett.

http://www.stargazing.net/kepler/moon2.

15. References

Mandeville, W.J., AMOS Conf. Paper. "Visible Cloud Imager for Autonomous Telescopes," (2015).

Cole, G.; Automating a Telescope for Spectroscopy. The Society for Astronomical Sciences 27th Annual Symposium on Telescope Science, p 103 (2008).

Lam, E.Y. (2015), "Camera-based forecasting of insolation for solar systems", Proceedings of SPIE 9405, ISBN: 978-1-62841-495-0.

Mandat, D. et. al., (2014) AtmoHEAD Conf. Paper "All Sky Camera instrument for night sky monitoring", https://arxiv.org/abs/1402.4762

A Community - Centered Astronomy Research Program

Pat Boyce
Boyce Research Initiatives and Education Foundation
3540 Carleton Street, San Diego, CA, 92016
pat@boyce-astro.org

Grady Boyce
Boyce Research Initiatives and Education Foundation
1433 Burroughs Street, Oceanside, CA, 92015
grady@boyce-astro.org

Abstract

The Boyce Research Initiatives and Education Foundation (BRIEF) is providing semester-long, hands-on, astronomy research experiences for students of all ages that results in their publishing peer-reviewed papers. The course in astronomy and double star research has evolved from a face-to-face learning experience with two instructors to an online – hybrid course that simultaneously supports classroom instruction at a variety of schools in the San Diego area. Currently, there are over 65 students enrolled in three community colleges, seven high schools, and one university as well as individual adult learners. Instructional experience, courseware, and supporting systems were developed and refined through experience gained in classroom settings from 2014 through 2016. Topics of instruction include Kepler's Laws, basic astrometry, properties of light, CCD imaging, use of filters for varying stellar spectral types, and how to perform research, scientific writing, and proposal preparation. Volunteer instructors were trained by taking the course and producing their own research papers. An expanded program was launched in the fall semester of 2016. Twelve papers from seven schools were produced; eight have been accepted for publication by the *Journal of Double Observations (JDSO)* and the remainder are in peer review. Three additional papers have been accepted by the *JDSO* and two more are in process papers. Three college professors and five advanced amateur astronomers are now qualified volunteer instructors. Supporting tools are provided by a BRIEF server and other online services. The server-based tools range from Microsoft Office and planetarium software to top-notch imaging programs and computational software for data reduction for each student team. Observations are performed by robotic telescopes worldwide supported by BRIEF. With this success, student demand has increased significantly. Many of the graduates of the first semester course wanted to expand their astronomy knowledge and experience. To answer this demand, BRIEF is developing additional astronomy research courses with partners in advanced astrometry, photometry, and exoplanets. The program provides a significant opportunity for schools, teachers, and advanced amateur astronomers to introduce high school and college students to astronomy, science, and STEM careers.

1. Introduction

The astronomy research seminar concept impressed the authors when they were first introduced to it by Russ Genet in 2014. Essentially the idea is to teach science by doing science as evidenced by the students publishing a peer reviewed paper based on their research (Genet et al. 2016). Research in astronomy is the means to introduce students to science and research as an exemplar of a STEM career.

The authors worked with Genet to introduce the classroom based seminar to San Diego from mid-2014 through mid – 2016. Based on this experience the authors created a new version of the seminar under their non-profit foundation, Boyce Research Initiatives and Education Foundation (BRIEF), and introduced it in the fall of 2016. The new seminar (now called "Double STARS") was initiated for 4 high schools, 2 community colleges, and one hybrid online seminar for the fall semester of 2016. Forty-four students participated in 12 teams. Twelve papers were written and eight have been accepted for publication by the *Journal of Double Observations (JDSO)* as of April, 2017; the remaining four are in varying stages of review. In addition, five other papers were produced in the fall of 2016 and three have been accepted for publication.

The new "Double STAR" (**S**TEM **T**hrough **A**stronomy **R**esearch for **S**tudents) course uses open source and relatively inexpensive tools to deliver content over the internet. The content and tools support classroom setting instruction at high school and community colleges and are also the basis for the hybrid in-person/online seminar. The new seminar is available to students of all ages, school enrollment, and financial means. The founders' mission is to develop the program within the greater San Diego

area to enable student team interaction and to develop a community-of-practice for the students to engage in easily (Wenger 1999). BRIEF has placed emphasis on the San Diego geographic area for this community-of- practice to limit logistical issues but more importantly to encourage the social interactions for students with the astronomy community. The learning objectives and skills acquired are broad; the astronomy learned is narrow but deep in double stars. (Figure 1.)

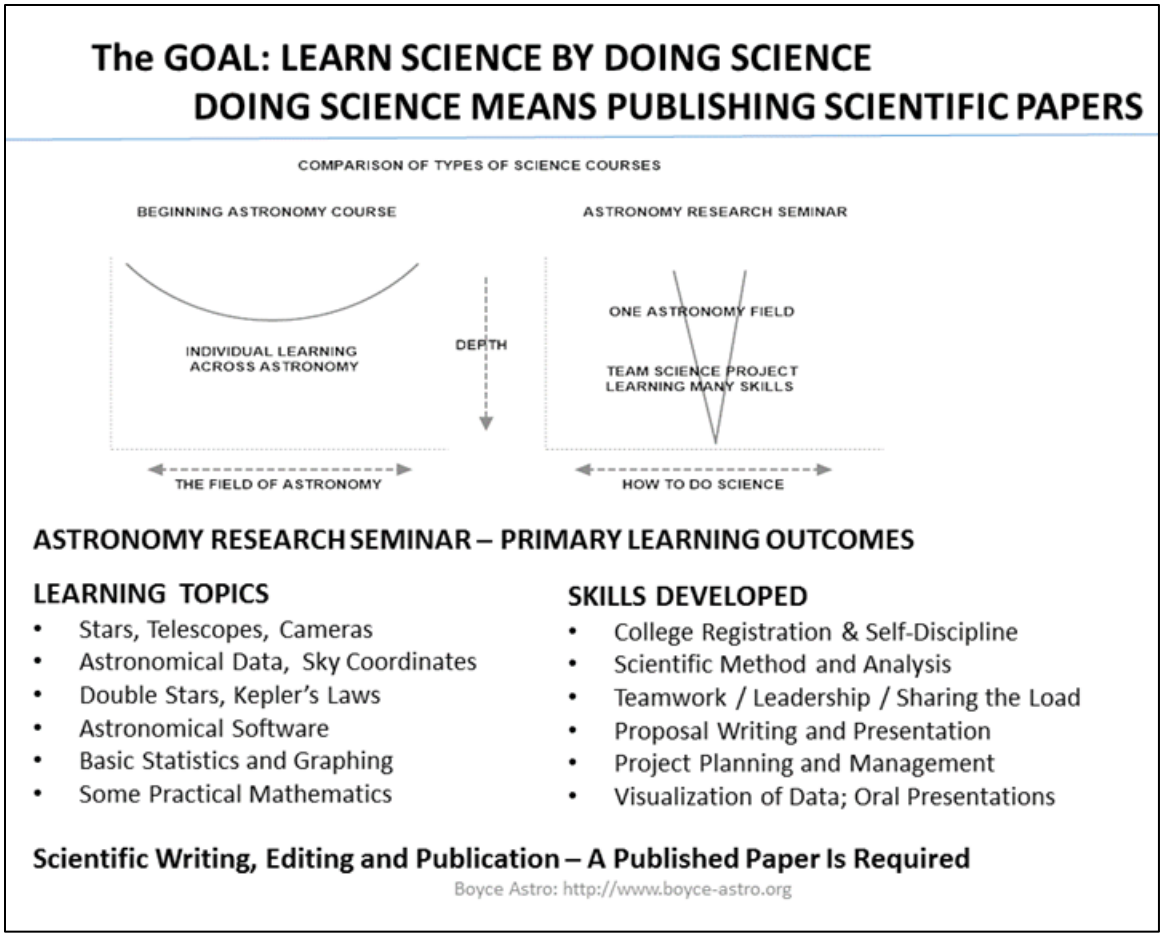

Figure 1. The learning objectives and skills acquired in the Astronomy Research Seminar.

Though initially offered as a one credit-hour community college credit course, experience has shown that this is not an important factor to many students who are interested in STEM careers. They see the experience and the recognition of being an author of a published scientific paper to be of greater value.

One measure of student acceptance so far: 50 % of the fall 2016 high school and online students enrolled in a new advanced, follow-on, not-for-credit seminar for the spring of 2017. This would seem to be a very high rate for volunteering to study further with no apparent reward other than self-satisfaction and the possibility of authoring another scientific report. This paper will describe the evolution of this STEM education program and the lessons learned over the past three years. Student and instructor experiences and outcomes will be provided. The future development into a three semester program will be outlined.

2. Background

Pat and Grady Boyce founded the non-profit BRIEF in September, 2013 with the following mission as stated in its articles of incorporation:

"The specific public, charitable, scientific and educational purposes of this corporation are to provide scientific and technical research opportunities to enhance the educational experience

of students and to introduce them to the scientific and technical communities."

An initial task was to acquire a modest observatory pad and RoboDome at the San Diego Astronomy Association (SDAA) site in east San Diego County, called Tierra del Sol (TDS), for education and outreach. The founders had already started an astronomy club t the Army Navy Academy (ANA) in Carlsbad, CA. This was shortly thereafter followed by their development and implementation of a University of California a-g accredited astronomy course that the founders then taught there for the 2014-2015 school year.

In the spring of 2014 the authors participated in an astronomy observation project at Kitt Peak National Observatory, met Genet, and learned of his research seminar. The authors introduced elements of the seminar in their ANA astronomy course in the fall of 2014 using speckle interferometry data from the Kitt Peak observations. Four papers were published from this in the *Journal of Double Star Observations (JDSO)* in 2015.

For the spring semester of 2015, the authors started the astronomy research seminar at ANA as a once-a-week evening class (Johnson et al. 2015). It was offered as a remote extension, one-hour credit Cuesta College class. The authors course content was developed in parallel with teaching the class. Occasional videoconferencing was used and an attempt was made to provide a simple single seat server to host data reduction tools for the students' data. A number of software problems and a lack of compatibility between client systems required spending significant instructional time on basic IT problems.

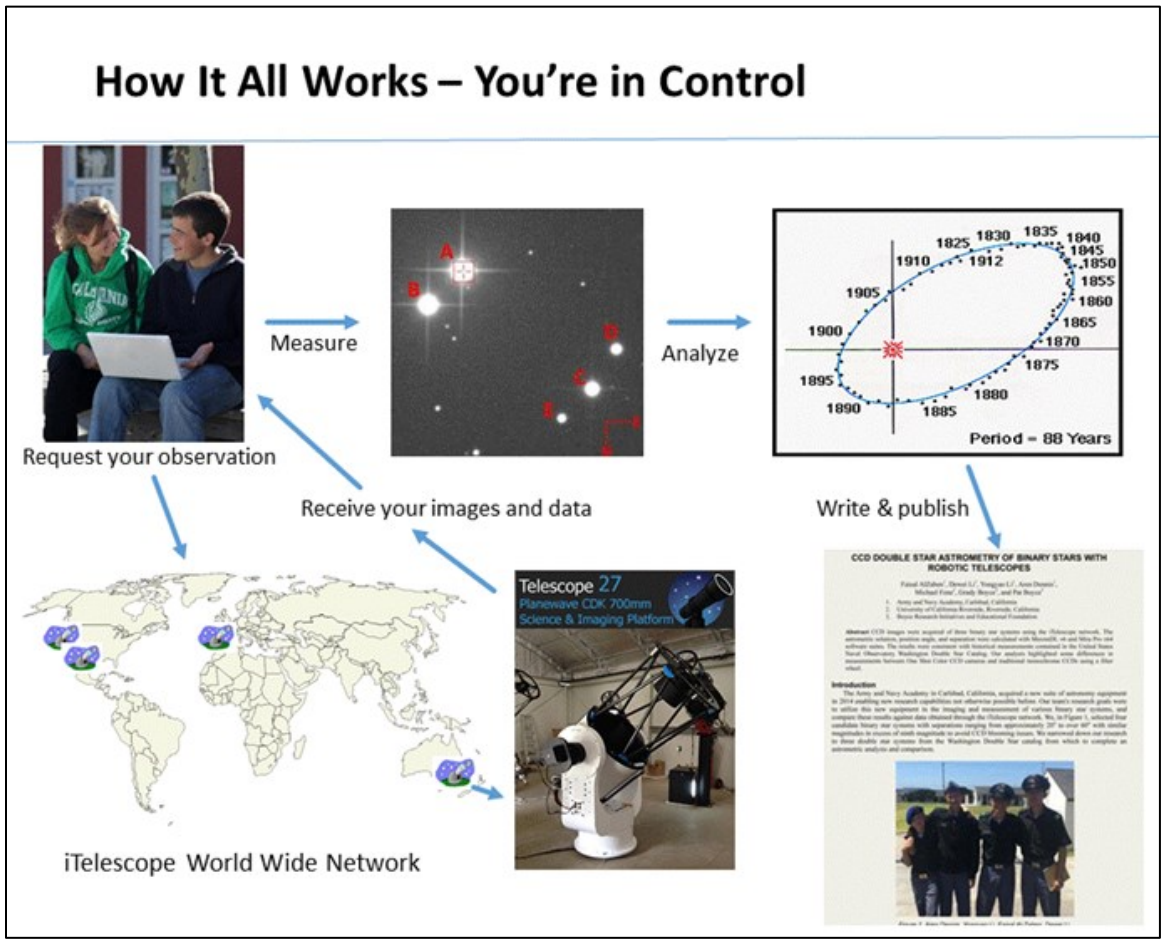

Figure 2. The Boyce-Astro student research workflow after the initial in depth instruction period.

Initial plans were to obtain double star observations locally, but seeing conditions on the coast of Southern California would not permit this in the short time period needed to complete the projects in one semester. To overcome this obstacle, the authors adopted iTelescope robotic observations paid by BRIEF using CCDs. Despite these difficulties 10 students participated in 3 teams to produce papers that were accepted for publication in the *JDSO*. The essential flow of the one-semester course using iTelescope stabilized. (Figure 2.)

By the fall of 2015, the seminar had settled on two basic software tools purchased by BRIEF: Maxim DL with Pinpoint Astrometry for plate solving and Mira Pro x64 for the astrometric measurements of position angle and separation of the double star images. However, the basic client compatibility problems of having students using a wide variety of platforms such as Windows-based computers, Apple based laptops and iPads, and iPhones and Android devices to process their data and collaborate on their presentations and papers still existed. Additional content was developed; refining the course with each semester. Having established an "alumni" base by this time, five students who passed the spring course returned despite not being able to receive another college credit for "taking the course again". This was the first sign that the experience and the authorship recognition were more important than receiving college credit. (Figure 3.)

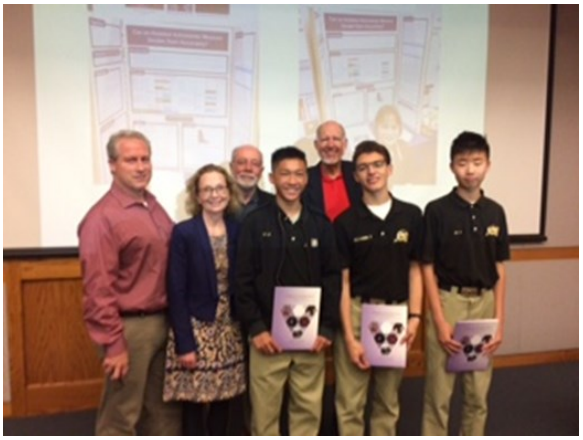

Figure 3. Army Navy Academy students were recognized at an SDAA meeting for publishing their papers.

For the 2015-2016 school year, the authors continued to teach the research seminar in the evenings but passed the teaching of the a-g astronomy class at ANA on to a physics teacher. It became more difficult to be a recognized program and be integrated into the boarding school's after school programs. Though the seminar was strongly supported by the administration, classroom time was slowly eroded by other evening programs. Additionally, the enrollment process with Cuesta College remained difficult, taking many weeks and many steps for a student to register, with much time required from the authors. Signs were emerging that the complicated and frustrating registration process was beginning to dampen the student interest and enjoyment. The rising demand for the seminar outside of ANA required time to make the program available to a greater metropolitan area. The founders reluctantly passed the instruction for the ANA seminar back to the school in the spring of 2016.

3. Initial Lessons Learned

The founders compiled many lessons learned from their first two years of experience. Double star astrometry was confirmed to be a sound topic area for an initial STEM experience, introduction and completion of scientific authorship, and understanding as to the style and structure of scientific papers. Making observations in a short two to three-week period of time could only be done reliably with a network of telescopes such as iTelescope's system to assure the seeing conditions and minimize any weather-related issues. Also, using robotic telescopes avoided the need to commit multiple long evenings for student observations – an almost impossible time commitment for most students. Training student teams to collaborate using a variety of PC, MAC, and other platforms can greatly detract from the intended learning experience and consume unnecessary hours of class time.

The course syllabus, first outlined during the ANA experience, evolved considerably from the initial half semester Cuesta design to a full semester class that incorporated much more of the content that the students wanted in astronomy and their research experience. The initial use of lecture and classroom recorded videos had to be replaced with self-paced learning modules for independent study so that classroom time could be devoted to questions and teamwork. Compelling research team development early in the semester had to be fostered and can be difficult. Instructor load could be substantially

reduced with the correct instructional materials, delivery methods, and supporting systems. (Table 1.)

Week	Topics	Activity
0	Introduction & Logistics & Teams	Meet fellow students
1	Double Stars, Kepler's Laws, Star Colors and Magnitudes	Establish Team Roles
2	Astrometry Fundamentals, Sky Coordinates	Begin coordinating as a team
3	Washington Double Star Catalog, How to access data	Begin selecting candidate stars
4	Online catalogs, Organizing data, Visualizing data	Request data from US Naval Observatory
5	Telescopes, Cameras, Filters, Imaging, Ordering Images	Begin drafting proposal
6	Planning research, Objectives, Schedules, Proposals	Finish proposal; Proposal Presentations
7	Review star images, Calibrating Images	Order images
8	Data reduction, measuring images	Send data to instructor for review
9	Statistics	Draft results of measurements and graph
10	Draft #1	Prepare and submit Draft #1
11	Review Drafts	Address comments & suggestions
12	Draft #2; Discussion: What is Science?	Submit Draft #2
13	Prepare for final presentation	Draft final presentation
14	Review Draft #2 suggestions	Prepare Draft #3 if necessary
15	Prepare final team presentation: Discussion: What have you learned?	Submit final paper
16	Prepare final team presentation:	Give final team presentation

Table 1. The Boyce-Astro first semester astronomy research seminar syllabus summarized by week.

To date, students of all ages from 7th grade to retirees have successfully taken the seminar, worked in teams, and a large fraction has continued on to other research topics. The mathematics required could be mastered but the writing and editing skills needed were the greatest challenges for the students. Educators and administrators can fail to realize that the seminar is a capstone learning opportunity that applies equally to science and liberal arts students. Just as Astronomy involves multiple disciplines, this course draws from many aspects of students' educational backgrounds culminating in publication. (Figure 4.)

For high schools, the seminar fits an after-school program, not a five-day-a-week class. To be sustainable at a high school it needs to have the same status as other after-school programs such as sports, drama or band. That provides the framework to fit it into the school's administration and operations. The seminar well suits a college curriculum which can be attended by students of all ages. On the other hand, not many high school students or adults are able to attend a college class during the daytime, and evening classes requiring driving can be difficult for many to attend as well.

Figure 4. Mount Everest Academy students proudly receiving their "diplomas" for completing the first semester seminar; the team members ranged from 8th grade to retirees.

4. The New First Semester Seminar (Double STARS)

From these lessons the authors developed a new and expanded seminar for launch in the fall of 2016 in the San Diego area. Instructors were solicited and trained from the community college ranks and from the seminar pro-am astronomy community well

represented by the San Diego Astronomy Association (SDAA) which has over 500 members. SDAA is over 50 years old, has a large observing site east of San Diego with public and private observing pads over a dozen observatories. The goal was to enable offering an adaptable seminar in multiple schools with differing venues and at different times rather than being limited to the span of time available to the authors alone. To enable this goal, new instructors not only needed to be trained, they also needed course content and support which BRIEF could provide. For efficiency, a common set of materials and systems were developed that could be used universally for classroom instruction in high schools and colleges as well as an online course. (Figure 5.)

Figure 5. Instructors posed for a photograph at a break in their training session in May, 2016.

The online venue is especially important to reach students throughout the San Diego area who are of varying backgrounds and means do not have access to a high school or college offering the seminar, or do not have transportation to brick and mortar venues. From an institutional perspective, due to many impediments in adopting new courses in most public institutions, the online seminar provides a path to institutional integration. San Diego spans a wide geographic area. The online seminar can easily reach and support the widely separated schools, many of which cannot devote resources to such a seminar. From a community perspective, the online course is especially useful and important for the underrepresented communities. The online seminar is a testing ground for content and systems to be used in the classroom instruction in the area's community colleges and high schools.

To increase instructors of the course, the authors' materials were converted to online self-paced video lessons with quizzes that were platform independent and could be accessed by students regardless of school venue. An online forum was established to provide supporting materials and support dialogue between teachers and students in each school. Administrative tools to handle registration, recording keeping, and student text notices and reminders were established using commonly available tools.

Most significantly BRIEF acquired a dedicated five-seat online server called Boyce-Astro Research Computer (BARC) with all the software tools needed by the students to perform and write their research papers. Among the packages included initially were the SkyX, MaximDL, Mirametrics Pro x64, Reduc, as well as a full suite of Microsoft Office products. Because BARC can be accessed by all common PC, MAC, tablet, and other client platforms, the time previously lost by students and instructors solving software compatibility problems was almost eliminated. Self-paced learning modules could be tailored to the exact same screens and experiences all students would have in common. The file systems were established to provide various levels of permission by student, instructor, mentors, and administrators.

Use of iTelescope for double star observations for the classes continues to be an efficient and reliable source of image data with many systems available around the world. iTelescope handles the initial data reduction – flat fielding and subtracting darks from the raw images – so that students are not required to learn these details in these initial experiences. This in turn stream lines the process even more. The pricing for short exposure double star astrometry observations on iTelescope is reasonable. BRIEF continued its educator discount program to provide the observations to students for free to date. The total minutes of time allotted to each team are sufficient for their project. Teams with especially interesting and well proposed projects are granted more minutes' time. Boyce-Astro schedules the images on iTelescope based on student requests and downloads the successful shots to the BARC server student folders for each team's access and data reduction. (Figure 6.)

A full semester syllabus is provided for use by all schools which can be readily adapted to individual school requirements. More stellar astronomy is taught in the first few weeks compared to the Cuesta College offering. This provides the students with more time to develop their own research proposal including selection of target stars and the rationale for their selection. Requiring students to select their targets compels them to apply what they have learned in their deep dive into the astrophysics and double star astrometry in the first few weeks of the course. The second half of the course focuses on writing.

Each student team is required to present their proposed research to all their peers and all instructors in a San Diego area conference at the eight-week

mark. They learn that real scientific research as well as other endeavors is typically competitive and funded by well-developed proposals. At this presentation, they have to defend their proposal and as a byproduct they learn much from observing the other team presentations. It is a bonding experience for each team and is increasingly an opportunity for the broader San Diego community to participate. The best proposals are awarded additional observation time.

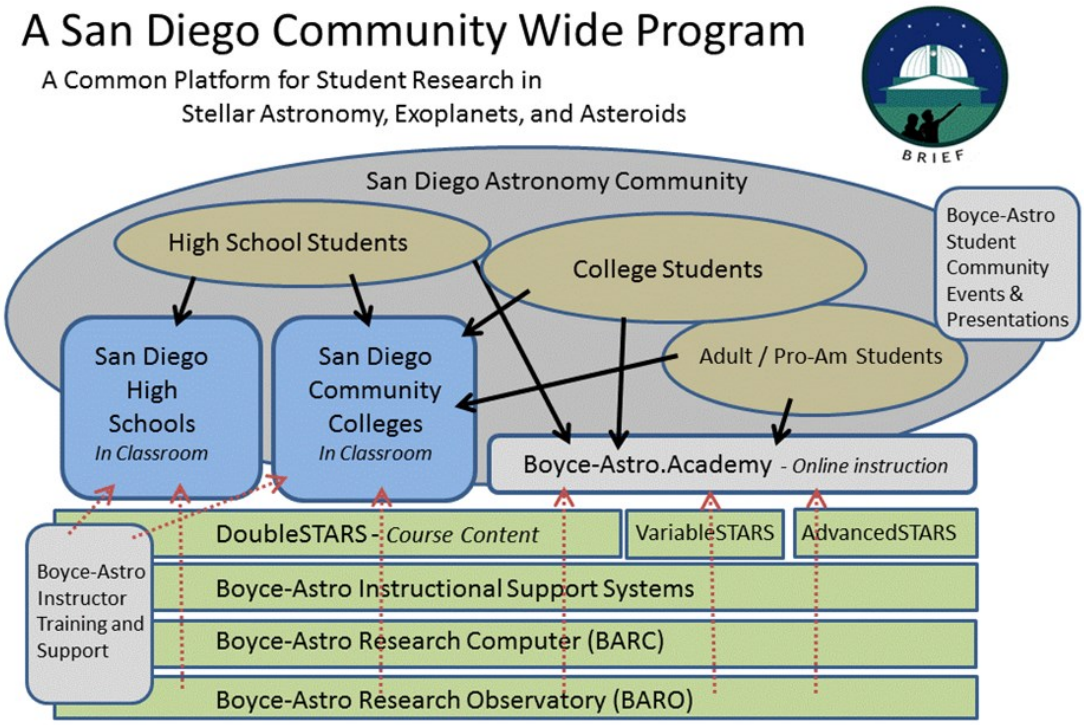

Figure 6. BRIEF's common community-wide instructional platform for the San Diego region.

Multiple observations are required typically over at least two nights and preferably from different telescopes. This introduces students to statistics and measurement of uncertainty. Then students are challenged to present their information graphically and hypothesize the possible alternative meanings of their results with special attention given to understanding outliers and the quality of the various past observations.

The semester culminates with a final presentation by each team, again in a community wide setting in a public library. Friendly but thoughtful criticism is offered by the instructor group as well as the students. At this stage, all teams are expected to have been through at least their third draft review by their instructors. The PowerPoint presentations provide useful feedback on their methodology, results and conclusions which can be incorporated into their final paper revisions. (Figure 7.)

5. New Lessons Learned

After conducting the new seminar for nearly two semesters in its various venues, a new set of lessons learned can be summarized.

Figure 7. Final presentation day at a public library. All San Diego teams meet to present their research to each other, the instructors and interested members of the community.

5.1 Overall Systems

In general, the new seminar has fared well, and evolved, through student and instructor evaluations. Self-paced learning units' using EdPuzzle are very well received by students and have reduced the instructor workload considerably. The text messaging system (Remind.com) is essential as most students do not read their email very often. Students did not use the online forum for discussion and would be better served for team collaboration through Google Hangouts or a similar free tool. The resource content on the forums will be moved to BARC which should simplify student interaction as well as administrative burden. Eventbrite has sufficed for online registration but a data management add-on will be added to simplify the enrollment process further in the future. In aggregate, the systems are an inexpensive, flexible and adequate alternatives for the current level of operations compared to the more cumbersome instructional systems such as Canvas and Blackboard mandated by various school systems.

BARC has overcome the compatibility and data management problems experienced in the past despite initial challenges in administering the server security protocols. To allow individual instructor software preferences and more research options, the BARC software suite has been expanded to include DS9, AstroimageJ, Stellarium, Sky Tools, Speckle Tool Box, and Astrometrica. iTelescope has continued to work well for the short exposure observations needed for double star astrometry. Still the administration of BARC and the observation management with iTelescope are time consuming even at the current levels and support staffing through student interns is being considered for the future.

5.2 First semester seminar syllabus and content

Students and instructors have been solicited for critical comments regarding the course content and methods. The replies especially from students were highly favorable. Considering where the seminars began in early 2015, the suggestions are really refinements.

When asked, the two most common suggestions are 1) to provide more time and guidance in target star selection, and 2) to provide a single consistent formatting guide for the papers. For the first the class segments describing the nature of science will be moved to the end of the semester for the point in time when students can appreciate the scientific research they have done. Enhanced guidance in paper formatting consistent with other astronomy journals and the JDSO, will be addressed with an updated "Elements of a Scientific Paper" handout as the sole guide. The BRIEF Advisory Board recommended adding basic photometric measurements to the astrometric data reduction now done and encouraging more historical research in the proposal phase. They recommended assessing individual student performance and their team contributions through final interviews. Some instructors experienced difficulty in establishing research teams and would appreciate receiving more guidance. All participants recommend even more training in writing – a common problem for all the past seminars that has proven difficult to fully resolve.

5.3 Experiences by Venue

Two high schools, Mount Everest Academy and the Cambridge School, were able to host the classroom seminar for students on their campuses, and Cambridge was able to include students from the nearby Westview High School. Professional-amateur ("pro-am") astronomer volunteers, Kent Smith and Allen Priest, were recruited from the ranks of the SDAA. They conducted the classroom instruction with occasional in person support from the developers. Both instructors performed admirably, and Kent Smith was even able to have all four of his team papers accepted for publication by the end of the semester. They were not able make this level of time commitment for the spring semester and there were no other trained instructors available to continue the high school classroom instruction in the second semester. Students ranged from junior high age to high school and community college instructors. High school teachers were not available as instructors, the reasons for which will be described later.

Two community colleges, Grossmont and Miramar Colleges, utilized the new Boyce Astro seminar content and support as the basis for honors "contracts" for interested science students. There is no course equivalent to Cuesta College's ASTR 299 one-hour credit course at their or other California Community Colleges. The honors contract approach allowed students to gain the added benefit of an honors class credit for the extra work and minimized the volunteer time commitment for the instructors. [See further discussion of these constraints later.] Both Jae Calanog at Miramar College and Sebastien Cormier at Grossmont College were able to continue their volunteer honors course instruction in the spring semester and Irena Stojimirovic was able to create a similar and larger honors program at Mesa College. All three instructors use the Boyce Astro content, BARC server and robotic telescope accounts to supplement their guidance and they collaborate with each other for added content and student support. Students enrolled at the community college seminars grew from 17 in the fall to 25 in the spring.

The hybrid online seminar conducted by the authors had 5 students in the fall semester and 26 students in the spring of 2017. It is called "hybrid" in that weekly online synchronous meetings (content is always available by asynchronous means) and at least two community-wide meetings are held each semester. Zoom, an online videoconferencing system, is the primary tool for online classes, whiteboard discussions and class discussions. These sessions are recorded so that students could return for review or do a makeup if absent. A second online seminar, Advanced Astrometry, was added for fall graduates and 13 students registered for it.

Fall students in the hybrid online seminar ranged from high school age to college graduates, including one high school teacher. The spring first semester hybrid online seminar grew five-fold for these reasons: no high school classroom instruction available and a new relationship with BEWiSE, a San Diego initiative that encourages young women (7^{th} to 12^{th} graders) to enter STEM careers. The BEWiSE group (Better Education for Women in Science and Engineering) epitomizes the power of the online course to reach underrepresented communities regardless of their school's ability to participate. Another paper will address the significance of this and how it can apply to other communities. (Figure 8.) A further student addition came from astronomy students at San Diego State University (SDSU) who wanted research publication experience and authorship that is not available at the University for undergraduates.

Figure 8. A screen shot of the online class in the spring of 2017; the course had more young women than young men thanks to BEWiSE support.

Of the 26 spring semester high school students 18 initially expressed interest in taking the course for one-hour college credit through Cuesta College; only 3 made it through the excruciating administrative hurdles to be registered. The rest were content to take the course for the experience and the value of authorship for their scholarship and college applications. After the above referenced registration difficulty, Cuesta had a change of policy and would only admit students if they joined their Canvas based online classes. When given the choice, all of the registered students chose to withdraw from Cuesta and remain with Boyce Astro even though they would not receive college credit through the Boyce Astro seminar. This is both an indication of the perceived value of the Boyce Astro online course and an expression of the power of community for student participation.

The proposal presentation and final presentation meetings have been held at public libraries with all students, instructors from all schools; other interested parties such as parents are encouraged to attend. In each instance the students have expressed a renewed vigor after seeing their peer's presentations. There is healthy competition between the teams.

6. Next Steps

The revised seminar program can be sustained at its current level as long as instructors from of the three community colleges and two high schools continue to volunteer their time. BRIEF is able to financially support the instructional systems, the BARC software and server, and the telescope resources required. The baseline hybrid-online course can be sustained as well at the thirty student level as well as provide the underlying school support. Thus the current capacity is approximately 60 to 75 students per 1^{st} semester students enrolled in the fall

and the same in the spring assuming some efficiencies can be attained.

Based on the past years' experience, BRIEF will streamline some of the administrative systems and consolidate the Forums content onto the BARC server. A number of 1st semester graduates are continuing to participate in follow-on classes. An internship program will be attempted in the fall of 2017 to provide support to the principals so that they can undertake further program development while supporting the 1st semester classes.

A primary focus for the next school year will be to address the interests of the graduating 1st semester students who want to go further into observational astronomy. The following three semester series will be developed using the new course acronym STARS (**S**TEM **T**hrough **A**stronomy **R**esearch for **S**tudents)

- ***Double STARS***: a refined version of the current 1st semester seminar
- ***Variable STARS***: a seminar in both single image (UBVRI) and time series photometry
- ***Advanced STARS***: guided independent research in stellar astronomy, exoplanets and asteroids

Rather than reinvent or compete with the excellent educational materials offered by the American Association of Variable Star Observers (AAVSO), BRIEF intends to make its Variable STARS seminar complement the courses offered by AAVSO. The Variable STARS course will focus on analysis and publication based on the variable star observation knowledge gained from the AAVSO CHOICE course. This collaborative project will begin in the summer of 2017 for a pilot seminar launch for the fall semester of 2017

A pilot seminar in currently underway for the Advanced STARS seminar with students who have completed the 1st semester binary star seminar. There was a strong demand for this course from the fall 2016 semester high school and online students. Projects are in astrometry, single image photometry, speckle interferometry, and exoplanet transit measurements.

The time series photometry and exoplanet observations needed for the new courses require long duration exposure sequences that are cost prohibitive using iTelescope. BRIEF has acquired a half time lease of an excellent 16" RC robotic telescope at the Sierra Remote Observatories (SRO) to support these long duration observations. In addition, BRIEF's own robotic observatory, the Boyce-Astro Research Observatory (BARO), is expected to come online initially with an 11" SCT in the summer of 2017 followed by a robotic 20" CDK. These will ultimately support CCD based astrometry and photometry and speckle interferometry. The San Diego Astronomy Association (SDAA) has offered student observation time to BRIEF on its Terry Arnold Robotic Observatory (TARO), a 14.5" fully robotic RC.

To tie the educational program and courses together, BRIEF is packaging the offering into an academy, Boyce-Astro.Academy, with a new website to integrate the instructional materials and support. The Academy will offer the three online non-credit courses listed above as well as continue to support the San Diego area classroom instruction at the community colleges and high schools that have trained instructors.

Boyce-Astro will continue its special projects, workshops and special events to encourage development of the San Diego area student, educator and pro-am astronomy community. For example, in October, 2016, Boyce-Astro offered a two-day exoplanet workshop taught by Dennis Conti of the AAVSO for San Diego area students and astronomers. In August, 2017, Boyce-Astro is manning one of the key observation sites for the total solar eclipse under the Citizen CATE (Continental-America Telescopic Eclipse) Experiment sponsored by several federal agencies (Penn 2015). The Boyce-Astro team is comprised of students, faculty, and pro-am astronomers from San Diego. For the 2018 Greater San Diego Science and Engineering Fair, Boyce-Astro will award a scholarship for a top-notch astronomy project as judged by the Instructional staff. The winner will be selected on the basis of the project that is most prepared for scientific publication. Boyce-Astro will continue to seek opportunities to collaborate with the SDAA and its membership to strengthen the San Diego astronomy research community. (Figure 9.)

Figure 9. BRIEF hosted a one-day workshop on small telescope research at the summer AAS conference in San Diego in 2016.

7. Further Growth

In March, 2017, possible future directions for the student research program were reviewed with BRIEF's Advisory Board. The Advisory Board is comprised of Russ Genet (Adjunct Professor at Cuesta College, and Research Scholar in Residence at California Polytechnic State University), Stella Kafka (Director, AAVSO Bob Buchheim (President, Society for Astronomical Sciences), Mike Chasin (President, SDAA), and Philip Blanco (Lecturer, Grossmont College). Based on this review the founders formulated the "baseline" plan above under "Next Steps".

The student potential in San Diego is many times greater than the 60 to 75 student level per semester in the baseline plan. The Advisory Board discussions centered on what would be required to raise the student enrollment to 250 or more students per year.

Despite the apparent student demand for the seminars, a number of factors constrain growth and can even affect the viability of the community-wide program. Theseneed to be addressed if one is to expand the program substantially. Most could be overcome with additional financial support.

7.1 Constraints to Growth

The growth to higher levels of operations depends on the rate of growth possible given these known constraints and the availability and timing of resources to overcome them.

- **Instructor compensation and reward**: To date the seminars have been staffed by volunteer instructors and the time commitment needed is not inconsequential. Though the authors intend to continue their volunteer time contributions one cannot expect others to make this commitment on a sustainable basis.

- **Instructor training**: To extend the seminar beyond its current schools to provide a more stable base of operations requires additional instructors who will need to be trained. If modest compensation for instructors were available, the ranks could be filled. An instructional team comprised of a school science teacher and a pro-am astronomer is best. It's the rare science teacher who knows the details of conducting astronomical observations. The pro-am astronomer complements the teacher's instructional skills as well as the knowledge of school practices and operations.

The current instructor training of having a qualified science teacher or pro-am astronomer take the seminar themselves is necessary but not sufficient. Knowledge of course systems and processes is needed as well which can be accomplished over a weekend workshop with reference materials. Taking the online seminar can then provide experience needed to lead a seminar.

- **Logistical support**: Course enrollment, systems administration (e.g. BARC) and observation management require time from the authors that can be accommodated at current operation levels, but additional support is needed if more schools and students are added. Student interns are the hoped-for solution in the near term but may not be a sustainable solution due to turnover in the long term.

- **Sufficient peer review resources**: Every paper requires considerable review and edit by the instructional staff. Despite this effort, the time required by the largely unrecognized peer reviewers is a significant time commitment for them. A broader pool of reviewers needs to be developed to assure adequate and timely review of all papers as produced.

- **Publication**: Almost all 1st semester papers have been published in the *Journal of Double Star Observations* (JDSO), an online peer-reviewed scientific journal. If for some reason the *JDSO* were to discontinue operations, the opportunity to publish papers in process at that time would be disrupted. If an alternate journal were not found, the basic premise of the course to publish a scientific paper would be seriously compromised.

School administrative regulations are significant barriers to grow operations rapidly even if the above constraints overcome. Here's a short digest of the factors:

- **High Schools**: A weekly seminar does not fit into a 5-day a week, two semester course, curriculum which is the mainstay of California qualified a-g courses needed for college admission. The seminar could be integrated into an existing qualified a-g course but that requires time and concerted effort from instructors and administration. The seminar can be offered as an after school program on a weekly basis substantially in its current form. Unions will not permit it to be offered on a volunteer uncompensated basis, so school or other funding is necessary to establish a recognized course or after school activity. At least for San Diego public schools, the internet security procedures require any accessible website or resource to be certified for student use. This impedes the use of the course materials and BARC to support the

seminar in the classroom or in after school programs.

- **Community Colleges**: The instructors are generally overloaded with classroom commitments and cannot take on a volunteer activity that is not recognized in their expected time commitments for teaching. Adequately attended and recognized courses do count though. For now, the seminar is used to create honors contracts which are recognized by the schools for students in science and other classes. It takes at least two years to get a new course such as the seminar through the curriculum adoption process. An effort has begun to gain approval for the seminar in the 2018 to 2019-time frame. In the interim the seminar instructors are volunteering their time as honors contract advisors.

7.2 A Possible Pathway

Community colleges are best suited to be the center piece of an expanded classroom program. High school, college and adult student communities are able to enroll in there with modest fees. The challenge is to establish a stand-alone (not honors) class in which all three student communities can enroll. A further enhancement would be to enable high school students to receive dual credit. Establishing such a class seems to be an arduous and slow process. Meanwhile students are having to be served by volunteers who are stretched for time.

A bridge financing until such time as the colleges adapt would put the program on sound footing and enable the growth to the higher level of operations. Such funding might be accomplished through a scholarship program or through direct contributions.

There is a new National Science Foundation (NSF) grant to California Polytechnic State University managed by Russ Genet (see Genet et al 2017). Its goal to evaluate the astronomy research seminar for broader implementation to other areas of science as well as to determine its STEM teaching effectiveness will span three years. It is expected that San Diego and the NSF grant team will share in lessons learned from the grant. BREIF intends to move San Diego forward at a possibly more rapid pace depending on resources and overcoming at least some of the constraints identified.

8. A Long Term Goal for San Diego STEM

With an expanded astronomy research seminar program, San Diego could become a national model for STEM education. If the resources were available to achieve the 250 student per year level of operations, triple the current level, the expanded STEM educational program through astronomy research for the San Diego area could look like this:

- ***Community Colleges:*** Four to six colleges conducting the first semester classroom seminar for two hours' credit with each school having 20 to 30 students; have cooperative programs in place with local high schools to encourage their students to attend the seminar at the community college
- ***High Schools:*** Four to six San Diego area public or private high schools conducting the classroom seminar with 15 to 25 students each; magnet schools for STEM would be the best candidates; the seminar could be integrated with their astronomy or physics a-g course or be offered as an after school program.
- ***Online first semester seminar***: Boyce-Astro.Academy would conduct one first semester hybrid online seminar (Binary STARS) to address underrepresented communities and instructor training each semester. Additional online seminars could also be led by trained instructors too.
- ***Online advanced seminars:*** Boyce-Astro.Academy would conduct the Variable STARS and Advanced STARS seminars for graduates of the first semester seminars from the San Diego community colleges, high schools, and the Binary STARS seminar.
- ***Community of Practice:*** Expand the community-wide proposal and final presentation programs to accommodate the larger student population; added workshops and teaming projects to encourage independent student experimentation and research mentored by experts in the San Diego community; encourage participation by the university community.

The consequences of such an expanded program need to be understood in their entirety. For example, about 40 papers per year would be produced needing peer review and publication. The *JDSO* currently publishes between 10 and 20 papers per quarter. The San Diego papers would increase the peer review requirements as well as the JDSO's content almost 40%. Other areas in California and Hawaii are also

ramping up. The total impact could be overwhelming for the *JDSO*.

The logistical support needed for the San Diego operations would require one to two full time staff members supported by interns. Server upgrades would be needed. BRIEF's projected telescope resources would, however, be adequate. An additional sustaining source of funding would be required to add these capabilities. On a cost per student basis, it would be inexpensive when compared to similar programs.

9. Initial Assessments

As the new seminar is in its second semester of operation, a formal evaluation is not possible yet. One measure of success with students is the number of fall 2016 first semester graduates who have chosen to take the Advanced Astrometry pilot seminar in the spring of 2017. Table 2 provides those figures for the high school classroom and online students. This course is not for credit. The community college students were not solicited for the second semester seminar; they have little time to take not-for-credit courses. Despite that a two are acting as voluntary mentors to first semester students now taking the seminar. In total 50 percent of the fall 2016 high school and online students chose to enroll in the not-for-credit second semester seminar.

Fall 2016 First Semester High School & Online		Students Continuing for Advanced Astronomy
Class Venue	Students	
Mount Everest Academy	11	4
The Cambridge School	4	2
Westview High School	6	4
Boyce-Astro Online	5	3
Total	26	13

Table 2. Many first semester students wanted to continue research in the spring of 2017 with the Boyce-Astro pilot seminar in advanced astrometry.

9.1 Classroom Instructor Feedback

The seminar community college and high school instructors provided these comments to an informal survey recently conducted.

Does it encourage critical thinking?

"I believe that it does encourage critical thinking. The students were required to provide evidence for all claims they made in their papers. I remember drafts being sent back to students with the comments, "Can you back up this claim?" and "Can you provide evidence?" or "This sounds like opinion." I don't think the high school students had ever had to write a paper that required so much rigorous evidence before. It hopefully helped to stress the difference between fact and opinion. "

"YES. … the whole process encourages critical thinking! For example, when students are trying to choose a double star system to study, they're thinking about: "Should I pick a star that's well studied and have multiple publications OR should I pick a star that has few observations?" There's pros and cons to both but ultimately, they have to weigh out their options. During the observations, they have to think about the many factors to consider since they have limited resources (telescope time). Questions such as: When should we observe it? How can we figure out an exposure time that doesn't saturate our images? Which filters do we use?"

What impact does it have on STEM career decisions (increases or decreases interest or no impact) and what factors seemed to be most influential?

"…there are many STEM careers that have nothing whatsoever in common with writing scientific papers, but it's hard to avoid planning, project management, communicating, working with other people, or having to meet standards or expectations in the real world; all things that students were exposed to the seminar. Authoring a published scientific paper gave some students, I believe, the taste to do it again. "

"It's a bit hard to answer this question since this would only apply to students who weren't STEM to begin with. As far as I know, from Fall to Spring, I've

had one student who was not of STEM background who I know is still deciding. However, I have had conversations with my students who were already interested in STEM. They've mentioned that this seminar has only encouraged them and reinforced why they picked the right field to begin with. I'm guessing that's a good thing! "

"Some may not enjoy having their results criticized or put on public display. Others may totally enjoy the process of scientific discovery and really be fired up about it. … Several of them loved the process and writing a scientific paper and will likely pursue a scientific course of study in the future."

Though the course uses double star astrometry as a topic area, do the students see the methodology to apply to other areas of science?

"In the seminar the students had to learn first-hand about the difference between accuracy and precision; worked with statistics, uncertainty, and error analysis; experienced project planning; were required to clearly state goals, summarize work done, and--something I really thought was excellent--deal with conclusions that were not what they expected."

"The students probably can't answer this right now because it's too early in their careers. Having gone through community college to a 4-year university to a PhD program, I can tell you that I definitely wish I had this experience early on! The methodology that we follow in writing the paper is the same methodology that I was introduced to not until graduate school! If these students continue to higher education, then I can only imagine that this experience will make their learning curve in research less steep. "

"I think they have a good handle of the use of the scientific method and how to go from a hypothesis all the way through to published work. I think they would definitely be able to apply this to other scientific fields and, in fact, I have seen some of them do that with science fair projects."

How would you change it to enhance its impact on high school and community college students?

"I think community college students need to be informed and aware of the actual impact it can make on their careers… I think they also need to understand that this seminar is a professional development opportunity for them. They can use the seminar to write about their experiences in their college applications, ask me for a letter of recommendation, and also use it as a basis for applying for other internships.

Professional development opportunities is what I'd like to improve on to enhance its impact. For example, workshops on how to make great presentations (I'm working on this one right now), great posters, incorporating the seminar in their resumes and personal statements, etc. would be extremely beneficial in helping our students reach their professional goals"

"I would bring in

scientists/astronomers/academics and have them talk about what their everyday work is like. Also, I would consider adding a field trip to Palomar Observatory."

Writing a peer-reviewed paper is almost always cited as the hardest part of the seminar. Instructors also noted these communication and social adjustments were challenges too:

"The seminar helped the high school students prepare for college by treating them like college students; for the first time, for many. One thing the students did in the seminar that they do not do in high school is interact with adults and experts who are not their "teachers," but mentors and peers."

"I think they actually struggle with the presentation. Many of them can't communicate their ideas or generate interest in a public speaking setting."

"I would also say communication, amongst each other and with me. They're still a bit culture shocked that the relationship between professor-student is different from advisor-student. I observe this during our meetings because sometimes they expect a lecture from me and everyone is really quiet, whereas it's actually the exact opposite."

9.2 Quotes from students

High school and online students from the fall 2016 first semester were surveyed; in addition to their other replies, they provided these quotes:

8th grade student (who won second place in the California State Science Fair):

"The Astronomy 299 [previous designation] course was a great experience. I learned how to write a scientific paper about my own measurements double stars and get it published!"

High School Students:

"As a high school student with a passion for science and Astronomy, I feel so lucky to have the opportunity to research under the expert guidance and support of Boyce-Astro. Learning that my research will soon be published has been the highlight of my education so far and will add valuable substance to my college applications."

"The Astronomy Research Seminar is a unique and enriching opportunity that allows students to participate in scientific research. Besides the incentive of becoming a published researcher (even

while in high school!), the program allows students to gain insight into how research is conducted and improve their teamwork, leadership skills, public speaking, presenting skills, and writing abilities. I would highly recommend this program to any students interested in science in general. Prior astronomy experience is not required to take advantage and benefit from this opportunity."

"The program taught me how to write an academic research paper - from conducting background research, to the proposal, to editing and submitting the paper. Furthermore, it helped me hone communication and organization skills through working and coordinating within a team setting, an aspect of utmost importance in STEM."

A Community College Student:

"Being a part of this research group really helped me in three areas of my life: gaining valuable research experience in the science field, learning how to work in a group setting, and networking with like-minded individuals."

Adult pro-am astronomer online student:

"This class solidified some astronomy concepts while introducing new ones. Grady makes it fun and accessible. Best of all, his relentlessly good attitude makes the challenges less daunting.

These initial student and teacher assessments, though only anecdotal, are encouraging. A further review and assessment is underway to identify enhancements to make in future semesters.

10. Conclusions

After three years of development the Boyce Research Initiatives and Education Foundation (BRIEF) has successfully launched a community wide astronomy research seminar to enhance STEM education in the San Diego area. BRIEF has established a common educational platform that serves high school and community college classroom instruction as well as hybrid online classes. The lessons learned and the model may be extensible to other communities to apply. BRIEF is proceeding with additional advanced hybrid online courses under its new Boyce-Astro.Academy and is committed to growing the San Diego area astronomy community.

11. Acknowledgements

BRIEF must acknowledge the indefatigable efforts of Russ Genet in pursuing his goal: teaching science by doing science as evidenced by authoring and publishing a peer reviewed scientific paper. He has shown the path to many and we are indebted to his advice and support.

BRIEF must acknowledge the efforts of its volunteer instructors who have made the expanded program possible: Philip Blanco (Grossmont College), Jae Calanog (Miramar College), Sebastien Cormier (Grossmont College), Allen Priest (The Cambridge School and Westview High School), Kent Smith (Mount Everest Academy), and Irena Stojimirovic (Mesa College). Their selfless commitment to this student experience must be commended. We must include Jerry Hilburn in our thanks for his donation of valuable time and resources in supporting BRIEF's educational systems.

The authors are especially indebted to Richard Harshaw for his excellent mentoring of our students as well unflagging ability to perform critical reviews. Thanks go to Vera Wallen for her amazing attention to detail in reviewing our papers for the inevitable grammatical error.

The members of BRIEF's Advisory Board have taken valuable time out of their very busy schedules to provide guidance and recommendations. In addition to Genet and Blanco acknowledged above, the other Board members are Stella Kafka (Director, AAVSO), Bob Buchheim (President, Society for Astronomical Sciences), and Mike Chasin (President, SDAA).

Finally, Pat and Grady must thank their wives, Debbie Fritsch and Katrina Boyce, for not only tolerating our long hours but also supporting BRIEF in ways that cannot be numbered. They have become an invaluable part of the BRIEF team.

12. References

Genet, R., et al, "A Student-Centered Astronomical Research Community of Practice", Proceedings for the 35th Annual Conference of the Society for Astronomical Sciences (June 2016), 59-74.

Wenger, Etienne, *Communities of Practice: Learning, Meaning, and Identity (1999),* Cambridge University Press, Cambridge

Johnson J, et al, "Astronomy Research Seminar", *Proceedings for the 34th Annual Conference of the Society for Astronomical Sciences* (June 2015), 139 – 148.

Penn, M., "Citizen CATE Experiment: Prototype Testing and Plans", *Proceedings for the 34th Annual Conference of the Society for Astronomical Sciences* (June 2015), 63 - 67.

Engaging Teenagers in Astronomy Using the Lens of Next Generation Science Standards and Common Core State Standards

Sean Gillette
Vanguard Preparatory School
sean_gillette@avusd.org

Debbie Wolf
Vanguard Preparatory School
debbie_wolf@avusd.org

Jeremiah Harrison
Sandia Academy
jeremiah_harrison@avusd.org

Abstract

The Vanguard Double Star Workshop has been developed to teach eighth graders the technique of measuring position angle and separation of double stars. Through this program, the students follow in the footsteps of a professional scientist by researching the topic, performing the experiment, writing a scientific article, publishing a scientific article, and finally presenting the material to peers. An examination of current educational standards grounds this program in educational practice and philosophy.

1. Introduction

Education standards within the United States are in a state of transition (NGSS, 2017; CCSS, 2017). Knowing discrete facts and figures are no longer a competitive advantage for today's youth. Knowledge once thought of as necessary for employment is only a few taps away on a modern smart phone. The Next Generation Science Standards (NGSS) and Common Core State Standards (CCSS) are focusing instruction on training students how to think and evaluate the plethora of modern information. With this shift, Vanguard Preparatory School, within the Apple Valley Unified School District, have developed programs to engage students with astronomy to become digital citizens of the twenty-first century.

2. Vanguard Double Star Workshop

With the help of Mark Brewer and the Apple Valley Double Star Workshop (Brewer et al, 2014), the Vanguard Double Star Workshop (VDSW) was created to teach eighth grade students how to measure the separation and position angles of double stars and publish and present their measurements as real professional astronomers would. To date around sixty students have been published, over three years (VDSW, VDSW2 & VDSW3) with about thirty-six in process (VDSW4). Students leave this program with experience on how to work with a team to make scientific measurements, write a scientific article fit for publications, and present their findings in front of peers, see Figures 1, 2, 3, 4.

Figure 1: VDSW - March 8-9, 2014

Figure 2: VDSW2 - March 20-22, 2015

Figure 3: VDSW3 - March 11-13, 2016

Figure 4: VDSW4 - March 3-4, 2017

Each year, approximately 36 students are selected from a pool of about 180 students. The entire eighth grade student body at Vanguard Prep are required to write an application astronomy essay. Within this essay, they must answer the following questions: a) what is astronomy, b) what do astronomers study, c) when/where are the best times/places to view astronomical objects, d) how do telescopes works and what are the different types, e) how do stars form, f) what are double stars, and g) why are they important. Students have the opportunity to attend several lunch-time instructional sessions, aimed at helping them understand the questions. With the internet available to students, most are not intimidated about doing scientific research.

A team of teachers reads each article and select students for inclusion in the program, with the final list posted on the gym wall. Typically, more students are selected (some as alternates) to provide for the fact that students will drop out once they understand the rigor and commitment required. Those selected students are required to sign a contract and a code of conduct form stating that they will participate in all the events, knowing their behavior reflects upon themselves and the school. To date, only one student has ever been removed due to behavior, however several students drop each year because of other outside activities.

Once committed, the students are provided with a glow-in-the-dark t-shirt. Most students report that the first thing they do when they get home is try on the shirt and step into a darkened closet. The glow-in-the-dark t-shirt provide a tremendous amount of excitement and novelty.

These students must attend approximately six hours of training, after-school, on the measurement technique and writing conventions of scientific papers. The students are also required to attend an evening program at the local observatory, to see first-hand how double stars are measured. The primary goal of this training is to grant the students a level of comfort using scientific equipment.

The workshop itself encompasses three days, Friday evening, Saturday evening, and Sunday afternoon, typically in late February or early March. The students are broken into three teams, with a volunteer adult amateur astronomer (familiar with the measurement technique) leading each group of students. During the workshop the students are treated to four all-you-can-eat meals, consisting of pizza on Friday night, taco bar on Saturday night, a continental

breakfast on Sunday morning, and subway sandwiches for Sunday afternoon. Cake and ice cream close out the event on Sunday. Glow-in-the-dark t-shirts and all-you-can-eat meals have proven to be successful motivators to the teen-aged participants, since they will put in approximately thirty volunteer hours once the workshop is complete.

The workshop is scheduled for late February or early March to take advantage of early evenings, but weather has often been a disadvantage. A back-up weekend has always been schedule, with its need to be utilized about fifty percent of the time. Wind, rain, and clouds have all contributed to scrub the scheduled events. On one occasion, the back-up weekend was equally poor so one set of adult volunteers filmed the process of measuring several double stars and the students performed the workshop indoors in front of computer screens. A large part of the thrill for the students is staying up late at night, hanging out with friends, and looking at the stars. Using computers, in lieu of telescopes, did not dampen the spirts of the students. Many past participants have related that this workshop was the highlight of their academic career leading into high school.

Friday night marks the students first opportunity to meet the students in their team and their adult team leaders. Each student is provided with an identification badge on a custom school lanyard, which they get to keep after the event. Upon arrival, the students are checked in and placed together with their new groups. Then, the students are lined up for a group picture followed by team pictures that serve as photos within their papers. After the photos, the students sit down together and eat their first of four all-you-can-eat meals. Once they have sufficiently bonded and have been fed, they follow their team leaders outside for the first round of double star measurements. The procedure used for measuring the separation and position angle of double stars are based upon those outlined in R.W. Argyle's book Observing and Measuring Visual Double Stars (Argyle, 2012).

Once outside, the first order of business is to calibrate the astrometric micro-guide eyepiece using the drift method, see figure 5. A calibration star is chosen and multiple measurements are taken using a stopwatch to determine how long the calibration star will take to drift across the linear scale of the eyepiece, once the drive motors are turned off. An average is computed using the following formula:

$$Z = \frac{15.0411\ t\ \cos(d)}{D}$$

Where Z is the scale constant in arc seconds per division; 15.0411 is the Earth's rotational rate in arc seconds per second; t is the average drift time in seconds; d is the declination of the calibration star in degrees; and D is the number of division marks on the linear scale, which for the eyepiece used is 60.

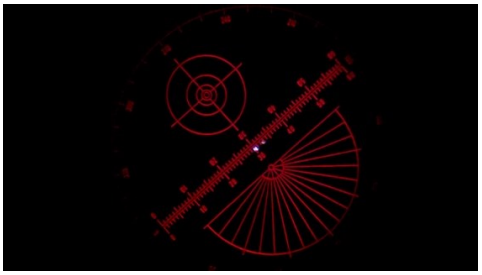

Figure 5: Astrometric Eyepiece used during VDSW2

To determine separation a double star is chosen and aligned on the linear scale, the division marks are counted between the primary star and the secondary star then multiplied by the scale constant. The position angle is determined by setting the primary star at the center of the linear scale and rotating the secondary star on the linear scale. The drive motors are once again disengaged and the double star is allowed to drift to the outside edge of the protractor on the astrometric micro-guide eyepiece, see figure 6. Averages are computed to arrive at a separation and position angle.

Figure 6: Students making measurements during VDSW2

Saturday night is designed as a back-up to Friday, allowing teams the chance to repeat their measurements. In years past, several of the amateur astronomers treat the students to a star party, providing background knowledge of night sky. Sunday is dedicated to the students so they can put their measurements together and write the first draft of their scientific paper. Previously published papers are provided as a guide, but the students are ultimately responsible for this stage of the workshop. After the first draft is competed the students must craft a presentation before they are able to eat lunch.

To simulate a scientific convention the students are required to present their papers as the concluding event. Parents are invited to watch, while their children deliver a public speech about something they have spent hour preparing for. Everyone goes home happy knowing they're put forth an honest effort to create scientific research.

The workshop only produced a first draft, often a very rough first draft. Students are required to attend three after-school editing sessions to fix and improve their paper, see figure 7. The students go through approximately three rounds of internal review and (depending on the quality of their paper) two rounds of external review before the papers are ready to submit to scientific journals.

Figure 7: Students editing papers after school (post workshop) for VDSW2

After four consecutive years of planning and hosting this event, six lessons have been learned: 1) students will work very hard for a free t-shirt and all-you-can-eat food, 2) with teenagers, it is important to point out that they will be able to stay up late at night with their friends, 3) to gain parent support, stress that a published paper provides a unique extracurricular activity on their child's college application, 4) plan all events ahead of time and make them mandatory, 5) use Google Docs to make collaboration easy, and 6) make the event fun and students will return as experienced high school team members.

3. Educational Standards

To better align the Vanguard Double Star Workshop with current educational theory, standards in math, language-arts, and science have been presented to allow other educators a better understanding of how to implement a program of this magnitude. Common Core State Standards (CCSS) cover math and language-arts instruction. While, the Next Generation Science Standards (NGSS) focus on science and engineering instruction.

3.1 CCSS – Math

Most educators agree that math education should be more focused and better sequenced in order to improve mathematical achievement for students. The Common Core Math Standards ware designed to correct the issue of past math curriculum being broad, but not very deep. Rather than teach students in generalities as instructors attempt to cover hundreds of topics in a given year, teachers are now able to focus on just a few key standards and teach them to much greater depth. This provides teachers the chance to teach both the conceptual understanding of mathematical ideas and the practical application of those concepts.

The Common Core Math Standards are organized by grade-level and sorted into sequential categories, with each year building on the prior year's knowledge. The standards were sequenced based on the most current studies of brain development, learning theory, and the rate at which student learning develops over time. This results in a deep and rigorous kindergarten-through-twelfth-grade sequence of the mathematics that students will need as they enter the workforce and/or continue their educations at the university level.

The five main standards for eighth grade students are The Number System, Expressions and Equations, Functions, Geometry, and Statistics & Probability.

3.1.1 CCSS Math Standards

- CCSS.Math.Content.8.EE.C.7 Solve linear equations in one variable.
- CCSS.Math.Content.8.G.A.3 Describe the effect of rotations using coordinates.
- CCSS.Math.Content.8.SP.A.1 Construct and interpret graphs for bivariate measurement data to investigate patterns between two quantities.

3.2 CCSS - English Language-Arts

The world we live in continues to change. For students to succeed in life, they will need more skills and knowledge than ever before. The English language-arts (ELA) Common Core Standards addresses this by not only setting requirements for ELA, but also for literacy in the other core subjects such as science and math. Students must learn to read, write, speak, listen, and use language effectively in a variety of content areas to prepare for college and career readiness.

Through Vanguard's Double Star Workshop, eighth grade students have the opportunity to research, write, and publish their findings.

3.2.1 CCSS ELA Standards

- CCSS.ELA-Literacy.W.8.4 Produce clear and coherent writing in which the development, organization, and style are appropriate to task, purpose, and audience.
- CCSS.ELA-Literacy.W.8.5 With some guidance and support from peers and adults, develop and strengthen writing as needed by planning, revising, editing, rewriting, or trying a new approach, focusing on how well purpose and audience have been addressed.
- CCSS.ELA-Literacy.W.8.6 Use technology, including the Internet, to produce and publish writing and present the relationships between information and ideas efficiently as well as to interact and collaborate with others.
- CCSS.ELA-Literacy.W.8.7 Conduct short research projects to answer a question (including a self-generated question), drawing on several sources and generating additional related, focused questions that allow for multiple avenues of exploration.
- CCSS.ELA-Literacy.W.8.8 Gather relevant information from multiple print and digital sources, using search terms effectively; assess the credibility and accuracy of each source; and quote or paraphrase the data and conclusions of others while avoiding plagiarism and following a standard format for citation.

3.3 NGSS

With the globalization of commerce and the shifting of manufacturing to cheaper oversea productions sites, the United States has embarked on a rewriting of science curriculum, titled the Next Generation Science Standards (NGSS). These new standards refocus science education to teach scientific methodology rather than scientific facts, facts which now can be easily located with a web browser. A second emphasis of NGSS is to introduce engineering as a curriculum, with the proposed benefit of bringing skilled manufacturing back to the US. In broad terms NGSS hopes to teach students how to think like a scientist or an engineer.

NGSS is multifaceted and is initially divided up into Performance Expectations (PE). These expectations spell out which broad topics are to be included in a grade level band. PEs are what the student is expected to be able to do by the end of the instruction. Each PE is further broken into (a) Disciplinary Core Ideas (DCI), (b) Science and Engineering Practices (SEP), and (c) Crosscutting Concepts (CCC). DCIs are specific scientific knowledge a student is responsible for, SEPs are skills students need in order to learn the material, and CCCs are broad topics that are present in all grade level bands, which tie several large scientific topics together into one overarching idea (NGSS, 2017).

The relevant NGSS Performance Expectation for this project are Earth and Space Systems MS-ESS1-2: Earth's Place in the Universe. This PE asks students to develop and use a model to describe the role of gravity in the motions within galaxies and the solar system. Within this PE there are applicable DCIs, SEPs, and CCCs.

3.3.1 NGSS Standards

Learning Goal (Performance Expectation – what the student should be able to do)

- Earth and Space Systems MS-ESS1-2: Earth's Place in the Universe.

Required Knowledge (Disciplinary Core Idea - what the student should learn)

- ESS1.A: The Universe and Its Stars - Earth and its solar system are part of the Milky Way galaxy, which in one of many galaxies in the universe

Required Skills (Science and Engineering Practices - what the student should do)

- SEP1: Asking Questions and Defining Problems - Students at any grade level should be able to ask questions of each other about the texts they read, the features of the phenomena they observe, and the conclusions they draw from their models or scientific investigations.
- SEP2: Developing and Using Models - Models include diagrams, physical replicas, mathematical representations, analogies, and computer simulations. Although models do not correspond exactly to the real world, they bring certain features into focus while obscuring others. All models contain approximations and assumptions that limit the range of validity and predictive power, so it is important for students to recognize their limitations.
- SEP3: Planning and Carrying Out Investigations - Scientific investigations may be undertaken to describe a phenomenon, or to test a theory or model for how the world works.
- SEP4: Analyzing and Interpreting Data - Students are expected to improve their abilities to interpret data by identifying significant features and patterns, use mathematics to represent relationships between variables, and take into account sources of error.
- SEP5: Using Mathematics and Computational Thinking - Students are expected to use mathematics to represent physical variables and their relationships, and to make quantitative predictions.
- SEP6: Constructing Explanations and Designing Solutions - Students are expected to construct their own explanations, as well as apply standard explanations they learn about from their teachers or reading.
- SEP7: Engaging in Argument from Evidence - In science, reasoning and argument based on evidence are essential in identifying the best explanation for a natural phenomenon.
- SEP8: Obtaining, Evaluating, and Communicating Information - Being able to read, interpret, and produce scientific and technical text are fundamental practices of science and engineering, as is the ability to communicate clearly and persuasively (NGSS, 2017).

Interrelated Scientific Topics (Crosscutting Concepts - broad topics within science)

- CCC1: Patterns - Observed patterns of forms and events guide organization and classification, and they prompt questions about relationships and the factors that influence them.
- CCC2: Cause and Effect - Events have causes, sometimes simple, sometimes multifaceted. A major activity of science is investigating and explaining causal relationships and the mechanisms by which they are mediated.
- CCC3: Scale, Proportion, and Quantity - In considering phenomena, it is critical to recognize what is relevant at different measures of size, time, and energy and to recognize how changes in scale, proportion, or quantity affect a system's structure or performance.
- CCC4: Systems and Systems Models - Defining the system under study—specifying its boundaries and making explicit a model of that system—provides tools for understanding and testing ideas that are applicable throughout science and engineering.
- CCC7: Stability and Change - For natural and built systems alike, conditions of stability and determinants of rates of change or evolution of a

system are critical elements of study (NGSS, 2017).

5. Conclusion

If students are to achieve in a global economy, where communication is instantaneous and digital borders are nonexistent, then they will need skills to effectively convey their learning and present evidence to support claims. Common Core Language-Arts and Math Standards and the Next Generation Science Standards attempt to bring students into the twenty-first century by providing them the tools to evaluate the plethora of information now available and promote assessment skills needed to succeed. The Apple Valley Unified School District has embraced these new standards and promote the real word application of this learning by supporting the Vanguard Double Star Workshop. As the program grows, establishment of additional eighth grade beginning workshops and high school advanced workshops is entirely possible.

6. References

Argyle, R.W. (2012). Observing and Measuring Visual Double Stars. The Patrick Moore Practical Astronomy Series. Springer. New York, NY. Second edition.

Brewer, M., Weise, E., Estrada, R., Estrada, C., Buehlman, W., Wasson, R., Rogers, A., Camunas, M. (2014). Apple Valley Double Star Workshop. Journal of Double Star Observations. Vol. 10, No. 2, p. 160.

CCSS (2017) Common Core State Standards. Retrieved from corestandards.org on April 14, 2017.

NGSS (2017). Next Generation Science Standards. Retrieved from ngss.org on April 12, 2017

An overview of ten years of student research and JDSO publications

Rachel Freed
Sonoma State University
416 4th St. W. Sonoma, CA 95476
r.freed2010@gmail.com

Michael Fitzgerald
Edith Cowan Institute for Educational Research
270 Joondalup Drive, Joondalup WA 6027 Australia
mfitzasp@gmail.com

Russell Genet
California Polytechnic State University, San Luis Obispo
4995 Santa Margarita Lake Rd
Santa Margarita, CA 93453
russmgenet@aol.com

Brendan Davidson
Desert Hills Middle School, St. George Utah
2564 E. 2150 S. Circle
St. George, Utah 84790
bjrocket141@gmail.com

Abstract

The astronomy research seminar, initially designed and taught by Russell Genet at Cuesta College over the past decade, has resulted in over 100 published student research papers in the Journal of Double Star Observations along with dozens of other papers and conference presentations. While the seminar began at a single community college it has now spread to include students from dozens of institutions and instructors, reaching students from middle school through graduate school. The seminar has integrated the large community-of-practice of amateur and professional astronomers, educators, students, and hardware and software engineers while providing an important experience for student researchers. In this paper, we provide an overview analysis of 109 publications authored by 320 individual students involved in the astronomy research seminar over the last decade.

1. Introduction

Cultivating a population that understands the true nature of science and science communication is critical to the future of this country and the globe now more than ever. Despite this, student interest in school science (Danaia et al. 2013) and science in general has stagnated (Osborne et al. 2003). An endeavor to redress this problem, an astronomy research seminar at Cuesta College, has been taught by Russell Genet for the past decade (Genet et al. 2010). Recently other schools have developed programs based on his model which provides the opportunity for undergraduate and high school students to conduct astronomical research and publish their findings within a well-established pro-am community-of-practice (Genet et al. in this proceedings). The program is unique in its requirement that students write papers and submit them for publication, thus teaching students about the entire research process from conception to submission. Perhaps also somewhat unique is that the students propose and manage their own research projects (rather than playing understudies to an experienced researcher).

Over the past decade, the seminar has influenced the future paths of many students. Some have gone on to repeat the seminar multiple times, therefore coauthoring several published papers, while others have ended up becoming instructors for the seminar. A few students have developed their own programs based on the research seminar, thereby multiplying the number of students gaining access to this kind of program.

In addition, some students who have taken the astronomy research seminar have been so inspired they went on to get science degrees, including advanced degrees in astrophysics. In this paper, we analyze 109 seminar research papers to look at the numbers of students who have taken the seminar, published papers and gone on to develop their own programs. We break down the types of research that have been done in the seminar and examine the number and types of institutions that have been involved in the research.

2. Analysis of the student coauthors and institutions

In this paper, we present a simple analysis of the student coauthors, the institutions from which they come, and the research techniques and commonly used equipment.

2.1 Students

This analysis is limited to student research papers published in the *Journal of Double Star Observations (JDSO)*. Many other student papers from the seminar have been published in the conference proceedings of the Society for Astronomical Sciences and elsewhere, and there are a couple of dozen papers in the pipeline for publishing in the *JDSO*. In analyzing 109 research papers we determined that there were 320 individual student coauthors. One hundred forty-two of the authors were female, while 178 were male. Of all of these students, 48 authored more than 1 paper, with the breakdown as follows. Seventeen high school students coauthored 2 publications. Four of these students had their first astronomy research seminar and publication when they were in middle school and their second in high school. Seventeen college students published 2 papers. One of these students first published in high school and then in college. Two high school and two college students each published 3 papers and 5 college students published 4 papers. One of these students published his first 3 in high school and another when he was in college.

There was a distinct difference between the numbers of male and female students taking the seminar and publishing more than one paper. There were roughly equal numbers of males and females who took the research seminar and published a single paper at all three educational levels; 48% female in middle school, 47% female in high school and 48% female in college (Table 1). However, the percentage of females dropped dramatically when looking at the number of students who published more than one paper. The percentage of female coauthors who published 2 papers was 29% for high school and 31% for college students (Table 2). Only 1 middle school student published 2 papers and it was a male. Two college and two high school students published 3 papers and there were all male (Table 3). Out of 5 students who published 4 papers, only 1 was female (Table 4). The five students who published more than 4 papers were all male.

Students who published 1 paper			
		number	%
College	Female	60	48
	Male	65	52
High School	Female	52	47
	Male	58	53
Middle School	Female	16	48
	Male	17	52

Table 1: The Number and percentages of female and male student coauthors who published a single paper.

Students who published 2 paper			
		number	%
College	Female	4	31
	Male	9	96
High School	Female	4	29
	Male	10	71
Middle School	Female	0	0
	Male	1	100

Table 2: The Number and percentages of female and male student coauthors who published two papers.

Students who published 3 paper			
		number	%
College	Female	0	0
	Male	2	100
High School	Female	0	0
	Male	2	100

Table 3: The Number and percentages of female and male student coauthors who published three papers.

Students who published 4 paper

		number	%
College	Female	1	20
	Male	4	80

Table 4: The Number and percentages of female and male student coauthors who published four papers.

2.2 Schools and other institutions

Involving students in actual scientific research is critical to helping them develop a true understanding of the nature of science. While the astronomy research seminar started out at Cuesta Community College and is still being taught there by Russell Genet, it reaches students far beyond the area. The seminar has expanded greatly over the years to really engage with the small telescope community-of-practice and many educational institutions. Student coauthors of the 109 papers we analyzed hailed from 22 different colleges and universities spanning 6 states (CA, HA, WA, OR, AZ and ID) and Australia, 18 different high schools from 4 states (CA, HA, OR, WA) and 3 different middle schools from California and Hawaii. The distributions of these schools is shown in Figures 1-4.

Other types of institutions have also become involved in the research seminar. Jo Johnson conducted observing sessions at the Gateway Science Museum in Chico CA. The Lewis Center for Educational Research in Apple Valley has an observatory and hosted 3-day workshops for double star observations (Gillette, 2013).

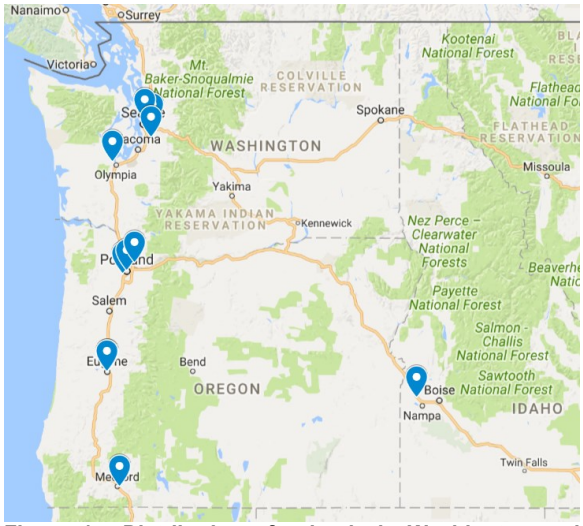

Figure 1: Distribution of schools in Washington and Oregon from which student coauthors of the papers hailed.

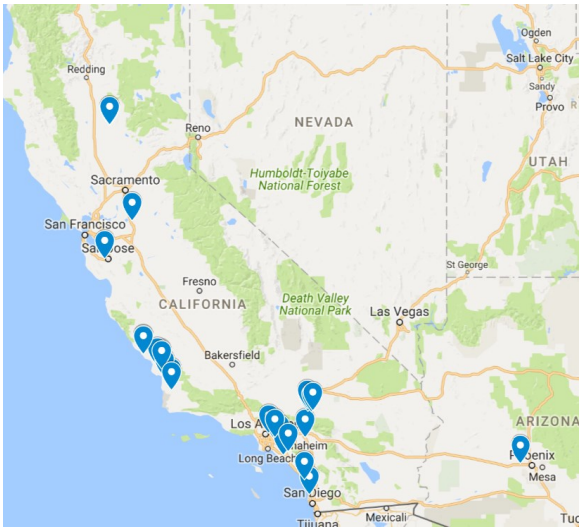

Figure 2: Distribution of schools in California and Arizona from which student coauthors of the papers hailed.

Figure 3: Distribution of schools in Hawaii from which student coauthors of the papers hailed.

Figure 4: One student coauthor participated in the research seminar from as far away as Australia.

3. Observational Techniques and Equipment

Within the 109 papers there are several main categories of observational techniques used. Measurements were made of the position angle and separation of one or more double stars using one of three techniques, 1) astrometric eyepiece measurements, 2) CCD measurements and 3) speckle interferometric measurements. Some published papers focused on technical issues comparing different telescopes or astrometric eyepieces. Another category of papers were devoted to producing tools for double star observations such as catalogues of neglected double stars. Still other papers were technical papers involving the development of observational techniques or equipment.

Forty-eight papers published separation and position angle data from astrometric eyepiece measurements of double stars. Seventeen published results from CCD measurements and eight published results from speckle interferometry measurements, four of which were analyses of the Kitt Peak data runs of 2013 and 2014 (Genet, 2015). Twenty-eight published papers introduced or described results of technical analysis of equipment or techniques.

The astronomy research seminar utilized telescopes and equipment from around the globe. The telescopes used belonged either to individual amateur astronomers, colleges and universities, or large local or global telescope networks. In terms of the greatest number of publications using a particular type of telescope, the most common telescopes were the 11", 10" and 8" Schmidt-Cassegrain (SCT) telescopes, (Carro, 2013; Buchheim 2008; Johnson, 2013; Brewer, 2016) and an 18" Newtonian telescope (Frey, 2014). This was a function of the fact that very active amateur astronomers owned these telescopes and shared them with many student groups at workshops or for individual team observing runs.

4. The Student Becomes the Teacher

A handful of students who went through the astronomy research seminar continued on to become prolific assistant instructors or instructors in their own right, or even developed their own programs to carry on what the seminar had begun and to bring the research and publication opportunities to other groups of students. Here we briefly describe a few of the more prolific authors:

Jolyon (Jo) Johnson first took the seminar in 2007 when he was in high school and then continued to work on double star observations as an assistant instructor and then ran his own workshops when he attended California State University, Chico and then graduate school at the University of Washington, Seattle. He quickly became adept at writing research papers on double star observations and he coauthored 20 papers in the *Journal of Double Star Observations* between 2007 and 2016 and has been a reviewer for many others. In addition, he is the co-editor of the *Small Telescope Astronomical Research Handbook* and several published collections of selected student research papers. He attended double star conferences and soon began chairing the conferences. Clearly the astronomy research seminar impacted his life steering it on a course of scientific research.

Eric Weise published his first two papers from the research seminar through Cuesta College in 2009 and 2010 as a student at Arroyo Grande High School. He then went on to the University of California, San Diego and continued to actively pursue double star research, coauthoring 13 papers in the *JDSO* between 2009-2015.

After first taking the course at Cuesta Community College and publishing a paper in 2011, Mark Brewer went on to help lead a number of groups of middle school students from Vanguard Preparatory School in Apple Valley, California through an independent version of the research seminar over the succeeding 5 years and he has coauthored 11 papers between 2011 and 2016, appearing as the first author on 9 of these.

Chris Estrada took the research seminar and published his first paper in 2010 and has been very active in double star research since then, publishing 10 papers in the *Journal of Double Star Observations* between 2010-2016, and working on a number of projects with Mark Brewer and others, including holding several weekend workshops for 8th grade students at Vanguard Preparatory School.

5. Amateur astronomers, an integral part of the Community-of-Practice

An important and indispensable part of the of the community-of-practice of small telescope research is the amateur astronomer community; they have provided invaluable assistance. They are an integral part of the research. In 38 out of the 109 papers amateur astronomers participated in the research in a variety of ways and were explicitly acknowledged. Some loaned their telescopes, astrometric eyepieces and other equipment to the students and helped them make observations and do the data analysis. Others reviewed student papers before publication. A total of 23 amateur astronomers were specifically thanked in the acknowledgement section of the published student papers that we analyzed. Many of these amateurs were actually co-authors of one or more

papers produced from the research seminar. Clearly, they were an indispensable part of the community-of-practice without whom it would have been very difficult to bring astronomical research to students.

Just as students can become inspired by the astronomy research seminar, so can amateur astronomers. One example is Joseph Carro, an amateur astronomer, who assisted in the research seminar in 2011 and then went on to publish seven papers on his own in the *JDSO*, between 2011-2015, in which he reported measurements of 126 double stars. He also published a paper describing the catalog he created to speed up the process of identifying double stars for future study (Carro, 2013).

Peer review is as critical to the process of science as developing solid questions. The small telescope community-of-practice provides vital service to students in this respect, allowing students to receive expert feedback on their papers before submission for publication. In addition to teaching them about what is required to conduct and communicate scientific research, it also helps them hone their critical thinking and writing skills. Many amateur and professional astronomers reviewed these student research papers and were specifically thanked. Tom Smith, of Dark Ridge Observatory, was acknowledged in 16 research papers for his helpful reviews, in addition to being part of the Kitt Peak Speckle Interferometry team which obtained over 1000 speckle interferometric measurements of close binaries for analysis by current and future students. Bob Buchheim, the president of the Society for Astronomical Sciences, was acknowledged for his help in reviewing 12 published student research papers. Dr. Vera Wallen reviewed almost all of the papers over the past 10 years for English and grammar. She was specifically acknowledged and thanked for her reviews in 29 of the papers.

6. Conclusion

The astronomy research seminar has clearly affected the education and career trajectory of a number of students and has most certainly given hundreds of students an understanding of the nature and process of scientific research. This approach has clearly shown that true student research can be undertaken for larger populations, a scaling problem for which a solution has been sought for many years (Fitzgerald et al. 2014).

Future directions for the research described in this paper should include interviewing students from the past 10 years about what they are doing now and how the seminar influenced their education and career choices. Information from these studies should help guide the continual development and evolution of the seminar, including the fully online version which is currently being piloted in the 2017 Spring semester with 43 students spread across five teams.

7. Acknowledgements

We would like to thank Vera Wallen for her review of this paper.

8. References

Brewer, M., Estrada, C., Estrada, R., Gillette, S. “A Weekend Workshop on Double Stars for Students.” (2016). *Journal of Double Star Observations.* **12:1**, 9-12.

Buchheim, R.K. “CCD Double Star Observations at Altimira Observatory: Spring 2008.” (2008). Journal of Double Star Observations.” **4:3**, 103-110.

Carro, J.M. “Useful Lists of Double Stars.” (2013). *Journal of Double Star Observations*. **9-3**, 203-206.

Danaia, L., Fitzgerald, M., McKinnon, D., “Students’ Perceptions of High School Science: What has Changed Over the Last Decade?” (2014). *Research in Science Education*. **43:4**, 1501-1515.

Frey, T.G., Hartshorn, B., Hernandez-Frey, N. “A Comparison of Two Double Star Astrometry Techniques: Visual and DSLR”. (2014). *Journal of Double Star Observations*. **10:1**, 52-51.

Fitzgerald, M. T., Hollow, R., Rebull, L. M., Danaia, L., & McKinnon, D. H. “A review of high school level astronomy student research projects over the last two decades.” (2014). *Publications of the Astronomical Society of Australia* 31, e037.

Genet R. M, Johnson J. M., Wallen V. “One-semester astronomical research seminars.” In: Genet RM, Johnson JM, Wallen V, editors. (2010) *Small telescopes and astronomical research*. 3rd ed. Santa Margarita (CA): Collins Foundation Press; 2010. p. 203.

Genet, R. M. “Kitt Peak Speckle Interferometry of Close Visual Binary Stars. (2015) *Journal of Double Star Observations,* **11-1s**, 234-244.

Gillette, S., Funk, B., Schlosser, R., Brown, A., Cruz, M., McCarthy, J., Rhoades, B., Spring, B. “Double Star Measurements of Beta Scorpii.” (2016). **12:6**, 586-588.

Johnson, J. Carro, J., Weise, E., Genet, R., Cahn, B., Chezum, B., Degnan, C. M. Ford, N., Greene, A., Jaeger, N., Johnson, R., Nicholson, K., Richards, D., Richardson, R., Thompson, S. "Two Cuesta College Teams Observe Albireo." (2013). *Journal of Double Star Observations*. **9:1**, 58-60.

Osborne, J., Simon, S., Collins, S. "Attitudes towards science: A review of the literature and its implications", (2003) *International Journal of Science Education.* **25:9**, 1049-1079

Use of the AAVSO's International Variable Star Index (VSX) in an Undergraduate Astronomy Course Capstone Project

Kristine Larsen
Central Connecticut State University
1615 Stanley St., New Britain, CT 06050
larsen@ccsu.edu

Abstract

The author discusses a capstone project that utilizes the AAVSO's International Variable Star Index (VSX), ASAS light curves and phase plots, and the SIMBAD astronomical data repository in a laboratory-based undergraduate Stellar and Galactic Astronomy course.

1. Introduction: Variable Stars as a Unifying Theme

AST 209 Stellar and Galactic Astronomy is an algebra-based four-credit course with a laboratory experience that serves both general education students and Astronomy Minors at Central Connecticut State University. For example, in the Spring 2017 semester, of the 36 students who completed the course 25% have majors in the School of Business, 27.8% in the Humanities, 19.4% in Social Sciences and the same percentage in Science/Technology/Engineering/Mathematical fields, with 8.3% in Education. Given the diverse audience of the course, it has proven a challenge to develop both course content and assignments that simultaneously engage and challenge both populations without targeting or neglecting one or the other.

The course begins with an overview of light, telescopes, and the sun, and then surveys stellar properties and evolution, galactic astronomy, and finally cosmology. Algebra is built into the course from the ground up, and is used in both lecture and lab. Students are given a formula sheet at the beginning of the semester that is used to complete all homework assignments and on in-class examinations. There are two telescope-based labs (simple observations of deepsky objects and double stars); the rest of the lab assignments involve analyzing provided data, graphs, or images.

Given the wide variety of topics covered, the course had been considered interesting but overwhelming by some general education students. It clearly needed a storyline to tie it all together; a refrain that would be introduced at the start of the course, periodically revisited and built upon, and would provide a cohesive message to the course as a whole. Given the instructor's long-time affiliation with the American Association of Variable Star Observers (AAVSO) as well as her research with students on reclassifying "miscellaneous" stars in the AAVSO's International Variable Star Index (e.g. Larsen 2016), it was decided to revise the course for the Spring 2017 to have a recurring focus on variable stars and their importance to our understanding of the universe.

On the first day of class, a PowerPoint slide containing a simplified taxonomy of variable stars (including only those types to be discussed over the course of the semester) was shared with the students, and it was described how this slide would be revisited over the course of the semester as different types of variable stars were integrated into the story of the universe. As described below, an appropriate assessment tool was required in order to evaluate student understanding of this new thematic approach.

2. Designing the Assessment Tool: Theoretical Considerations

Scriven (1967) is considered the first to classify assessments as either formative or summative. As applied to education, formative assessments take place periodically during the learning process and provide feedback as to both the current mastery of the material by the learner and the effectiveness of the pedagogy being utilized by the instructor (for the purpose of making needed strategic changes by both sides in real time). Summative assessment occurs at the end of a learning module (e.g. the end of a unit or semester), and measures the final mastery of the material by the learner. In well-crafted assignments, meaningful information should also be provided to the instructor as to the overall effectiveness of the pedagogy used within that module. In a lab-based science course, such assessments have typically included both in-class final exams based on the

lecture material and lab exams (either paper-and-pencil or so-called lab practicums that ask the student to "redo" parts of experiments already completed but without the aid of their lap partners and within a highly structured, timed environment).

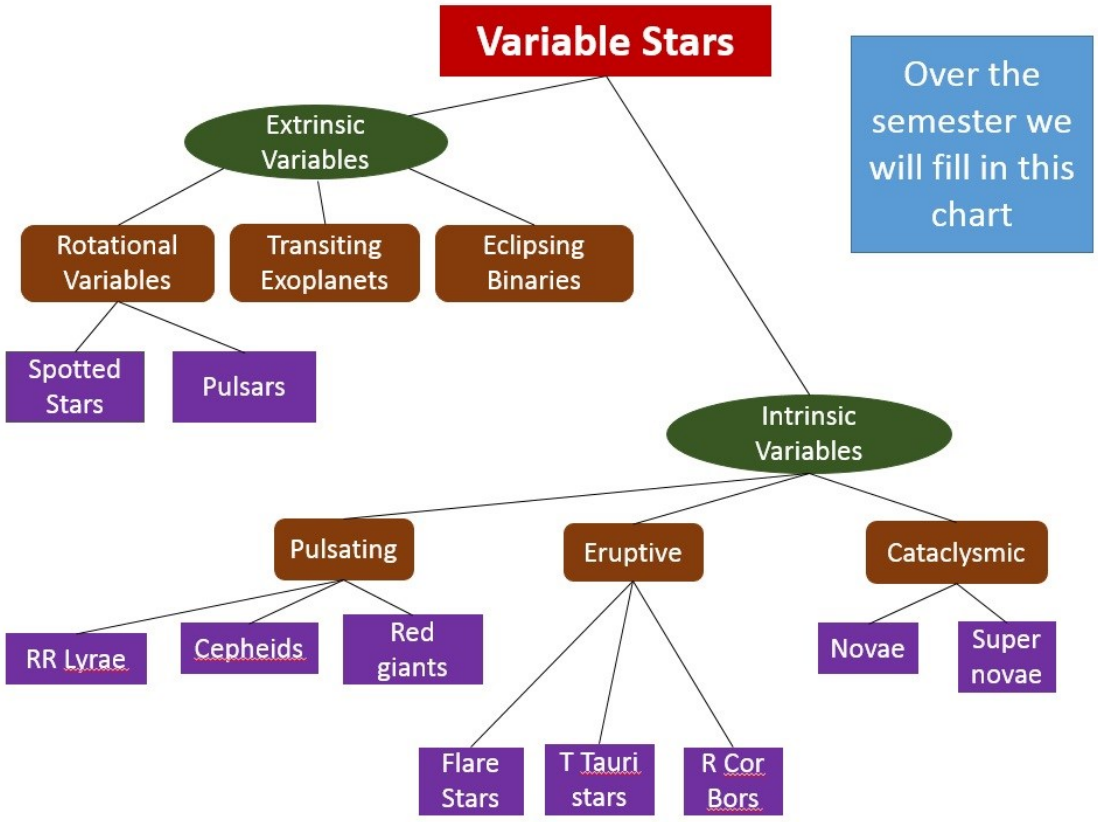

Figure 1. Diagram of variable star taxonomy that provide the storyline for the course.

Unfortunately, such a bifurcated assessment structure can lead students to the erroneous conclusion that the material taught in lab and lecture is unrelated, rather than highlighting the true nature of the lab experience, which is to demonstrate the way that science is actually conducted and that theory and observation/experimentation are equally important to the scientific endeavor (something that is particularly true in astronomy). Therefore it was decided in 2008 to switch from lab practicums to capstone projects that integrate lab and lecture content and techniques for both AST 208 Planetary Astronomy and AST 209 Stellar and Galactic Astronomy (Larsen & Piatek 2009).

While the instructor of AST 209 was initially satisfied that the assignment (based on HST photographs of high redshift galaxies) was a fair assessment of both content (including Hubble's Law and electromagnetic spectrum) and lab techniques (e.g. using a plate scale and classification based on morphology), as well as opportunities for students to both calculate and explain, there was push-back from the students, a significant number of whom considered the assignment to be busy-work that was not worth the 5% weight towards the overall course grade. As a result, a not insignificant number of students who were otherwise passing the course opted to skip the assignment and lose the points (as high as 12% of the entire class in some semesters). It was therefore decided to rethink the entire capstone project simultaneously with revising the course to follow the aforementioned storyline of the importance of variable stars to our understanding of the universe.

While educators often debate the required characteristics of an effective summative assessment, the "top seven" list provided by Gillespie (2014) summarizes some key points: effective summative assessments should (1) be crafted by instructors (rather than publishers) with student input/choice; afford students the opportunity to (2) demonstrate their understanding of the course material through (3) applying it to authentic situations via the use of (4) "21st century skills"; (5) be aligned with key course concepts; (6) include opportunities to "provide meaningful feedback to both the student; and avoid being limited to high-stakes exams. These key points were central to the creation of the Variable Star Capstone project described in the following section.

3. The Variable Star Capstone

It was decided that a central feature of the new capstone would be to introduce students to the AAVSO's VSX as well as other online repositories of astronomical data. It was also decided that since students already plotted light curves from provided data in a lab exercise near the midpoint of the semester, the emphasis would instead be placed on analyzing a light curve. It was important that the assignment provide meaningful information to both the student and the instructor as to what the student had successfully mastered (and what was still unclear) since the assignment was due a week before a cumulative final exam worth 20% of the overall course grade, and was graded and returned to the students 48 hours after submission. In order to accomplish this goal, the project integrated concepts that students often demonstrate confusion with (e.g. the magnitude scale, spectral classes, HR diagram) as well as affording them opportunities to apply equations and mathematical techniques (e.g. unit conversions) that had been used throughout the semester. Students were given a month to complete the assignment on their own time outside of class and was still worth 5% of the total course grade.

In order to integrate student choice into the assignment, each student selected a unique variable star from a pre-approved list provided by the instructor. Students were able to select a star from several different types of variable stars: eclipsing binaries, rotational variables, RR Lyrae stars and Cepheids, and Long-period variables/Semiregulars (termed "pulsating red giants" in general within the course). These types were selected based on the availability of sufficient examples with the necessary accompanying data that could be found in VSX.

Students were given an electronic template for their project (a Word document that was to be completed) as well as a detailed instruction sheet with screen captures detailing how to use VSX to look up information on "their star." Both documents are available from the author via email upon request. ASAS light curves and phase plots for one Cepheid and one rotational variable were also provided on the instruction sheet, along with an explanation of the apparent differences between each, in order to provide pointers to the students as to what to look for in the behavior of their star.

The basic outline of the project was as follows. Students first used VSX to look up the constellation, variability type (including subtype), spectral class, magnitude range, and period of their star. Students then had to decide whether their star was an intrinsic or extrinsic variable, and whether its variations were caused by rotation, eclipses, or pulsations. Students then followed the ASAS light curve link in VSX to copy/paste the ASAS light curve and phase plot into their template and briefly analyzed them in a qualitative way (focusing on the regularity – or lack thereof – in the period and amplitude range).

The SIMBAD astronomical database link in VSX was then used to record the star's parallax and proper motion. This data was in turn used to calculate the star's tangential velocity and distance. In the final calculation, students estimated the star's mean apparent magnitude, and using the computed distance to calculate the star's absolute magnitude, which was then used in conjunction with the spectral class to plot the star (and the sun, for comparison) on a provided HR diagram. Students were then asked whether or not their star was intrinsically brighter or dimmer than the sun. It is important to note that all calculations included in this project had been previously done on homework problems during the semester.

4. Student Outcomes

Every student in the course successfully completed the assignment and on time. The main difficulties demonstrated fell into three categories: computational errors (either in utilizing the distance-modulus formula or converting from milliarcseconds to arcseconds), lapses in remembering that more negative magnitudes are brighter, and forgetting to plot the sun on the HR diagram. The perfect completion rate is at least anecdotal evidence that the students found the assignment to be reasonable work for 5% of their course grade and relatively interesting and worthwhile.

The assignment ended with a set of open-ended reflection questions asking the students to explain the most important and surprising things they learned about both their individual star and variable stars in general. A number of students gave particularly

interesting answers, a sample of which are reproduced here:

"Stars don't look that much different in the night sky to us but when people study them we learn that they have so many differences."

"This project helped me understand not only what the variables are, but how they differ from a main sequence star, or even how they go from being a 'normal' star to leaving the main sequence."

"There are tons of variable stars in the universe. Looking at the catalog, you could see how impressive the numbers just are."

"Since my star was 277000 pc away it looked much dimmer than our sun. However, when calculating the absolute magnitude of my star it ended up being much brighter than our sun. Distance really does make a huge difference in the way we see how bright stars are."

"The most surprising thing about variable stars in general is that by studying these stars we can find out vital information about other stars…. By observing how variable stars behave, we can predict how other stars will behave."

5. Conclusion: Completing the Assessment Loop

Meaningful assessment is a continual loop; students provide evidence of what they know through the assignment, and the instructor further focuses attention on the misconceptions and errors that still exist through providing the student with meaningful feedback. Given the timing of the capstone, students could benefit directly from that feedback in preparing for the final exam. Simultaneously, students provide valuable feedback to the instructor in terms of how successful the assignment was in meeting its assessment goals. Based on observed student difficulties with the assignment, directions can be improved and portions of the assignment modified as needed in the future.

In order to expedite this process, an optional bonus question was included, asking students to provide constructive feedback on how to improve the assignment in the future. Such feedback included the expected specific examples for rewording the directions, but additionally offered the unexpected suggestions of including more work in the assignment, such as the visual observation of the star by the student, writing a short paper on the star summarizing its characteristics, or the comparison of several stars to each other. These and other suggestions will be taken into account in future iterations of this assignment.

6. References

Gillespie, R. "7 Characteristics of Quality Summative Assessments." (April 7, 2014). *Brilliant or Insane: Education on the Edge*. http://www.brilliant-insane.com/2014/04/7-characteristics-of-quality-summative-assessments.html.

Larsen, K. "Utilizing the AAVSO's Variable Star Index (VSX) in Undergraduate Research Projects." AAS Meeting #227, #247.08, 2016. http://aas.org/files/resources/aas_227_abstract_pdf.pdf.

----- & J. Piatek. "Utilizing Realistic Problem-based Projects to Assess Student Learning in Laboratory-based Introductory Astronomy Courses." CCIC/Project Kaleidoscope/CSU Conference. Yale University, New Haven, October 30, 2009.

Scriven, M. "The Methodology of Evaluation." (1967). In *Perspectives of Curriculum Evaluation*, eds. R.W. Tyler, R.M. Gagne, & M. Scriven, pp. 39-83. Chicago: Rand McNally.

Student Scientific Research within Communities-of-Practice

*Russell Genet, California Polytechnic State University, San Luis Obispo, CA**
James Armstrong, Univ. of Hawaii, Maui, HI
Philip Blanko, Grossmont College, San Diego, CA
Grady Boyce, Boyce Research Initiatives and Education Foundation, San Diego, CA
Pat Boyce, Boyce Research Initiatives and Education Foundation, San Diego, CA
Mark Brewer, California State University, San Bernardino, CA
Robert Buchheim, Society for Astronomical Sciences, Ontario, CA
Jae Calanog, Miramar College, San Diego, CA
Diana Castaneda, University of Hawaii, Honolulu, HI
Rebecca Chamberlin, The Evergreen State College, Olympia, WA
R. Kent Clark, University of Southern Alabama, Mobile, AL
Dwight Collins, Collins Educational Foundation, San Rafael, CA
Dennis Conti, American Association of Variable Star Observers, Annapolis, MD
Sebastien Cormier, Grossmont College, San Diego, CA
Michael Fitzgerald, Edith Cowen University, Perth, Australia
Chris Estrada, California State University, Los Angeles, CA
Reed Estrada, Northrop Aviation, Lancaster, CA
Rachel Freed, California State University, Sonoma, CA
Edward Gomez, Los Cumbres Observatory, Santa Barbara, CA
Paul Hardersen, Planetary Science Institute, Tucson, AZ
Richard Harshaw, Brilliant Sky Observatory, Cave Creek, AZ
Jolyon Johnson, Sammamish High School, Belleview, WA
Stella Kafka, American Association of Variable Star Observers, Cambridge, MA
John Kenney, Concordia University, Irvine, CA
Kakkala Mohanan, Leeward Community College, Pearl City, Oahu, HI
John Ridgely, California Polytechnic State University, San Luis Obispo, CA
David Rowe, PlaneWave Instruments, Rancho Dominguez, CA
Mark Silliman, Waipaha High School, Waipaha, Oahu, HI
Irena Stojimirovic, Mesa College, San Diego, CA
Kalee Tock, Stanford Online High School, Palo Alto, CA
Douglas Walker, Estrella Mountain Community College, Avondale, AZ
Vera Wallen, Coast Unified School District (retired), Cayucos, CA
* Corresponding author russmgenet@aol.com

Abstract

Social learning theory suggests that students who wish to become scientists will benefit by being active researchers early in their educational careers. As coauthors of published research, they identify themselves as scientists. This provides them with the inspiration, motivation, and staying power that many will need to complete the long educational process. This hypothesis was put to the test over the past decade by a one-semester astronomy research seminar where teams of students managed their own research. Well over a hundred published papers coauthored by high school and undergraduate students at a handful of schools substantiated this hypothesis. However, one could argue that this was a special case. Astronomy, after all, is supported by a large professional-amateur community-of-practice. Furthermore, the specific area of research—double star astrometry—was chosen because the observations could be quickly made, the data reduction and analysis was straight forward, and publication of the research was welcomed by the *Journal of Double Star Observations*. A recently initiated seminar development and expansion program—supported in part by the National Science Foundation—is testing a more general hypothesis that: (1) the seminar can be successfully adopted by many other schools; (2) research within astronomy can be extended from double star astrometry to time series photometry of variable stars, exoplanet transits, and asteroids; and (3) the seminar model can be extended to a science beyond astronomy: environmental science—specifically atmospheric science. If the more general hypothesis is also supported, seminars that similarly feature published high school and undergraduate student

team research could have the potential to significantly improve science education by increasing the percentage of students who complete the education required to become professional scientists.

1. Specific Hypotheses

We do not expect students who want to be professional basketball players to take classes in the theory of basketball and participate in dunking and dribbling labs for years on end without ever actually playing a basketball game as a team member. So why, without ever doing any actual research, should we expect high school or undergraduate aspiring scientists to somehow appreciate that the individual lecture courses and technique labs they will take for many years will somehow all come together in a coherent manner?

One of us (Genet) formulated Hypothesis #1 that, given appropriate circumstances, teams of undergraduate and high school students could themselves, within the confines of a single semester, systematically produce published research by following the same process that professional research teams use to conduct their research. As is the case for professional research, the students would develop ideas for projects, formulate teams, and write up project proposals for approval by their researcher supervisor (the instructor). The teams would then conduct their research, write up their results, and send their papers out for external review and publication.

A related Hypothesis #2 is that conducting real, published research as a member of a student research team within an established research community-of-practice will transform student identities. Students will, at least for a semester, become scientists. This identity will provide them with determination, persistence, and staying power that many will need to navigate the long educational road to become professional scientists. In psychology, this is referred to as grit, a positive, non-cognitive trait based on an individual's passion for a particular long-term goal or end-state, coupled with a powerful motivation to achieve an objective.

Social learning theorist Etienne Wenger (1998) provided the theoretical foundation for this hypothesis in his pioneering book, *Communities of Practice: Learning, Meaning, and Identity.* He pointed out why students will benefit from immersion within an existing research community-of-practice:

> Learning [within a community-of-practice] transforms our identities; it transforms our ability to participate in the world by changing all at once who we are, our practices, and our communities.
>
> Learning is a matter of engagement: it depends on opportunities to contribute actively to the practices of communities that we value and that value us, to integrate their enterprises into our understanding of the world, and to make creative use of their respective repertoires.
>
> Learners must be able to invest themselves in communities of practice in the process of approaching a subject matter. Unlike in a classroom, where everyone is learning the same thing, participants in a community-of-practice contribute in a variety of interdependent ways that become material for building an identity. What they learn is what allows them to contribute to the enterprise of the community and to engage with others around that enterprise.

There is a problem, however. Membership in most scientific research communities-of-practice is restricted to scientists with doctoral degrees (full members) and their graduate students (junior members). Furthermore, access to the community's research facilities is usually limited to PhD scientists and their graduate students. Although this is the case for most areas of scientific research, there are a few important exceptions where professional researchers have teamed up with amateur (unpaid) researchers to form professional-amateur (pro-am) communities-of-practice (Stebbins 1980). These pro-am communities exist in research areas where professional scientists are too few in number to make the needed observations, yet the equipment costs and training required to make high-quality observations are modest.

Astronomy has a large and successful pro-am scientific research community, replete with its own societies, journals, and vendors (Stebbins 1982). This pro-am community not only welcomes professional and amateur researchers but also undergraduate and even high school student researchers as full members.

The American Association of Variable Star Observers (AAVSO) is a good example of a pro-am research organization that has served the greater astronomical community with distinction for over a century. Research results are published in the *Journal of the AAVSO.* The Society for Astronomical Sciences is another example of pro-am research cooperation. The proceedings from its annual

symposium have been published for over three decades. Other examples include the Center for Backyard Astrophysics and the International Occultation Timing Association.

The pro-am astronomical research community also features stand-alone journals, such as the *Journal of Double Star Observations (JDSO),* that are independent of any society. For double star observations to be included in the *Washington Double Star Catalog,* they must first be published. The *JDSO* serves this need by publishing the observations as well as details on instrumentation, software, and observational techniques of interest to the entire double star research community. Other journals that serve this need include *El Observador de Estrellas Doubles,* and *Il Bollettino delle Stelle Doppie*.

It might be noted that many amateur astronomers are professional engineers or computer programmers. They bring their skills to the development of telescopes, instruments, and software that benefits the entire small telescope astronomical research community-of-practice. The development of robotic telescopes, for instance, greatly benefited from the contributions of amateur astronomers who were also professional engineers.

2. Testing the Specific Hypotheses: The Astronomy Research Seminar

The experience of Cuesta College's Astronomy Research Seminar provides an informal test of specific Hypotheses #1 and #2. The Seminar initially featured student observations of fairly bright, widely-separated double stars using low-cost astrometric eyepieces. Amateur astronomers provided and operated the telescopes, while multiple student teams—often consisting primarily of high school students taking their first college course on the side—recorded the astrometric observations. Calibration and repeated target observations provided practical examples of the role of accuracy and precision in scientific research. After external review by professional or highly experienced amateur researchers, team papers were published in the *Journal of Double Star Observations.*

This successful combination of published student research teams, astrometric eyepieces, and amateur telescopes validated Hypotheses #1, that students can do "real research" in a single semester. This success soon spread to a summer workshops at the University of Oregon's Pine Mountain Observatory (attended by high school and college students from Oregon as well as many students from Evergreen State University in Olympia, WA), California Polytechnic State University, and Apple Valley area schools. A winter workshop was initiated at Leeward Community College in Oahu. The Boyce Research Initiatives and Educational Foundation (BRIEF) initiated full-semester seminars at the Army and Navy Academy and then spread them to other high schools and community colleges in the greater San Diego area, and also initiated hybrid in-person/online seminars (see Boyce et al. these proceedings). The Vanguard Academy developed a highly structured version of the seminar that has been successfully completed by some thirty eighth grade students every winter for the past several years (see Gillette et al. these proceedings).

As the seminar matured, an increasing number of student teams have used CCD cameras—most often on remote, robotic telescopes—to reach fainter double stars, and high-speed, low-readout-noise cameras to reach closer doubles via speckle interferometry. Observational time was also requested and granted on the 2.1-m telescope at Kitt Peak National Observatory—one week in the fall of 2013 and one in the spring of 2014—to obtain observations of over a thousand very close double stars. The observations were made by sizeable pro-am-student teams and have been featured in a number of student team papers.

Although all of the early seminars were totally in-person, the seminars have increasingly become a hybrid in-person/online mix or totally online. This year, for instance, the first half of the spring 2017 seminar (offered by Leeward Community College in Oahu) was in person, while the last half was online. Most of the students were participants in the Early College High School Initiative Program at Waipahu High School. Students in this program graduate, simultaneously from high school and community college. The Astronomy Research Seminar, with its published papers, made an ideal "capstone" course for the Program's STEM students.

The Early College High School Initiative began in 2002, with generous support from the Bill and Melinda Gates Foundation and many other philanthropic contributors and resulted in the formation of a non-profit organization known as Jobs for the Future (JFF). Since its inception, the JFF partnership have given rise to more than 240 redesigned schools serving more than 75,000 students in 28 states and the District of Columbia. Early College High Schools are specifically designed so that low-income youth, first-generation college students, English language learners, students of color, and other young people underrepresented in higher education can simultaneously earn a high school diploma and an Associate's degree or up to two years of credit toward a Bachelor's degree—tuition free.

Many of the Early College schools subscribe to a radical notion: challenge, not remediation. This underlying concept inspires, engages and motivates educationally underserved young people to tackle college rigor, and has resulted in accelerated academic programs that have dramatically increased postsecondary attainment rates of lower income students.

The Waipahu High School Early College Program—the first in the State of Hawaii—was launched in the summer of 2012 and followed up with an expansion of the program to include vertically articulated pathways leading to an Associate in Arts or Associate in Science degree by the time students graduate from high school.

To demonstrate the potential of fully on-line seminar, Cuesta College's eight-week seminar is being done totally online this semester (spring of 2017). Some 43 students were divided into five teams. The fully online seminar features a preliminary textbook (the *Small Telescope Astronomical Research Handbook*), video lectures, self-paced learning units, and weekly synchronous on-line staff meetings—all integrated into the Canvas learning management system (LMS). For the spring of 2017, the San Diego area featured in-person teams with 25 students at three community colleges—Grossmont, Miramar and Mesa—and two online seminars that reached 40 high school and adult students throughout the greater San Diego metro area; all are supported by the Boyce Research Initiatives and Educational Foundation through a common instructional platform (see Boyce et al. paper these proceedings). The Vanguard Academy had another two dozen students formed into three teams. Altogether, the spring 2017 Astronomy Research Seminars featured about 150 students formed into teams at a dozen schools.

Having student teams reliably complete papers and submit them for publication within the constraints of a one-semester course or short summer research experience is very demanding. We have learned, in the past decade, how to do this successfully on a regular basis (Johnson 2016). We found that it is important to:

- Pick a student-friendly area of scientific research within an with existing, sizeable professional-amateur (pro-am) community-of-practice.
- Immerse the student research teams within this supportive pro-am community.
- Avoid prerequisites, as they would bar from participation the non-AP/STEM-track students we are trying to entice into considering STEM majors.
- Place high school, community college, and university students together on the same teams, often with amateur or even professional astronomers as additional team members.
- Form diverse teams with a wide range of student talents, backgrounds, and experience.
- Embrace this large variation in student expertise and motivation. Such variation, it should be noted, is also the norm within professional research teams.
- Encourage varying levels of participation as some students have more time than others. The same is true in professional research. Justice, with respect to the degree of participation, is handled by author order.
- If team projects are falling behind, as happens on occasion, do not hesitate to add experienced researchers to the team (former seminar graduates or experienced amateurs). Failure is not an option!
- Require that student teams take ownership of their projects and manage the projects themselves but, at the same time, limit the scope of team projects and provide close supervision to assure project success.
- Require that student teams plan their projects, make their proposals, and collect and analyze their data in a prompt manner, leaving ample time for writing and rewriting team papers.

The Astronomy Research Seminar in its many variations has been very productive, significantly contributing to the science of double star astrometry. Some 300 students have coauthored over 100 papers (see Freed et al. these proceedings for details).

Students have also been coauthors or coeditors of seven books:

Small Telescopes and Astronomical Research (Genet, et al. 2010)
The Alt-Az Initiative: Telescope, Mirror, and Instrument Developments (Genet et al. 2010)
The Double Star Reader (Clark et al. 2013)
Speckle Interferometry of Close Visual Binaries (Genet et al. 2015)
Double Star Astrometry: Collaborations, Implementations, and Advanced Techniques (Weise et al. 2015)
Small Telescope Astronomical Research Handbook (preliminary edition, Genet et al. 2016)
Double Star Research: A Student-Centered Community of Practice (Johnson 2016)

and have co-chaired numerous workshops and three major conferences:

Small Telescope Astronomical Research, 2008, San Luis Obispo, California
Galileo's Legacy, 2009, Makaha, Oahu, Hawaii
Maui International Double Star Conference, 2013, University of Hawaii's Institute for Astronomy, Maui

We have also seen anecdotal evidence supporting Hypothesis #2: students have reported dramatic changes in their appreciation for science and related skills; some have changed their major area of study to science and engineering; and some have received scholarships on the strength of their publication record.

3. Student Research within Communities-of-Practice: a General Hypothesis

A decade of published student-team double-star research has clearly answered the original Hypothesis #1 in the affirmative, namely that students can indeed conduct real, published research early in their educational careers as members of student research teams within an established pro-am research community-of-practice. Anecdotal evidence supports Hypothesis #2 in the affirmative, namely that: conducting published research as a member of a student research team can transform student identities and provide them with determination that many will need to become professional scientists.

A more ambitious hypothesis is now being tested: Hypothesis #3. Can the seminar's concept be extended from a few schools and instructors to many schools across the United States or even internationally? Also, can the seminar concept be extended from double star astrometry to other, areas of astronomical research, and to sciences beyond astronomy?

We also intend to develop quantitative evidence for Hypothesis #2, establishing through surveys, interviews, and focus groups of the hundreds of seminar graduates over the past decade, that conducting real, published research, early on as a member of a student research team within an established research community-of-practice, leads to the transformation of student identities. Do students, at least for a semester, actually feel that they became scientists, mathematicians, or engineers? If so, did this identity provide them with determination, persistence, and staying power that they needed to navigate the long educational road to become professionals?

4. A Development, Expansion, and Evaluation Program

A recently launched development, expansion, and evaluation program is testing Hypothesis #3 and developing quantitative evidence for Hypothesis #2. This program is being supported by a modest grant from the National Science Foundation, as well as support from many other institutions including the Boyce Research Initiatives and Educational Foundation (BRIEF), the Collins Educational Foundation (CEF), and almost a dozen schools including Cuesta College, California Polytechnic State University, and Concordia University.

Expansion from the current four community colleges in California to a number of other community colleges in the state is being is being considered, perhaps as an Astronomy Research Certificate Program that would include not only the basic seminar, but advanced research seminars and selection of several courses from an array of other astronomy, physics, and mathematics courses. Leeward Community College in Hawaii is considering expanding its participants in the Early College High School Initiative Program from Waipahu High School students, to students from other high schools on Oahu or even on Maui and the big island of Hawaii. Plans are being formulated to extend the seminar to community colleges in Arizona. Stanford Online High School plans, next year, to offer a totally online version of the seminar to its students—many which are international. Other national and international online high schools and colleges are being considered as hosts for the seminar.

Expansion of the seminar beyond double star astrometry to time series photometry of eclipsing binaries, intrinsically variable stars, exoplanets, and asteroids is being actively pursued. The considerable observing time required by time series photometry is being made available on a PlaneWave Instruments CDK-17 telescope at Sierra Remote Observatories (compliments of PlaneWave Instruments), a number of 0.4-meter telescopes on a global network (compliments of Los Cumbres Observatory and the University of Hawaii), and a PlaneWave Instruments CDK-700 telescope at Great Basin Observatory (compliments of Concordia University). It might be noted that the prototype for the CDK-700 telescope was developed by student engineering teams at California Polytechnic State University.

These expansions are being supported by the refinement of existing training materials and the development of new material to support the expansion of the seminar into research areas beyond double star astrometry. Workshops and conferences are being organized to bring together the seminar development community, including instructors,

students, education researchers, and supporting professional and amateur astronomers.

Efforts are underway to establish contact with the many hundreds of student coauthors of published papers and invite them to participate in a professionally devised survey and online interviews and focus groups to determine if conducting published team research within a community-of-practice significantly affected their educational and professional career trajectories.

Finally, a pilot project is exploring the extension of the seminar's model of published student team research to an area beyond astronomy. After careful consideration, environmental science was selected as the general area for expansion, with atmospheric science specifically for the pilot project. Concordia University (Irvine) is leading this pilot project with support from the University of California, Irvine (UC-Irvine), the National Center for Atmospheric Research (NCAR), and the National Oceanic and Atmospheric Administration's Earth Systems Research Laboratory (NOAA/ESRL). The pilot project, funded as a component of the NSF grant, is focusing on student measurements of atmospheric gasses and particulate matter with of low-cost Arduino-based and similar sensors calibrated at Concordia University's extensive laboratory facility. The pilot project is also conducting research that uses the nuclear reactor and a gamma-ray spectrograph at UC-Irvine to identify the elements in atmospheric particulate matter.

5. Conclusions

The Astronomy Research Seminar has firmly established, over the past decade, that undergraduate and high school student teams can, within the confines of a single semester or short summer camp, conduct published research on a regular basis when such research is made in a carefully selected area (double star astrometry) and conducted within and supported by a pro-am community-of-practice. The seminar has also demonstrated that in-person, hybrid in-person/online, or fully online formats are all effective in producing published research.

An organized program, supported by the National Science Foundation and others, is currently exploring the expansion of the seminar from a few schools in California and Hawaii, to many more schools, and from double star astrometry to time-series photometry of eclipsing binaries, intrinsically variable stars, exoplanets, and asteroids. The effectiveness of such seminars to positively impact the educational and professional career trajectories of students is being methodically examined. Finally, a pilot program is exploring the extension of the seminar's model from astronomy to environmental science.

The research seminars have the potential to positively transform undergraduate science education in a significant manner by involving students at the outset of their college careers in scientific communities-of-practice where they join a research team, conduct real science, and actually become—both sociologically and technically—real scientists themselves. Being a scientist changes students' lives.

The seminar integrates a key social learning theory, Communities-of-Practice, into the teaching of science. Each student contributes as their time, talents, knowledge, and experience dictates, democratizing the research process. This encourages women, underrepresented minorities, persons with disabilities, and non-STEM-track students to participate in a genuine research experience, completing the seminar as published scientists and, eventually, becoming professional research scientists or science-informed citizens that contribute to increasing our nation's economic competitiveness and discover innovative solutions to the many problems we face as a global community.

6. Acknowledgements

We thank the National Science Foundation for their support via a grant #1610350, Student Research within Communities of Practice. We also thank the Boyce Research Initiatives and Educational Foundation, the Collins Educational Foundation, and the W.M. Keck Foundation for their support.

7. References

Boyce, P. and Boyce, G, 2017. A Community-Centered Astronomy Research Program. Proceedings of the Society for Astronomical Science.

Clark, R. Genet, R., Johnson, J., Wallen V., and Weiss, E. 2013. *The Double Star Reader.* Santa Margarita, CA: Collins Foundation Press.

Freed, M., Genet, R., Fitzgerald, M., and Davidson, B. 2017. Analysis of Ten Years of Student Research and Publications. Proceedings of the Society for Astronomical Science.

Genet, R., Johnson, J., Buchheim, R., and Harshaw, R. 2016. *Small Telescope Astronomical Research Handbook* (Preliminary Edition). Santa Margarita, CA: Collins Foundation Press.

Genet, R., Johnson, J., and Wallen, V. 2010. *The Alt-Az Initiative: Telescope, Mirror, and Instrument*

Developments. Santa Margarita, CA: Collins Foundation Press.

Genet, R., Johnson, J., and Wallen, V. 2010. *Small Telescopes and Astronomical Research.* Santa Margarita, CA: Collins Foundation Press.

Genet, R., Weise, E., Clark, R., Wallen, V. 2015. *Speckle Interferometry of Close Visual Binaries.* Santa Margarita, CA: Collins Foundation Press.

Johnson, J. 2008. Double star research as a form of education for community college and high school students. In *Proceedings for the 27th Annual Conference for the Society for Astronomical Sciences*, eds. B. Warner, J. Foote, D. Kenyon, and D. Mais. 25-27.

Johnson, J. (Ed.). 2016. *Double Star Research: A Student-Centered Community of Practice.* Santa Margarita, CA: Collins Foundation Press.

Stebbins, R.A. 1980. Avocational science: The avocational routine in archaeology and astronomy, *International Journal of Comparative Sociology,* 21(March-June), 34-48.

Stebbins, R.A. 1982. Amateur and professional astronomers: A study of their inter-relationships, *Urban Life,* 10(January), 433-454.

Weise, E., Genet, R. & Wallen, V. eds. 2015. *Double star Astrometry: Collaborations, Implementations, and Advanced Techniques.* Santa Margarita, CA: Collins Foundation Press.

Wenger, E. 1998. *Communities of Practice: Learning, Meaning, and Identity*. Cambridge: Cambridge University Press.

The SPIRIT Telescope Initiative: six years on

Paul Luckas
International Centre for Radio Astronomy Research, The University of Western Australia
35 Stirling Hwy, Crawley, Western Australia 6009
paul.luckas@uwa.edu.au

Abstract

Now in its sixth year of operation, the SPIRIT initiative remains unique in Australia, as a robust web-enabled robotic telescope initiative funded for education and outreach. With multiple modes of operation catering for a variety of usage scenarios *and* a fully supported education program, SPIRIT provides free access to contemporary astronomical tools for students and educators in Western Australia and beyond. The technical solution itself provides an excellent model for low cost robotic telescope installations, and the education program has evolved over time to include a broad range of student experiences—from engagement activities to authentic science. This paper details the robotic telescope solution, student interface and educational philosophy, summarises achievements and lessons learned and examines the possibilities for future enhancement including spectroscopy.

1. Introduction

It is a reality that much of modern observational astronomy is undertaken using highly automated telescopes. Situated often in remote locations, these instruments provide researchers the means to acquire high quality data with great efficiently. Robotic minor planet survey telescopes map the sky adding dozens of new discoveries each week, and satellites command ground based telescope systems to respond rapidly to distant transient phenomena such as gamma ray bursts. Sensitive digital imagers and sophisticated processing software have long replaced the chemical emulsions and analogue analysis of days' past and professional astronomers are now served astronomical data via the internet from the comfort of their campus offices. Yet despite this renaissance, high school text books still often characterise the *astronomer* as someone who *looks* though a telescope—with many that portray astronomy with a picture of Galileo alongside his primitive telescope 400 years ago. Dispelling these notions and providing school students access to the tools used by modern observational astronomers has formed the core of a program of activities within the SPIRIT initiative at The University of Western Australia (UWA) for the past 6 years. Commissioned in 2010 and followed by a second instrument in 2012, SPIRIT comprises two web enabled robotic telescopes located on the roof of the School of Physics at UWA. The initiative is currently hosted by the International Centre for Radio Astronomy Research (ICRAR) as part of its outreach and education program and includes a full life cycle of workshops and student activities.

The provision of robotic telescopes for use in education is not a new. Seminal projects such as the Bradford Robotic Telescope, the Faulke's telescope project, and in more recent years the Las Cumbres global telescope network among many others have done much to increase student participation in contemporary astronomy. Some of these examples are characterised by large observatory-class instruments that, while delivering research quality data potential, incorporate significant operational and maintenance overhead and commensurate operating budgets. In addition, the proprietary nature of their technical solutions (often a consequence of pre-existing observatory infrastructure) presents most as poor models for replication. At the same time, small robotic telescope technology has advanced considerably, evidenced most notably in its use among the amateur community. Advanced amateurs have increasingly made significant contributions to astronomical research in areas such as the discovery and monitoring of transient events—supernovae surveys, minor planet astrometry—as well as photometric measurements of variable stars, exoplanet research and spectroscopy. As a consequence of being part-time astronomers, many have found themselves at the forefront of telescope automation in order to improve output while balancing other 'life commitments'. This is exemplified by the number of vendors of commercial telescope hardware and software who are themselves, amateur astronomers. The small robotic telescope revolution of recent years has impacted not just professional and amateur astronomy, but also education and outreach,

particularly in regions where access to established observatory outreach programs is otherwise absent.

Of critical importance has been the realisation that *just* providing access to robotic telescopes does not guarantee that they will be used effectively in science education. Without access to relevant and engaging educational resources, many except for the very enthusiastic of teachers may be reluctant to incorporate the use of such telescopes in their day to day teaching—particularly when the curriculum does not prescribe it. Supporting programs that include teacher workshops and the provision of student activities often typify aspects of a remote telescope initiative that are yet to be fully realised, as is ongoing study and research into the educational effectiveness of the individual programs themselves.

The SPIRIT initiative began with a set of goals that informed a proposal and design in early 2009. Since that time, SPIRIT I & II have proven themselves successful models for modest sized and comparatively low cost web-enabled telescopes exhibiting high levels of reliability. The supporting education program, initially developed through a collaboration between the Western Australian Department of Education and UWA has evolved to include opportunities for students to participate in genuine science.

Figure 1: Students visiting SPIRIT I & II observatories at UWA.

2. Technical Solution

Vendor information has been omitted from the text in this section for reasons of clarity but can be found in tables at the end of this paper and in the references.

2.1 Hardware

The SPIRIT telescopes are located on the roof of UWA's School of Physics, housed within fibreglass domes manufactured by Sirius Observatories. Dome rotation and shutter control are fully automated utilising the MaxDome interface, and each includes automated and redundant weather monitoring via a Boltwood cloud sensor located adjacent to each observatory. Both optical tube assemblies are mounted on Paramount ME robotic mounts manufactured by Software Bisque. These mounts deliver robust targeting and tracking as well as the capability for remote initialisation via a proprietary homing feature. The Paramount robotic telescope mounts also include advanced periodic error correction, pointing and tracking algorithms through included software. As a consequence, the SPIRIT telescopes do not use auto-guiders—improving the efficiency of data collection. Exposures of up to 300 seconds (limited mostly due to light pollution) are easily achieved at all telescope orientations with stellar profiles exhibiting negligible trailing artefacts.

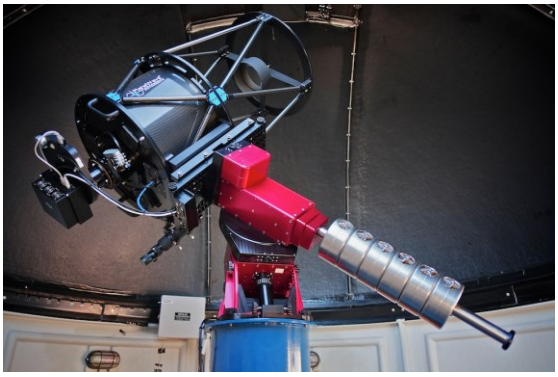

Figure 2: The SPIRIT II telescope.

2.2.1 Imaging System

SPIRIT I utilises a 0.35m f/11 Schmidt-Cassegrain telescope paired with an Apogee Alta U6 CCD camera incorporating a front illuminated Kodak KAF-1001e sensor with an array of 1024x1024 pixels of 24µm size. This combination provides a square field of view of 20 arc minutes and a native resolution of 1.2 arc seconds per pixel, considered ideal for the sky conditions at UWA. SPIRIT II includes a more sophisticated 0.43m f/6.8 Corrected Dall-Kirkham telescope manufactured by Planewave Instruments. A Finger Lakes Instruments Proline camera utilising a Kodak KAF-16801 sensor with an array of 4096 x

4096 pixels of 9µm size provides a square field of view of 40 arc minutes and a resolution of 0.63 arc seconds per pixel at bin 1. As a consequence, SPIRIT II is nominally used at bin 2 or bin 3 to provide for more appropriate stellar sampling under the skies at UWA. Both systems have been optimised to produce stellar profiles that meet the 2-3 pixel FWHM ideal. The CCD cameras employ non anti-blooming CCD sensors, and as a result exhibit excellent linearity up to saturation.

The SPIRIT I and II image trains include software controlled filter wheels that provide access to photographic red, green and blue filters, and photometric B, V and R filters sourced from Astrodon. A clear (non-IR blocked) filter is provided on both instruments to provide for parfocal 'non-filtered' imaging. SPIRIT I also includes a narrow band H-a filter with a 5nm bandwidth at 656.3nm.

The image train on SPIRIT I is supported by an Optec TCF-S3 temperature controlled focuser which provides a reliable means of maintaining focus throughout the night via a temperature probe attached to the side of the aluminium telescope tube. Initial focus measurements undertaken over a range of temperatures determined a highly linear relationship between temperature and focus position, with the resulting coefficient permanently programmed into the focuser's control software. Only occasional, seasonal re-focusing is necessary. The carbon fibre truss construction of the SPIRIT II telescope provides a thermally stable support for the optics and rarely requires focus adjustment over the course of a typical observing year.

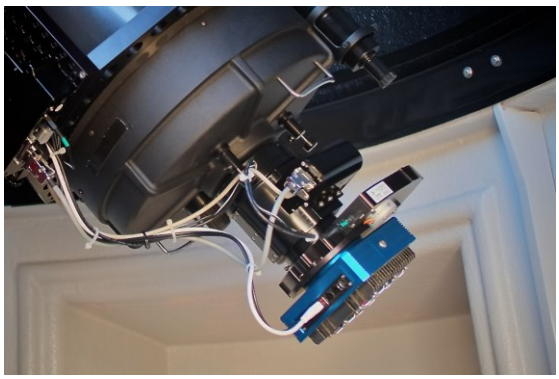

Figure 3: SPIRIT I optical train, showing the Optec TCF-S3 temperature controlled focuser and Apogee U6 CCD camera and filter wheel.

It has been difficult to precisely define the magnitude limits of both instruments owing to the constantly changing local sky conditions and pollution gradients over the city of Perth. Using stacking techniques, measurements of a magnitude 19.5 minor planet were achieved with the 0.35m SPIRIT I telescope and successfully submitted to the Minor Planet Centre in 2011. Photometric studies by students of brighter than magnitude 16 stars with exposures of 120s or less routinely yield magnitude errors of around 0.03 or better, as determined by software for targets whose brightness is well above sky background and read noise levels.

2.2 Software

The SPIRIT software technical design is centred around an implementation of ASCOM compliancy and utilises ACP Observatory Control Software to provide interoperability between control applications. ACP also includes components necessary for the provision of web-enabled access, fundamental to the SPIRIT design, and at time of writing is still the only commercial observatory control suite with built in web functionality. Users can access and control the SPIRIT telescopes using any modern browser on both desktop and mobile platforms.

The SPIRIT ACP web interface has been customised significantly in a number of areas including:

- Disabling buttons that allow users to undertake unnecessary or undesirable actions, such as opening or closing the dome, modifying the CCD camera's cooling state and viewing non-essential sidebar tools and superfluous information.
- Streamlining the look, feel and text to cater for an audience age range from school students to adults.
- Adding functionality, such as a webcam view, a link to the bookings calendar, enhancing the default help information, and in the case of SPIRIT II, access to the 'SPIRIT Bright Star Spectroscope' (see section 7.1).

A secure, single server model is employed in each of the SPIRIT observatories, with all control software, web server and user file systems installed on a single PC. Back-end interoperability is achieved through commercially available telescope and camera control software as well as a number of ASCOM components which require only minimal adaptation in order to engineer robust unattended

dusk until dawn operations. A commercially available telescope sequencing application (CCD Commander) has been employed to automate daily start-up and shutdown tasks invisible to the end user. Functions such as sun-angle timed camera cooling, dome opening, dusk calibration frame acquisition and activation of the ACP web interface are encapsulated within an easily modified daily script. These daily scripts can also be daisy-chained to allow a repeating multi-day operation for weekend use.

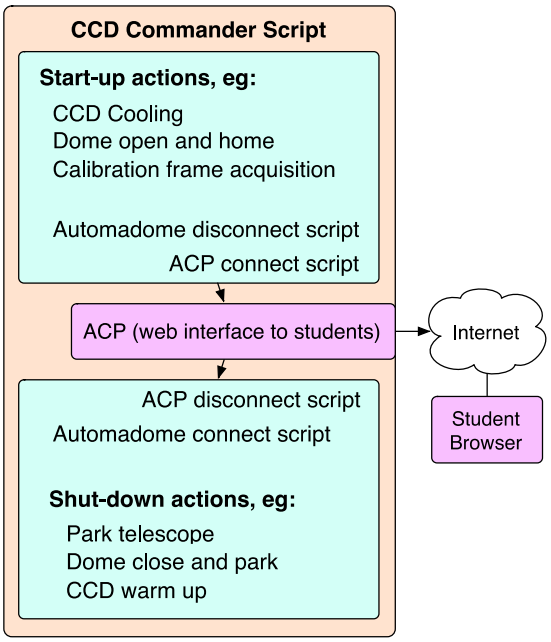

Figure 4: Daily script flow. The entire pre-dusk until post-dawn daily sequence is embedded within a CCD Commander 'action file'.

Remote administration is provided using a third-party cloud based solution (GoToMyPC) which enables non-device and non-location dependant administration. SPIRIT can be administered via smart phone from anywhere in the world!

Users acquiring images with SPIRIT can download both RAW and calibrated FITS files directly from within the web interface or using File Transfer Protocol (FTP), which also provides access to log files and calibration frames for advanced analysis. A high quality JPEG version of each image is also automatically generated at the completion of each acquisition. This provides students with a level of instant satisfaction as images appear on the screen before them, as well as an efficient means to monitor image quality without the need to download large FITS formatted image files. Moreover, the JPEG version has proven sufficient for the vast majority of basic student engagement activities including colour astrophotography.

2.3 Modes of Operation

Central to the SPIRIT philosophy is a novel approach to cater for a varied student and user demographic—encompassing a range of abilities from primary school students to post graduate tertiary students and researchers. The web interface provides an intuitive choice of operating modes providing a pathway for students to develop more skills and embark on more research-oriented projects.

'Mode 1' allows novice students to 'drive' the telescope, acquiring either a single image, or a series of images through different filters of a single target. This is undertaken in real time, while observing telescope and dome movements together with image acquisition progress via the web interface. 'Mode 2' provides the more experienced student with multi-target unattended options. It is most suited to survey work, and is typically utilised by experienced users of SPIRIT undertaking long term monitoring of variable stars, minor planet astrometry or other survey work. Mode 2 also provides an alternate means of servicing collaborative or large class work—where many students submit observation requests which are coordinated by a teacher or group leader.

A third mode of operation uses *Tools for Automated Observing* (TAO)—a fully automated user acquisition system, including submission and scheduling and operates as a customised script within the ACP control software environment. It ensures maximum telescope utilisation through the use of an advanced scheduler at the expense of real time interaction. It is, essentially, an image request system. Perhaps as a consequence of this, it has not been used within the educational outreach and engagement model characterised by the SPIRIT philosophy.

For the vast majority of students, mode 1 continues to offer an engaging and reliable means of acquiring images. For improved data gathering efficiency and more advanced student science projects such as the *SPIRIT light curve photometry project* (see section 4), mode 2 provides for fully unattended operations. In both cases, students can monitor operations regardless of whether in direct control or running an automated plan.

3. Telescope Access

Access to SPIRIT is provided through the SPIRIT web site (spirit.icrar.org) which also presents a 'base of operations' for all things SPIRIT. The site contains a description of the program, access to guides, documents and activities, image galleries and a news blog. The telescope access page provides authorised users with a clearly defined 5 step booking process with links to weather information, calendar and booking form. Access to the web interface for each telescope is also provided on the access page.

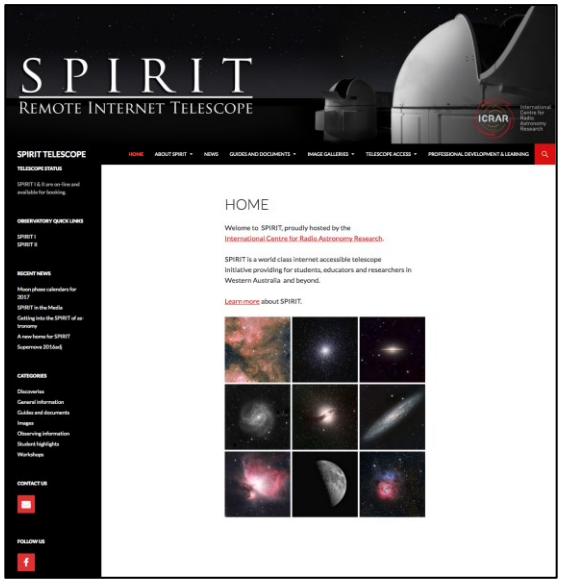

Figure 5: The SPIRIT initiative home page.

3.1 Telescope Web Interface

The web interface for each telescope provides a modified ACP web presentation including both content and control. Imaging options, together with file access, system status information, a web cam view and other items are contained within a logical side bar menu structure, allowing the users to customise the view according to their requirements.

Targeting objects is facilitated by an object database contained within the ACP software. It contains a subset of the most common deep sky objects so that novice users need only input the catalogue name and select "get coordinates" to target these objects. Similarly, ACP has been configured to facilitate targeting of moving objects such as planets, asteroids and comets—the latter two through an updated minor planet orbital file downloaded periodically and providing updated ephemerides of recently observed or discovered objects. Moving object ephemerides are automatically calculated at the time of imaging for such objects specified in the targeting dialogue.

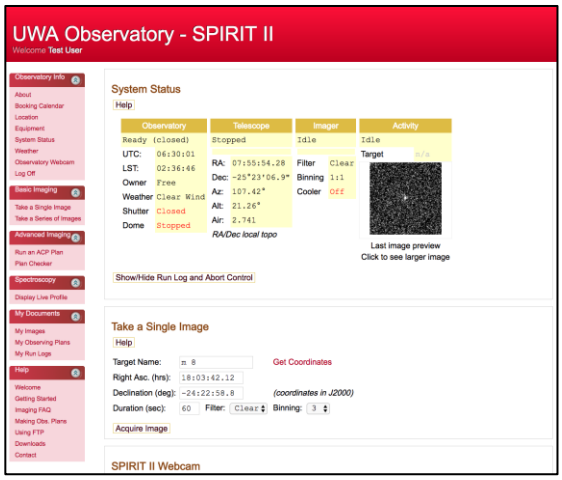

Figure 6: The SPIRIT II telescope web interface.

The flexibility of the advanced imaging options allows for fully unattended, multi-target imaging using a range of exposure and filter options. Utilising ACP's intuitive directive-based format, sophisticated text based observing plans can be uploaded and run at the time of booking. The advanced imaging mode allows experienced students to embark on more sophisticated observing programs, such as high cadence variable star photometry observations or 'all night' target monitoring.

4. Education Program

The education program has evolved from an initial teacher-centred program to a student-centred program. In-school or on site at UWA workshops are offered for small groups of students embarking on school-based programs. These usually start with an engagement cycle of activities, where students are introduced to the mechanics of the night sky, learn how to remotely access and use the SPIRIT telescopes, acquire images and undertake basic image processing. Packaged as "SPIRIT 101", these activities provide an engaging way for students to learn about contemporary observational astronomy before embarking on more challenging activities. The SPIRIT 101 program of activities has also shown great promise in increasing mainstream participation by less motivated and low achieving students.

With the completion of SPIRIT 101, a number of advanced activities become available:

- *Targeting and imaging asteroids with SPIRIT.*

Students learn how to target and observe visible minor planets using the SPIRIT telescopes.

- *Astrophotography with SPIRIT.*

A workshop covering both basic and advanced image processing techniques, enabling users to create stunning colour images of astronomical objects using the SPIRIT telescopes.

- *Advanced astrometry with SPIRIT.*

An advanced minor planet workshop intended for upper school investigations and advanced studies. This workshop provides the tools and techniques necessary to undertake minor planet astrometry and submit observations to the Minor Planet Centre for publication.

- *Variable star photometry with SPIRIT.*

This comprehensive program of activities provides detailed information on how to undertake photometric observations of short period variable stars using SPIRIT. Workshop sessions introduce students to the same tools and techniques used by professional astronomers to create light curve photometry that is submitted to the American Association of Variable Star Observers (AAVSO) database.

All SPIRIT activities are supported by on-line guides and manuals and offered at no cost as part of the ICRAR outreach mandate. Where practical, a visit to the SPIRIT observatory at UWA and ICRAR research institute including presentations by leading astronomers as a component of the outreach program is also encouraged.

Advanced activities often form a component of existing academic extension programs in what is an astronomy-poor state and federal science curriculum in Australia. Remote and regional schools are uniquely positioned to take advantage of SPIRIT's web-enabled interface and tailored learning programs are available to service regional schools at a small cost.

4.1 State Curriculum

The results of pilot teacher professional development activities undertaken early in the program informed the development of curriculum specific activities for teachers planning to utilise SPIRIT as part of the astronomy components of the then Western Australian state curriculum. These resources were made available as part of a secondary science teacher enrichment program jointly funded by the WA Department of Education and UWA. These resources are separately available for download through the department's portal.

5. Results

5.1 Technical Implementation

Reproducibility of the technical design itself was tested early in the program during the commissioning of SPIRIT II—a near exact 'copy and paste' of the SPIRIT I deployment. Aside from variations in device dependencies and their configuration, software installation was substantially achieved by restoring a backup of the SPIRIT I observatory server directly onto the new SPIRIT II server.

Reliability of the original technical design has exceeded expectations, with both the SPIRIT I and SPIRIT II telescopes operating essentially 24x7x365 and experiencing no significant or costly hardware failures over the past 6 years. The original Windows PCs are still in use in both observatories despite considerable temperature and humidity fluctuations over a typical observing year. The Sirius and MaxDome hardware in particular have proven surprisingly robust. Notable issues and replacements include:

- Ice formation on the sensor of the sealed Apogee Alta CCD housing requiring servicing by vendor.
- Replacements fans for both CCD cameras (a near annual requirement).
- Replacement or repair of both Boltwood cloud sensors (continuous working life ~ 2 years).
- Replacement of the computer motherboard in SPIRIT I observatory PC.
- Minor corrosion on exposed USB cables
- Replacement of the dome shutter's 12V DC sealed lead acid batteries every 2 years (precautionary).

In general, it has been found that instrumentation and computer devices are less likely to be problematic if left powered on—with most items at their most vulnerable during cold start up. The solid-state circuitry employed in modern computers, telescope mounts and cameras and in the dome automation used by SPIRIT does not appear to suffer by being left in a powered-on

state. Even the modest sized solar panel used to maintain dome shutter battery charge has proven sufficient with the dome shutter mechanism left powered on 24x7.

The use of commercially available components has helped mitigate risks associated with proprietary in-house developed solutions with replacement items available 'off-the-shelf' and often delivered within a short time frame. A modest ~ $5,000 AUD annual maintenance budget for the two facilities has proven adequate over the current operating life. The use of commercially available components has also helped to 'future-proof' the initiative with respect to staff changes, given the ubiquitous use of many of the components in the SPIRIT technical solution, in both professional and advanced amateur installations.

5.2 Education and Science

SPIRIT has proven a welcome tool in providing for student engagement in science as is routinely affirmed through the positive feedback received from teachers and an increasing annual user base. Both basic and advanced (colour) imaging has proven a popular means of capturing interest and introducing basic astronomical concepts, such as object types and classification, distance scales and the basics of astronomical data acquisition.

Figure 7: Eta Carina Nebula, SPIRIT II. Credit: Alex King, John XXIII College Perth, 2014.

The potential for student participation in 'real science' was demonstrated conclusively in the attainment of UWA's Minor Planet Center observatory code by local high school students during the commissioning of SPIRIT I. Further afield, Students at a school in Japan successfully determined the rotation period of minor planet (15552) sandashounkan in 2015, after an extensive observation program using SPIRIT. Their results, together with others, appear in the IAU's *Minor Planet Center* publications.

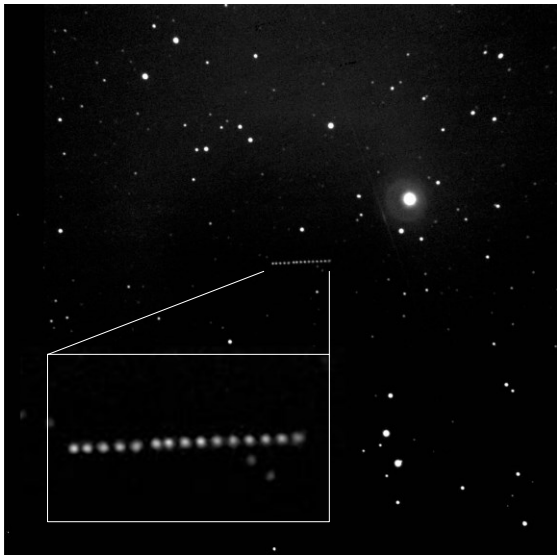

Figure 8: Time lapse composite image of minor planet 909 Ulla, SPIRIT I. Credit: Gurashish Singh, Mt Lawley Senior High School Perth, 2010.

At part of an annual 'Girls in STEM' initiative, students from Iona Presentation College in Perth use SPIRIT to undertake observations of RR Lyrae stars, analysing and preparing light curves of these short period variables for submission to the AAVSO. Many of the southern stars observed by these students have little in the way of published photometry and as such provide yet more opportunities for students to undertake novel observational work.

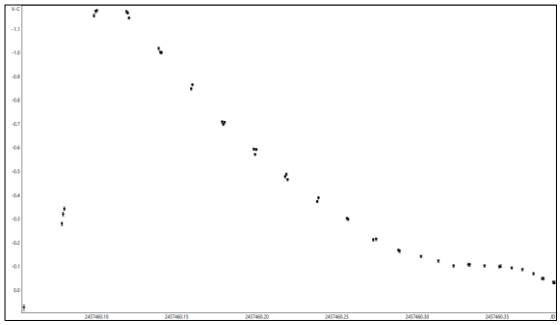

Figure 9: High school student light curve of FX Hya, a type RR Lyrae variable star in the constellation of Hydra. Credit: Victoria Wong, Iona Presentation College Perth, 2016.

SPIRIT also enjoys successful use in undergraduate and postgraduate study and research. As part of coursework, UWA astrophysics students use SPIRIT to acquire data of stellar clusters in order to create colour magnitude diagrams using crowded field photometry techniques. Students as far afield as the UK enrolled in on-line post graduate courses in astrophysics have also used SPIRIT to acquire data for Masters level projects.

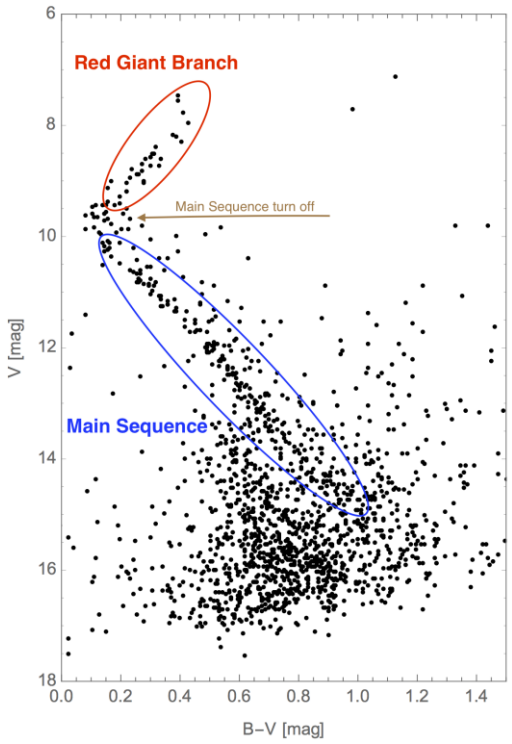

Figure 10: Crowded field photometry using SPIRIT: a colour magnitude diagram of the cluster M93. The main sequence and turn-off points are clearly visible. Credit: Adam Watts, UWA, 2015.

While still in its infancy, the publication of spectroscopic observations from prototype testing of both high and low resolution spectrographs has affirmed the enormous potential that spectroscopy offers for advanced student projects in the coming years (see section 7.1 for more information).

6. Lessons Learned

Not withstanding the availability of commercial robotic telescope hardware and software, successfully implementing a diverse suite of hardware and software components benefits from prior expertise in the field. Marrying precise electro-mechanical control with contemporary software platforms and the requirements of a diverse user demographic is a non-trivial endeavour. The term 'robotic' should not be confused with 'easy' and a percipient understanding of the potential for problems should not be underestimated, particularly for continuous operation scenaria. The scalability from single owner/operator to a multi-user environment requires careful consideration, particularly in areas of client interface, access control and user management, as these concepts generally lay outside the domain of commercial telescope control software offerings.

Consideration should also be given to the skill set requirements, useful in the construction, implementation and maintenance of an advanced Internet telescope. These include:

- the ability to operate hand tools and possessing general electrical and mechanical adeptness particularly during construction phases;
- proficient project management skills and a well-developed capacity to solve complex technical problems in areas often characterised by the terms 'cutting edge' or 'bleeding edge';
- experience in astronomy including a working knowledge of the observational techniques used in contemporary CCD equipped telescope implementations;
- understanding of astronomical software design as well as proficiency and experience in the implementation of robotic telescope technologies.

Fostering good relationships in an industry represented by a comparatively small number of commercial vendors is considered advantageous. Likewise is the ability to participate effectively in the broader community of advanced amateurs and professionals who represent the robotic telescope

fraternity. In any cutting edge field, achieving success in troubleshooting difficult problems is more often a result of 'who you know' rather than 'what you know'.

Not withstanding these atypical aspects, it is nevertheless the view of this author that this type of project represents both a viable and realistic undertaking given enough impetus.

Of note has been the realisation of the time required to maintain and manage both the telescope facility and the educational program itself. While funding for capital investment in telescope hardware may be comparatively easy to justify, securing on-going funding for staff and program initiatives is much harder.

In a similar vein has been the realisation that without a mature and well produced education program, use of the SPIRIT telescopes within the current educational environment in Western Australia would be significantly reduced. Expertly maintaining a well-structured educational program has proven the most fundamental requirement of the SPIRIT initiative.

7. Future Enhancements

7.1 Spectroscopy

The provision for web-enabled spectroscopy has long been a consideration for enhanced use and a number of projects have been commissioned in order to identify the requirements and characterise the issues. A small web enabled, low resolution spectroscope was added to SPIRIT II in late 2014. The 'SPIRIT Bright Star Spectroscope' (SBSS) consists of an 80mm refracting telescope, a 100 lines/mm transmission grating and a video camera. It produces a real time, low resolution spectral image of bright stars with a spectral dispersion of approximately 10 Angstroms per pixel. The entire spectral image—from ultraviolet to infrared—is contained in the field of view. Video from the spectroscope is processed in real time and presented as a spectral profile in a customised view created in the ACP web interface. Together with a snapshot of the live spectral profile, the original spectral image can be downloaded for calibration and analysis off-line.

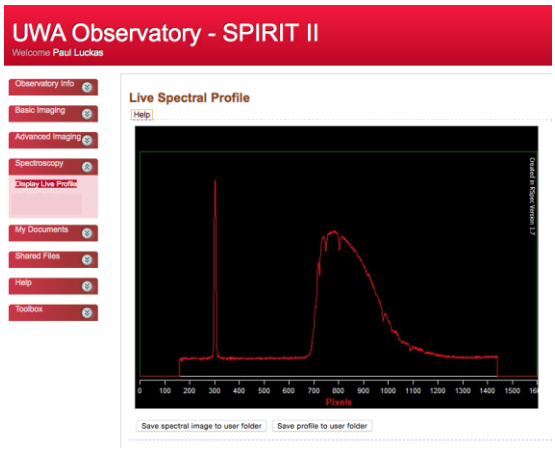

Figure 11: The uncalibrated spectral profile of a type-A star as it appears in real time on the SPIRIT II web interface. The zero order stellar image appears at far left.

Students using the SBSS extend their photometric knowledge of the universe into the realm of spectroscopy, learning about the temperature profiles and chemical signatures of stars, and reproducing the foundational work of those such as Edward Pickering and his team at Harvard in the early 20th century.

Deployment of the SBSS was facilitated by software created in-situ, and depends heavily on the functionality of the imaging software used, in this case *RSpec*. As a consequence of this and limitations of control and observatory software, the solution is still prototypical in nature and requires further development.

The scientific capabilities of a high resolution ($R > 10000$) slit spectrograph on small telescopes under urban conditions have also been tested in a number of configurations since 2013. These tests continue to yield surprising results, affirming the potential for spectroscopy and its tolerance for challenging sky conditions. Pro-am collaborations have resulted in over 500 spectra submitted for publication on a number of massive and 'exotic' star campaigns including those associated with BRITE satellite monitoring and the 2014 eta Carinae periastron campaign (Teodora et al, 2016).

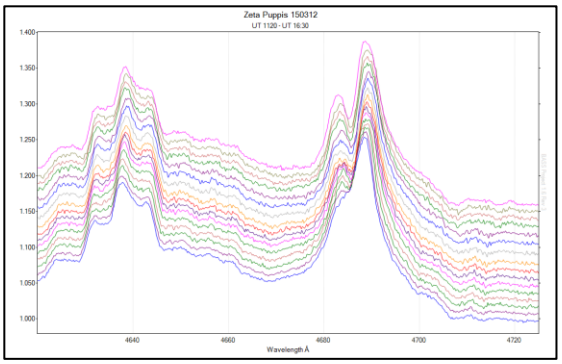

Figure 12: High resolution time series of the blue supergiant zeta Puppis. Changes in the HeII emission feature can be detected in just a few hours of spectroscopic observation. 257 spectra spanning several months have been included as part of a major study into the large-scale wind structures, due for publication in 2017. Similar high cadence spectra of other massive stars including, gam2 Vel, mu Sgr, uw Cma and WR 6 have produced publication quality spectra as part of other professional collaborations.

In addition to high-resolution spectroscopy, two galactic novae in 2016 were confirmed in testing of a low resolution (R ~ 600) slit spectroscope in late 2016 (Luckas, 2016).

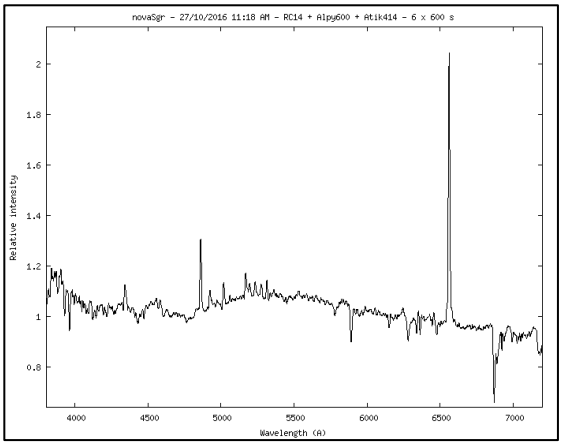

Figure 13: Confirmation spectra of galactic nova ASASSN-16ma acquired using a Shelyak Alpy600 spectrograph (Luckas, 2016).

These publications—a number still in draft—allude to the enormous potential for spectroscopy as a means for students to contribute at the very cutting edge of contemporary astronomy using modest sized robotic telescopes equipped with spectrographs and operating under challenging urban skies.

7.1.1 Technical Hurdles

Transforming in situ use of a spectrograph into a web enabled solution requires significant modification of the current commercial slit spectroscope offerings. The basic operational requirements for slit spectroscope control include:

- The ability to centre a target on the slit in real time.
- Telescope mount auto-guiding capability.
- Remote control of the calibration arc lamp.
- Adjustment of the grating angle to the target wavelength of interest.
- Collimator focus.

A number of prototype solutions for robotising the above functions have been developed, including *Arduino* control of the Ne arc lamp in two slit spectrographs tested to date. Video monitoring through the spectrograph's conventional auto-guiding port has proven successful as a means of positioning bright targets and the slit, though this requires a separate telescope auto-guiding capability. Rudimentary designs for servo controlled micrometre and collimation lens controls have also been completed. However, commercially available observatory control software does not provide well for multi-device and multi-instrument package scenarios. Limitations presented by the MaxIM DL imaging application within the ACP control environment in particular, have prevented progress in this area. A more plausible solution using a fibre-fed echelle spectrograph, such as the *Shelyak eShel* within a separate image control environment is likely to present the best option for medium term web-enablement.

Figure 14 shows a prototype multi-instrument package including both high and low resolution spectrographs and a photometric CCD camera for conventional imaging. All instruments are selectable via a 'flip mirror'. The auto-guiding ports on both spectrographs have been repurposed with video feeds to aid in remote positioning of the target on the slit. Auto-guiding is accomplished separately using a pick off mirror integrated into the flip mirror device. Care has to be taken to ensure back focus requirements of the telescope design are adhered to, and that the image planes for all sensors are, ideally, at focus.

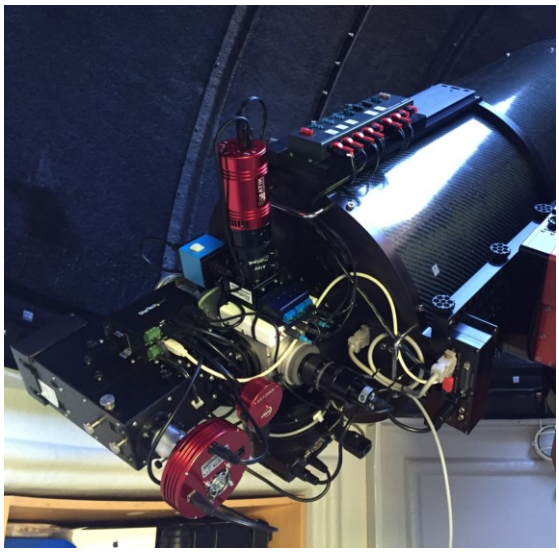

Figure 14: The author's home observatory and SPIRIT test bench. The multi-instrument optical train includes both high and low resolution spectroscopes, and a conventional CCD imager for photometry.

This solution has been rigorously tested in number of spectrographic and photometric applications, and can be remotely controlled only using direct remote control software. Web enabling this technology for mainstream multi-audience use remains a goal for the future.

7.2 SPIRIT Radio

Multi-wavelength astronomy, and in particular those that include radio wavelengths, is of significant interest to the outreach goals at ICRAR. Radio astronomy presents an exciting opportunity for student observation as it extends into day light (class time) hours. Preliminary testing of a small 'Haystack' design radio telescope at UWA's *Gingin Observatory* located approximately 1 hour north of Perth in a [relative to UWA's Crawley Campus] radio-quiet zone, has provided baseline information on the capabilities of a 1.8m small radio telescope. Projects include measuring the temperature of the sun's photosphere, and detecting HI regions in the galactic plane and in other galaxies. The system is currently only controlled using remote access software, but plans for an in-house developed web interface are being explored.

8. Conclusion

The SPIRIT initiative has helped to show that the use of well-designed and maintained contemporary web-enabled, robotic telescopes in astronomy education can be both engaging and relevant. That these telescopes need not be multi-million dollar facilities to provide opportunities for students to participate in authentic and cutting edge science appears also to be well established. The development and delivery of educational support is considered fundamental to the effectiveness of such initiatives, and when done well can do much to create high levels of student participation and engagement in science.

9. References

Apogee CCD Camera Series. Retrieved March 15, 2017, from https://www.andor.com/scientific-cameras/apogee-camera-range

American Association of Variable Star Observers. AAVSO Home Page. Retrieved March 29, 2017, from http://www.aavso.org.

ASCOM Initiative. ASCOM Standards Home Page. Retrieved March 2, 2017, from http://ascom-standards.org/.

Baruch, J. E. F. "The future of robotic telescopes for education." *Publications of the Astronomical Society of Australia* 17.2 (2000): 119-124.

Beare, R. Investigation into the Potential of Investigative Projects Involving Powerful Robotic Tele- scopes to Inspire Interest in Science. *International Journal of Science Education 29*, 3 (2007).

Buchheim, Robert. *The sky is your laboratory: advanced astronomy projects for amateurs*. Springer Science & Business Media, 2007.

Danaia, L. Perceptions, knowledge outcomes and experiences of students in junior secondary science: Impact(s) of using a remote telescope and associated curriculum materials. In *AARE 2007 International education research conference, Fremantle, Western Australia* (2007).

Deep Sky Instruments. Ritchey-Chretien Astrographs Series. Retrieved August 11, 2012, from http://deepskyinstruments.com/products.htm.

Denny, R. "ACP Observatory Control Software". Retrieved March 14, 2017, from http://acp.dc3.com.

Diffraction Limited. “Diffraction Limited Home Page”. Retrieved March 23, 2017, from http://www.cyanogen.com/.

Eversberg, T., et al. "World-wide amateur observations." *Wolf-Rayet Stars: Proceedings of an International Workshop held in Potsdam, Germany, 1–5 June 2015. Edited by Wolf-Rainer Hamann, Andreas Sander, Helge Todt. Universitätsverlag Potsdam, 2015., p. 71-74*. Universitätsverlag Potsdam, 2015.

Field, Tom. "RSpec: New Real-time Spectroscopy Software Enhances High School and College Learning." In *Bulletin of the American Astronomical Society*, vol. 43. 2011.

Fitzgerald, Michael, David H. McKinnon, and Lena Danaia. "Inquiry-based educational design for large-scale high school astronomy projects using real telescopes." *Journal of Science Education and Technology* 24, no. 6 (2015): 747-760.

Gomez, Edward L., and Michael T. Fitzgerald. "Robotic telescopes in education." *Astronomical Review* (2017): 1-41.

Harrison, K. “Astronomical Spectroscopy for Amateurs”. Springer Verlag, 2011.

Hidas, M., Hawkins, E., Walker, Z., Brown, T., and Rosing, W. Las Cumbres Observatory Global Telescope: A homogeneous telescope network. *Astronomische Nachrichten 329*, 3 (2008).

Holvorcem, P. Tools for Automated Observing. Retrieved March 12, 2016, from http://sites.mpc.com.br/holvorcem/tao/readme.html

Howell, Steve B. *Handbook of CCD astronomy*. Vol. 5. Cambridge University Press, 2006.

Kaler, James B. *Stars and their spectra: an introduction to the spectral sequence*. Cambridge University Press, 2011.

Lewis, F., Street, R., Roche, P., Stroud, V., and Russell, D. Robotic Astronomy with the Faulkes Telescopes and Las Cumbres Observatory Global Telescope. *Advances in Astronomy* (2010).

Luckas P. The design, construction and use of an internet accessible, robotic optical telescope initiative for student research projects [master’s thesis]. Western Australia: *The University of Western Australia* (2013).

Luckas, Paul. "Spectroscopic confirmation of ASASSN-16ma as a classical nova in the Fe-curtain stage." *The Astronomer's Telegram* 9678 (2016).

Luckas, Paul. "Confirmation of TCP J18102829-2729590 in Sagittarius as a classical nova in the optically thick stage." *The Astronomer's Telegram* 9658 (2016).

McKinnon, David H., and Andrew Mainwaring. "The Charles Sturt University remote telescope project: Astronomy for primary school students." *Publications of the Astronomical Society of Australia* 17, no. 2 (2000): 125-128.

Robinson, Keith. *Spectroscopy: The Key to the Stars*. Berlin;: Springer, 2007.

Sirius Observatories. Retrieved March 27, 2017, from http://www.atscope.com.au/sirius.html

Software Bisque. Software Bisque Home Page. Retrieved March 24, 2017, from http://www.bisque.com.

Teodoro, M., et al. "Emission from the Massive Binary System in λ Car: Constraints to the Orbital Elements and the Nature of the Periodic Minima" *The Astrophysical Journal* 819.2 (2016): 131.

Thizy, Olivier, and François Cochard. "Spectrographs for small telescopes." *International Astronomical Union. Proceedings of the International Astronomical Union* 6.S272 (2010): 282.

Thomas, M. CCD Commander Automated Imaging. Retrieved April 12, 2012, from http://ccdcommander.com/.

Warner, Brian D., and Alan W. Harris. *A practical guide to lightcurve photometry and analysis*. New York: Springer, 2006.

10. Additional Figures and Tables

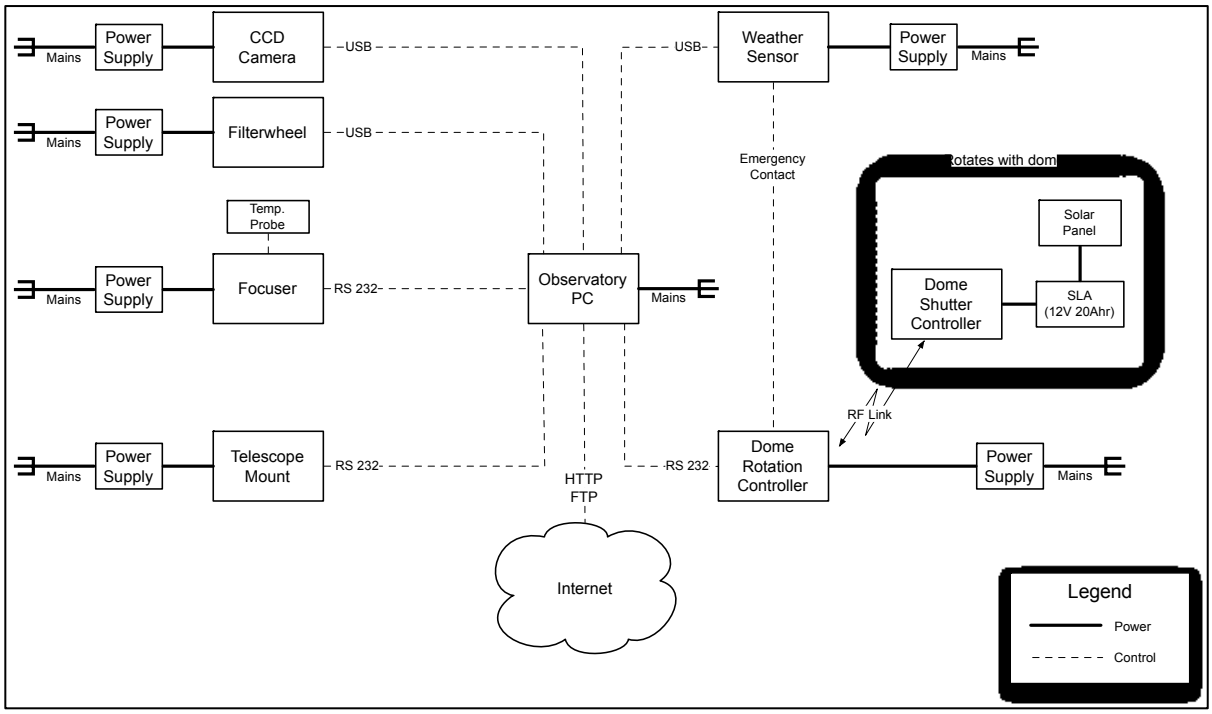

Figure 15: SPIRIT Hardware Block Diagram

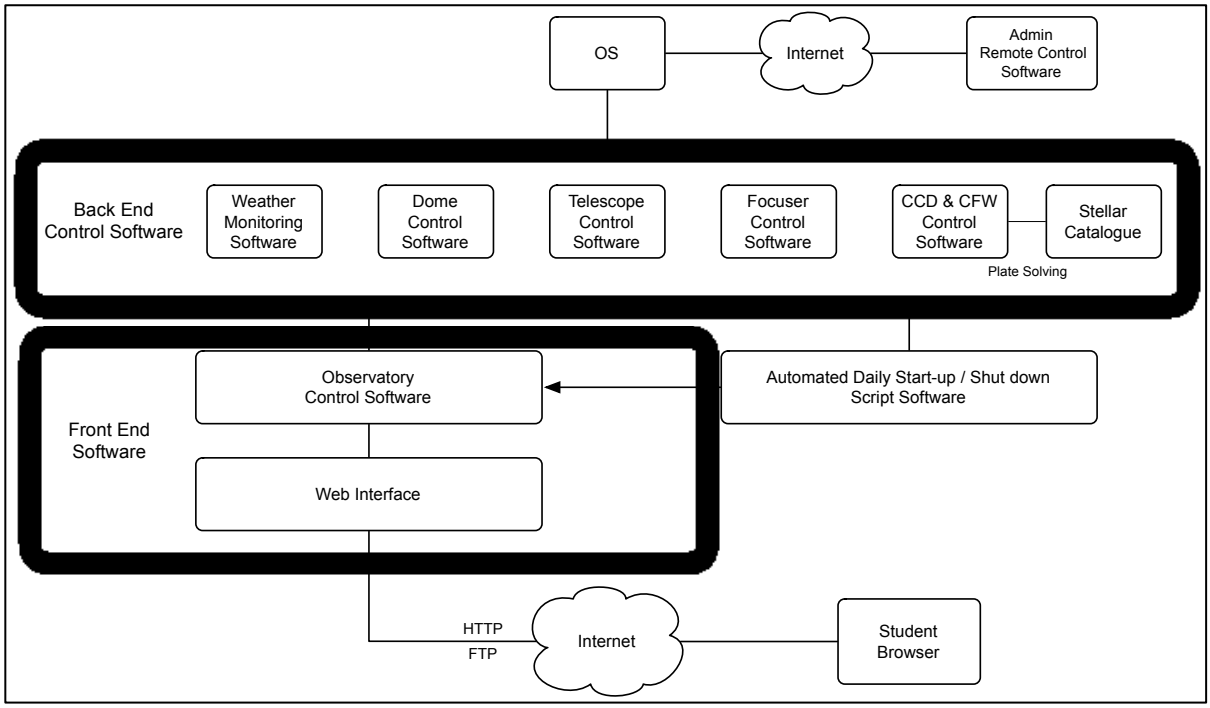

Figure 16: SPIRIT Software Block Diagram

Table 1: SPIRIT major hardware items and vendor list.

Device	Model	Vendor
Telescope Mount	Paramount ME	Software Bisque
Telescope OTA (SPIRIT I)	C14 Schmidt-Cassegrain	Celestron
Telescope OTA (SPIRIT II)	CDK 17	Planewave Instruments
CCD Camera (SPIRIT I)	Alta U6	Andor (formerly Apogee)
Filter wheel (SPIRIT I)	AFW50-9R	Andor (formerly Apogee)
CCD Camera (SPIRIT II)	Proline PL-16801	Finger Lakes Instrumentation
Filter wheel (SPIRIT II)	CFW5-7	Finger Lakes Instrumentation
Filters	CRGB + BVR + H-a	Astrodon
Focuser SPIRIT I	TCFS-3	Optec Inc.
Dome enclosure	2.3m & 3.5m models	Sirius Observatories
Dome automation	MaxDome	Diffraction Limited
Weather monitoring	Boltwood Cloud sensor II	Diffraction Limited

Component	Software	Vendor
Weather monitoring	Clarity II	Diffraction Limited
Dome control	MaxDome	Diffraction Limited
Telescope mount control	TheSkyX	Software Bisque
Focuser control (SPIRIT I)	FocusMax	CCDWare
Focuser control (SPIRIT II)	Planewave Interface	Planewave Instruments
CCD and filter wheel control	MaxIM DL	Diffraction Limited
Observatory control software	ACP Observatory Control	DC-3 Dreams
Web interface	ACP Observatory Control	DC-3 Dreams
FTP Server	BulletProof FTP	BulletProof Software
Backup software	Acronis True Image	Acronis International GmbH
Remote administration	GoToMy PC	Citrix Systems, Inc.

Table 2: SPIRIT primary software list.

Techniques of Photometry and Astrometry with APASS, Gaia and Pan-STARRs Results

Wayne Green

Abstract

The databases with the APASS DR9, Gaia DR1 and the Pan-STARRs 3π DR1 data releases are publicly available for use. There is a bit of data-mining involved to download and manage these reference stars. This paper discusses the use of these databases to acquire accurate photometric references as well as techniques for improving results. Images are prepared in the usual way: zero, dark, flat-fields and WCS solutions with Astrometry.net. Images are then processed with Sextractor to produce an ASCII table of identifying photometric features. The database manages photometic catalogs and images converted to ASCII tables. Scripts convert the files into SQL and assimilate them into database tables. Using SQL techniques, each image star is merged with reference data to produce publishable results. The VYSOS has over 13,000 images of the ONC5 field to process with roughly 100 total fields in the campaign. This paper provides the overview for this daunting task.

1. Introduction

Automating the reduction of a large number of images requires accurate photometry and position data. The recent DR1 (DR2 pending) release of the Pan-STARRs 3π data [Chambers et al (2016)] provides the public access to accurate magnitudes for roughly 3 X 10^8 stars. DR1 of the ESO Gaia [Gaia Collaboration et al (2016a,b)] program provides very accurate positions and one "clear" filter's photometry for roughly 1.4 X 10^6 stars. DR9 of the APASS catalog from AAVSO [Henden, et al (2009)] provides good coverage of roughly 4 X 10^6 stars between 7 to 17^{th} magnitude, with a program goal of 1% photometric accuracy. For each of a campaign's target fields, the data are downloaded from the public databases and converted by Python scripts into tables following a PostgreSQL schema for each target field. Caveats apply to all data (see 3.1).

These external data are collected for an area approximately 1.5 times the size of the images and put into a PostgreSQL database using Python scripts. A uniform translation scheme is applied to critical keywords e.g.: various terms for right ascension and declination are simply called "ora" and "odec". This lends a consistency to cross catalog comparisons. The database uses built-in rules to create a qualified proper subset (indexed materialized views) of stars to use with images. All decisions are retained in the code.

Pan-Starrs, located on Haleakala, in Hawaii, covers 3 out of 4 π steradians of the sky (hence its name) using the Pan-STARRs' Sloan's filters for the "grizy" photometric bands. The catalog is very deep but does not include stars brighter than about 13 magnitude and avoids areas with "texture" like nebulae and galaxy fields. The APASS catalog complements the Pan-STARRs 3π catalog adding BV bands and brighter magnitudes. The space-based Gaia mission's database has very precise positions for all the stars in the Hipparcos and Tycho databases. Gaia's ancillary TGAS (Tycho-Gaia Astometric Solution) database provides a wealth of proper motion data. Gaia 'G' magnitudes are essentially the quantum efficiency curve of its sensor. With a proper transfer curve, the Gaia magnitude standard will be of great interest to small telescope observers using a 'clear' filter to maximize their photon-counts. This paper uses the VYSOS project's [Reipurth et al (2004)] 20-inch Ritchey-Chretien images for ONC5 as the basis for the pipeline development. The images contain both bright and dim stars and lots of texture.

The PostgreSQL database is widely used in astronomy. It is more compliant with standard SQL, platform agnostic and easily extended with 'C' language routines that greatly accelerate machine operations. This work uses Python scripts running under a special Anaconda Continuum Analytics (2017)} astronomy recipe allows merging Python 2.7x, IRAF and the Jupyter notebook environment on "*nix" platforms. The reduction parts of the pipeline can be used on all platforms. Special scripts are used to download data from Gaia, Pan-STARRs, AAVSO's APASS/UCAC4, together with SIMBAD and NED database queries to form a complete basis for developing a photometric reference base.

1.1. Database Overview

A database for each campaign is created with a separate schema for each target field. Into each target

schema, tables are created by their names: "panstarrs", "ucac4", "apass", and "gaia". Pre-canned views and routines are used to winnow stars below a quality threshold leaving those with the best statistics for use. The rule for Pan-STARRs 3π candidates requires more than 9 observations with a variance of less than 0.005 magnitude. This helps assure no covert variable stars are accidently used. This shortened list is reduced by throwing out stars that fail a color test (r>g and i>r>g for example) using g,r, and i filters. The data-subset is further reduced by eliminating stars located within a seeing-radius of any other star, SIMBAD or NED object not conducive to a clean reduction of small telescope objects. Any star that has more than one entry in the Gaia table falling within the seeing radius of the candidate is also eliminated. This assures a higher confidence of having no background contaminants. Sergey Koposov's github repository" q3c" [Koposov and Bartunov (2006)] provides well optimized PostgreSQL routines for indexing objects in a celestial coordinate system.

The initial Pan-STARRs 3π database contained 158,156 stars across the ONC5 sub-region ra/dec of (81.3996424-7.83926452), to (86.45441702, -2.82696554). Figure 1 shows overall raw magnitude distribution in column 1, column 2 qualified stars, column 3 has stars selected for the area of the images (82.721835, -6.9612661) to (90.0344403 -3.5166481). Column 4 has the APASS data for comparison. Using a quality metric of number of observations greater than 9 and magnitude error < 0.005 drops the count, in Figure 1c to 11,372 (7%). A total of 118,433 raw Sextractor entries resulted from 54 images in the r' band from one night's observations. Directly, this requires $O(n^2) \sim 10^{10}$ comparisons. Winnowing data results in n X 400 selections in the each image, for $O(n^2) \sim 10^6$.

	Pan-STARRS				APASS	
mag	count (158156)	mag	count (22850)	mag	count (11372)	mag	count (16295)
						8	8
						9	115
						10	154
						11	273
						12	258
13	12					13	940
14	1815	14	565	14	222	14	1549
15	4978	15	2283	15	1134	15	2643
16	8904	16	4817	16	2331	16	5477
17	14281	17	7980	17	3923	17	10334
18	22166	18	6242	18	3241	18	20481
19	31134	19	938	19	503	19	28068
20	40586	20	25	20	18		
21	32244						
22	2036						

Figure 1: The extractions, using an artificial zpt=25 magnitude estimate, for Pan-STARRs 3π and APASS

2. Image Preparation

Preliminary processing of the images uses Python scripts leveraging standard IRAF routines. Successful images are plate-solved with Astrometry.net [Lang et al (2015)], running locally on a Linux server. A properly tuned Sextractor [Bertin (2015), Holwerda (2015)] script is run, and the resulting table of results are then loaded into the database on a field-by-field basis. Python is used to update the database of master files and to populate reduction directories with the latest images obtained before or immediately after the observation run.

3. ONC5 V1118 Analysis

V 1118 Ori, (RA 5:34:44.745, Dec -5:33:42.18) is a T Taurii-type star, classified as an EXor variable with a recent outburst described by Giannini [Giannini et al (2016)].. While its V mag ~ 14.4, its odd behavior is tied to a mass accretion rate of 10^{-6} to 10^{-8} $M_\odot$ yr^{-1} leading to changes in emission lines and in overall photometric color. This puts it near the limit of small-telescope spectroscopy in its quiescent period but accessible to amateurs during periods of outburst. Obtaining high cadence data over many days by the small telescope community will greatly contribute to understanding this object.

3.1 Caveats

During initial examination of images, the close proximity of a bright star caused a diffraction spike to enter into the area of V 1118.

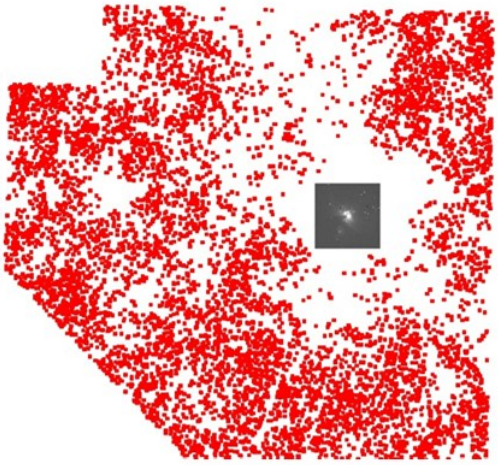

(a) Elevated optimism plummets to despair noting not one Pan-STARRs star is on the image.

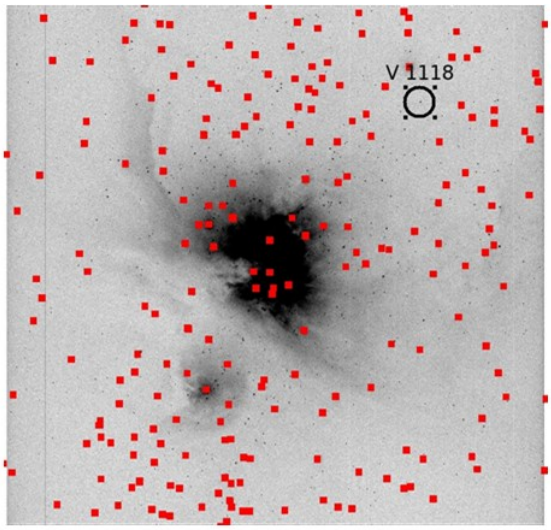

(b) and cautiously rises noting that stars from APASS are on the image.

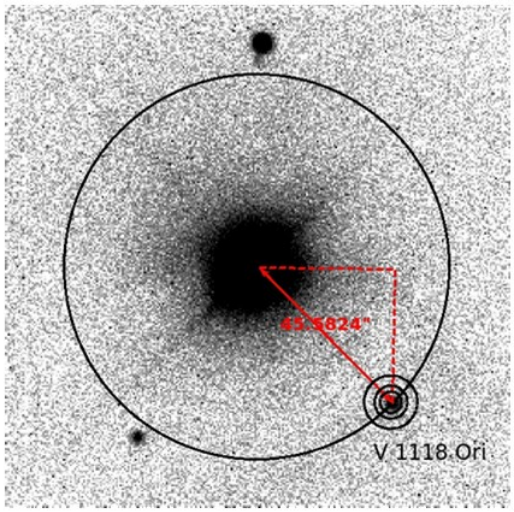

(c) Diffraction spike contaminates part of a standard aperture.

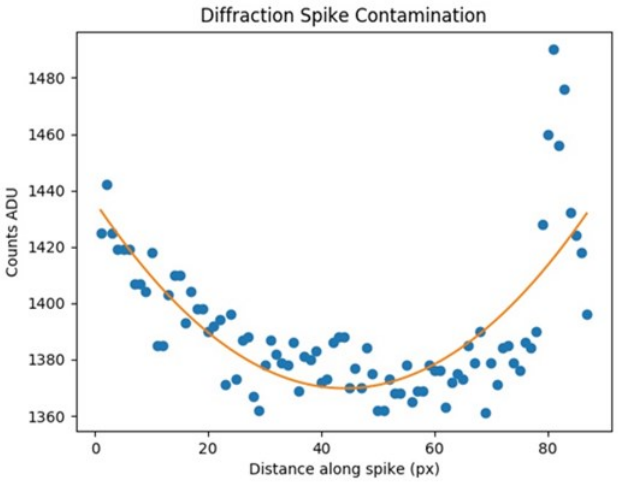

(d) Cut along spike between bright star and target

Figure 2: Caveat Examples: Diffractipn Spike contamination and Pan-STARRs data avoids areas with nebulae, galaxies.

The command

```
getapass 83.68590224 -5.561377544 1 > apass.csv
```

resulted in 2256 stars for the 1-degree field centered on V1118. Removing entries where 'rmag' (Sloan r' band) is missing or the number of observations of that star was < 4 results in 1129 or one half the catalog size. Matching the star to an image reduces this list down to 189 matches.

Figure 3 is the code snippet where `60.0` is the exposure time in seconds, `1.6` is the gain value for the camera (caveat: missing from the headers), `flux_iso` and `background` are from Sextractor and `rmag` is from the large initial APASS catalog. The rules of

"rmag is not null" (missing data for a catalog),
"a.number_of_obs > 3" (assuring more than three) observations and
"(b.flux_iso-b.background) > 20000"
(to assure 1% photometry)
produces a decent sub-set of 110 reference stars. This makes O ~ 110 times 118433 =1.x X 10^6 for the entire dataset.

```
create table apass_ref as (
      select ora,odec,rmag,rerr,zpt from
   (select a.ora,
          a.odec,
          sdist(s2r('5:34:44.745'), s2d('-5:33:42.18'),b.ora,b.odec) * 60,
          a.rmag,
          a.rerr::numeric(7,4),
          zptmagnitude(b.flux_iso,
                       b.background, a.rmag,
                       60.0,1.6)::numeric(6,3) as "zpt",
          a.number_of_obs,
          (b.flux_iso -  b.background)::numeric(12,4) as "flux",
          b.mag_auto
   from apass a   join image1 b
   on vnearby(a.ora,a.odec,10,b.ora,b.odec)
   where a.rmag is not null
   and a.number_of_obs > 3
   and (b.flux_iso -  b.background) > 20000
   order by (b.flux_iso -  b.background)
   ) x   ); -- 110 ref stars
```

Figure 3: Code snippet showing the recipe to develop the APASS reference table for use with the V1118 field.

```
# aliases defined for the system:
alias myconda='source ~/.myconda'
alias myastroconda='source ~/.mycondairaf'

Three steps to make the recipe

myconda
conda config --add channels http://ssb.stsci.edu/astroconda
conda create -n astrocondairaf python=2.7 iraf pyraf stsci jupyter
```

Figure 4: Code to include in the .alias user file tied to the small programs to be activate the "conda" environment}

4. Conclusions}

Professional astronomers are under increasing pressure to perform administrative duties at the expense of time for research and teaching undergraduate courses. This leaves a door wide open for the small telescope observing community to fully participate with contributions ranging from data analysis during the usual waking hours to making detailed, high cadence observations of selected targets at night. Essentially the biggest telescopes in the world are available to everyone with a willingness to learn and contribute. The basic VYSOS data reduction approach will be expanded to cover the other roughly 100 targets in the campaign.

5. Acknowledgments

The author gratefully appreciates access to the VYSOS large data set from Drs. Bo Reipurth and

Josh Walawender from IfA. The reductions used The European Space Agency (ESA) Gaia data DR1, APASS DR9 data from AAVSO , Pan-STARRs 3π DR1. Reductions use IRAF [Tody (1986, 1993)], distributed by the National Optical Astronomy Observatories, which are operated by the Association of Universities for Research in Astronomy, Inc., under cooperative agreement with the National Science Foundation. Numerous additional packages and papers are cited throughout this paper.

A. Reduction Environment

Continuum Analytics, Inc. offers its rich "Anaconda" data analytics package at no charge to the community. Anaconda comes in two flavors: a Python 3x and Python 2.7 environment. For the most part, Anaconda is platform agnostic. At the time of this writing, astronomy is split between the two Python flavors, with an emphasis on Python 2.7 still remaining. IRAF/PyRAF requires a Unix™ derivative system as it requires a Python 2.7 environment. It is possible to load the popular iPython notebook environment using the special "Anaconda recipe":

where ~/.myconda is:

Listing 1: Snippet of code for *sim*/.myconda

```
export
PATH="/home/wayne/anaconda3/bin:$PA
TH"
echo $PATH
source activate astroconda
echo "This shell ready for conda"
```

and ~/.mycondairaf is:

Listing 2: snippet of code for *sim*/.mycondairaf

```
export
PATH="/home/wayne/anaconda3/bin:$PA
TH"
echo $PATH
source activate astrocondairaf
echo "This shell ready for conda
with iraf"
PS1='V \h:(\j) \w [\!]>'
```

A number of Python and bash shell scripts facilitate acquiring, translating and loading data from web data repositories into the local PostgreSQL database.

References

Bertin, E. e. (2015). Sextractor v2.13 draft. WEB/URL https://www.astromatic.net/pubsvn/software/sextractor/trunk/doc/sextractor.pdf.

Chambers, K. C., Magnier, E. A., Metcalfe, N., Flewelling, H. A., Huber, M. E., Waters, C. Z., Denneau, L., Draper, P. W., Farrow,
D., and Finkbeiner; and 93 coauthors (2016). The Pan-STARRS1 Surveys. ArXiv e-prints.
Continuum Analytics, I. (2017). Anaconda leading open data science platform powered by python. WEB/URL. https://docs.continuum.io/.

Gaia Collaboration, Brown, A. G. A., Vallenari, A., Prusti, T., de Bruijne, J. H. J., Mignard, F., Drimmel, R., Babusiaux, C., Bailer-Jones, C. A. L., Bastian, U., and et al. (2016a). Gaia Data Release 1. Summary of the astrometric, photometric, and survey properties. Astronomy & Astrophysics, 595:A2.

Gaia Collaboration, Prusti, T., de Bruijne, J. H. J., Brown, A. G. A., Vallenari, A., Babusiaux, C., Bailer-Jones, C. A. L., Bastian,
U., Biermann, M., Evans, D. W., and et al. (2016b). The Gaia mission. Astronomy & Astrophysics, 595:A1.

Giannini, T., Lorenzetti, D., Antoniucci, S., Arkharov, A. A., Larionov, V. M., Di Paola, A., Bisogni, S., and Marchetti, A. (2016). On the 2015 Outburst of the EXor Variable V1118 Ori. Astrophys. J., Lett., 819:L5.

Henden, A. A., Welch, D. L., Terrell, D., and Levine, S. E. (2009). The AAVSO Photometric All-Sky Survey (APASS). In American Astronomical Society Meeting Abstracts #214, volume 214 of American Astronomical Society Meeting Abstracts, page 669.

Holwerda, B. (2015). Source extractor for dummies. don't panic. WEB/PDF. http://mensa.ast.uct.ac.za/~holwerda/SE/Manual_files/Guide2source_extractor.pdf.

Koposov, S. and Bartunov, O. (2006). Q3C, Quad Tree Cube – The new Sky-indexing Concept for Huge Astronomical Catalogues and its Realization for Main Astronomical Queries (Cone Search and Xmatch) in Open Source Database PostgreSQL. In Gabriel, C., Arviset, C., Ponz, D., and Enrique, S., editors, Astronomical Data Analysis Software and Systems XV, volume 351 of Astronomical Society of

the Pacific Conference Series, page 735. https://github.com/segasai/q3c.

Lang, D., Hogg, D. W., Mierle, K., Blanton, M., and Roweis, S. (2010). Astrometry.net: Blind astrometric calibration of arbitrary astronomical images. The Astronomical Journal, 137:1782–2800. arXiv:0910.2233,doi:10.1088/0004-6256/139/5/1782](http://dx.doi.org/10.1088/0004-6256/139/5/1782) summary http://astrometry.net/summary.html latest release 0.70.

Reipurth, B., Chini, R., and Lemke, R. (2004). The VYSOS robotic telescope project. Astronomische Nachrichten, 325:671–671.

Tody, D. (1986). The IRAF Data Reduction and Analysis System. In Crawford, D. L., editor, Instrumentation in astronomy VI, volume 627 of Proceedings: Society of Photo-Optical Instrumentation Engineers, page 733.

Tody, D. (1993). IRAF in the Nineties. In Hanisch, R. J., Brissenden, R. J. V., and Barnes, J., editors, Astronomical Data Analysis Software and Systems II, volume 52 of Astronomical Society of the Pacific Conference Series, page 173.

Exploring the Unknown: Detection of Fast Variability of Starlight

Richard H. Stanton
Jet Propulsion Laboratory (Retired)
Big Bear City, CA 92314
rhstanton@gmail.com

Abstract

In previous papers the author described a photometer designed for observing high-speed events such as lunar and asteroid occultations, and for searching for new varieties of fast stellar variability. A significant challenge presented by such a system is how one deals with the large quantity of data generated in order to process it efficiently and reveal any hidden information that might be present. This paper surveys some of the techniques used to achieve this goal.

1. Introduction

Although there are astronomical objects that vary optically on timescales of milliseconds, these objects are few in number. One of the reasons for this dearth might be that fast optical variability is an intrinsically rare phenomenon. Another factor might be a selection effect stemming from astronomers spending relatively little telescope time searching for such objects. Amateur observers could play a role in this pursuit as appropriate equipment and analysis tools become more readily available. Detector and computer technology have improved over the years, paralleled by the discovery of some interesting behavior and bizarre targets. The field is wide open for amateur exploration to those willing to invest the required resources and effort.

2. Background

The "road less travelled" of photon counting has enticed the author for more than forty years. Early on (Stanton, 1983) it was recognized this technology has the potential to provide measurements of star intensity at their most fundamental level. Since light arrives in discrete energy packets (photons), one merely needs to count these arrivals to achieve a fundamental measurement of starlight intensity. Such signals never require an analog-to-digital conversion since they arrive in digital form—integer counts. Of course, there are many excellent reasons why charge-coupled devices (CCDs) and other area-array detectors have almost completely dominated astronomical photometry in recent decades. Without recounted these here, it should just be mentioned that the technology for photon counting has also reached a state of maturity similar to that achieved by CCDs. Excellent photomultiplier modules are available where one simply connects a 5V power supply to the input and receives a nearly noiseless stream of detected photon pulses at the output (Hamamatsu, 2015).

Details of the instrument used for the author's observations have been described previously (Stanton, 2012 & 2015). Table 1 summarizes system characteristics and typical processing parameters for the output data. Although the counters are capable of continuous operation with sample times as short as one microsecond, most observations are made using 50μs bins. This is a compromise to avoid storing and processing 50 times more data samples!

The nearly 150 million time samples for each observation are stored as simple tab-delimited ASCII integers. The initial analysis performed uses a single program to bin the data by successive factors of 4 (up to 4096x), search each of the resulting files for significant pulses, transform each file into spectra (optical power vs frequency) and summarize the results in forms that can be easily displayed in tables and plots. This computation takes approximately five minutes with an ordinary PC, enabling "quick look" evaluation to be accomplished in near-real-time. Figure 1 shows a typical time-series plot illustrating simultaneous Y and B color data (the plot of Background data has been deleted for clarity). The large difference between Y and B indicates that this object, V404 Cyg, is a very red object.

Telescope System

30" Dobson operating at prime focus

ServoCat tracking system

SBIG Guider + MaximDL

Photometer: 3-Channels simultaneously

Y = 500-700nm

B = 350-500nm

Background = 350-700nm

Typical Run

Duration: 2400s

Sample Rate: 20,000/s

Total raw samples: 144 million

Typical Processing

Binning: 4x to 4096x

Pulse search with background subtracted
Power spectra: 10 to 47,000 overlaps

Table 1 Typical Observation Characteristics

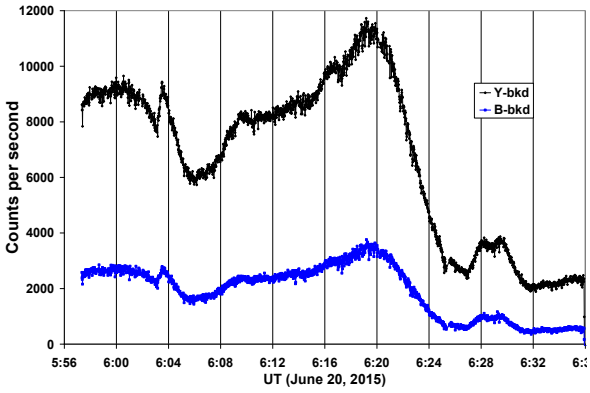

Figure 1 40 minute time series (1 sample/s) taken during the recent outburst of the "X-Ray Nova" V404 Cyg. Many oscillations similar to the 1.6 magnitude drop seen here were observed during 10-day outburst

Before describing the processing steps in more detail, it is interesting to contrast this problem with that of analyzing a typical light curve generated by more conventional means (CCDs and visual observations). Most traditional light curves (AAVSO and others) rely on observations submitted by many individuals over extended periods of time. This is, of course, the great strength of these databases. But this strength comes at the price of irregular spacing in time, diurnal gaps in the data, variations between observers and equipment that suffers from poorly-known calibrations. Each of these factors has the potential of significantly degrading the information content of a light curve. Such deficiencies can often be effectively ameliorated, but uncovering hidden information often requires using a variety of analytical tools and techniques, such as those described by Foster (2010). In contrast, the observations described here suffer from none of these issues, making it much easier to apply the powerful tools designed for analyzing continuous, equally-spaced data series.

3. Searching for Pulses

This equipment is well-suited for searching for optical pulses over a large range of pulse duration. Samples as short as one microsecond are possible with this system, implying that pulses of this duration should be readily detectable. [Note that to search for even shorter "SETI" pulses one has to use more specialized equipment such as that developed by Howard (2015).] To search for optical pulses in the type of time-series data described here one must take into account at least three important factors: separation from noise, variations in background level, and use of appropriate time samples.

3.1 Separation from noise

3.1.1 Statistical noise

Statistical noise can be readily addressed based on the assumption that the data statistics are purely Poisson (or Gaussian for large signals). One simply calculates the probability of having a single event in the entire data set of the detected amplitude. This probability is typically a very steep function of pulse amplitude, so one can usually reject all questionable pulses, even those with only a 10% probability of being random events.

3.1.2 Environmental noise

Noise arising from the surrounding environment can be dealt with taking advantage of information in the Background channel. A suspect pulse can often be identified in the Background channel, whether it is due to a passing airplane, a neighbor's lights or a background flash from lightning or a meteor. If it is detected without passing through the photometer's diaphragm (i.e. is detected in the Background channel) it is certainly not associated with the target being observed!

3.1.3 Instrument noise

Noise arising somewhere in the telescope or instrument is often the most difficult to deal with since it can arise from unexpected sources. In a memorable example, the author detected a "signal" that was well above any possible noise threshold (Stanton, 2015). It was detected only in the Y & B

channels, but not in the Background. This was ultimately found to be due to wind-induced vibrations in the telescope that were only visible when the star occasionally wandered to the edge of the diaphragm (also due to wind). One of the best ways to build confidence that a new signal is not caused by the instrument is to observe many similar targets on the same night, and in the same region of the sky.

3.2 Variations in Background Level

A search for pulses should also take into account variations in the background signal intensity caused by seeing, sky transparency variations or changes in the star itself. Without taking such local changes into account, one is much more likely to miss significant pulses when the background level is low, or potentially detect noise when it is high. This factor can be effectively handled by averaging N values of the background both preceding and following each time sample, and then subtracting this average from the sample count.

3.3 Use of appropriate time samples

The time resolution of the data samples (bins) should match the duration of the pulses being sought. If the samples are too short, the longer pulse will be "washed out" over many samples and probably not be detected. Conversely, if the samples are too long, a short pulse will be lost in the background integrated during the long sample time.

The author addresses this issue by scanning each of the binned files mentioned above, one sample at a time. The computer keeps track of the five largest pulses found at each color channel and each resolution (raw, bin 4x, bin16x, …), and compares these to what is expected due to random noise.

4. Power Spectra

Time-series data can be readily converted to the frequency domain "spectra" using the Fast Fourier Transform (FFT). Performing a FFT on the raw data described above will sample frequencies up to 10,000 Hz (with 50μs samples). Higher resolution spectra for lower frequencies can be generated by performing FFTs on binned data. With this approach, displays of the power spectra for a large range of optical variability can be part of the routine processing of time series data.

Signals whose frequency content does not change significantly during an observation are said to be "stationary" during the observation. This is in stark contrast to many audio signals familiar in every day experience such as voices or bird chirps. But if we assume that there are astronomical signals of interest that are stationary, the signal-to-noise ratio for power spectra can be greatly improved by averaging many such spectra together. For the long time series discussed here it is possible to average thousands, or even tens of thousands of spectra together. The resulting reduction in background noise can be a factor of 100 or more. Weak signals that are completely invisible in a time series display can often be clearly seen in the power spectrum of the same data.

Figures 2 and 3 show this effect very clearly. In the time series data (Fig. 2) we see data from the Y, B channels consisting of light from the pulsar, nebula, sky background and moonlight (the crescent moon was ~25° away). The pulsar itself contributes less than 2 photons per revolution to this total, or roughly 50 photons/s. Since this is less that 1% of the Y or B count rates, the pulsar rotation is hopelessly lost in noise of the total signal, regardless of what time resolution one chooses to display.

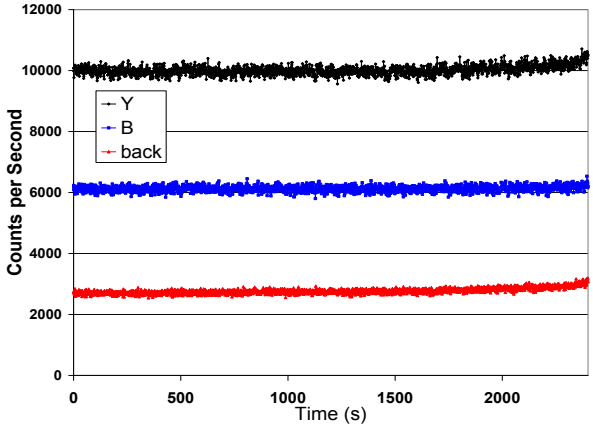

Figure 2 Time variability of the Crab Pulsar buried in surrounding light. The lower curve shows that the background is increasing as the stars move lower in the west. The middle curve (B) is searched for signs of the pulsar signal (below)

Due largely to our ability to average thousands of individual spectra together, the power spectrum in Figure 3 clearly shows the presence of the time-varying pulsar generating a repeating pulse at its rotation frequency (~29.6Hz). It also shows four harmonics of this frequency, with the first harmonic apparently more powerful than the fundamental. Such harmonics are a clear sign that a complicated waveform lies buried in the time series data. The sharpness of the lines suggests that the frequency of the variation is unchanging (stationary) at least for the duration of the observation.

Once the rotation period of the pulsar is determined from the power spectrum, it is possible to

add data from repeated pulsar rotations together and bring the waveform out of the noise. During this 40 minute observation the pulsar rotated approximately 70,000 times. But in order to add data from these 70,000 cycles together *without smearing out the resulting waveform,* the repetition period must be known to better than 1 part in a million! Starting with the spectral information in Fig 3 (frequency ~29.64Hz), the sampling period around this frequency was iterated until a waveform emerged. At the end of this process the waveform was found to show best at a repetition rate of 674.7669 samples per cycle. This corresponds to a frequency of 29.6399Hz if the system clock were a perfect 20,000Hz. But during this observation the system clock was running faster, at 20,000.684Hz, implying that the measured pulsar rotation frequency was 29.64088Hz on the night of the observation (March 31, 2017).

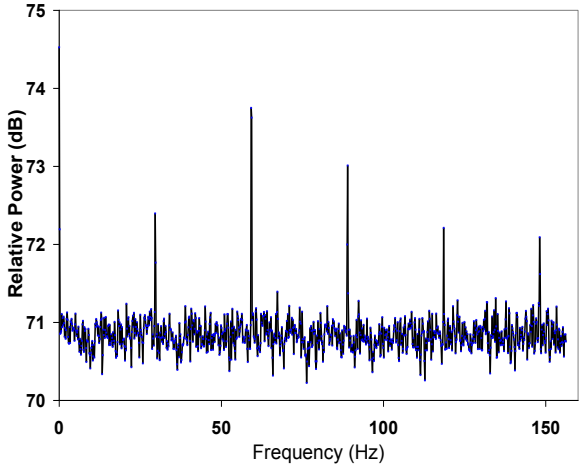

Figure 3 Power spectrum of the Crab Pulsar optical pulsations (B channel)

The waveform shown in Figure 4 is actually the result of a two step process. First 70,000 cycles of the B channel data were added together with a period of 674.7669 samples for each cycle (50μs/sample). Second, the resulting 674 point waveform was then re-binned by a factor of 10 to give the resolution of 0.5ms shown in the figure. This double peak waveform, familiar in the literature (Warner, 1988), clearly shows why the second and higher harmonics are so prominent.

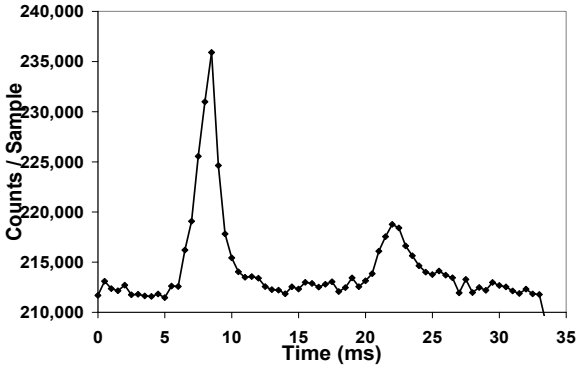

Figure 4 Crab Pulsar optical variation (3/31/17)

Another interesting example of a "signal" that can be clearly seen and characterized in the spectral domain is that due to atmospheric seeing. Amateurs well know how seeing both distorts and modulates incoming starlight. A quantitative characterization can often be best achieved by looking at the power spectrum of the seeing-driven scintillation . Figure 5 illustrates this for a relatively bright star (V~9). Note that seeing power is very high for low frequencies, being more than 10dB above the background noise level for frequencies below 10Hz, but essentially disappearing above ~120 Hz. This tells us that any light curve for this bright star will be affected by seeing at frequencies below 100Hz, but that above this, the signal is essentially what could be achieved above the atmosphere (except for a small amount of absorption). Notice that seeing doesn't seem to affect the power spectrum of the Crab pulsar data in Figure 3. Since the background signal in this case is much weaker, and that signal is largely due to extended sources (moonlight and nebulosity), the data are much more immune to the effects of seeing.

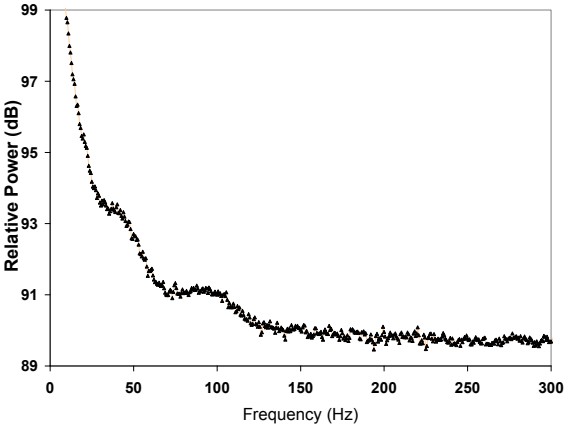

Figure 5 Typical power spectrum of atmospheric scintillation

Finally, the search of the unknown has turned up a number of "signals" in some of the author's power spectrum data. Almost all of these have been explained due to extraneous light sources, mechanical vibrations in the telescope or problems in cabling carrying the photon pulses. But the power spectrum measurement is so sensitive that not all detections have yet been fully explained. Fig 6 shows an example of one such "signal" from a bright star showing a small resonance at 371Hz. As is usually the case, more observations are needed to find the culprit actually responsible for this "signal"!

5. Digital Filtering

In addition to providing data that can be used for power spectrum analysis, high cadence photon counts can be easily re-binned and digitally filtered to bring out subtle light variations that might otherwise be missed. Figure 7 is an example of a flare captured by the B channel for BL Lacerta on July 27, 2015. These data have been binned to 250ms resolution in order to show the star's rapid variation during the flare event. But much of this variation is masked under a substantial band of noise.

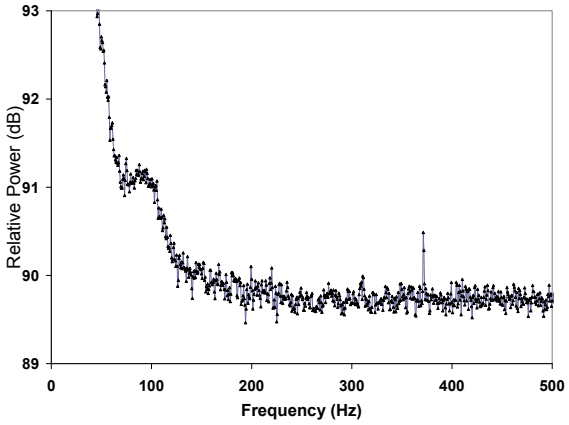

Figure 6 Power Spectrum of bright star showing unexplained resonance @ 371Hz

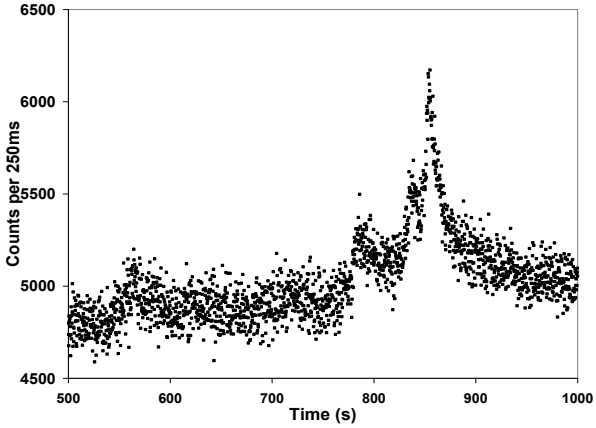

Figure 7 Flare in BL Lac, B channel (250ms/point)

One way to reduce this noise is to apply digital filtering to remove higher frequencies while leaving unaffected any frequencies below the filter cutoff. These filters can be easily developed and applied to evenly-spaced time-series data (Rabiner, 1975). The results for two different filters are shown in Figures 8 and 9. Figure 8 results from applying a low-pass filter that allows only the lowest 25% of the frequencies in the original data to be displayed and also discards every other data point. By eliminating higher frequency information that is mostly noise, this strategy gives in a much clearer picture of the several small pulses that precede the major outburst.

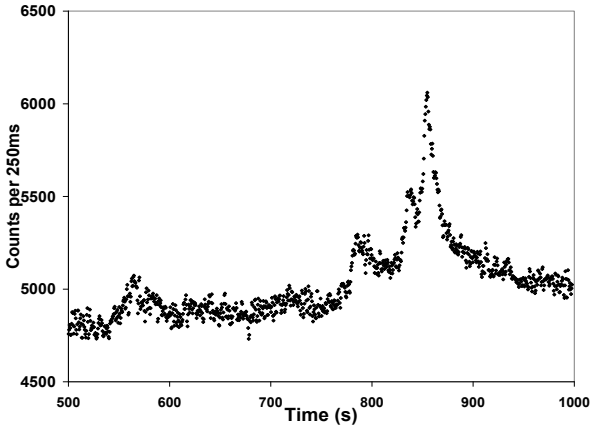

Figure 8 Flare shown in Fig 7 after applying a 4x low-pass filter

Figure 9 shows the same data, this time using a filter that only passes the lower 1/8th of the frequency content in Fig. 7. This may be an example of too much filtering since the correlation between adjacent data points introduces a level of unreal waviness.

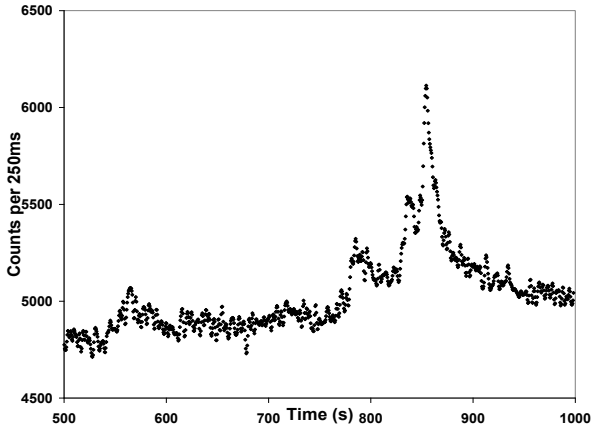

Figure 9 Flare shown in Fig 7 after applying an 8x low-pass filter

6. Conclusion

Every astronomer knows that there is much to be learned by analyzing starlight. In many cases amateurs provide valuable data for professionals in their study of unusual stars and in their efforts to understand new phenomena. Recording and analyzing high speed time-series data provides a different avenue for possible discovery and collaboration. The sensor technology and analyses needed are really no more challenging than those required for taking beautiful CCD photographs or generating the high precision light curves required for finding and characterizing extra-solar planets.

7. Acknowledgement

The author thanks Rook Andalus for his review of the paper and many helpful suggestions.

8. References

Foster, Grant, *Analyzing Light Curves—A Practical Guide* (2010), Lulu Press, Inc.

Howard, B., "Optical SETI Using a 3-Beam Coincident Photometer" (2015), Proc. SAS, 34, Buchheim, Foote & Mais eds., 79-82.

Hamamatsu Corp. *Photon Counting Head H8259 Series* (2015), Hamamatsu Corporation, Bridgewater, NJ

Rabiner, L.R, & Gold, B, *Theory & Application of Digital Signal Processing* (1975), Prentice-Hall, Englewood Cliffs, NJ.

Stanton, R.H. "Design and Use of a Computer-based Photon Counting System" (1983), *Advances in Photoelectric Photometry, Vol. 1,* R.Wolpert & R.Genet, eds., Fairborn Observatory, Fairborn, Ohio, 87-129.

Stanton, R.H. "Triple Photometer: Design and Initial Results" (2015), Proc. SAS, 34, Buchheim, Foote & Mais eds., 69-77.

Stanton, R. H. "Photon Counting—One More Time" (2012), Proc. SAS, 31, Warner, Buchheim, Foote & Mais eds., 177-184.

Warner, Brian, *High Speed Astronomical Photometry* (1988). Cambridge University Press, Cambridge, p182-194.

A Wide Band SpectroPolarimeter

John Menke
22500 Old Hundred Rd
Barnesville, MD 20838
john@menkescientific.com

Abstract

This is the third paper in a series describing experiments in developing amateur spectropolarimetry instrumentation and observational methods. Spectropolarimetry (SP) can provide insight into the extra-stellar environment, including presence of dust and alignment forces (e.g., magnetic fields). The first two papers SAS 2014,6 described the SP1, a spectropolarimeter based on the medium-resolution spectrometer on our 18in. f3.5 Newtonian. The desire to observe fainter stars led to the development of the SP2 reported here that uses a low resolution spectrometer. The SP2 has been used with a C11 f10 telescope, and has allowed observations down to about mag. 8. This paper describes the SP2 and observational results to date.

1. Introduction

Polarimetry measures the total relative net polarization of the light from an object (such as a star), while spectropolarimetry (SP) measures the polarization as a function of wavelength. Measurements of the polarization, coupled with other observations and theoretical models of what is going on in, on, and near the star, can allow a researcher to detect and measure possible matter (e.g., dust) in the neighborhood of a star, as well as the presence of forces that may align the matter so as to polarize the light passing through it (e.g., magnetic fields). Polarization can also occur far from a star, so some interstellar spaces may also be investigated.

The net polarization that one expects to see from observing, for example, a uniform star is zero: even if polarization is present in the light from part of the disc, presumably it will be balanced by contrary polarization from other points on the star disc. Where asymmetric emitters or intervening polarized materials exist, polarization can occur, but usually at low levels, e.g., less than a few percent. Thus, due to the very low levels of polarization in most situations, the measurement of polarization is inevitably challenging. This is because one measures polarization by observing the change in intensity as one varies the angles of a polarizer that can be rotated in conjunction with an analyzer. To measure 1% polarization to a precision of 10% will require comparing brightness measurements to precisions of 0.1%, i.e., one millimagnitude. In practice, one would like to be substantially more sensitive to polarization that this!

Of course, in practice, there are additional problems. For example, when performing spectropolarization (SP), the spectrometer portion of the instrument has already spread the light over wavelength thus reducing the intensity in each wavelength bin by hundreds to thousands compared to the object brightness. Each wavelength bin must still be measured to precisions of better than 0.1%. A second problem is that many optical systems impose polarization onto the light passing through them, causing offset errors. A totally symmetric system such as a refractor or an SCT will add minimal polarization, while a non-cylindrically symmetric Newtonian reflector, will add more. Even simply having a dirty region on the telescope optics can cause net polarization as the polarizations imposed may no longer cancel out.

2. SP2 Design

Because of the challenges in taking such high precision data, special observational and analytic methods have long since been developed to help cancel out as many errors as possible. Figure 1 shows the overall design of the SP2, which is quite similar to the SP1 (please see SAS2014 and SAS2016 Menke for more detail on the theory of SP measurements).

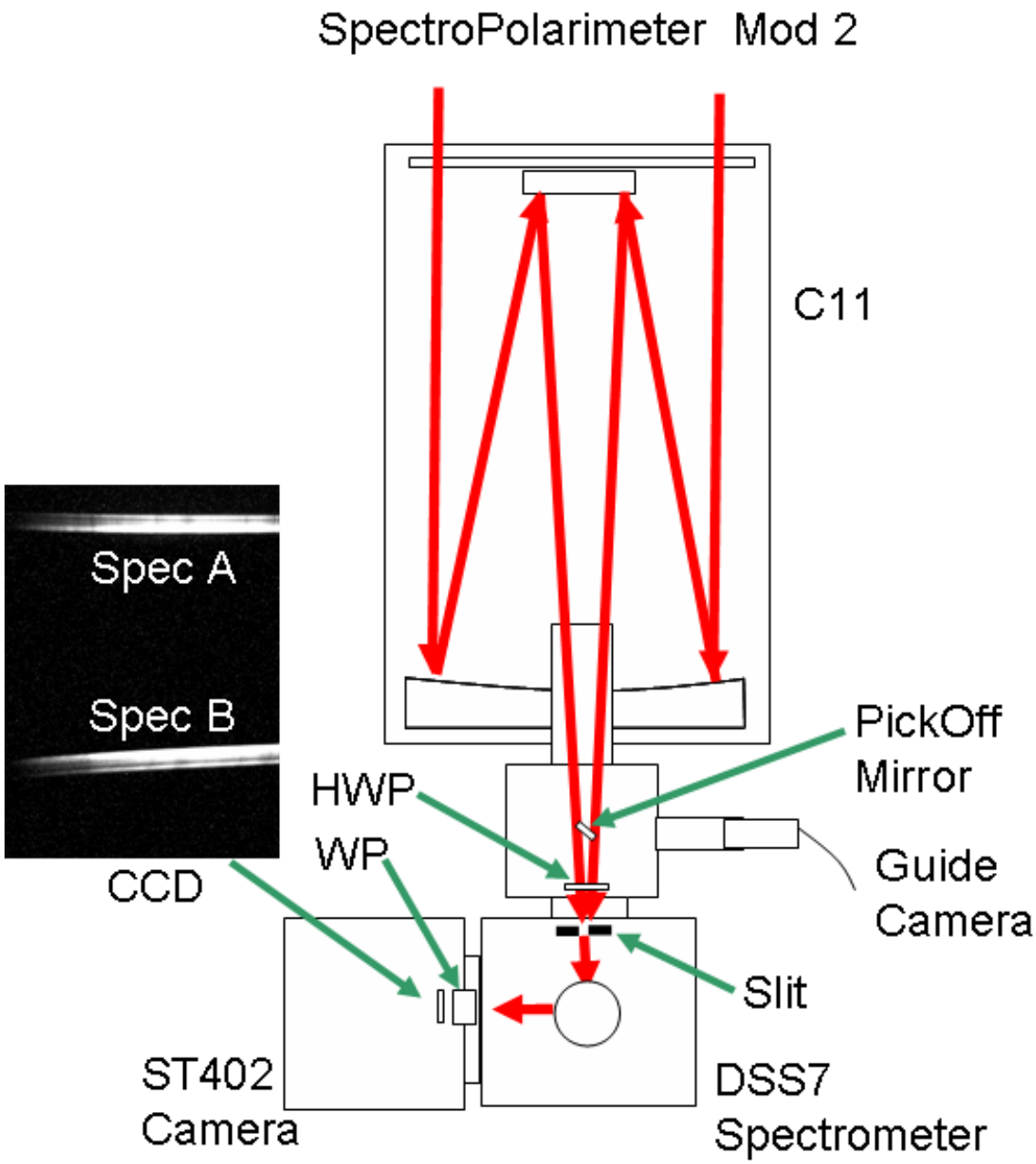

Figure 1 Schematic of SP2 Optical System

Following the light path as it leaves the telescope, the light passes through a rotatable HalfWavePlate (HWP) and then enters the DSS7 spectrometer (more on the details below). To achieve observation of fainter stars than the SP1 could achieve, we used a modified low resolution spectrometer, i.e., the SBIG DSS7 coupled to an SBIG ST402 CCD camera. Light enters the DSS7 through the (modified) slit, strikes the diffraction grating, and is reflected and focused through the output port into the camera. However, just before it reaches the camera sensing chip, the light passes through the analyzer Wollaston Prism (WP). The WP splits the light beam containing the polarized light into two orthogonally polarized beams that leave the WP at different angles and which then land on the CCD chip. The result is an image containing two spectra (A & B), whose intensity ratios are related to the relative polarization at each wavelength.

Let us now discuss each major component. The HWP is a device that rotates the direction of the polarization of the light passing through it: if it is

rotated, say 22deg, the **direction** of polarization out will rotate twice as much, or 44 deg. The purpose of rotating the HWP is to introduce known polarization angle changes into the system, so that appropriate ratios can be taken that can remove the effects of downstream instrument polarization. The DSS7 provides full visual band coverage of the spectra, so the HWP used in the SP2 must be achromatic. Because large HWPs are expensive, a small (1inch) HWP was used and it is placed just before the DSS7. In contrast, the SP1 had much lower bandwidth, so a larger, **non**-achromatic HWP could be placed before the Newtonian secondary, thus allowing cancellation of polarization imposed by that secondary).

The HWP is rotated by a small stepping motor that is normally directed to nominal 67, 89, 112, 134 degrees physical rotation. In the same housing is provided a guiding camera that uses a small (4mm) mirror that intercepts about 15% of the light from the telescope that is reflected into a small CCD camera. Once calibrated against the DSS7/ST402, the image from this camera not only guides the telescope, but allows placement of the star on the spectrometer slit to a precision of better than one pixel.

After the HWP, the light enters the slit of the DSS7. The standard DSS7 slit is actually comprised of four slits, above one another, that have widths ranging from 50u to 400u. After much testing, the DSS7 slit was replaced by a single 200u slit (wider to get as much light in as possible) that is masked off to reduce its height from 3mm to about 1mm.

After leaving the spectrometer grating, the light passes through the WP. Because this particular WP causes relatively highly divergent output beams (about 30deg), when the two beams (A & B) arrive at the CCD chip they will not both fit onto the horizontal chip causing the camera to be used in the vertical orientation. With care, the full wavelength range of the spectra is accommodated. Finally, because the WP adds to the optical path length and defocuses the DSS7/ST402, a weak positive meniscus lens was added just before the output port of the DSS7 so as to achieve reasonable focus of the spectra into the camera.

3. Observing and Analytic Routines

The target star (or planet) is obtained, and focused onto the DSS7 slit. At this point a custom control program (written in Visual Basic VB), with the controls shown in Figure 2A) is started that controls the system via direct serial commands and commands from MaximDL. This program is very similar to that used in the SP1. This program begins taking data which includes

* rotating the HWP to one of the four preset angles

* exposing the image as desired (typically 30-240 seconds)

* rotating the HWP to the next setting, and so on.

The program cycles through the HWP angles, taking the four images (each with two spectra). The program continues recycling through the angles until the observing session is finished (5 min-3 hours).

After the data (e.g., 50-100 fits files) are taken, they must be reduced. For most work, MaximDL under the control of a VB program (see Figure 2B) is used. Once the images are loaded into MaximDL, the software directs Maxim to apply calibration corrections (darks), rotating and mirroring the images as needed. Various means are used to improve the resulting data, such as hot and cold pixel repair and median corrections, but no overall image manipulations are performed The software runs through all the images, summing the data for each spectrum (i.e., A & B) and HWP angles. The software then writes the eight spectral data sets into a text file.

The text file is then copied and pasted into an Excel spreadsheet that displays the measured spectra. The sheet also performs a series of ratio calculations, yielding the final value of the polarization and angle at each wavelength. As discussed in the SP1 papers, these ratios cancel out most variations in observing conditions that might have occurred during the session. The entire analytic process takes about five minutes.

To simplify my own files, I have chosen to leave all polarization measurements as decimal fractions, e.g., 0.002, rather than use the percent units (e.g., 0.2%) used in the literature.

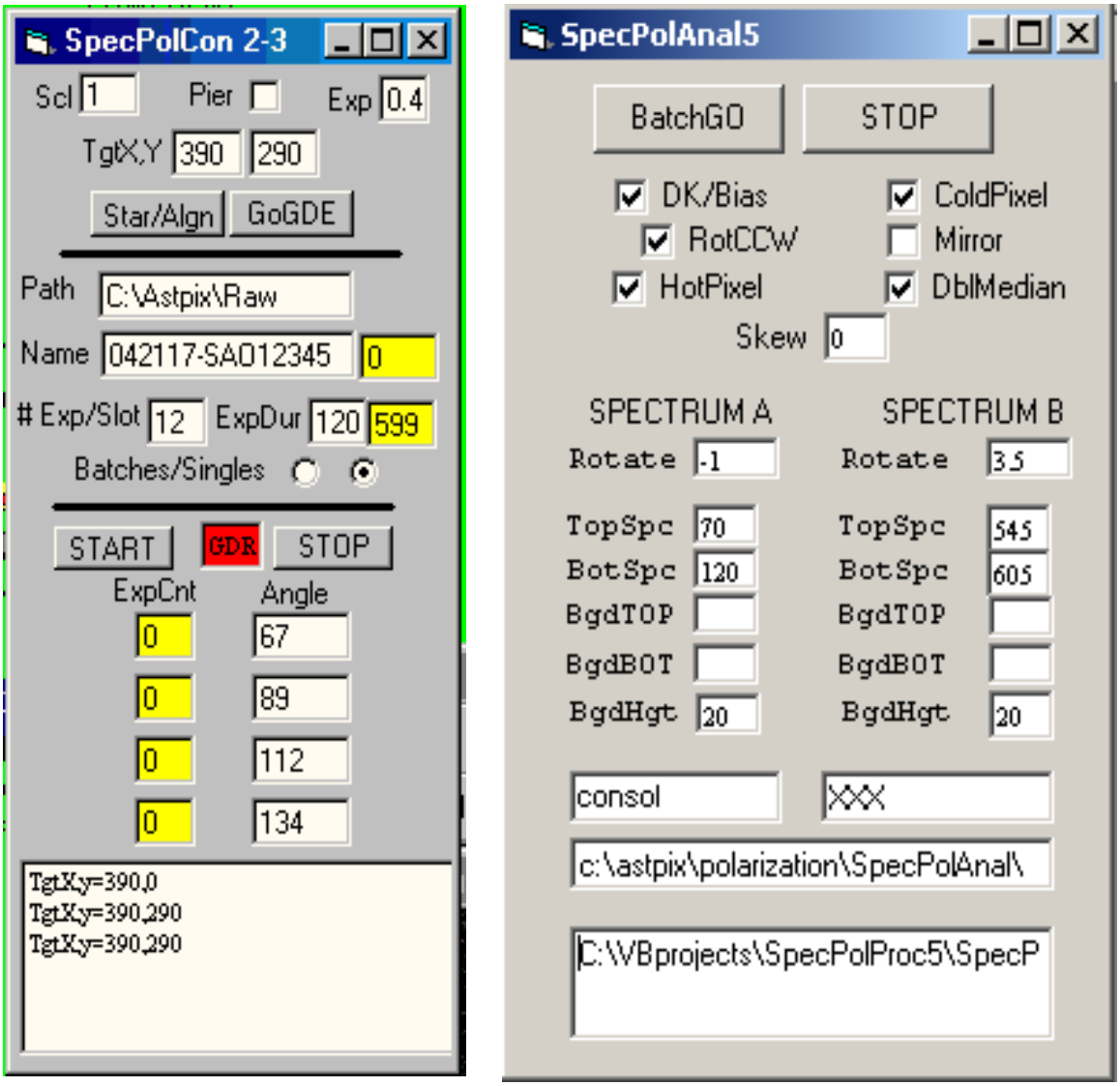

Figure 2 Imaging and Analysis Control Windows

4. Initial Operation and Shakedown

An impetus for building the SP2 was the Alert Notice 546 by AAVSO of the Wolf Rayet star WR140 campaign as follows: "WR 140 (HD 193793 = SAO49491) is a long-period (P~8yr), highly eccentric (e=0.8964) system with a carbon-rich Wolf-Rayet star and an O star in the orbit [6.8mag]. Both stars lose mass, which collides, and the density at the collision point is much higher around the periastron passage, which should occur on the 18th of December [2016]. In the months just after periastron, the system creates a large amount of dust."

While the AAVSO campaign was primarily after photometric data, the presence of dust in a highly perturbed system made this a potential target for SP.

To observe the polarization of this system required a new instrument--the earlier SP1 (even using the 18in. telescope) had a faint target limit of about 5-6mag. Clearly, one avenue to achieve fainter objects would be to reduce the wavelength resolution as a tradeoff--hence, using the DSS7 in the SP2. To avoid the problem of a Newtonian mirror, a Schmidt-Cassegrain C11 was chosen for the telescope. General design occurred in the summer/fall of 2016; however, the request was that data taking begin in Oct. 2016. The SP2 was barely "finished" by then, but data taking began while continuing to test and modify the instrument and observing and analytic methods. Through the winter of 2016-7, until the target began setting too soon after sunset for observation, data were taken every night that stars

were visible (approx 40 out of 90). During this time, the slit size was 100u x 3mm.

Because of the desire to capture possible transient behavior in the WR140 system, interruptions of the campaign were minimized with only limited observations of other targets. However, results of these observations showed several design deficiencies in the SP2, as well as changes needed in observation and analytical methods.

As noted, the original SP2 had problems placing the two spectra onto the horizontal camera chip. The initial solution was to place a custom converging (acrylic) prism between the WP and the camera chip partially to converge the two beams. This would be a good solution, except that due to tight spacing the two spectral beams are not fully spatially separated when they enter the converging prism. Thus, there is the potential for producing unknown contamination of the A & B spectra or the backgrounds. Although the prism helped, the final solution was to remove the prism and instead rotate the camera 90deg to the vertical orientation.

In general, guiding was not a problem as the guider normally achieves <1 pixel stability. Once calibrated against the SP2 camera, a target could be placed on the DSS7 slit to a precision of <1 pixel.

Experiments were performed in which the slit was entirely removed. The precision of guiding still allowed the system to maintain full wavelength calibration, i.e., the slit was no longer necessary to assure calibration. Removal of the slit yielded about 30% more intensity but at the cost of much higher background in the spectral images, which was unacceptable. A return was made to a 200u slit, wider than the original 100u, but still effective in quelling sky background. The height of the slit was reduced to about 1mm further to reduce sky background entering the instrument.

One concern was that the guider mirror (3 mm across), because it was upstream of the HWP/WP, could be imposing a net polarization that would create an offset on measurements. However, several objects were measured with polarizations as low as 0.001 (0.1%), seeming to show that instrumental offsets are not a problem, at least at this sensitivity.

Aside from the optical issues of obtaining clean spectra, the biggest challenge in operating the SP2 has been assuring proper treatment of sky background. As the objects became fainter than about mag 4, the signal to background ratio became significant. Recall that the basic measurement is the ratio (at a particular wavelength) of the intensity in Spec A vs. Spec B. On the one hand, if background or gradients in the background are present and remain unchanged throughout the session, then their effects will ratio out. However, if there is the slightest change in background or gradient (at the <0.1% of signal level), then an offset error (i.e., apparent polarization) will be introduced. These errors can be very large, often creating what appear to be polarizations >0.01 (1%) or even more, and often containing wavelength related artifacts.

This issue is most important early in the evening when there is substantial sky background, including strong gradients, and that are changing during the observing run. This was particularly a challenging problem for WR140 late in the campaign (Jan-Feb), as it was sinking into twilight.

The issue of handling background is very much a concern during data analysis. Given the less than ideal sharpness of the spectra, there is little delineation of where to set the analysis software to measure the spectral intensity at each wavelength, nor to include a well defined background measurement. Obviously, the fainter the object and/or the greater the background, the worse this challenge becomes, thus requiring scrupulous attention to detail.

5. Observational Results

As of the writing of this paper, some 150 measures of 35 objects (both stars and planets) have obtained. Many measurements were under poor weather conditions, or were early in use of SP2 so involved deficiencies in equipment, observation, or analysis which were corrected for later observations. The general result has been a trend of results having lower noise and more consistency. In general, in polarization work, the expected polarization for most objects is very low (i.e., < 0.001), and this is what is seen in these results. Of course, the most interesting results are targets having polarizations >0.001!

Here is a sampling of some of the results.

WR140. As noted, this observing campaign provided a part of the impetus for constructing the SP2, and resulted in about 40 measurements though the winter of 2016-7. The early results were not of high quality; however, there were recurring changes in the measured polarization that appeared to originate in WR140 (observations of other both bright and faint targets during the same months did not show the same kinds of changes).

Figure 3 is a good example, and shows the very first evening of WR140 data on Oct. 10, 2016. The black line is the spectrum summed over all the spectral images. As one can see, the "average" counts are about 1million, so the observation has good statistics. The red curve shows the polarization

calculated from the data. Because the polarization involves ratios of virtually identical spectra having slightly differing polarizations, there is no expectation that the polarization will follow the shape of the spectrum itself. In general, the wavelength resolution is about 100A in this system (will be improved).

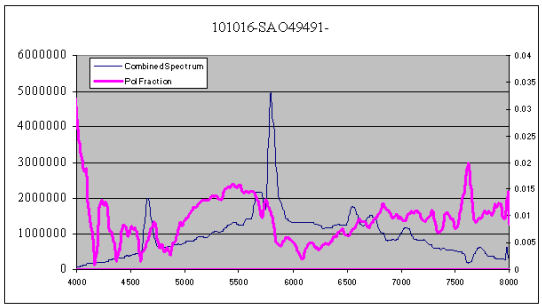

Figure 2 Example of WR140 Data Oct. 10, 2016

In low signal level regions, e.g., below 4500A in this case, the spectral data are relatively weak (low counts) , leading to relatively large fluctuations in the measured polarization. On the other hand, where there is a substantial spectral peak having good statistics, e.g., 4700A, there is usually a bipolar swing in the polarization due to slight differences in the shape and amplitudes of the slopes of the peak between the A & B spectra.

In this Figure, the most obvious polarization feature is the large hump centered at 5500: is it real? Although a somewhat similar artifact was seen occasionally in other targets, various tests seem to show that this one may be real. The second feature is the minimum at about 6100A and the ramp up to about 6800A. These have appeared in many other WR140 curves but not in other targets. Interestingly, very similar results showed 14 days later in WR140 but not in the intervening observations. It is still not proven whether these features are real or some type of artifacts.

About 40 usable nights of data were obtained, although a significant number of these had apparent background problems. Early in the campaign, these were from poor definition of the spectra and apparent intermixing due to the convergence prism, while later the effects of twilight sky background levels and gradients were apparent. Even with these challenges, the data did appear to be sufficient to demonstrate several significant changes in the polarization behavior over the period. The data were submitted to the project sponsors; however, no comment has ever been received.

Because of the complexity of the results -a mix of observational issues and apparent real changes in the WR140 system- they are difficult to summarize. Clearly, there is polarization >0.001 present. Often, but not always, features include the 5500A polarization ramp and the 6500A polarization ramp. There is no question that WR140 polarization curves differ from any other object so far observed in this project.

Assorted Stellar Observations. Many repeated observations were made of both bright and faint stars of differing spectral characteristics. Special studies were made of polarization vs. altitude (to below AM=5) or of changes due to clouds as thick as 50% obscuration. In general, except for issues of twilight sky background, none of these studies showed polarization effects at the sensitivity of this instrument.

Fig 4A shows a typical result for Navi, a class B0 emission star (note the Ha emission at 6563A), while Fig 4B shows the result for Kochab, a class K2 star. The large majority of observations show polarizations <0.001-2.

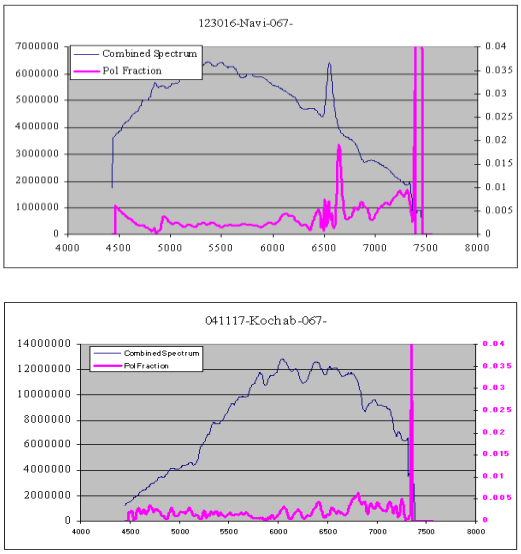

Figure 3 Example Stellar Results

Assorted Planetary Observations. One would expect the gas planets to show minimal polarization, but that the solid planets might well show polarization, and this is what is seen. Venus, Uranus, Jupiter, and Neptune all showed very small (<.003) polarization.

Solid planets (and moons) can be very different. Fig 5A shows Ganymede as essentially zero (a single observation). However, Figure 5B shows Mars having a large polarization (eg., 0.01 or 1%) that changes radically according to the Earth-Sun-Mars

phase angle. This effect has been widely studied, but would appear to be fertile ground for additional observation.

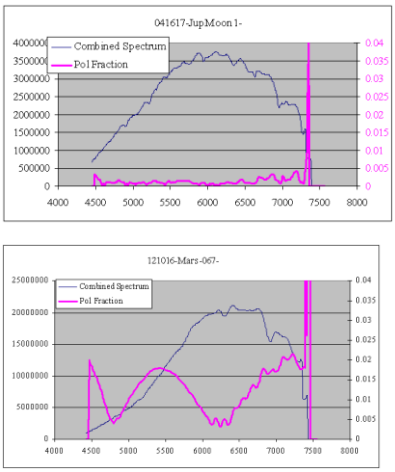

Figure 4 Example Planetary Results

6. Conclusion

The project to construct and operate an amateur, wide band, low cost spectropolarimeter has been successful. Even at this rather early stage of development, the polarization sensitivity appears to be ~0.001, and when using a C11 can operate down to about mag 8. Because the SP measurements are very sensitive, observations must be carried out with a high degree of care to avoid major error. Whether such amateur observations are of use to research science is not yet clear; however, very little amateur work has been done in SP so the potential for discovery is certainly present.

7. References

SAS2014. Spectropolarimetry: Another New Frontier. John Menke http://www.socastrosci.org/publications.html

SAS2016. A Bespoke Spectropolarimetrist. John Menke http://www.socastrosci.org/publications.html

Isaac Newton Group of Telescopes (ING) website provides standard star data and some general advice. See following and related pages http://www.ing.iac.es/Astronomy/observing/manuals/html_manuals/wht_instr/isispol/node39.html Also for discussion of calculating polarization see http://www.ing.iac.es/astronomy/observing/manuals/html_manuals/wht_instr/isis_hyper/subsubsection1.7.0.2.5.1.html#SECTION07025100000000000000

Joint Astronomy Center (JAC) website includes several lists of reference polarized and non-polarized stars. http://www.jach.hawaii.edu/UKIRT/instruments/irpol/irpol_stds.html

Clarke, D. Theoretical Considerations in the Design of an Astronomical Polarimeter. Royal Astronomical Society. This 1964 paper is a good introduction to polarimeter design and use. See http://adsabs.harvard.edu/abs/1965MNRAS.129...71C

HPOL Spectrometer at Univ. Wisconsin has excellent website with both instrumental and astronomical information. See http://www.sal.wisc.edu/HPOL/Warner, B.D., "Asteroid Photometry at the Palmer Divide Observatory." (2004). *Minor Planet Bulletin* **31**, 12-14.

A Slitless Spectrograph That Provides Reference Marks (revised 2017)

Tom Buchanan
Atlanta Astronomy Club
Post Office Box 187
Hiwasse, AR 72739, USA
tombuchan@hughes.net

Abstract

The author designed and built a slitless spectrograph to record reference marks along the spectrum of a point light source. Spectra can be taken of transient, clustered, or moving lights when a spectrograph cannot be accurately aimed at the lights to capture slit spectra. Three beams of undispersed light, directed by mirrors and lenses, provide reference marks. Near each end of the spectrum a reference mark barely varies from the corresponding point on the spectrum when the aim toward the light source varies. Within 2 degrees of perfect aim toward the light source, the variation is less than 7 angstroms. The third reference mark enables this variation to be quantified. The locations and orientations of the optical components are mathematically derived. Additional features of the spectrograph enable the use of a slit and comparison spectrum, and the recording of higher orders by moving the camera and using specific Wratten filters.

1. Introduction

The need for this spectrograph became evident to the author during his pursuit of a hobby studying nocturnal luminous phenomena. The mysterious Brown Mountain light of North Carolina was the primary target. Appalachian State has been investigating these lights (Appalachian State). The following versatile characteristics were desired in the design of the spectrograph:

1. Reference marks in the slitless mode for short-lived, moving, and clustered lights, when precise aim toward target is not possible for use with a slit spectrograph and a comparison spectrum.
2. Ability to record entire visible spectrum at one time in first order.
3. Fast optics.
4. Highest feasible resolution.
5. Portability by hand to a site some distance from the nearest parking area.
6. Self-contained, not attached to a telescope.
7. Comparison spectrum while operating in the slitless mode.
8. Portability in a suitcase aboard an airplane.
9. Ability to record higher orders by means of filters and various positions of the camera.
10. Automatic frame advancer for recording fast-changing phenomena.

2. Previous Methods of Providing Reference Marks for Slitless Spectra

In a commonly-uses method, the undispersed or "zero order" light from the source is used for a reference mark, although recorded far from the spectrum, as reported by Liu (1962) and Remus (1978).

Various methods have been proposed for providing spectral reference marks on the spectrogram recorded by a slitless spectrograph. One category of methods consists of inducing dark lines on the spectrum. One method uses transparent plane-parallel glass plates within the optical path for recording interference bands as reported by Linnik (1971). Another method records absorption lines generated by an absorbing medium in the optical path as reported by Fehrenbach (1947, 1966) and Millman (1931). Griffin (1973) reported still another method using telluric absorption lines.

Another category of methods uses convex cylindrical surfaces both to reflect the source light as a narrow image and to reflect a laboratory source of light for comparison as reported by Baskett (1970) and Lebedinsky (1955). These methods are used primarily for taking spectra of extended illuminated areas.

Still another category of methods uses a second beam from the light source to provide either a relatively undispersed point of light along the spectrum or a second spectrum. In one method, the spectrum of a star is simultaneously photographed next to a reversed spectrum of the same star as described by Fehrenbach (1966, 1947a), Millman

(1931), Geyer (1979), Gieseking (1979), and Comstock (1906).

Kirillovykh (1980) reports another method using a prism and light filters in front of a diffraction grating to produce reference points on the spectrum.

3. Description of the Spectrograph

The method described in this paper uses redirected light beams from the source to provide accurate and correctable reference marks as previously described by Buchanan (1984).

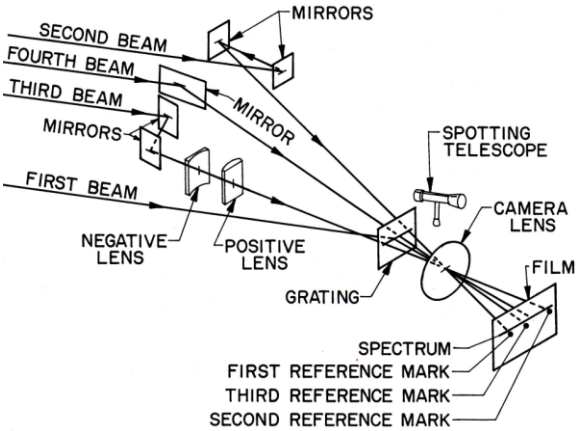

Figure 1. Isometric View of Light Beams in Slitless Spectrograph.

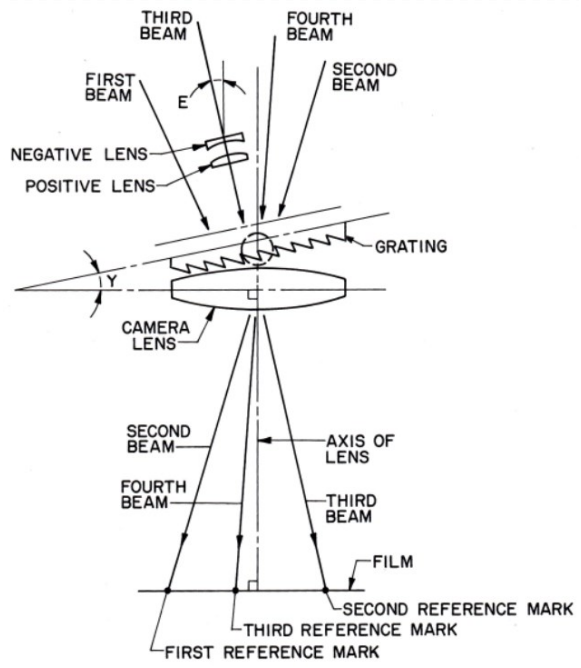

Figure 2. A Diagrammatic Plan View of Light Beams Passing through Diffraction Grating and Lens to Film.

Figure 1 is an isometric view of light beams in the slitless spectrograph. Figure 2 is a diagrammatic plan view of the light beams passing through the diffraction grating and camera lens to the film.

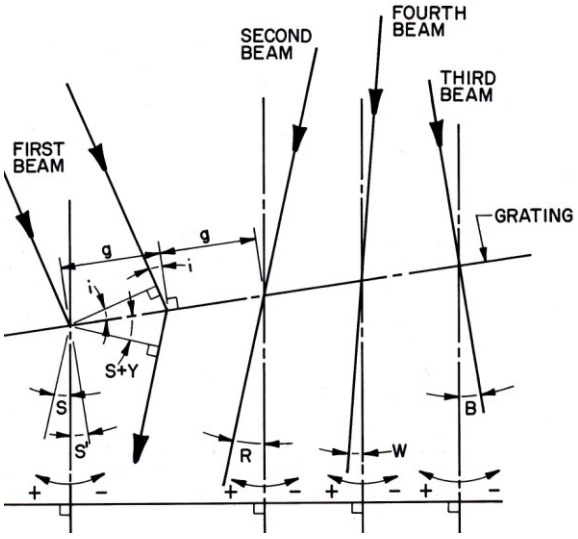

Figure 3. Enlarged View of a Small Portion of Diffraction Grating, the Circle on Figure 2, Showing Detail of Incident and Emerging Beams.

Figure 3 shows an enlarged view of a small portion of the grating surface, showing detail of the incident and emerging beams.

Ideally, the light source is a point sufficiently distant so that all photons from it are essentially parallel. A spotting telescope containing cross hairs is used to align the spectrograph toward the source. The optical elements consist of plane mirrors, lenses and a diffraction grating. All optical elements are mounted in the plane which is perpendicular to the grooves of the diffraction grating. These elements are positioned to direct four beams of light through a camera lens which focuses the light onto a recording medium. Although various recording media, such as photosensitive film or a charge couple device can be used, film is assumed in this paper.

The first beam of light strikes the diffraction grating, which disperses the light, then passes through a lens which focuses the spectrum on the film. The first beam makes an incident angle "i" with the normal to the surface of the diffraction grating, is dispersed by the grating, and emerges at an angle "S" with respect to the axis of the camera lens.

The second beam strikes a plane mirror which reflects the beam onto another plane mirror which reflects the beam through the grating, from which the camera lens. The undispersed or zero order light passes through the lens which focuses the light onto

the film at a selected position on the spectrum, forming the first reference mark.

The third beam strikes a plane mirror which reflects the light onto another plane mirror which reflects the light through a negative lens and a positive lens, resulting in collimated light at a selected magnification. This pair of lenses can also be placed in front of the mirrors. The third beam emerges from the grating at an angle "B" from this axis. The undispersed light passes through the grating and the lens, which focuses the light onto the film at a selected position on the spectrum, forming the second reference mark.

The fourth beam is reflected by a mirror directly through the grating. The lens focuses the undispersed light of the fourth beam on the film to form a third reference mark at a varying position on the spectrum. The fourth beam emerges at an angle "W" from this axis.

4. Equations for the Four Light Beams and the Optical Constants

The formulas and numerical constants of the spectrograph are derived. The number of digits used is for mathematical demonstration, and does not imply physical precision. Angles are in radians unless noted otherwise. All terms calculated with subscript "$_O$" are constants, referring to the condition when the spectrograph is perfectly aimed toward a light source.

4.1 First Beam

The equation of diffraction of light by the grating for a first order spectrum is

$$\lambda / g = \sin i + \sin (S + Y) \qquad (1)$$

where "λ" is the wave length of a spectral line in a dispersed light beam. The term "Y" is the angle between the normal to the diffraction grating and the axis of the camera lens. The term "g" is the groove spacing on the diffraction grating. A grating of 600 grooves per mm is selected. The groove spacing is

$$g = 10^7 \text{ Å} / 600 = 16{,}666.67 \text{ Å} \quad (2)$$

4.2 Second Beam

The first and second reference marks are positioned near the opposite ends of the first order of the visible spectrum. The first mark "λ_1" is set at the B-solar line due to oxygen, according to The Chemical Rubber Company (1967),

$$\lambda_1 = 6{,}869.955 \text{ Å} \qquad (3)$$

When the spectrograph is perfectly aimed,

$$R_O = S_O \qquad (4)$$

where "S_O" is the angle of the diffracted first beam with respect to the axis of camera lens at the first reference mark.

To make angle "R" of the undiffracted second beam to change at the same absolute rate as angle "S", when the angle "i" changes,

$$dR / di = dS / di = -1 \quad (5)$$

To differentiate Equation (1) with respect to "i", when "λ", "g", and "Y" are constant,

$$0 = (\cos i)\, di + \cos (S + Y)\, dS \quad (6)$$

$$dS / di = -[\cos i / \cos (S + Y)] \quad (7)$$

When "i_O" and "S_O" are substituted,

$$\cos (S_O + Y) = \cos i_O \quad (8)$$

$$\text{Solution 1: } i_O = S_O + Y \qquad (9)$$

$$\text{Solution 2: } i_O = -(S_O + Y) \qquad (10)$$

Solution 1 applies for the diffracted first order of the first beam, the condition desired. Solution 2 applies to the zeroth order of the first beam, and is of no further interest.

To solve for angle "i_O", the incident angle of the first beam at precise aim, appropriate constants are substituted into Equation (1):

$$\lambda_1 / g = \sin i_O + \sin (S_O + Y) \quad (11)$$

Since $(S_O + Y) = i_O$, from Equation (9),

$$\lambda_1 / g = 2 \sin i_O \qquad (12)$$

$$\sin i_O = \lambda_1 / 2g = 0.20609865 \quad (13)$$

$$i_O = 0.20758633 \text{ radian} = 11.893821° \quad (14)$$

4.3 Third Beam

The second reference mark "λ_2" is set at a wavelength of HI, according to the Massachusetts Institute of Technology (1969),

$$\lambda_2 = 3889.055 \text{ Å} \qquad (15)$$

This wavelength is also known as hydrogen-zeta.

To make the two reference marks to be equally spaced in angle from the axis of the camera,

$$S_O = - S'_O \quad (16)$$

where "$-S'_O$" is the angle of diffracted first beam with respect to axis of the camera lens at the second reference mark. Substituting into Equation (1),

$$\sin (Y + S_O) \quad (17)$$

and

$$\lambda_2 / g = \sin i_O + \sin (Y + S'_O) \quad (18)$$

or

$$Y + S'_O = Y - S_O = \arcsin [(\lambda_2 / g) - \sin (i_O)] = 0.027248022 \text{ radian} = 1.5611967° \quad (19)$$

To subtract Equation (19) from Equation (9), by use of Equation (14):

$$Y + S_O - (Y - S_O) = 2\ S_O = i_O - 0.027248022 \quad (20)$$

$$S_O = 0.09016915 \text{ radian} = 5.1663117° \quad (21)$$

$$S'_O = - 0.09016915 \text{ radian} \quad (22)$$

$$Y = i_O - S_O = 0.11741718 \text{ radian} = 6.727509° \quad (23)$$

Solving "R_O" by substituting in Equation (1),

$$\lambda_1 / g = \sin i_O + \sin (R_O + Y) \quad (24)$$

$$R_O = 0.09016915 \text{ radian} = 5.166312° \quad (25)$$

Solving ''B_O" by substituting in Equation (1),

$$(\lambda_2 / g) = \sin (i_O) + \sin (Y + B_O) \quad (26)$$

$$B_O = - 0.09016915 \text{ radian} = - 5.166312° \quad (27)$$

When the spectrograph is precisely aimed,

$$S'_O = B_O \quad (28)$$

The angle "B" of the undiffracted second beam is selected to change at the same rate as angle "S" of the diffracted first beam, when angle "i" changes. This condition can be satisfied only if the third beam is magnified.

$$dE / di = 1 \quad (29)$$

$$dB / di = m_O (dE / di) = dS / di \quad (30)$$

where "E" is the incident angle of the unmagnified third beam as shown in Figure 2, and "B" is the incident angle after magnification. To solve for the required magnification ratio "m_O":

$$dS / di = - m_O = - \cos (i_O) / \cos (S'_O + Y) \quad (31)$$

$$m_O = [\cos (i_O)] / \cos (S'_O + Y) = 0.9788946 \quad (32)$$

4.4 Fourth Beam

The fourth beam emerges from the grating at an angle "W", which changes in the opposite direction from the emerging diffracted beam when the angle of incidence changes. The fourth beam is reflected once and is unmagnified. For determining "W_O", the fourth beam can be set to be midway between the second and third beams when "$i = i_O$". Therefore,

$$W_O = (R_O + B_O) / 2 = 0° \quad (33)$$

Therefore,

$$R - R_O = W_O - W = (B - B_O) / m_O = i_O - i \quad (34)$$

5. Positions of Reference Marks on Film

Figure 4 contains a diagrammatic plan view showing the camera lens, the emerging angles of the undiffracted second, third, and fourth beams, the film, and the corresponding reference marks when the spectrograph is precisely aimed at the light source. The dimension "f" represents the focal length of the camera lens, which is selected to be 135 mm. The lower portion contains a diagrammatic rear elevation view of the spectrum and reference marks.

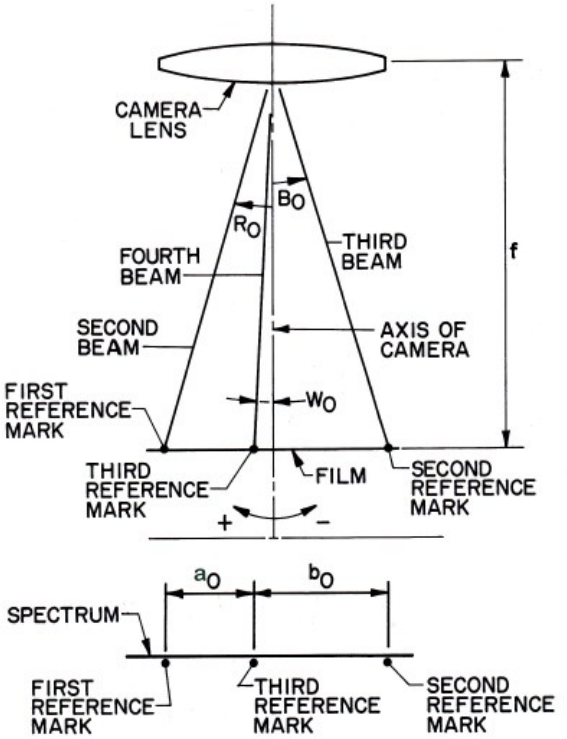

Figure 4. Diagrammatic Views of Camera Lens, Emerging Undiffracted Beams, Film, and Reference Marks When Spectrograph is Precisely Aimed at Light Source.

Figure 5 contains a diagrammatic plan view showing the camera lens and film, the emerging undiffracted beams, an unknown diffracted component of the first beam, the reference marks, and the position along the spectrum of the unknown spectral line, when the spectrograph is not precisely aimed at the light source. The dimension "a" is the distance between the first and third reference marks, and "b" is the distance between the second and third reference marks. The dimension "d" is the distance from the first reference mark to a spectral line. The lower portion contains a diagrammatic rear elevation view of the spectrum and reference marks.

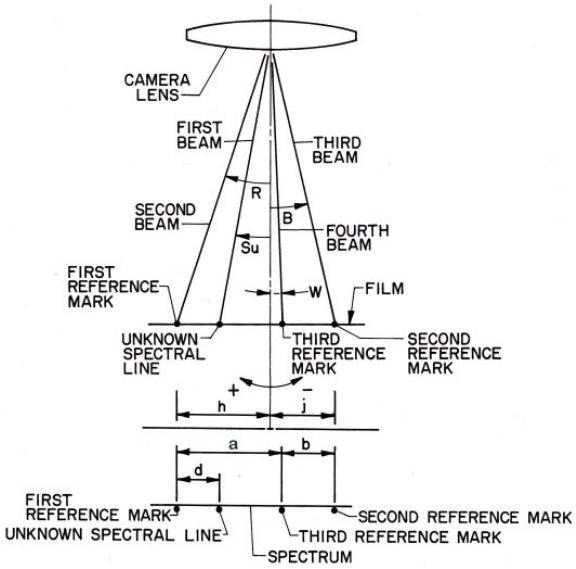

Figure 5. Diagrammatic Views of Camera Lens, Emerging Undiffracted Beams, Film, and Reference Marks When Spectrograph is Not Precisely Aimed at Unknown Light Source.

From Figures 4 and 5 these equations can be deduced:

$$f = 135 \text{ mm} \quad (35)$$

$$a = f(\tan R - \tan W) \quad (36)$$

$$b = f(\tan W - \tan B) \quad (37)$$

and that specific equations for perfect aim are:

$$a_O = f(\tan R_O - \tan W_O) = 12.205934 \text{ mm} \quad (38)$$

$$b_O = f(\tan W_O - \tan B_O) = 12.205934 \text{ mm} \quad (39)$$

Figure 6 is a diagrammatic representation of a spectrogram recorded when the spectrograph is aimed generally toward a group of three light sources having various elevations and directions. When the spectrograph records multiple point sources of light, the spectra of all sources along with their respective reference marks are simultaneously recorded.

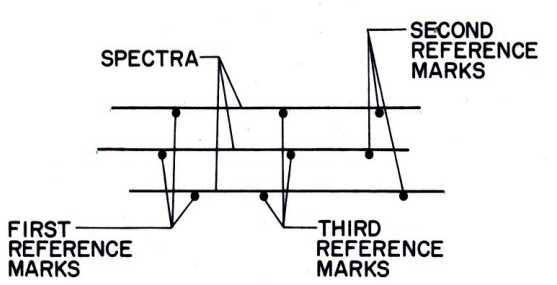

Figure 6. Spectrum Recorded When Spectrograph Is Aimed toward a Group of Three Light Sources.

6. Derivation of Formula for Calculating an Unknown Spectral Line

Subtracting Equation (38) from Equation (36):

$$(a - a_O) = f (\tan R + \tan W_O - \tan R_O - \tan W) \quad (40)$$

When substitutions for "R" and "W" are made from Equation (34):

$$(a - a_O) / f + \tan R_O - \tan W_O = - \tan [(i - i_O) - R_O] - \tan [(i - i_O) + W_O] \quad (41)$$

Since $W_O = 0$, from Equation (33):

$$a_O / f = \tan R_O \quad (42)$$

and

$$a / f = - \tan [(i - i_O) - R_O] - \tan (i - i_O) \quad (43)$$

where "a" is the independent variable and "i" is unknown. Separating the "i" term and placing all terms containing "i" on the left side of the equation:

$$\tan [i - (i_O + R_O)] + \tan (i - i_O) = - a / f \quad (44)$$

To use this trigonometric identity:

$\tan (x - y) \equiv (\tan x - \tan y) / [1 + (\tan x)(\tan y)]$:

$$\frac{\tan i - \tan (R_O + i_O)}{1 + (\tan i)[\tan (R_O + i_O)]} + \frac{(\tan i)(\tan i_O)}{1 + (\tan i)(\tan i_O)}$$

$$= - a / f \quad (45)$$

To facilitate algebraic manipulation, the following terms are substituted:

$$I = \tan i \quad (46)$$

where "I" is a dependent variable to be solved.

$$J = \tan (i_O) = 0.21062041 \quad (47)$$

$$L = \tan (R_O + i_O) = 0.30687866 \quad (48)$$

Therefore:

$$(I - L) / (1 + IL) + (I - J) / (1 + IJ) = - a / f \quad (49)$$

Using the common denominator:

$$\frac{[(I - L)(1 + IJ) + (I - J)(1 + IL)]}{[(1 + IL)(1 + IJ)]} = - \frac{a}{f} \quad (50)$$

Expanding terms and multiplying equation through by: "f [(1 + IL)(1 + IJ)]":

$$If + I^2Jf - Lf - IJLf + If + I^2Lf - Jf - IJLf = - a [1 + IJ + IL + (I^2) JL] \quad (51)$$

Collecting terms in descending exponents of "I":

$$I^2 [f(J + L) + (JL)a] + I [2 f(1 - JL) + (J + L)a] + [- f (J + L) + a] = 0 \quad (52)$$

$$A_qI^2 + B_qI + C_q = 0 \quad (53)$$

Since the solution to the quadratic equation is

$$x = \frac{-b \pm \sqrt{b^2 - 4ac}}{2a}$$

$$I = \frac{- B_q +/- [(B_q)^2 - 4 A_qC_q]^{0.5}}{2A_q} \quad (54)$$

Setting $A_q = 1/2$:

$$I = - B_q +/- [(B_q)^2 - 2C_q]^{0.5} \quad (55)$$

Setting $A_q = 1/2$, and dividing Equation (52) through by "2 [f (J + L) + JLa]":

$$\frac{I^2}{2} + \frac{I[2f(1 - JL) + (J + L)a]}{[2f(J + L) + 2JLa]} + \frac{[- f(J + L) + a]}{[2f(J + L) + 2JLa]} = 0 \quad (56)$$

Putting "a" terms on the right and dividing numerator and denominator of "B_q" by "2JL":

$$B_q = \frac{[a(J + L) / (2JL) + f(1 - JL) / (JL)]}{a + [f(J + L) / JL]} \quad (57)$$

The denominator is divided into the numerator, resulting in only one input term "a":

$$B_q = \frac{J + L}{2JL} - \frac{(f / JL)(1 - JL) - f[(J + L)^2 / 2(JL)^2]}{a + [f(J + L) / JL]} \quad (58)$$

Quantifying all known terms:

$$B_q = 4.0032474 - [2373.3627 / (a + 1080.8768)] \quad (59)$$

From Equation (55):

$$C_q = [a - f(J + L)] / [2JLa + 2f(J + L)] \quad (60)$$

The numerator and denominator of "C_q" are divided by "2JL", and the "a" terms are placed on the right:

$$C_q = \frac{(a / 2JL) - (f / 2JL)(J + L)}{a + [f(J + L) / JL]} \quad (61)$$

The denominator is divided into numerator, resulting in only one input term "a":

$$C_q = \frac{1}{2JL} - \frac{(f/2)(J+L)[(1/JL^2) + (1/JL)]}{a + [f(J+L)/JL]} \quad (62)$$

Quantifying all known terms:

$$C_q = 7.735758 - [8901.839/(a + 1080.8768)] \quad (63)$$

To compare actual measurement of "(a + b)" against theoretical value, "(a_O + b_O)" is solved as a function of "i" from Equations (33) and (36):

$$a + b = a + f \{\tan [(i - i_O) + W_O] - \tan [B_O - m_O (i - i_O)]\} \quad (64)$$

Since $W_O = 0$:

$$a + b = a + f \{\tan [(i - i_O)] + \tan [m_O (i - i_O) - B_O]\} \quad (65)$$

$$a + b = a + 135 \tan [iI - 0.20758633] + \tan [0.9788946 (i - 0.20758633) + 0.09016915)] \quad (66)$$

7. Calculation of an Unknown Spectral Line

The spotting scope is aimed imprecisely at an unknown light source, and an exposure is made. Measurements on the developed film disclose that:

$$a = 19.237 \text{ mm}, \quad (67)$$

$$b = 5.265 \text{ mm}, \quad (68)$$

$$d = 4.856 \text{ mm} \quad (69)$$

From Equations (46, 55, 59, 63):

$$i = 0.18168767 \quad (70)$$

From Equation (34):

$$R = i_O - i + R_O = 0.11606781 \quad (71)$$

$$h = f \tan R \quad (72)$$

where "h" is the distance of the first reference mark from axis of camera lens.

$$h = 135 \tan R = 15.739899 \quad (73)$$

$$j = - f \tan B \quad (74)$$

where "j" is the distance of second reference mark from axis of camera lens.

The term "Su" is the angle of the unknown spectral line with respect to axis of camera lens:

$$\tan Su = (h - d) / f \quad (75)$$

$$Su = \text{Arctan} [(h - d) / f] = 0.08044748 \quad (76)$$

The wavelength of the spectral line, "λu", is determined by substitutions in Equation (1):

$$\lambda u = g [\sin i + \sin (Su + Y)] = 6287.8 \text{ Å} \quad (77)$$

8. Spreadsheet Solution

Based on the known parameters of the spectrograph, the term "i" is solved for each value of "a" and . "d" in Table 1.

The term "d" is first input at column A; therefore, the values on lines 7 to 17 are repeated from line 18 downward. They are omitted in columns C to E and in columns G to I, since they are not used in subsequent calculations.

Table 1 shows that the error between the first reference mark and the target wavelength position ranges up to 7.02 Å. The error between the second reference mark and the target wavelength position ranges up to 3.94 Å. Figure 7 shows the errors as related to "a / a +b".

The average dispersion for "$i_O = 0.2065$" is:

$$(6869.955 - 3889.055) / 24.415 \text{ mm} = 122.09 \text{ Å / mm}.$$

The width of exposed film for 35-mm film is 36 mm. The half length of exposed area on film is:

$$36 \text{ mm} / 2 = 18 \text{ mm}$$

When "a = 0", first and third reference marks coincide. From Equation (74) and Figure 5:

$$j = - f \tan B = - f \tan[-m_O(i - i_O) + B_O] = 18.240 \text{ mm} > 18 \text{ mm}$$

The second reference mark lies outside exposed area.

When "a" = 24.5 mm, and "a + b" = 24.591 mm, the second and third reference marks almost coincide.

From Table 1, h = 18.39 mm > 18 mm, indicating that the first reference mark falls outside the exposed area. Therefore, when all three reference

marks are present, the third mark normally lies between the first and second marks.

Figure 7 graphically shows the errors as functions of imprecise aim.

	A	B	C	D	E	F	G	H	I	J	K	L	M	N
1	Table 1. Calculation of Wave Lengths for a Slitless Spectrograph													
2		io= 0.20758633		mo= 0.9788946		Bo= -0.09016915		Ro= 0.09016915		g= 16666.667		Y= 0.11741718		f= 135.000
3	d	a	Bq	Cq	tan i = I	i	tan (i - io)	tan B	a + b	h, Fig. 5	Su	Lambda	a / (a + b)	Error
4			Eq. (59)	Eq. (63)	Eq. (46), (55)	atan (E5)	tan(F6 - B$2)	Eq. (34)	B6+(N$2	N$2*tan	atan((J6-A6)	J$2*(sin(F6)+	B6 / I6	L7-L$12
5									*(G6-H6))	(B$2-F6+H$2)	/N$2)	(sin(K6+L$2)))		
6	4.856	19.237	1.8458681	-0.35598578	0.18371328	0.18168734	-0.025904778	-0.06490770	24.502	15.739944	0.08044781	6287.76	0.78511	
7	0.000	0.000	1.8074720	-0.49999930	0.25818858	0.25267059	0.045114833	-0.13511523	24.331	6.090588	0.04508489	6862.97	0.00000	-6.98
8	0.000	2.500	1.8125390	-0.48099447	0.24835561	0.24343040	0.035859432	-0.12591592	24.340	7.341109	0.05432508	6865.54	0.10271	-4.41
9	0.000	5.000	1.8175826	-0.46207715	0.23856934	0.23419180	0.026611752	-0.11673912	24.352	8.592673	0.06356368	6867.52	0.20532	-2.43
10	0.000	7.500	1.8226031	-0.44324673	0.22882946	0.22495637	0.017371791	-0.10758482	24.369	9.845278	0.07279911	6868.92	0.30777	-1.03
11	0.000	10.00	1.8276005	-0.42450263	0.21913564	0.21572570	0.008139550	-0.09845300	24.390	11.098926	0.08202978	6869.73	0.41000	-0.22
12	0.000	12.50	1.8325751	-0.40584424	0.20948757	0.20650136	-0.001084971	-0.08934367	24.415	12.353617	0.09125412	6869.95	0.51198	0.00
13	0.000	15.00	1.8375270	-0.38727098	0.19988494	0.19728492	-0.010301772	-0.08025681	24.444	13.609349	0.10047056	6869.59	0.61365	-0.36
14	0.000	17.50	1.8424564	-0.36878226	0.19032743	0.18807795	-0.019510853	-0.07119242	24.477	14.866124	0.10967753	6868.65	0.71496	-1.30
15	0.000	20.00	1.8473634	-0.35037752	0.18081474	0.17888200	-0.028712215	-0.06215048	24.514	16.123940	0.11887348	6867.13	0.81585	-2.83
16	0.000	22.50	1.8522481	-0.33205619	0.17134657	0.16969861	-0.037905857	-0.05313098	24.555	17.382799	0.12805687	6865.02	0.91630	-4.93
17	0.000	24.50	1.8561400	-0.31745879	0.16380388	0.16236197	-0.045255212	-0.04593154	24.591	18.390637	0.13539351	6862.93	0.99629	-7.02
18	6.000	0.000				0.25267059				6.090588	0.00067102	6130.08		
19	6.000	2.500				0.24343040				7.341109	0.00993381	6134.01		
20	6.000	5.000				0.23419180				8.592673	0.01920262	6137.54		
21	6.000	7.500				0.22495637				9.845278	0.02847584	6140.66		
22	6.000	10.00				0.21572570				11.098926	0.03775188	6143.39		
23	6.000	12.50				0.20650136				12.353617	0.04702912	6145.72		
24	6.000	15.00				0.19728492				13.609349	0.05630597	6147.64		
25	6.000	17.50				0.18807795				14.866124	0.06558081	6149.16		
26	6.000	20.00				0.17888200				16.123940	0.07485204	6150.27		
27	6.000	22.50				0.16969861				17.382799	0.08411807	6150.98		
28	6.000	24.50				0.16236197				18.390637	0.09152606	6151.26		
29	12.000	0.000				0.25267059				6.090588	-0.04374550	5393.26		
30	12.000	2.500				0.24343040				7.341109	-0.03449661	5397.85		
31	12.000	5.000				0.23419180				8.592673	-0.02523411	5401.82		
32	12.000	7.500				0.22495637				9.845278	-0.01595955	5405.79		
33	12.000	10.00				0.21572570				11.098926	-0.00667452	5409.55		
34	12.000	12.50				0.20650136				12.353617	0.00261938	5413.09		
35	12.000	15.00				0.19728492				13.609349	0.01192054	5416.42		
36	12.000	17.50				0.18807795				14.866124	0.02122736	5419.53		
37	12.000	20.00				0.17888200				16.123940	0.03053821	5422.43		
38	12.000	22.50				0.16969861				17.382799	0.03985148	5425.11		
39	12.000	24.50				0.16236197				18.390637	0.04730274	5427.09		
40	18.000	0.000				0.25267059				6.090588	-0.08799008	4656.89		
41	18.000	2.500				0.24343040				7.341109	-0.07879130	4660.83		
42	18.000	5.000				0.23419180				8.592673	-0.06957144	4664.74		
43	18.000	7.500				0.22495637				9.845278	-0.06033204	4668.63		
44	18.000	10.00				0.21572570				11.098926	-0.05107461	4672.50		
45	18.000	12.50				0.20650136				12.353617	-0.04180070	4676.35		
46	18.000	15.00				0.19728492				13.609349	-0.03251188	4680.18		
47	18.000	17.50				0.18807795				14.866124	-0.02320973	4683.99		
48	18.000	20.00				0.17888200				16.123940	-0.01389584	4687.77		
49	18.000	22.50				0.16969861				17.382799	-0.00457183	4691.52		
50	18.000	24.50				0.16236197				18.390637	0.00289360	4694.51		
51	24.331	0.000				0.25267059			24.331	6.090588	-0.13430128	3885.12	0.00000	-3.94
52	24.340	2.500				0.24343040			24.340	7.341109	-0.12525610	3886.57	0.10271	-2.49
53	24.352	5.000				0.23419180			24.352	8.592673	-0.11621248	3887.69	0.20532	-1.37
54	24.369	7.500				0.22495637			24.369	9.845278	-0.10717196	3888.48	0.30777	-0.58
55	24.390	10.00				0.21572570			24.390	11.098926	-0.09813610	3888.94	0.41000	-0.13
56	24.415	12.50				0.20650136			24.415	12.353617	-0.08910644	3889.06	0.51198	0.00
57	24.444	15.00				0.19728492			24.444	13.609349	-0.08008451	3888.86	0.61365	-0.20
58	24.477	17.50				0.18807795			24.477	14.866124	-0.07107185	3888.33	0.71496	-0.73
59	24.514	20.00				0.17888200			24.514	16.123940	-0.06206998	3887.47	0.81585	-1.59
60	24.555	22.50				0.16969861			24.555	17.382799	-0.05308041	3886.29	0.91629	-2.77
61	24.591	24.50				0.16236197			24.591	18.390637	-0.04589861	3885.12	0.99628	-3.94

Table 1. Calculation of Wave Lengths for a Slitless Spectrograph.

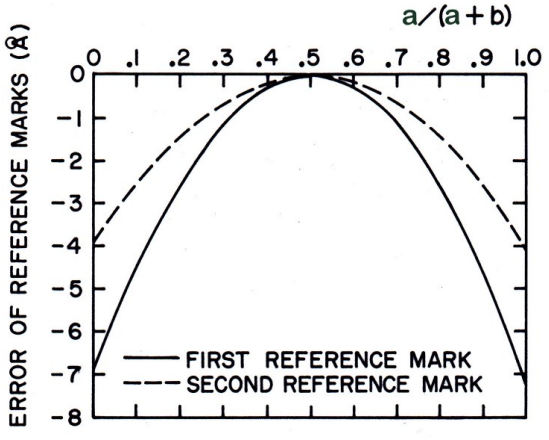

Figure 7. Errors of Reference Marks as Functions of Imprecise Aim of Spectrograph toward Light.

Figure 8. The Author with the Spectrograph on an Equatorial Mount. The Round Mask Reduces Sky Glow. Picture Was Taken after Two Holes in Front Were Enlarged and Combined.

9. Description of Components in the Constructed Prototype

The wooden housing of the spectrograph measures 13 inches by 26 inches by 6.75 inches (66 cm by 33 cm by 17 cm) and weighs 16 lb. (7.3 kg), including 35-mm camera and lens. The spectrograph can be operated in either the slitless mode or the slit mode. Figure 8. shows the mounted spectrograph.

A separate unit weighing 5.5 lb. (2.5 kg) and containing an objective lens, a slit, a 45-degree mirror, and a collimating lens can be inserted into the spectrograph housing, and a comparison spectrum can be exposed adjacent to the target spectrum. Both of these lenses have a focal length of 135 mm and an aperture of 71 mm. The unknown light focused by the objective lens illuminates one half of the slit; a known emission source shines onto a mirror which reflects the light through the other half of the slit. The calibration lamp, usually a small fluorescent light, is placed under a hole in the bottom to reflect from the mirror through the slit. This light produces spectral lines of mercury for a comparison spectrum.

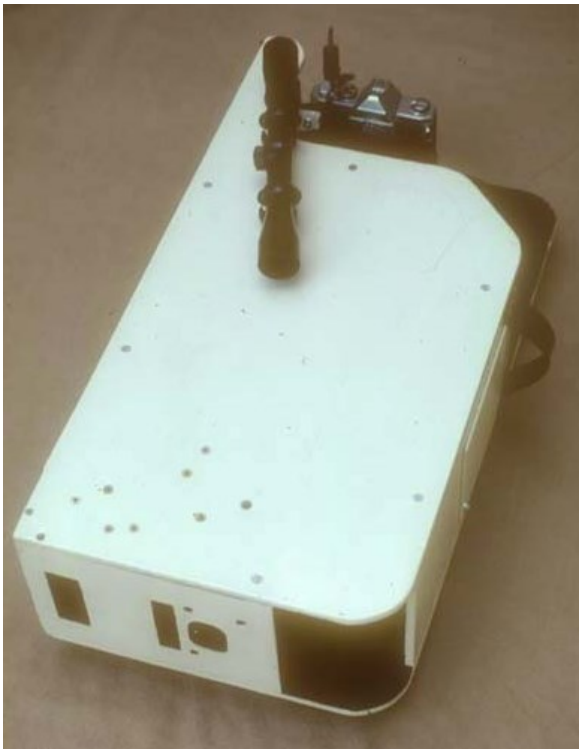

Figure 9. Front Top View of Spectrograph.

The dispersing element of the prototype is a blazed transmission diffraction grating having 600 grooves per millimeter. The lens and film are mounted in a commercial 35 mm camera. The camera lens has a focal length of 135 mm and an aperture of 71 mm. An automatic film winder is attached to the camera.

All mirrors are plane first surface mirrors to avoid ghost reflections. Spherical lenses in the third beam cause a slight shift of the vertical position of the second reference mark with respect to the horizontal spectrum. Cylindrical lenses magnify light only in the direction perpendicular to the grating grooves. cylindrical lenses are preferred in order to limit the distance of shift. When the incident light varies vertically from the horizontal axis of the system, the reference marks vary somewhat in vertical position with respect to the spectrum due to the distortion of the spectrum, according to Miranda (1965).

Figure 10. Top Rear View of Spectrograph with Camera in Position 3.

10. Additional Features of the Spectrograph

The spectrograph contains additional features for versatility. A hinged flap can be lowered to cover the paths of the second, third, and fourth beams to prevent reference marks from being recorded. For most stars, the spectrograph is aligned with the grating grooves perpendicular to the pole and the drive is turned off for one second at regular intervals. The spectrum is spread vertically. The beams providing the reference marks are blocked about two thirds of the exposure time, since they do not need to be spread as much as the spectrum.

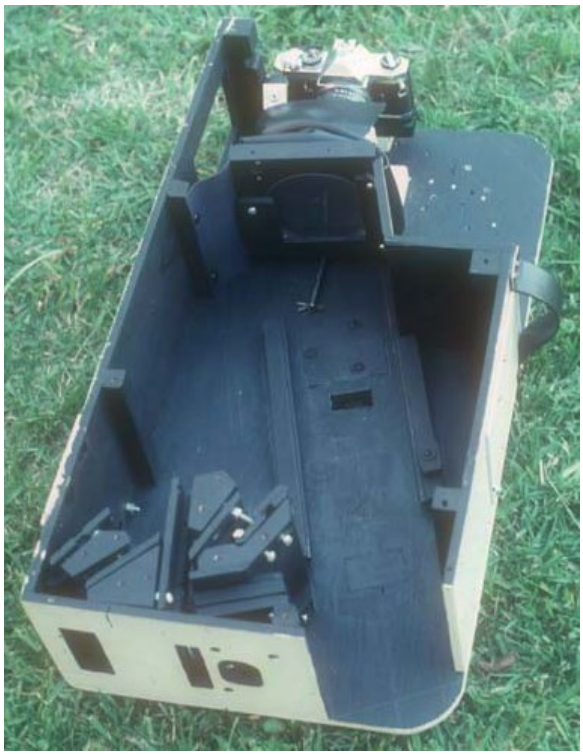

Figure 11. Inside Front View of Spectrograph.

Figures 9 through 12 show various views of the inside and outside of the spectrograph. The camera lens with camera and film are mounted on a board which can be locked by two wing bolts at any of several positions about an axis vertically aligned with the center of the diffraction grating. Spectra for adjacent positions overlap slightly. The approximate angle between positions 1 to 2, 2 to 3, 3 to 4, and 4 to 5 is 12.5 degrees. The angle between positions 5 to 6 is 12.3 degrees. The angle between positions 6 to 7 is 11.9 degrees. The camera mount is underlain by a steel channel, open on the bottom, which pivots on a peg set in the housing base under the center of the grating.

The first order of the visible spectrum can be photographed in one position, and parts of the second and third orders can be photographed in other positions. Various Wratten filters are used to prevent overlapping of orders. The filters are described by Eastman Kodak Company (1973). Table 2 lists each position, with corresponding order, approximate range of wave lengths, and filter.

Table 2. Positions, Orders, Ranges of Wave Lengths, and Filters			
Position	Order	Range, Angstroms	Wratten Filter #
1	1	3800 - 7000	none
2	2	3800 - 5200	none
3	2	5150 - 6870	8
3	3	3800 - 4450	34 and 38A
4	3	4400 - 5350	38A
5	3	5270 - 5950	12
6	3	5910 - 6400	22
7	3	6390 - 6600	22
5	4	3950 - 4450	34 and 38A
6	4	4435 - 4820	38A
7	4	4800 - 4900	2B and 38A

Table 2. Positions, Orders, Ranges of Wave Lengths, and Filters.

Figure 12. Inside Top View of Spectrograph Showing Slit Unit in Place. A Corner of Camera Support Is Set on a White Dot, Position # 1, for First Order. Seven Dots Mark All Positions.

Figure 13 identifies parts of the inside of the spectrograph without the slit unit.

11. Examples of Spectra Obtained

Spectra have been obtained of stars as dim as magnitude 5.0. Several primary emission lines have been obtain for nebulas as dim as magnitude 8.5. Figures 14 through 19 show examples of stellar and solar spectra, and a flash spectrum of a total solar eclipse.

This instrument provided much data on the natural and man-made light sources near publicized mystery lights at several geographic locations. It also provided useful spectra of Comet Halley as reported by Edberg (1996).

12. Conclusions

This slitless spectrograph has particular applicability to determining spectra of moving, multiple, and transient luminous events. The film version requires no outside power source or internal light. The operator roughly points the instrument at a light source and takes a photograph. The practical field width approaches 2 degrees in every direction from the light source.

The author is currently replacing the film camera with a digital camera, with expectations of higher quality spectra.

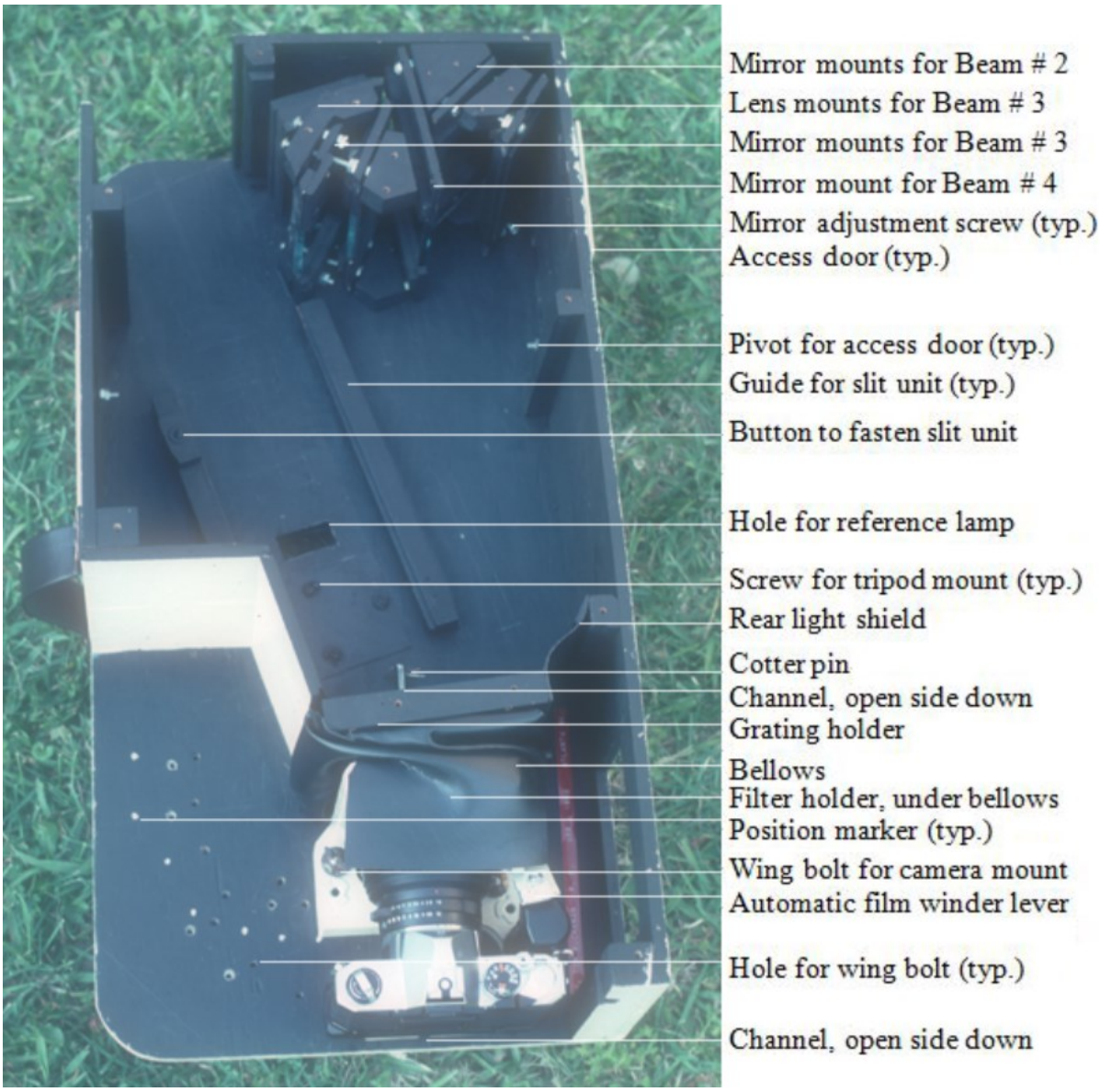

Figure 13. View of Inside without Slit Unit, Showing Identified Parts.

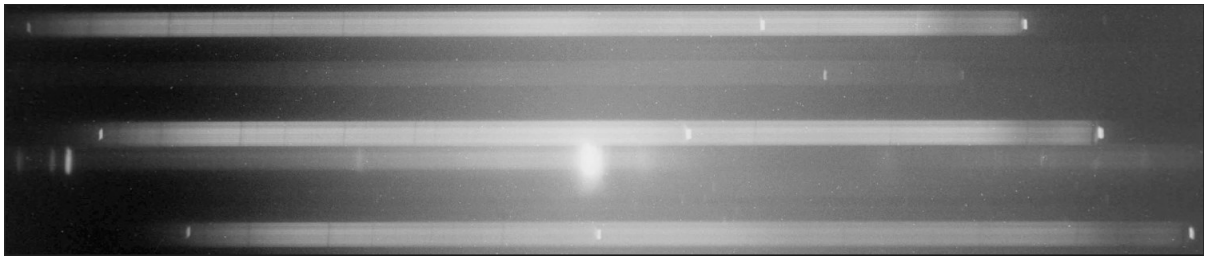

Figure 14. Slitless Spectrum of Belt of Orion, Showing Spectral Reference Marks, One at Each End and One Between.

5890^ Figure 15. Slitless Spectrum of Second Order of AlpOri from 5890 to 6563 Angstroms. 6563^

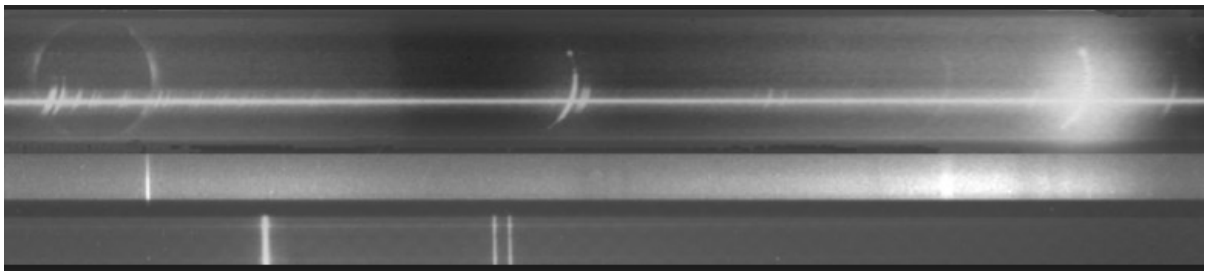

Figure 16. Flash Spectra of 1983 Total Solar Eclipse. Top Section Shows Slitless Spectrum. Bottom Half Shows Slit Spectrum of Corona and of Fluorescent Light.

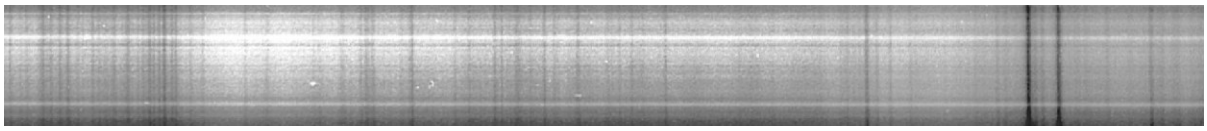

Figure 17. Slit Spectrum of Sun, Showing Third-Order Sodium Doublet at 5890-5896 Angstroms. ^ ^

Figure 18. Slit Spectrum of ^ Sun, Showing Fourth-Order Hydrogen Gamma Line, 4340 Angstroms.

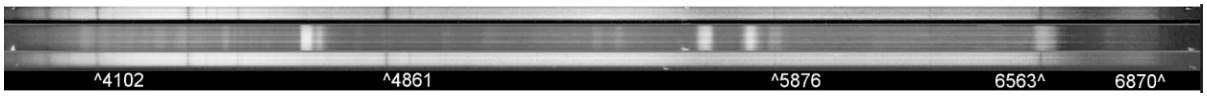

Figure 19. Slitless Spectra of EpsCen, GamVel, and AlpLup on 11 Apr 1986 and Juxtaposed.

13. Acknowledgments

W. R. Buchanan, the author's father, who assisted in the construction of the spectrograph.

The drafter, whose name is lost, who drew the original Figures 2 to 7 in India ink on 100% cotton paper in 1985.

J. R. Washburn, who primed the author's interest in spectroscopy while both were college students.

R. G. Bostrom, who taught the author much about spectroscopy.

14. References

Appalachian State
, (http://brownmountainlights.org/)

Baskett, J. R. and Liu, I. D.; "Anamorphic Condensing Optics for a Slitless Spectrograph." (1970). Applied Optics, Vol. 9, No. 1, 49-52

Buchanan, William T.; "Spectrograph Providing Spectral Reference Marks." (April 1984). U. S. A. Patent # 4,441,814

Comstock, George C.; "A Proposed Method for the Determination of Radial Velocities of Stars." (1906). The Astrophysical Journal, Volume XXIII, 148-151

Eastman Kodak Company, "Kodak Filters for Scientific and Technical Uses." (1973). Standard Book Number 0-87985-029-9, First Edition

Edberg, Stephen J., "The Archive of The Amateur Observation Network of The International Halley Watch." (1996). National Aeronautics and Space Administration, Jet Propulsion Laboratory, Publication 96-3, Vol. 2; vii, 22-23, 32

Fehrenbach, Charles; "Recherches sur la Mesure des Vitesses Radiales au Prisme Objectif." (1947). Annales D'Astrophysique, vol. 10, No. 3, 257-281

Fehrenbach, Charles; "Recherches sur la Mesure des Vitesses Radiales au Prisme Objectif." (1947a). Annales D'Astrophysique, Vol. 10, No. 4, 306-328

Fehrenbach, Ch.; "Objective Prisms and Measurement of Radial Velocities." (1966). Advances in Astronomy and Astrophysics, Vol. 4, 1-26

Geyer, E. H. et al.; "On the Use of a Focal-reducer System for Slitless Fieldspectroscopy." (1979). Astronomy and Astrophysics, vol. 80, 248-251

Gieseking, Frank; "Measuring Radial Velocities with an Objective Prism." (1979). Sky and Telescope, 142-144

Griffin. R. and R.; "On the Possibility of Determining Stellar Radial Velocities to 0.01 Km/S." (1973). Monthly Notices of the Royal Astronomical Society, Vol 162, 243-253

Lebedinsky, A. I.; "A Slitless Spectrograph Designed to Photograph the Spectra of Aurorae." (1955). The Airglow and the Aurorae, 388-394

Linnik, V. P.; "A Slitless Stellar Spectrograph with Guiding and Spectral Reference Lines." (1971). New Techniques in Astronomy, Chap. I-29, 289-295

Kirillovykh, V. A.; "Diffraction grating spectrograph - uses prism and light filters in front of grating to produce reference points on recorded spectrum." (December 1980). U. S. S. R. Patent #787-909

Liu, I. D.; "Spectra Associated with High-Speed Projectiles in Rarefied Air Obtained with a Large-Aperture Slitless Spectrograph." (1962). Applied Optics, Vol. 1, No. 5, 675-677

Harrison, G. R., Wavelength Tables (Cambridge MA: The M. I. T Press), (1969), 37, 106, 151, 176, 192, 202.

Millman, Peter M.; "Objective Prism Radial Velocities." (1931). Journal of the Royal Astronomical Society of Canada, Vol. XXV, No. 7, 281-293

Miranda, Henry A., Jr.; "Apparent Distortion in a Slitless Spectrograph. " (1965). Applied Optics, Vol. 4, No. 7, 809-813

Remus, G. and Sastri, V. D. P.; "Fisheye field spectrograph. " (1978). Applied Optics, Vol. 17, No. 19, 3076-3080

Weast, C. & Selby, S., The Chemical Rubber Company, "CRC Handbook of Chemistry and Physics. " (1967). 48th Edition, E-133

Astronomical Instrumentation Systems Quality Management Planning: AISQMP

Jesse Goldbaum
Tierra Astronomical Institute
23717 Miranda St., Woodland Hills, CA 91367
jesse@tierra-astro.org

Abstract

The capability of small aperture astronomical instrumentation systems (AIS) to make meaningful scientific contributions has never been better. The purpose of AIS quality management planning (AISQMP) is to ensure the quality of these contributions such that they are both valid and reliable. The first step involved with AISQMP is to specify objective quality measures not just for the AIS final product, but also for the instrumentation used in its production. The next step is to set up a process to track these measures and control for any unwanted variation. The final step is continual effort applied to reducing variation and obtaining measured values near optimal theoretical performance. This paper provides an overview of AISQMP while focusing on objective quality measures applied to astronomical imaging systems.

1. Introduction

Typically associated with manufacturing, quality management pertains to all types of deliverables. Results from an astronomical instrumentation system (AIS) can be regarded as deliverables provided to the scientific community. Quality management not only ensures the quality of results, it's also helpful in preventing and assisting with the early detection and rapid resolution of AIS performance issues. Some larger observatories already have quality management practices in place[3].

Ensuring quality means that results from an AIS are both valid and reliable. Validity asserts that results are accurate to a verifiable precision, such that they're reproducible by other AISs. Reliability ensures that valid results are consistently obtained. Certification of validity and reliability is based on adherence to and thorough documentation of the quality management process.

Quality management can be divided into four areas: planning, control, assurance and improvement. Planning begins by recognizing the need to set quality goals for an AIS. It next identifies the components of an AIS that independently play a role determining the quality of the final product. Planning next specifies the measurements taken and control procedures used in the control process. Control implements the above procedures which typically involve recording and tracking the objective measurements identified in the planning process. Assurance verifies that the measurements are within a specified performance range, while improvement focuses on adjusting planning in looking for ways to minimize variation and improve precision and reliability. The degree of quality management for an AIS should be based on result requirements and resources available. In general, the stricter the result requirement, the more demanding the quality management effort becomes. While this paper will focus on quality management planning for AISs dedicated to producing astronomical images (hence the 'I' in AIS can now stand for imaging) the basic principles can be extended not only to other AIS instances but to almost any type of instrumentation system producing a standard result.

2. AISQMP Overview

The first step in AIS quality management planning (AISQMP) starts with defining objective quality measures of an astronomical image and the instrumentation used to produce it. After these measurements have been defined, target values for these measurements are identified. The target values are often constrained by the practical limits which an AIS can achieve. That is, an astronomical image can be no better than the AIS used to produce it. For example pixel size and aperture diameter define a theoretical limit to an image's resolution. In practice theoretical limits are rarely achieved because of natural variation and degradation from external sources. Site conditions such as seeing typically induce an expected degradation from the theoretical

[3] See for example http://www.eso.org/observing/dfo/quality/ and http://ccdqc.ing.iac.es/

target limit for resolution. Mechanical (e.g. mount) and electronic (e.g. camera) systems have a natural variation in their noise contributions about the target value. These contributions generate a range of output values that provide the boundary conditions to the acceptable variation. The extent of this natural variation is often not known a priori, in which case an initial set of measurements is used to come up with a starting estimate. As time progresses, quality management planning looks at ways to reduce the initial variation estimate, with the goal of converging on an optimal value.

The next step is to determine the method and frequency of obtaining measurements for tracking purposes. These values must be repeatable to the extent that they can be reliably compared to determine variation. The method of tracking these values depends on their nature of variation. Tracking may be as simple as recording the dates of a maintenance activity or it may involve a quality control chart[4] using e.g. standard spreadsheet software. One caveat to using a standard control chart is the requirement that the variation of quality measure follow a normal distribution and this may often not be the case. For example, the distribution of an image's average half flux radii (described below) measured over the course of a year is likely to show a positive skew due to the selection of evenings with relatively better seeing. For this reason one may not want to place too much initial emphasis on setting absolute control limits for tracking measurements, keeping in mind that the primary goal in tracking is to monitor and control for *trends* and *outliers*. Establishment of specific control limit values and reducing their range, if warranted, then becomes part of the continual improvement process.

The frequency of obtaining quality measurements can depend on several factors that are generally related to the overall requirements and resources available for quality management. For example, the frequency may be reduced for measurements with low expected variation or measurements that require extensive resources to obtain. So a goal of AISQMP is to define relevant quality measurements whose cost to obtain and maintain is kept low.

In summary, AISQMP defines a quality control process centered on two requirements; first that the performance of the AIS is measured regularly and tracked and second, that unwanted variations are investigated for extreme values and patterns that could indicate quality issues. Unwanted variation could relate to procedural error, a changing specification e.g. due to age, or potential hardware issues. Minimizing the amount of unwanted variation and reducing its range is the goal of quality improvement. Variations that remain within a specified range or tolerance ensure that the system is in 'control'. Note that the quality measurements and measurement frequencies identified in this paper are mostly suggestions. They're not meant to form an exhaustive or required list to be followed to the letter. It's up to each observatory to decide on what type of AISQMP to implement based on its unique quality requirements.

[4] For readers who aren't familiar with quality control charts, the concepts are straight forward and several sources can be found on the internet.

3. Image Quality Measures

A subjective definition of the quality of an astronomical image might include three components: sharpness, contrast (or dynamic range) and noise.[5] Sharpness can typically be ascertained from the size and shape of the stars in an image. While often associated with focus, sharpness can be a function of many other things including optical alignment, tracking and weather (seeing). Contrast is determined by the ability to resolve detail over a wide range of intensities and noise is spurious information added to an image during its acquisition. Contrast and noise are typically a function of camera electronics and settings (e.g. exposure time, read noise &c.) and the environment (e.g. weather, city lights, &c.). Contrast and noise may also be difficult to separate when making objective measurements as, depending on the noise source, a noisy image typically has reduced contrast.

Many 'off the shelf' (OTS) software applications provide the functionality to turn these subjective quality values into objective measurements useful for quality management. For example, some applications provide objective measures of 'sharpness' by finding stars in an image and measuring their size (e.g. full width half maximum, FWHM, or half flux radius, HFR) and shape parameters (e.g. roundness or eccentricity). Applications may count the number of stars in an image set (taken of the same field) to provide a relative measure of contrast, such that the

[5] For the mathematically inclined, the quality of an image is affected by spatial convolution of the ideal image with a degradation function (sharpness), quantization (contrast) and additive unwanted information (noise). In the ideal the convolution function is the Dirac delta, the signal is continuous (and infinite) and of course the noise is zero. A multiplicative 'noise' source due to non-uniform flat field response (vignetting, dust &c) must also be considered.

more stars counted equals better relative contrast, and average 'background' levels may provide an objective measure of noise. Table 1 identifies some OTS applications and their image quality measures.

	DSS	FIG	MAX	CCDI
# stars	x	x		
FWHM			x	x
HFR		x		
SigmaR	x			
Roundness	x		x	x
Score/Rank	x	x		
Ave Intensity			x	
Sky	x			x
Contrast			x	

DSS - DeepSkyStacker
FIG - FITS Image Grader
MAX - MaxIm DL
CCDI - CCD Inspector
blue - sharpness
red - contrast/noise
green - relative score/rank

Table 1: OTS image quality measures.

Most small observers, if they bother to obtain these image quality measures, might use them only for determining whether the images qualify for additional processing (typically registration and stacking). However, for AISQMP these values can be recorded, tracked and analyzed with the quality goals of a) obtaining values as close as possible to optimal theoretical performance and b) reducing the measured variation of these values. For example, let's say a set of thirty astronomical images are obtained on a given night. Then for each image the HFR is measured for each star and an average HFR value for the image is calculated. A control chart can be established that tracks standard deviation[6] of the average HFR values. The quality goal then is to record and track this standard deviation over several observing nights to ensure that its value is minimized to the most reasonable extent possible and that any variation of its value is within a desired range.

A critical point, particularly in the case of astronomical images, is that tracked values derived from an image set for a particular night must match with values taken on another night. In the above example, an HFR standard deviation value measured one night from an image set obtained with no binning can't be tracked on the same chart with a value obtained on another night where binning was used, unless the HFR is converted from pixels to arc seconds. Other factors, such as filter(s) used might also have to be controlled for.

4. AIS Instrument Quality Measurements

For purposes of quality management planning it is useful to break an AIS into its constituent instruments. Following the AIS instrument definitions used in the AISML paper (see References), this paper will cover the mount, optical tube assembly (OTA), camera, focuser, site and filter wheel[7]. The definitions for these instruments enable quality control for each of them to be maintained independently such that the final quality of an astronomical image becomes something of a linear sum of the quality of its constituent instruments. This independence means that issues found with the quality of an astronomical image can often be isolated to a specific instrument, facilitating issue resolution. For example, sharpness issues might be traced to the focuser, roundness issues to the mount (tracking) or OTA collimation, and background noise issues to the camera or site. As a rule, AIS instrument quality measures essentially test to see whether the instrument is performing to desired specifications.

Summarizing the instrument definitions, the camera is defined as the instrument that records incident light. The OTA is the instrument that collects light from an astronomical source and focuses it. The mount positions the OTA. The site positions the mount. The focuser positions the image's focal plane and the filter (wheel) filters the incoming light from an astronomical source.

Although the above instruments are independently subjected to quality control measures, in practice it's not necessary to physically separate them from the AIS. This is accomplished by establishing quality measurements for each instrument in a specific order, such that quality measurements for a given instrument only require that previously measured instruments meet quality assurance criteria. Starting with the camera, it can effectively undergo stand-alone quality testing without physically being removed from the AIS[8].

[6] The distribution of HFR standard deviations should be closer to a Gaussian than the distribution of HFR averages.

[7] The exact instruments depend on the specific AIS configuration.

[8] Though the camera's typically the easiest device to remove from an AIS.

After the camera has achieved the necessary level of quality assurance, it can then be used when performing quality testing on the OTA. As with the camera, the OTA may be attached to the mount but not rely on mount meeting quality assurance criteria for its own quality tests. Finally, the mount may undergo quality tests using the camera and OTA which have already been tested. Thus initial quality control testing for an AIS begins with the camera, progresses to the OTA and mount, and concludes with either the filter wheel or focuser. Another fortunate aspect of starting with the camera is that it is typically a COTS device, which means that it's more likely to have an existing set of manufacturer performance specifications that can be used as a baseline for quality control purposes.

1.1 Camera Quality Measurements

For quality measurement purposes, the camera can be thought of as a 2D sensor array of pixels mounted in a camera body. The sensor array reacts with incident light and converts it to another format, typically electron charge, which can be used to derive the intensity of the incident source. Cameras used in astronomy typically have CCD or CMOS sensor arrays. The camera body controls exposure of the sensor array, processes the exposed sensor array information and outputs an image frame. The image frame is a 2D array of pixel values or ADUs (analog to digital unit, sometimes called DN or digital number). There can be various types of image frames depending on the target. For example a 'light' frame has a target of an astronomical source. A 'dark' frame has no target and is an image resulting from an exposure when the sensor array is completely shielded from incident energy (e.g. camera shutter is closed). Camera quality control is centered on certifying the validation and reliability of all types of image frames produced by the camera. Objective quality measurements derived from image frames include read noise, gain and the number of bad pixels. These are scalar values that characterize the performance of the camera and whose variation is easily tracked for quality control purposes. Unfortunately there isn't the same availability of COTS that determines these values as there is for the image quality.

Read noise relies on data obtained from bias frames. Bias frames are the shortest exposure dark frames that a camera is capable of taking[9]. Gain and bad pixel values rely on data obtained from dark corrected flat frames. Flat frames (or flats) are exposures taken of flat or uniformly illuminated fields. Dark corrected means dark frames of exposure times matching the flats have been subtracted from the flat frames. 'Master' frames are typically the estimated average of several individual frames of identical type. Each of the above frames is typically exposed at nominal camera operating temperatures (if the camera has cooling capability). For cooled cameras with short flat frame exposures, bias frames can also be used to dark correct flats. Since dark corrected flat frames are typically acquired during standard imaging sessions, little extra effort is required for quality purposes. Bias frames also require little extra effort. Obtaining a uniformly illuminated field for flats is not always easy. Either an artificial flat field source is used[10] or a set of sky flats are taken.

1.1.1. Read Noise

The ideal bias frame would consist of an array of uniform values (typically some offset value pre-defined in the camera body electronics). A real bias frame will of course show variation. Not only is there intensity variation within the pixels of a given bias frame, but the intensity of a specific pixel will vary between bias frames. Read noise is determined from the statistics of this intensity variation. It's important to note that statistical calculations for read noise assume the intensity values within and between bias frames are independent of each other, or uncorrelated. This means that bias frames look random, i.e. they contain no patterns or regular features, and the histogram of the bias frames are roughly Gaussian in appearance. If the bias frames contain a feature that encompass a relatively small number of pixels, such as a bad row or column on the edge of the frame, or a few bad pixels scattered across the array, then those pixels can either be excluded from the calculations or ignored if their number is relatively small. Larger scale patterns such as ramps or periodic variations can be more problematic. If possible they should be eliminated or minimized such that they become statistically insignificant. Patterns and features in bias frames can be determined from visual inspection, using contrast enhancement if necessary. A 2D FFT of the bias frame can be useful to help identify and characterize periodic patterns.

The simplest method for calculating read noise requires two bias frames (ref 3). One frame is

[9] Bias frames must have short enough exposures for zero dark current.

[10] The uniformity of an artificial flat field source should be tested by comparing master, corrected flats taken by a camera before and after a ninety degree rotation.

subtracted from the other, and the read noise is the standard deviation of the pixel values in the resulting frame divided by the square root of two. Note that the units for read noise in this instance are in ADUs. Keep in mind that manufacturer specified read noise is typically provided in electrons where the gain (see below) is multiplied in. For a little more accuracy (and because bias frames are easy to obtain) it's recommended to take a set of bias frames, calculate the read noise for each unique pair, and then take an average. For example, a set of five bias frames results in ten unique pairs. An ideal bias frame of consistent uniform values would have zero read noise.

As noted above, the manufacturer will provide read noise as a camera specification. This value becomes the initial center line for a read noise control chart. The measured read noise is regularly plotted and the variation from the specification is observed. In general a manufacturer's specification is based on an average of several cameras values. By regular measurement, the specific read noise of a particular camera can be determined and the center line adjusted if necessary. Regular measurement will also provide an idea of what the normal variation in read noise should be. Large variations should immediately be investigated to determine the cause. Sometimes a large variation can be due to a software parameter that was changed from a nominal value. Other non-random control chart patterns should also be examined for their cause.

1.1.2. Gain

The gain, used to convert ADUs to electrons, is critical for accuracy in measuring the flux from an astronomical source. There are two methods for determining gain. The more precise method uses a 'gain plot' (ref x), where the measured gain is the slope obtained from a linear fit of 'gain points' derived from pairs of corrected flats, where each pair has a unique average intensity value[11]. For quality control purposes only a single gain point needs be determined on a regular basis, though a complete gain plot is initially required. Calculating a gain point starts with two corrected flats taken at the same exposure. Then the average flat frame value is calculated. This is the gain point's ordinate. To determine the abscissa, one corrected flat is subtracted from the other for a difference frame. The statistical variance is determined for the difference frame and then divided by two (due to the subtraction). Unlike bias and dark frames, flats are expected to have imperfections such as dust rings on filters or occasionally vignetting due to limits of the optical system or field of view (FOV) obstructions. Gain points should be calculated from the largest sub frames in a corrected flat that are free from significant imperfections. As noted above, the initial gain plot is created using several gain points obtained from flats with different average intensities, and the measured gain is slope of the least squares fit. Subsequent gain points used for quality control are overlaid on the initial gain plot and their deviation from the least squares fit is noted.

A simpler, though less accurate method for measuring the gain relies only on two corrected flat frames (ref x). The method involves dividing the average of the two flats by the variance of the difference. As with read noise, multiple pair values can be averaged in either case.

Also, as with read noise, the gain value for a camera is typically provided by the manufacturer. Measured gain values should be compared against the manufacturer's specification to be sure it's a reasonable value. Determining gain (points) on a regular basis provides a good validation of whether the camera is performing according to spec. Gain points with a large deviation from the least squares fit to a gain plot are likely an indication of a quality issue. Note that gain plots may not be truly linear and that deviation of between gain points of similar average intensities (if available) is more significant than the deviation from the linear fit.

1.1.3. Bad Pixels

In general, if a suspect pixel is not obviously defective[12] it is somewhat subjective whether to mark it as 'bad'. Fortunately, for quality control what's important is not whether a pixel is intrinsically bad but rather that the number of bad pixels is measured in a consistent fashion. An example of such a method is provided below. For bad pixels, any trend involving the total number as a function of time is important to note. A sudden, dramatic increase could mean a serious issue with the camera. While undesirable, the total number will typically increase with a camera's age. Air leaks in the chamber containing the sensor array can allow moisture to creep in. When the camera's cooled, crystals can form on the sensor array which can show up as an increase in the number of bad pixels.

A method the author uses for determining the number of bad pixels involves obtaining a master corrected flat of nominal average intensity value and counting the number of outlier pixel values. It's

[11] The gain plot should not be confused with the quality control plot.

[12] That is, outputting a constant value regardless of the intensity of incident light.

important that the optics be clean and the flat uniformly illuminated across the whole array. If vignetting is an issue then a 2D surface fit is subtracted before counting outliers. The author typically uses Chauvenet's criterion for determining whether a pixel is an outlier. As noted earlier, master flats are typically created during an observing run, making it fairly simple to keep track of the bad pixel count, though it typically does not need to be measured with any great frequency.

1.1.4. Other Camera Quality Measures

Other camera quality measures use less quantitative assessments. As can be seen from the above, the quality of the flat field is important for gain and bad pixel determination. If an artificial flat field is used it should be periodically checked to ensure that the response remains uniform over time. A simple test for uniformity involves comparing one master corrected flat with another that's exposed after the camera has been rotated ninety degrees.

Dark current is another quality measure that can optionally be tracked and compared with the vendor specification. To measure dark current, create a master bias and a set of master darks at different exposure times with the camera operating at nominal temperature. Then create a plot of the average frame value vs. exposure time and keep track of plot's slope over time.

Master darks and biases should also regularly be inspected for overall uniformity where unwanted patterns or thermal effects coming from the camera body can reach the sensor.

1.2 Optical Tube Assembly (OTA) and Focuser Quality Measurements

The OTA is the next instrument to undergo quality measurements. Like the camera, the OTA can be divided into two sub components, in this case the optics (i.e. mirrors, lenses, masks and baffles) and the optical mounting (i.e. tube assembly, optic mounts). The optics act on the incoming light and the optical mounting acts on the optics. Since the focuser works in close conjunction with the OTA its quality measurements are also included in this section. While some quality measures of the OTA such as the optics' figure and tube flexure are expected to remain fairly static over time, i.e. without noticeable variation, there are regular quality measurements of the OTA that can be included for AISQMP purposes.

1.2.1. Optical Surfaces

Exposed optical surfaces should regularly be inspected for cleanliness and coating quality. The optics should be properly cleaned when necessary and the cleaning dates recorded. If cleaning dates become more closely spaced than normal the observatory environment should be inspected for sources of contamination. In general, a cursory visual inspection before telescope use should be adequate. The inspection should be part of a startup checklist. Also note any dates if or when the optics are (re)coated or if any other type of work is done on the surfaces

1.2.2. Collimation

The next quality measurement of the OTA is stable collimation. After initial collimation adjustments have been made, additional testing is performed with the tube pointing at different altitudes and azimuths to verify stability of the optical mounting hardware. The nature and frequency of the collimation tests depend on the quality of the original OTA designand imaging requirements of the AIS. Fortunately there are a few OTS applications that will measure collimation quality in real time via focus testing. Results from collimation testing should be saved so that they can be compared with values obtained from later tests. Collimation test dates should be recorded. Increased frequency of collimation adjustments may indicate a problem with the optical mounting hardware.

1.3 Mount Quality Measurements

Optimal performance of the mount, particularly in tracking, is obviously critical for quality images. The mount is sub-divided into three components for quality tracking purposes. These are the controller, the motors (which include any additional feedback mechanism to the controller such as shaft encoders) and the mechanics which consists primarily of gears, shafts, coupling to the OTA and their housing. A quality plan for the mount should include verifying any controller firmware is up to date, and visually inspecting and maintaining the quality of mechanics including establishing and following a schedule for any lubrication, cleaning or other maintenance that may be required or recommended.

1.3.1. Periodic Error (PE) and Polar Alignment (PA)

PE and PA are critical measurements for tracking. PE and PA should be checked at least once per year. As with collimation, it's helpful to use OTS applications to perform these measurements and a single application such as PEMPro[13] will often measure both PE and PA. For PE values one should record primary frequency and amplitude. Note any unusual frequency component(s) which typically are due to a problem, e.g. a rough spot, in the worm gear. For PA any drift rate should be recorded. PA issues come from unexpected displacement of the mount which can be due e.g. to adjustment screws getting accidently tweaked or even to earthquakes (if an observatory is in that type of region).

1.3.2. Pointing Characterization

Pointing characterization essentially creates a model of a mount's pointing accuracy based on differences between where the mount is actually pointing (determined by plate solves) vs. where mount's controller thinks it's pointing (based on motor or encoder feedback). As with PE and PA, OTS applications are available for pointing characterization[14]. The application should be run at least once a year, if no changes to the overall mechanics/balance of the telescope are made in the meantime. When no changes have been made, the parameters for each model run should be compared for any major differences in values which could indicate something indeed has changed without prior knowledge.

1.4 Filter Wheel Quality Measurements

The filter wheel has two primary features that contribute to image quality. These are based on the filters[15] which act as optical surfaces and the filter wheel's mechanical accuracy.

1.4.1. Filter Surfaces

As with the optical surfaces in the OTA, each of the filters in the filter wheel should be periodically inspected to ensure they're free of dust and other defects. Flat frames can be used for this purpose by tracking the number and type of dust donuts which appear in the master frames for each filter. The type or size of dust donuts and their repeatability across filters can help discriminate whether the dust is on the filter, the CCD window or on the CCD surface itself. Since flats are often taken during observing runs this data does not require much extra effort to obtain. Periodic visual inspection of master flats taken at different dates should suffice in lieu of a literal count and control plot.

1.4.2. Filter Wheel Positioning

Precise repeatability of filter positioning is necessary for accurate flat correction and stacking (especially if filters are rotated after each exposure). Since filter positioning is a mechanical process it's subject to degradation over time as components wear. As with filter surfaces, master flats again can be used. In this instance masters created before and after a rotation are compared, e.g. by simple subtraction, to determine whether there's any measurable shift between the two.

5. Notes on Tracking

As noted earlier, objective quality measures can be tracked via a control chart where the target value can start with a manufacturer's specification or a locally determined average after a set of initial measurements have been made. For a chart to be of the most use, the measurements should be taken with some regularity and follow a normal distribution. For measurements that are non-numerical and/or are taken irregularly a delta-date can provide a useful measurement for tracking. For example, the cleaning dates for optics can be tracked in this fashion to ensure a regular cleaning schedule and to note any trends such as increased frequency of cleaning due to some issue, e.g. improper dust protection. As noted in Section 2, non- normally distributed data can often be transformed. The delta cleaning dates in the above example ideally should be normally distributed about a scheduled maintenance interval.

Measurements can be recorded by hand or via text files, spreadsheets, databases, or custom applications. The later three can also be used in tracking to generate control charts or other types of quality reports. The author uses his text/XML based AISML format to either record the quality measure or

[13] http://www.ccdware.com/products/pempro/

[14] E.g. http://www.tpointsw.uk/

[15] This is one instance where the independence of each AIS instrument can get fuzzy. The camera's CCD window and any Bayer mask overlaying a camera sensor essentially act as filters though they're not part of the filter wheel.

point to a csv format file with the raw data. AISML files can easily be read by a variety of applications.

Figure 1 shows an example of a plot obtained from the European Southern Observatory (ESO) website[16] that tracks the rms of bias levels (similar to read noise) for one of their cameras.

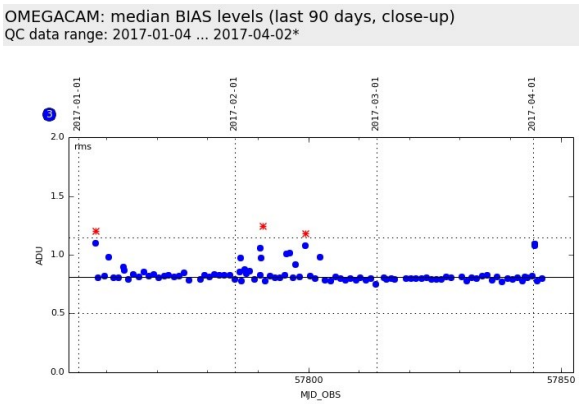

Figure 1: Control chart tracking rms of bias levels

Note the non-normal distribution of values and red data points indicting values exhibiting excessive variation. The ESO even developed their own application[17] for creating these plots.

6. Conclusion

Quality results are an important objective for small, amateur observatories aiming to make scientific contributions. Quality management helps meet that objective. Quality management planning is the part of quality management that a) identifies the various components that contribute to the quality of the final output, b) defines objective quality measurements for each component, and c) establishes procedures to track these measurements and control for unwanted variation.

AISQMP assists with quality management planning by specifying not just the quality measurements of the final product[18] but also in identifying the instruments comprising an AIS and specifying their quality measurements that can be used for tracking. The level and degree of quality desired play an important role in the determination of the amount of resources available to dedicate to the quality management effort. Neither the instruments nor measurements mentioned in this paper are meant to be a rigid or comprehensive list nor necessarily followed in toto. They should be customized for each observatory's unique configuration and needs.

7. Acknowledgements

The author would like to thank Robert Bucheim and the SAS program committee for their assistance with the preparation of this paper.

8. References

Goldbaum, Jesse M. "Astronomical Instrumentation System Markup Language (AISML)." (2016). *SAS 2016 Proceedings* **35**, 131-144.

Jamieson, Archibald, 1982, Introduction to Quality Control (Reston Publishing Company, Inc.).

Read Noise: Photometrics Whitepaper. https://www.photometrics.com/resources/whitepapers/read-noise.php

Tech Note: Pixel Response Effects on CCD Camera Gain Calibration. http://www.mirametrics.com/tech_note_ccdgain.php

Chauvenet's Criterion. https://en.wikipedia.org/wiki/Chauvenet%27s_criterion

Alnitak XL Flat Fielder Test Results http://optecinc.com/astronomy/catalog/alnitak/xl_testing.htm

Dark Current https://www.photometrics.com/resources/learningzone/darkcurrent.php

16 http://www.eso.org/observing/dfo/quality/OMEGACAM/reports/HEALTH/trend_report_BIAS_level_HC.html

17 http://www.eso.org/~qc/tqs/trendPlotter.html

18 Astronomical images for the purpose of this paper.

Scintillation Reduction using Conjugate-Plane Imaging

Gary A. Vander Haagen
Stonegate Observatory
825 Stonegate Road, Ann Arbor, MI 48103
garyvh2@gmail.com

Abstract

All observatories are plagued by atmospheric turbulence exhibited as star scintillation or "twinkle" whether a high altitude adaptive optics research or a 30 cm amateur telescope. It is well known that these disturbances are caused by wind and temperature driven refractive gradients in the atmosphere and limit the ultimate photometric resolution of land-based facilities. One approach identified by Fuchs (1998) for scintillation noise reduction was to create a conjugate image space at the telescope and focus on the dominant conjugate turbulent layer within that space. When focused on the turbulent layer little or no scintillation exists. This technique is described whereby noise reductions of 6 to 11/1 have been experienced with mathematical and optical bench simulations. Discussed is a proof-of-principle conjugate optical train design for an 80 mm, f-7 telescope.

Introduction

High accuracy photometric measurements are directly related to the level of turbulence within the atmosphere and our ability to compensate for both the instantaneous and time average intensity changes. As the star's plane wavefront passes through the atmosphere both phase changes caused by variations in the total air column and intensity variations are caused by diffraction at high altitudes. These effects result in in intensity variations at the telescope as the turbulence is continuously blown across the field of view. Of particular concern are portions of the incoming flux that are entirely lost or propagate into the field from these refractive changes. Viewed with the naked eye and smaller scopes we see twinkling of the image. With larger telescopes the effect is less but significantly reduces the photometric measurement accuracy.

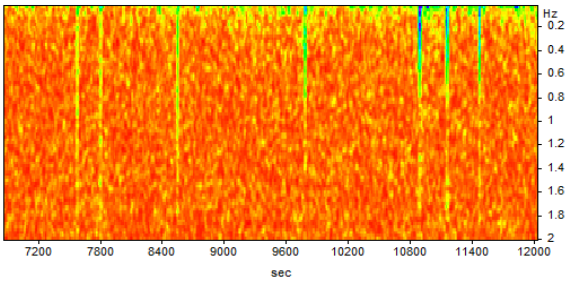

Figure 1. FFT power spectrogram of scintillation noise from observations of CR Dra on 2016-5-23 over a 5000 sec period. There is significant noise below 0.4 Hz over the full period with a large spikes approaching 2 Hz at multiple times. The yellow to green regions represent higher energy level noise.

Figure 1 shows a spectrogram, an FFT power spectrum over time, with scintillation noise scattered from sub-Hz to 2 Hz over a 5000 sec measuring period.

Figure 2 shows the origin of the scintillation process pictorially. Consider first what might happen if an aperture was placed in the sky within the turbulence layer. With the detector close to the aperture no scintillation would be detected since all the flux would be contained within the aperture irrespective of any diffraction occurring. Moving back the detection to a practical position at the telescope aperture, any diffraction-taking place has sufficient distance for light to redirect either outside the aperture or come within the aperture from outside the field. Those optical rays are shown with the large dots.

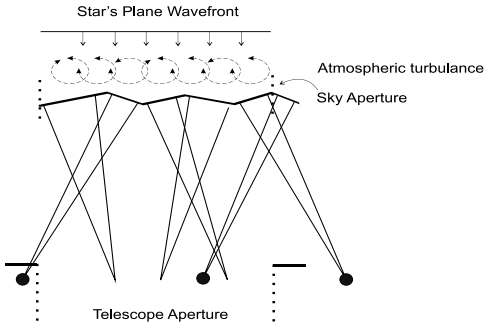

Figure 2. The star's plane wavefront enters a layer of turbulence causing diffraction zones to redirect the incoming light far below at the telescope aperture. This effect causes some light to pass outside the aperture and be lost and likewise other areas to pass inwards. The sweeping changes are driven by atmospheric conditions within the air column e.g., wind, turbulence, temperature, humidity, pressure, etc.

It seems intuitive that an optical system allowing access to the turbulent region would offer an opportunity for scintillation reduction. The math and

simulations for such an optical system was done by Fuchs, Tallon, and Vernin (1996, 1998) followed up by additional work and a prototype by Osborn et al. (2010). These researchers described an optical train using conjugate imaging to provide access to the atmospheric plane within a land-based telescope. The motivation was to further reduce the optical noise of large earth based telescopes where a dominant turbulent layer typically exists and, further improvement is still needed to augment installed adaptive optics and other techniques.

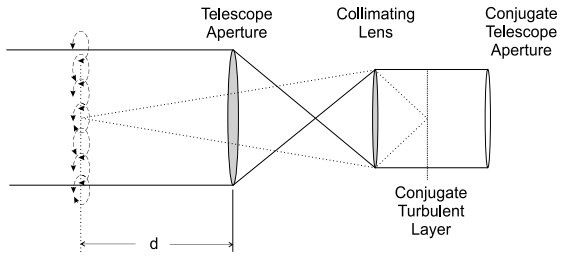

Figure 3. An optical system providing a conjugate image space and access to the turbulence plane and target plane.

Figure 3 depicts the ray diagram for the conjugate image space. A collimating lens provides the image space for the turbulent layer with infinite image position to the left and the entrance aperture to the right. The distance to the upper dominant turbulence layer (d) at many observing sites is typically 10 km.

With a detector assumed at the conjugate turbulent plane, Osborn et al. (2010) ran mathematical simulations of this configuration using actual SCIDAR (scintillation detection and ranging) turbulence data recorded at San Pedro Martir. The results showed the median reduction in intensity variance improved by a factor of 11. With a wider range of data, including nights without a dominant turbulent layer, the median reduction was a factor of 6. Also, optimum telescope size was found to be 1.2 to 2m with smaller scopes improving less due to aperture diffraction effects and larger being shot noise limited. The data for telescopes below 0.5m also looked promising.

During an investigation of this technique Fuchs et al. (1996) had developed a physical optical simulator. The key to the optical simulation was an airflow channel where two different air temperature and speed columns were mixed in a controlled environment with optical windows allowing for light passage through the turbulent region. This turbulent zone was placed at distance (d) and measurements were made to determine the refractive index spatial power spectrum for correlation with the mathematical simulation. A movable photomultiplier was placed at the conjugate turbulent layer image space and moved both directions along the axes to measure the turbulence intensity. The turbulence was eliminated when the detector was focused on the layer and increased parabolically either side. The improvement in scintillation index was found greater than 50/1.

Bench Simulation of the Conjugate Imaging System

An attempt was made to repeat this experiment using a smaller optical bench and a very different approach to the turbulence generation. The optical bench length available was considerably shorter at 275 cm. A slowly spinning acrylic disk with refractive areas of various sizes replaced the complex dual column airflow chamber. Several versions of the refractive discs were tried; small thin epoxy blobs, controlled surface scratches, and distortion of the acrylic surface by solvents. Single and multiple spaced layers were also tried. The solvent induced surface irregularity, single layer disc worked the best. Most of the configurations produced excessive beam divergence and sharp flaring. While the turbulence disk did demonstrate feasibility it showed turbulence reduction ratio of only 4/1, considerably below the results shown by Fuchs et al. (1996). Likely causes were the poor beam quality due to laser multi-moding, excessive disc scattering, insufficient distance between the turbulence wheel and the telescope aperture, and stray light scattering along the optical path.

A second bench setup was tried with a substantially longer optical path of 780 cm between the turbulence disc and the telescope aperture. The setup is shown pictorially in figure 4 with laser illuminating a collimator and expanded beam passing through the rotating turbulence wheel into the telescope aperture, collimated, and generating the conjugate image space. The detector was placed at focus of the imaging lens and contained its own 2 mm aperture. The aperture should be approximately the size of the telescope entrance aperture divided by the magnification ratio of the telescope-collimator combination.

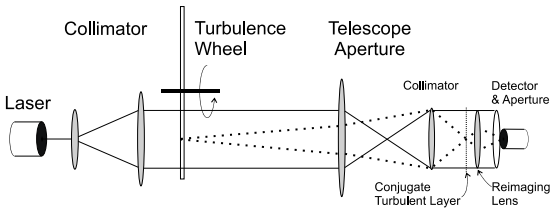

Figure 4. The bench setup for simulating the turbulent layer in an optical path. The field-limiting aperture is contained at the entrance to optical detector.

With the simulated turbulent layer located 780 cm from the telescope aperture the conjugate layer focus was approximately 20cm behind the imaging lens. The rotational speed of the turbulence wheel was adjusted to permit a reasonably stable noise output at the AC voltmeter resulting in a 35Hz centered noise spectrum. The optical detector was a Thorlabs PDA36A amplified high-speed photodiode with bandwidth over 5 MHz. The actual optical bench setup is shown in figure 5.

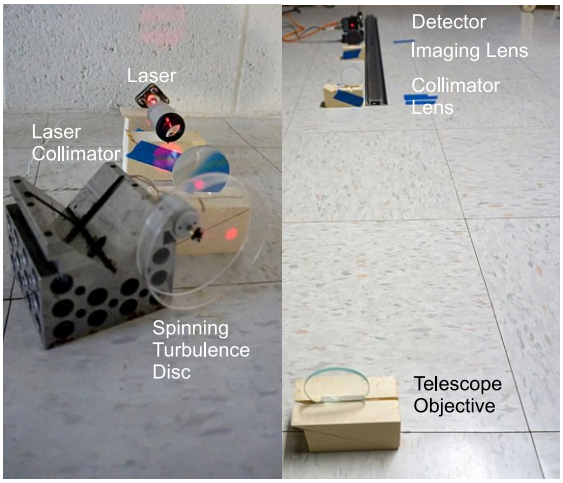

Figure 5. The left panel shows the source end of the 950cm total length bench: the laser, collimator, and motorized spinning turbulence disc. The right pane shows the telescope objective in the foreground, the collimator lens, reimaging lens, and optical detector.

The change in scintillation noise as a function of the detector position within the conjugate turbulent layer is shown in figure 6. The two different curve shapes represent different refractive profiles generated by two different radial positions on the turbulence disc. Improvement ratios for the measurement range shown are 7.9/1 for the lower and 3.6/1 for the upper curve.

The optical simulation demonstrates that the technique works. The overall insufficiency of the turbulence disc, laser, and available optics may not give an accurate picture of the level of expected improvement possible. However, it appears from the previous research and the simulations that a telescope proof-of-principle is worth pursuing.

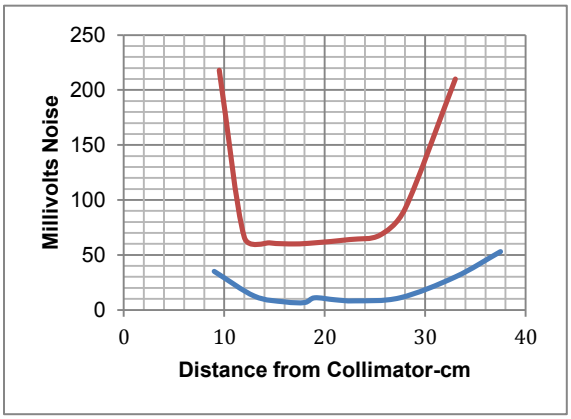

Figure 6. Noise as a function of detector position within the conjugate turbulent image layer shown in figure 4. Two separate measurements were made with the laser striking two different regions of the turbulence disc.

A Conjugate Optical Train Prototype for an 80 mm, f-7 Telescope

Design of the optical train uses conventional geometric optical relationships with p_1 and q_1 respectively representing the distance of object and image from the lens centerline and, f_1 the lens focal length, Pedrotti (2017). For convex lenses the signs are positive for real objects to the left and real images to the right. For a convex lens f is positive and concave is negative. Equation (1) shows the relationship for thin lenses:

$$1/p_1 + 1/q_1 = 1/f_1 \qquad (1)$$

For a 80mm diameter f-7 lens the focal length is 560mm. Placing the object p_1 at infinity results in:

$$1/q_1 = 1/f_1 \qquad \text{or}$$

$$q_1 = f_1$$

The image is (+) real and located 560mm to the right of the lens. Equation 1 results are now coupled with the same relationship for the collimator but adding another variable, lens separation, making (separation-q_1) the input to the collimator or p_2. The same sequence is used for the final imaging lens. A spreadsheet was used for this iterative process. The collimating lens was chosen for a commonly available focal length of 12mm or a 47/1 magnification. A value of 10^{14} mm was used for the infinite object (p_1) position and 10^7 mm for the high altitude dominate turbulent layer position. The telescope objective to collimator separation will be slightly larger than the sum of the two focal lengths.

Here is where design direction is less clear. Referring to table 1, upper pane exhibits the optical bench setup. The near and far field imager focal points were equal and worked properly over the very limited object range studied. The same direction was followed for the 80 mm design. For both designs the imager focal length was chosen for availability. Numerous iterations were tried varying focal length and spacing with the final focal positions closely matching. When fabricated, the 80 mm proof-of-principle optical train should answer whether this direction was correct.

Optical Bench Conjugate System

Lens	Focal Length mm	Lens Separation	Q3 mm	
			10^{14}	10^{7}
Tel Objective	570			
Collimator	230	800.01	10^{6}	10^{6}
Imager	200.5	410	200.5	200.5

80 mm Telescope Conjugate Optical Train

Lens	Focal Length mm	Lens Separation	Q_3 mm	
			10^{14}	10^{7}
Tel Objective	560			
Collimator	12	572.0001	10^{8}	10^{6}
Imager	50	20	50	50.5

Table 1. Upper table, the specifications for the optical bench setup. Lower table, the set of trial lens specifications for a 80mm diameter conjugate lens system.

For initial optical alignment, the collimated laser will be used to set the collimation distance between the telescope and collimation lens with the imaging lens removed. The imaging lens will be installed per dimension and the aperture just forward of the image focal point. A detector will be set at the imaging lens focus and moved outward through the conjugate turbulence layer to measure effectiveness.

Conclusions

The concept of using the conjugate image space for scintillation reduction is predicated on the presence of at least one dominant turbulence layer. While this is true in most good viewing regions many sites areas have at least a second turbulent area near the ground, generally within 100-meters or less. However, with the optical system focused on a dominant high altitude layer and a lower layer(s) still present Osborn (2010) noted there was still a 6/1 median improvement in noise. This improvement was orchestrated by a reasonable knowledge of where the upper dominant layer is located so proper focus could be achieved. Without such knowledge a conjugate optical system as described could rely on use of its inherent capability as a SCIDAR by running through the focus manually to find the minimum turbulence region and the focal position set accordingly.

The previous discussion represents a very abbreviated version of the research available on this topic. While of great interest to the large land based adaptive optics telescopes, it may also represent productive area for amateur telescope study.

The actual design approach would benefit immensely from dialog with other interested astronomers to better understand the boundaries and limitations of this optical system. The author would welcome such collaboration.

References

Fuchs, A., Vernin, J., Tallon, M. 1996, Appl. Opt., 35 1751

Fuchs, A., Tallon, M., Vernin, J. 1998, PASP, 110, 86-91

Osborn, J., Wilson, R. W., Dhillon, V. S., Avila, R., Love, G. D. 2010, *Conjugate-plane photometry: Reducing scintillation in ground-based photometry*, Mon. Not. R. Astron. Soc., 000

Pedrotti, L. S. 2017, *Basic Geometrical Optics,* https://spie.org/Documents/Publications/00%20STEP%20Module%2003.pdf , CORD, Waco, TX,

Thorlabs 2017, https://www.thorlabs.com, PDA36A amplified photo detectors